

Advances in HDS catalysts design

- Relation between catalyst structure
and feed composition -

Advances in HDS catalysts design



Narinobu Kagami

Narinobu Kagami

Propositions accompanying the thesis
Advances in HDS catalysts design
- Relation between catalyst structure and feed composition -
by Narinobu Kagami

- 1) Although the final proof has not been given that type II active phase consists of several stacked layers of MoS₂ slabs or edge-bonded layers, the insight that the type II active phase has weaker interaction with the support is very useful in developing highly active catalysts.
Chapter 3, 4 and 7 of this thesis
- 2) 3-Dimensional Transmission Electron Microscopy will be the most powerful technique to reveal the morphology of type II active phase in the future, although statistical analysis will still be necessary if they exist as a mixture of the specific morphologies.
U.Ziese et al., Preprint of ICC 13th, Paris, **O1-048** (2004)
- 3) H₂S inhibition has to be taken into account for the ranking of HDS catalyst activity because the susceptibility of catalysts to H₂S is sometimes significantly different, as shown in the difference between CoMo and NiMo catalysts.
Chapter 4 of this thesis
- 4) It is promising to apply catalysts with high hydrogenation activity for ultra deep desulfurization of diesel, but the nitrogen compound concentration in feedstocks should be taken into account since the hydrogenation pathway is relatively strongly inhibited by them.
Chapter 4, and 6 of this thesis
- 5) Although statistical techniques can reveal the inhibiting effect of nitrogen compounds for deep desulfurization of diesel using real feed, the study of model reactions is a rewarding challenge to discover how it retards the catalyst activity.
Chapter 5, and 6 of this thesis
- 6) Oil refining is one of the oldest scientific fields, but still one of the most challenging topics because oil is a mixture of uncountable number of compounds.
- 7) Although high-throughput experimentation is intrinsically efficient, from the enormous efforts by forerunners should be learned and well utilized for planning of the experimentation in order to avoid disappointing results.
- 8) For the production of sulfur free transportation fuels, the conversion level has reached more than 99% for diesel HDS. This changes fuel processing technology into a chemical field.
- 9) When the density is high and there is not so much space, we need technology to build high buildings like skyscrapers. The same is the case for structure of the active phase on the surface of HDS catalysts.
- 10) Industrial catalysis is not a field where typically Nobel Prizes are awarded, but it is highly relevant because it allows the synthesis of products in an environmentally friendly way.

These propositions are considered defensible and as such have been approved by the supervisor, Prof. dr. J. A. Moulijn.

Stellingen behorend bij het proefschrift
Advances in HDS catalysts design
- Relation between catalyst structure and feed composition -
door Narinobu Kagami

- 1) Hoewel het definitieve bewijs niet geleverd is dat type II actieve fase bestaat uit een stapeling van lagen MoS₂ of uit lagen gebonden via de ribben, is het inzicht dat type II een lage interactie heeft met de drager van groot belang bij de ontwikkeling van katalysatoren met een hoge activiteit.
Hoofdstuk 3, 4 en 7 van dit proefschrift
- 2) 3-Dimensionale Transmissie Elektronen Microscopie zal in de toekomst de krachtigste techniek zijn voor het onthullen van de morfologie van type II actieve fase, hoewel statistische analyse nog steeds vereist zal zijn indien de actieve fase zou bestaan uit een mengsel van specifieke morfologie.
U.Ziese et al., Preprint of ICC 13th, Paris, **O1-048** (2004)
- 3) Mogelijke remming door H₂S moet in aanmerking worden genomen bij het rangschikken van katalytische activiteiten omdat de gevoeligheid voor H₂S van katalysatoren heel verschillend kan zijn zoals bijvoorbeeld is gevonden voor NiMi en CoMo katalysatoren.
Hoofdstuk 4 van dit proefschrift
- 4) Katalysatoren met een hoge hydrogeneringsactiviteit zijn veelbelovend voor ultradiepe ontzwaveling van diesel, hoewel de stikstofconcentratie in aanmerking genomen moet worden aangezien stikstofverbindingen het hydrogeneringsreactienetwerk sterk hinderen.
Hoofdstuk 4 en 6 van dit proefschrift
- 5) Hoewel statistische technieken de inhibitie-effecten van stikstofverbindingen kunnen karakteriseren voor realistische diesel voedingen, is het toch dankbaar werk om modelverbindingen toe te passen voor het vinden van het onderliggende mechanisme van de inhibitie.
Hoofdstuk 5 en 6 van dit proefschrift
- 6) Olieraffinage is weliswaar een klassiek technisch onderwerp maar tegelijkertijd nog steeds een van de meest uitdagende onderwerpen omdat olie een complex mengsel is van een ontelbaar aantal verbindingen.
- 7) Hoewel 'High-Throughput Experimentation' in principe een tijdsbesparende techniek is moeten toekomstige gebruikers er voor zorgen te leren van de zeer uitgebreide ervaringen van de eerste gebruikers om teleurstellingen te voorkomen.
- 8) Voor de productie van zwavelvrije brandstoffen ligt het HDS conversieniveau hoger dan 99%. Dit verschuift de technologie van brandstofverwerking meer en meer naar een chemisch gebied.
- 9) In onze maatschappij passen we hoogbouw toe wanneer de bevolkingsdichtheid hoog en de ruimte schaars is. Dezelfde redenering is van toepassing op ontzwavelingskatalysatoren.
- 10) Het feit dat Industriële Katalyse niet een gebied is waar Nobel prijzen voor worden uitgereikt zou ten onrechte kunnen suggereren dat het gebied minder belangrijk is. Immers, milieuvriendelijke productieprocessen zijn slechts mogelijk dankzij de Industriële Katalyse.

Deze stellingen worden verdedigbaar geacht en zijn als zondanig goedgekeurd door de promotor, Prof. dr. J. A. Moulijn.

Advances in HDS catalysts design

- Relation between catalyst structure and feed composition -

Advances in HDS catalysts design

- Relation between catalyst structure and feed composition -

Proefschrift

ter verkrijging van de graad van doctor
aan de Technische Universiteit Delft,
op gezag van de Rector Magnificus prof. dr. ir. J.T. Fokkema,
voorzitter van het College voor Promoties,

in het openbaar te verdedigen op maandag 25 september 2006 om 12:30 uur

door Narinobu KAGAMI

Master of Science (Applied Chemistry), Waseda University, Japan.
geboren te Osaka, Japan

Dit proefschrift is goedgekeurd door de promotor:

Prof. dr. J.A. Moulijn

Samenstelling promotiecommissie:

Rector Magnificus,	voorzitter
Prof. dr. J.A. Moulijn,	Technische Universiteit Delft, promotor
Prof. dr. F. Kapteijn,	Technische Universiteit Delft
Prof. dr. J.A.R. van Veen,	Technische Universiteit Eindhoven
Prof. dr. J. Grimblot,	Université des Sciences et Technologies de Lille
Dr. A.D. van Langeveld,	Technische Universiteit Delft
Dr. ir. M. Makkee,	Technische Universiteit Delft
Dr. E.T.C. Vogt,	Albemarle Catalysts, Amsterdam
Prof. dr. A. Schmidt-Ott,	Technische Universiteit Delft (reservelid)

This research was supported by Idemitsu Kosan Co. Ltd., and Japanese Cooperation Center Petroleum (JCCP).

ISBN: 4-9903244-0-4

Copyright © 2006, by Narinobu Kagami

Contents

Chapter 1: Ultra deep hydrodesulfurization for diesel fuel -General Introduction-	1
Chapter 2: Testing of HDS catalysts	17
Chapter 3: Characterization of NiMo type I and type II catalysts -The effect of metal loading-	33
Chapter 4: Reaction pathways on NiMo/Al ₂ O ₃ catalysts for hydrodesulfurization of diesel fuel	49
Chapter 5: Application of datamining method (ID3) to data analysis for ultra deep hydrodesulfurization of straight-run light gas oil -Determination of effective factor of the feed properties to reaction rate of HDS -	69
Chapter 6: Modeling of inhibition of deep hydrodesulfurization by competitive adsorption of carbazole	81
Chapter 7: New highly active Ni-Mo catalyst for deep HDS of diesel	105
Chapter 8: Summary and evaluation	119
Samenvatting en evaluatie	127
List of Publications	137
Acknowledgement	141
Curriculum Vitae	143

1

Ultra deep hydrodesulfurization for diesel fuel -General Introduction-

Abstract

An overview of ultra deep hydrodesulfurization of diesel fuel is given. The background of this study is based on the legislation for sulfur in transportation fuels, including the demand for ultra low sulfur fuel. Recent studies about the active phase of hydrodesulfurization catalysts (CoMoS, NiMoS) and the catalyst preparation techniques are evaluated. The reaction mechanism of different sulfur compounds and the inhibiting effect of hydrogen sulfide and non-sulfur compounds in the feed are also crucial in this reaction.

1. Introduction

Promoted molybdenum catalysts have been the work-horses in HDS processes since the 1940's. The incorporation of cobalt or nickel to the MoS_2 increased catalyst activity significantly. As the consumption of oil had been increasing significantly since the 1960's, acid rain caused by air pollution of sulfur dioxide gas that was produced during the combustion of the fuel oils, raised the environmental disruption. These catalysts take an active part in the removal of sulphur from fuel oils by a selective hydrogenation process, referred to as Hydrodesulfurization (HDS). Since the late 1980's, these catalysts have been getting increasing attention in the field of HDS for transportation fuels, to reduce emission, such as NO_x , and Particulate Matter (PM). For a sustainable society, the targets are not only reducing NO_x and PM, but also CO_2 emission. To achieve the use of new high fuel efficiency and anti-pollution technology for vehicles, the demand of ultra clean fuel has been urging the oil industries.

In principle, many improvements are conceivable for responding to this situation, on the one hand, chemical engineering solutions, and on the other hand, the development of advanced catalysts. The aim of this work is to contribute to the development of advanced catalysts and also to the optimal use of the catalysts.

2. Legislation for diesel

The demand to improve diesel-exhaust emissions urged stringent legislation for diesel fuel. World-wide fuel charter can be regarded as a representative future trend of legislation for transportation fuels by automotive manufactures all-over the world. Sulfur content is one of the important specifications, and in the Category 4 essentially sulfur free diesel fuel was demanded. Table 1 shows the specifications of diesel fuels [1].

Table 1. Major specifications of diesel fuel in WWFC category 4

Sulfur	/ ppm	max	5-10
Aromatics	/ vol%	max	15.0
Polyaromatics	/ vol%	max	2.0
Density	/ kg/m^3	max	820
Cetane number		min	55.0
Distillating point (T90)	/ $^{\circ}\text{C}$	max	320

Generally speaking, decreasing the content of sulfur in fuel will prevent the sulfur poisoning of deNO_x and combustion catalysts that contain noble metals to reduce NO_x and PM (particulate matter). In Table 2, trends of current and planned limits for emission for the EU are shown for heavy-duty vehicles diesel engines [2].

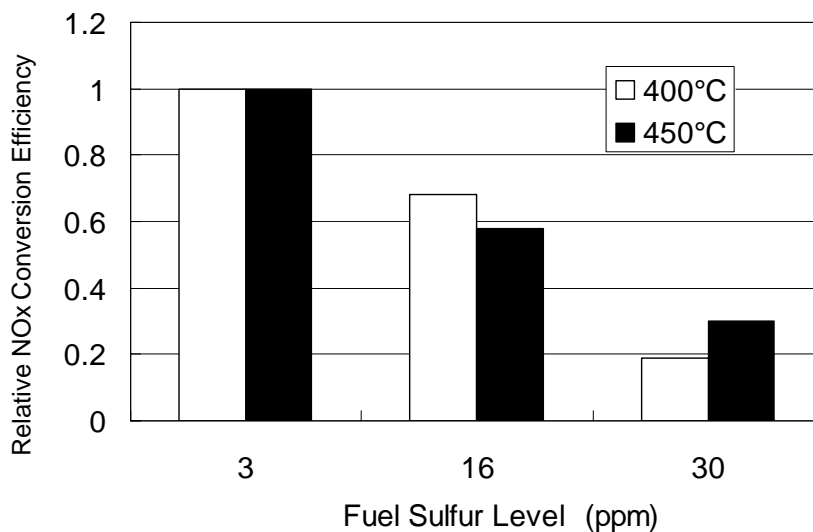
In particular, the main reason for the requirement of sulfur free (below 10ppm) fuels is the sensitivity for sulfur of the NO_x -trap system. To raise engine efficiencies, the control of NO_x emissions is one of the major challenges. The higher oxygen content of the exhaust gases from lean-burn gasoline and diesel engines that have higher fuel efficiencies disrupts the application of conventional three-way catalysts. A new developed system is the NO_x -trap that adsorbs and stores the NO_x as nitrates during oxygen rich operation, and releases them as nitrogen during short, fuel-

rich (reducing) desorption steps. The major active components in modern NO_x-traps are alkaline earths metals, for instance barium oxide as the storage metals of NO_x. The NO_x-trap works only with low sulfur fuels, as SO₂ has been found to form sulfates with the barium oxide. Because the sulfates are more stable at the operation temperature than the nitrates, there is competition for the active sites between NO_x and SO_x, and the sites are deactivated significantly by sulfate [3]. In Fig. 1 the effect of fuel sulfur level on NO_x conversion efficiency of NO_x -trap for diesel emissions is shown [1].

Table 2. Legislative limits for heavy duty diesel engines (truck and bus), g/kWh (smoke in m⁻¹).

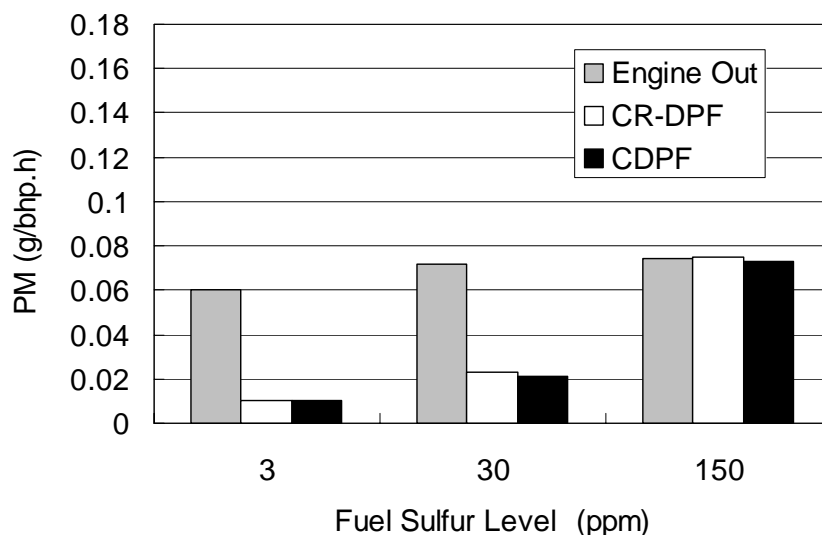
Tier	Date & Category	Test Cycle	CO	HC	NOx	PM	Smoke
Euro 2	1998.10	ECE R-49	4.0	1.1	7.0	0.15	
Euro 3	1998.10, EEVs	ESC/ELR	1.5	0.25	2.0	0.02	0.15
	2000.10	ESC/ELR	2.1	0.66	5.0	0.10	0.8
Euro 4	2005.10	ESC/ELR	1.5	0.46	3.5	0.02	0.5
Euro 5	2008.10	ESC/ELR	1.5	0.46	2.0	0.02	0.5

ECE: old steady-state engine test cycle (Economic Commission of Europe), ESC: stationary cycle (European Stationary Cycle), ELR: transient cycle (European Load Response), EEV: enhanced environmentally friendly vehicles



*Engine tested: 1.9 liter, high speed direct injection, common rail, 81kW

Figure 1. Effect of fuel sulfur level on NO_x conversion efficiency (150 hours aging) [1].



*Engine tested: Caterpillar 3126, 7.2 liter, in line 6 cylinder, 205kW, @ 2200 rpm; g/(bhp.h): grams/ (break horse-power. hour).

Figure 2. Effect of fuel sulfur level on PM emissions [1]. CR-DPF: continuous regenerating diesel particulate filter, CDPF: catalysed diesel particulate filter.

Especially in the case of diesel engine, the reduction of PM is also crucial. The most promising regenerative DPFs are CR-DPF (continuous regenerating diesel particulate filter), and CDPF (catalysed diesel particulate filter). The CR-DPF accomplishes regeneration by continuously generating NO_2 from engine-emitted NO over a diesel oxidation catalyst placed upstream of the CR-DPF. NO_2 is a more effective low-temperature operative oxidizing agent for diesel PM than oxygen. One of the components in PM is sulfate formed after sulfur compounds in the exhaust are oxidized over the CR-DPF. Sulfur oxides also compete for the reaction of NO to NO_2 , making the regeneration of the trap less effective.

The CDPF accomplishes DPF regeneration by using a catalyst coated on the DPF element to combust PM. However, sulfates from oxidized sulfur in the exhaust cover the CDPF and deactivate the catalyst. The effect of fuel sulfur level on PM emissions of CR-DPF and CDPF is shown in Fig. 2 [1].

There could be a reasoning in oil refinery and automotive manufacture that the over all environmental emissions from a vehicle can be included in "well to tank" (from oil well to vehicle fuel tank), in addition to "tank to wheel" (vehicle operation). "Well to tank" includes refinery emissions distribution and drilling or production emissions and accounts for only approximately 15% of the total lifecycle CO_2 emissions. In some cases, refinery changes to produce cleaner fuels could result in higher energy use, but the overall environmental benefits are far beyond these concerns.

Therefore refining technologies also have been able to produce cleaner fuels with less impact on the environment. The overview of legislations for sulfur content in diesel fuel in EU, US (California/CARB), and Japan are summarized in Table 3 [4-6]. Several reviews about the

legislations on ultra deep desulfurization and the changes in refining technology associated herewith have been reported [7-10].

Table 3. Overview of sulfur legislations for diesel fuel, ppm

	Sulfur ppm	Year							
		2001	2002	2003	2004	2005	2006	2007	2008
EU	350					50		←	[10]
Germany	350	<50>		<10>					
US/California	500						15		
Japan	500			(50)	← 50	(10)	←	←	[10]

* determined, [planned], <tax incentive>, (self imposed)

** Arrows denote that it will come earlier.

3. Structure and morphology of supported molybdenum sulfide

3.1. Active phase structure models

Active phase structure of HDS catalyst has been a focus of constant attention. Although they are not fully proven yet and there are still several proposals, the most plausible structure for the active phase in $\text{CoO-MoO}_3/\text{Al}_2\text{O}_3$ is the so-called CoMoS phase, proposed by Topsoe et. al [11]. In their study, $\text{CoO-MoO}_3/\text{Al}_2\text{O}_3$ was presulfided and measured by MES. In addition to Co_9S_8 and Co trapped in spinel sites of alumina, the CoMoS phase was found. They concluded that Co in CoMoS phase has a correlation to thiophene HDS activity. The CoMoS phase is believed to consist of hexagonal layers of Mo atoms between two layers of sulfur atoms and the edge of MoS_2 phase is covered by Co (see Fig 3); this picture is based on the outcome of various characterizations by MES, FT-IR, XPS, and XAFS [12].

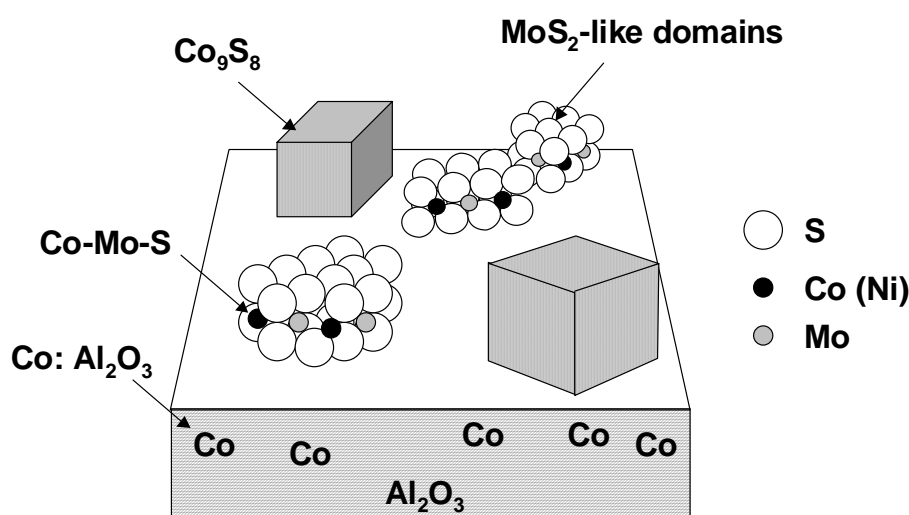


Figure 3. Schematic view of the different phases in a typical alumina supported catalyst (by Topsoe et. al [11]).

Nowadays, the preparation of model catalysts that have a simplified active phase can be a convenient way to characterize the active phase in an industrial catalyst. Okamoto reported that $\text{Co}(\text{CO})_3\text{NO}$ can be adsorbed selectively on the edge site of MoS_2 slabs. The catalyst made by this CVD method contains only CoMoS phase. They also treated the CoMo catalyst prepared by impregnation method by $\text{Co}(\text{CO})_3\text{NO}$ CVD. Then their activity for thiophene HDS increased when the edge site was not saturated by impregnation method [13]. The results supported the conclusion that the Co adsorbed on MoS_2 slab form the active CoMoS phase.

The active site of promoted MoS_2 catalysts is widely discussed. As the Mo layer is sandwiched by sulfur layers, the edge is believed to be the active site of HDS. At the edge of MoS_2 crystal, sulfur atoms can be removed, forming so-called coordinatively unsaturated sites (CUS). In the MoS_2 structure, a Mo-edge and a S-edge can be distinguished, and hydrogen may react with the S-edge, creating sulfur vacancies. On the other hand, hydrogen sulfide may dissociatively adsorb on the Mo-edge. DFT calculations are powerful techniques to investigate the stability of the model structures theoretically. Recently, the location of promoter such as cobalt and nickel has been investigated, to elucidate their promoting effect [14].

Atomic scale structure observations could give us information to understand the HDS catalyst active site. Helveg et al. made a model catalyst by vaporizing Mo in H_2S ; this resulted in a single layer MoS_2 cluster on the Au (111) surface. Then atomic scale structure of MoS_2 cluster was successfully observed by STM [15] and it appears to be a triangular MoS_2 , terminated by Mo edge fully covered with S_2 dimers. Co was also doped during model catalyst preparation, but then MoS_2 slabs showed a hexagonal shape that could be an indication of CoMoS phase [16]. It has been concluded that the equilibrium shape of MoS_2 clusters is sensitive to the different $\text{H}_2\text{S}/\text{H}_2$ pressure, forming triangular species at sulfiding condition ($\text{H}_2\text{S}:\text{H}_2=500$) and hexagonal species at more reducing condition ($\text{H}_2\text{S}:\text{H}_2=0.07$) [17]. Thiophene adsorption in this system was also examined and according to DFT calculations thiophene C-S cleavage can occur [18]. The results supported the suggestion that S-H (hydrogen adsorbed sulfur) groups are involved in the first hydrogenation steps [19]. Although it is a model catalyst under different sulfiding condition, the results strongly suggest that MoS_2 clusters can be transformed, depending on the conditions (H_2S presence) and on the absence or presence of promoters.

3.2. Catalyst preparation conditions and morphology of molybdenum slabs

Candia et al. proposed so-called type I and type II active phases [20]. CoMo catalysts were presulfided at different temperatures. High temperature sulfided form was called type II active phase and low temperature sulfided one is referred to as type I. The results of thiophene HDS showed that type II active phase have higher activity than type I at the same amount of Co atoms in CoMoS phase, as determined by MES. It was suggested that type II active phase has weaker interaction with support than type I. HRTEM measurement showed that type II active phase consist of more stacking MoS_2 slabs than type I. Then they suggested that the different HDS activity of those phases depends on these morphologies.

It was reported that type II active phase can be made using chelating ligands like NTA [21]. These catalysts are just dried after impregnation, skipping calcination. Almost the same results were obtained as Candia et al., viz., compared to type I, type II active phase determined by MES

was twice as active in thiophene HDS. Moreover, type II active phase was studied with several characterization techniques such as EXAFS, MES and XPS, and it was reported that the CoMoS type II phase is present as a multilayer structure and is fully sulfided and not chemically bonded on alumina [22]. Moreover, various chelating agents have been studied and it was suggested that the agents which complex with promoters (Co, Ni) were effective and the role of the chelating agent is retarding sulfiding of promoters until Mo has been sulfided, resulting in the effective coordination of promoters at Mo edges [23, 24].

Besides chelating agents addition, phosphorus addition has been studied to increase HDS activity. Several effects of phosphorous addition have been reported. When phosphate is added to the impregnation solution, it reacts with the molybdenum precursor, forming a variety of phosphomolybdate anions, such as Keggin type ($\text{PMo}_{12}\text{O}_{40}^{3-}$, $\text{PMo}_{12}\text{O}_{40}^{7-}$), Dawson type ($\text{P}_2\text{Mo}_{18}\text{O}_{62}^{6-}$), and diphosphopentamolybdate ($\text{P}_2\text{Mo}_5\text{O}_{23}^{6-}$) anions [25]. Co or Ni can be solved as an aqueous complex or become complexed by phosphomolybdate. The improvement of the stability of the impregnation solution and the acidity of the catalyst aiming to increase hydrogenation activity was reported. Moreover, the effect to increase the stacking of MoS_2 slabs has been also reported [26-28]. Therefore, it was reported that phosphorus addition in NiMo leads to the partial formation of type II phase [29].

Recently, other water insoluble organic compounds such as glycols have been added in the metal impregnation solution, although it is unlikely that they have strong chelating effect on cobalt, nickel or molybdenum [30, 31]. The authors suggested that polyethylene glycol somehow blocks the aggregation of cobalt and molybdenum until the active metals interact with the alumina support during the calcination step, resulting in the improvement of HDS activity.

Moreover, another type of catalyst without calcination that contains phosphate and glycol has been reported [32-35]. Based on Laser Raman spectroscopy, ^{31}P ^{13}C NMR, and Mo K-edge EXAFS, it was concluded that it does not interact with metal precursors in impregnation solution. The main role of the glycol was suggested to be as follows: it reacts with the basic OH groups on alumina, and hinders the interaction between metal precursors and the alumina support, resulting in a close proximity of promoter and molybdenum. They suggested that the weakening of the interaction of the molybdate with the alumina surface increases the stacking of MoS_2 and thus the formation of the more active type II structure.

Recently, similar type of catalyst without calcination, prepared with phosphoric acid and citric acid monohydrate, has been reported. From TEM measurement, it was observed that MoS_2 was present as multilayer species that would be so-called CoMoS type II structure [36].

Summarizing the points of preparation of type II catalysts, it should be noted that the catalyst is prepared without calcination after active metal impregnation. The other point is the addition of organic compounds that would weaken the interaction between active metals and support. Moreover, phosphorus addition could be effective to enhance the formation of type II phase.

As described above, generally alumina is a typical support for HDS catalysts. The main reasons are that it has sufficiently high surface area and active metal molybdenum can be supported at high dispersion state. Recently titania has been focused upon as an alternative support or as an additive for alumina. It has been known that unpromoted Mo catalysts on titania show higher HDS

activity than that on alumina [37]. However, titania tends to have lower surface area than alumina and is less cost effective. For overcoming the first weak point, pH swing method was applied for the precipitation of titania gel, resulting in titania with a comparably high surface area as alumina [38]. The CoMo/titania catalysts showed high HDS activity for dibenzothiophene. In other ways, CVD method has been utilized to coat the alumina support with titania [39, 40]. The surface area of alumina did not decrease after CVD up to 10 wt% titania loadings. The catalyst showed higher HDS activity, especially for 4,6-dimethyldibenzothiophene, i.e. the most refractory sulfur compound in diesel. This was explained by the hypothesis that Mo has weaker interaction with titania than with alumina, forming fully sulfided phase with high activity.

One of the candidates for the highly active catalyst for ultra deep hydrodesulfurization can be a NiW catalyst. Although W is relatively difficult to be sulfided, resulting in insufficient activity for HDS [41], it has been reported that the catalyst has high hydrogenation activity as it has been utilized as lubricant oil hydrotreating catalysts. Moreover, it was suggested that W on titania can be sulfided easier than that on alumina [42]. Therefore, catalysts including W and titania may be very interesting to investigate for ultra deep hydrodesulfurization of diesel [43].

3.3. The method of presulfiding

The presulfiding method has been also important and studied to get higher activity. One of the aspects is the difference between gas and liquid presulfiding. It is not surprising that liquid phase presulfiding can reduce the sintering of the active phase by the exothermicity during the sulfiding. In gas presulfiding, a low heating rate procedure can be effective, as it was reported that mild presulfiding is necessary to get higher activity for type II catalyst [22].

Recently, Eijsbouts et al. reported that the morphology of type II catalyst was affected by gas or liquid presulfiding [44]. Whereas MoS₂ stacking is apparently increased by gas presulfiding, presulfiding in the liquid phase seems to prevent it. Dugulan, Craje, and Kearley tested the effect of pressure during presulfiding by MES. It was reported that Type II active phase could be formed also after calcinations at high temperature (above 400 °C), following presulfiding under high pressure and high temperature [45]. The pressure of presulfiding might be also an important aspect. It has been reported that the catalyst sulfided above 1.1 MPa can form CoMoS (or NiMoS) selectively [46, 47].

The other aspect is the effect of sulfiding agents such as molecules containing –SH, –S–S, and C–S–C. It was reported that butanethiol, H₂S, DMDS, CS₂, and thiophene were tested as presulfiding agents [48]. Thiophene did not work effectively and CS₂ was not effective due to coke formation. Sulfur atom in –SH groups can be easily consumed during presulfiding and –S–S– can also be beneficial as the decomposition of –S–S– with hydrogen forms –SH groups. Polysulfides such as CS-40 were suggested as an effective presulfiding agents for ultra deep HDS of diesel [49].

4. Reaction mechanism of HDS of relevant sulfur compounds

Typical boiling point range of diesel is approximately from 180 to 360 °C. Consequently, main sulfur compounds in diesel are thiophenic compounds such as benzo- and dibenzothiophenes [50]. Historically, thiophene often has been a model compound in HDS research, because of its convenience. However, thiophene is exceptionally reactive and, as a

consequence, its use as model compound is not straightforward. Dibenzothiophene and its derivatives, especially β -substituted DBTs, are more refractory and therefore more appropriate model compounds for the evaluation of the HDS activity in deep diesel desulfurization. It is well known that cyclic sulfur compounds react through two pathways, so-called direct desulfurization (DDS) and hydrogenation (HG), and that the ratio of DDS to HG depends on the reactant molecules, the catalysts properties and the reaction conditions [51-53]. The reaction pathways are shown in Fig.4.

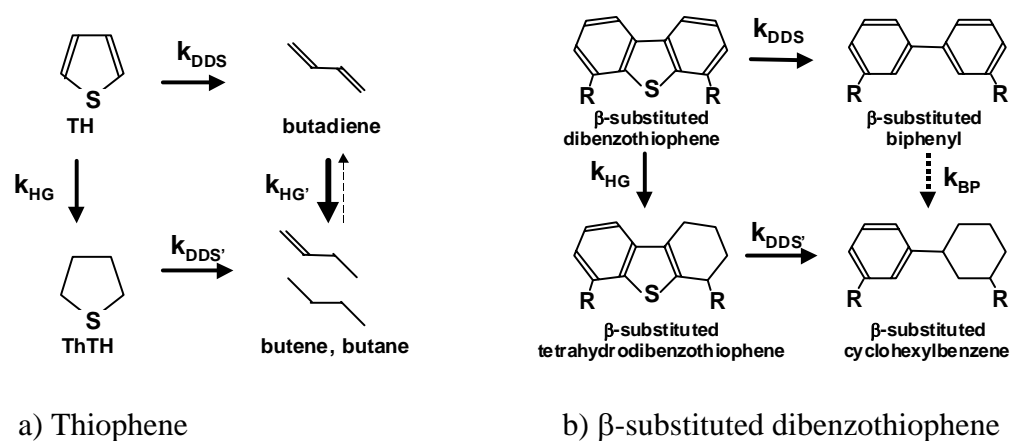


Figure 4. Reaction pathways of thiophene-ring type sulfur compounds.

4.1. Thiophene HDS reaction

In thiophene HDS, it is difficult to discriminate between those two pathways from product yields, as the butadiene that might be produced via DDS pathway is rapidly hydrogenated to butene and butane, the products of hydrogenation. Most researchers now conclude that thiophene reacts via both DDS and HG pathways. Usually thiophene HDS has been tested at atmospheric pressure because of its convenience. In few literatures [54, 55], thiophene HDS at high hydrogen pressure has been reported. The authors suggested that at atmospheric pressure, the total HDS is limited by hydrogenation of thiophene ring and at high pressure hydrogenolysis of C-S bond is the case. It is not fully proven, but it can be supported that thiophene also reacts mainly via the HG pathway. First it is known that the polarized C-S bond is shorter in thiophene (1.71 Å) than in dibenzothiophene (1.74 Å). Therefore, essentially the C-S bond cleavage of thiophene is more refractory than that of DBT. In literature support for this can be found [56]. Recently, a mechanism of HDS of thiophene via HG pathway has been proposed in a theoretical study, using molecular simulations [57]. According to the literature, the most stable coordination geometry of thiophene is flat adsorption configuration (η^5 -bondings), and after the ring is saturated, hydrogenolysis occurs. This confirms that HG pathway could be the main pathway.

As a representative reaction for DDS in the gas phase, HDS of tetrahydrothiophene could be applicable, as it has been proposed to be one of the most important intermediates for HDS of thiophene [58, 59]. In order to assess the potential of using tetrahydrothiophene as a model compound, the ranking of thiophene and tetrahydrothiophene will be informative.

4.2 (β -substituted) Dibenzothiophene HDS reaction

In HDS of DBTs, DDS and HG pathways can be easily distinguished as the consecutive hydrogenation of (substituted) biphenyls is very slow [60, 61], especially under H_2S rich conditions [62, 63]. As shown in Fig. 4b, (substituted) biphenyl and (substituted) cyclohexylbiphenyl were observed showing the reaction pathways of DDS and HG, respectively. Moreover, (substituted) tetrahydro-DBT was observed, supporting the reaction scheme.

It has been reported that the most refractory sulfur compound in diesel is 4,6-dimethyldibenzothiophene (4,6-DMDBT), and it is 3 to 6 times more refractory than DBT. This can be explained by the strong steric hindrance of the two methyl groups in the coordination of sulfur on the active sites, needed for DDS [8]. In contrast, DDS of the hydrogenated intermediates occurs relatively fast. The opposite effects of steric hindrance and the electron density on sulfur atom in the molecule could explain that the difference between DBT and 4,6-DMDBT is small after hydrogenation. Compared with DBT and 4,6-DMDBT, the steric restrictions of the hydrogenated intermediates are reduced. By the two methyl groups the electron density on sulfur atom is increased, which strengthens the coordination of the molecule to the active site [64].

DFT calculations are powerful techniques to support these reaction mechanisms theoretically [65]. It has been suggested that $\eta_1(S)$ adsorption on the sulfur edge of the active phase is at the origin of the DDS of the molecules whereas benzene ring adsorption on the molybdenum edge is at the origin of the HG pathway. The authors also suggested that the presence of stacking defects on the molybdenum sulfides would allow the adsorption and the activation of 4,6-DMDBT, although a combination of aromatic and steric effects strongly inhibits its adsorption.

The experimental adsorption behavior at 50 °C of 1-methylnaphthalene (1-MN), DBT, 4-MDBT, and 4,6-DMDBT were also reported on $CoMo/Al_2O_3$ after presulfiding followed by reduction [66]. The adsorptive affinity increased in the order of $1-MN < 4,6-DMDBT < 4-MDBT < DBT$. It was concluded that the interaction between the S atom and the adsorption sites plays an important role and that methyl substituents adjacent to the sulfur atom inhibit the interaction between the S atom and the adsorption sites.

5. Inhibiting effect for HDS reaction

5.1. Effect of hydrogen sulfide

It is well known that H_2S inhibits the HDS reaction significantly for (substituted) DBT, especially with respect to the DDS pathway [63],[67]. Furthermore, it was reported that the adsorption constant of H_2S is much higher than that of thiophene at atmospheric pressure [68], while the heat of adsorption of H_2S is comparable or slightly higher than that of DBTs [69].

In hydrotreating for diesel, the inhibiting effect of H_2S on sulfur, nitrogen, and aromatics content is lower at high temperature, in agreement with the conclusion that H_2S adsorbs on the active site competitively [70].

In recent reports, the difference of susceptibility to H_2S of $CoMo$ and $NiMo$ for 4,6-DMDBT HDS reactions has been highlighted [71, 72]. Some authors suggested that $CoMo$ shows less susceptibility to H_2S . However, others suggested an opposite trend [63]. It was

suggested that the DDS pathway is more inhibited by H₂S than the HG pathway, and that would suggest that the CoMo catalyst could suffer more from inhibition by H₂S [8].

5.2. Effect of Nitrogen and aromatics compounds

It is reported by many authors that nitrogen compounds inhibit HDS reaction significantly. However, it is not so clear which nitrogen compound inhibits the most for ultra deep desulfurisation reaction. Recently results have been published concerning both model reactions using nitrogen compounds, and real feedstocks.

In the feed of straight run light gas oil, typical nitrogen content is from 100-500 ppm [50]. Three types of nitrogen compounds are mainly present: non-heterocycles, heterocycles of 6 membered ring (6MR), and heterocycles of 5 membered ring (5MR). We do not have to consider non-heterocycles, anilines and aliphatic amines, as they undergo HDN quickly. Among the heterocycles nitrogen compounds, 6MR pyridinic species are basic and 5MR pyrrole species are non-basic or even acidic [73]. The ratio of the content of basic to non- basic nitrogen compounds is 0.2 – 0.3.

Generally, the inhibiting effect of basic nitrogen compounds is the strongest. Koltai et al. compared the reaction rate of 4,6-DMDBT in the presence of acridine or carbazole on NiMo catalysts, using an autoclave [74]. They found that the inhibiting effect on initial HDS activity by acridine is higher than by carbazole, due to its stronger adsorption.

However non-basic nitrogen compounds such as carbazole are also known to be comparable strong inhibitors for the course of deep HDS reactions. It is noteworthy that non-basic type pyrolic type nitrogen transforms to the strong basic compound by hydrogenation. Little work has been published about the difference of susceptibility by nitrogen on catalysts properties (CoMo, NiMo, Mo, W, or additives). That will be crucial to choose optimal catalyst or establish the best catalysts combination, as nitrogen inhibition is significant, especially for ultra deep desulfurization range.

It was generally accepted that the aromatic compounds inhibit HDS reaction substantially [62, 75, 76]. In real feedstocks, LCO (light cyclic oil from cracking units) is generally regarded to be refractory, as it contains extremely high amount of aromatic compounds, especially for ultra deep desulfurization range. Aromatic rings can be nucleophilic, as π electron is polarized to be negatively charged by the access of electron defect site of catalysts. However, inhibiting effect of aromatics is an order of magnitude smaller than the effect of nitrogen compounds. It was reported that 10 wt% of naphthalene addition severely retarded the HDS of 4,6-DMDBT [75]. Moreover, an aromatic hydrocarbon of larger ring number has a stronger retarding effect on the HDS rate. The addition of phenanthrene decreased the HDS rate of DBTs in the order DBT > 4-MDBT > 4,6-DMDBT, while 1-methylnaphthalene did not affect the HDS rate. The effect of phenanthrene on the HDS rate appeared to be related to the differences in the adsorption ability of DBTs [76].

6. Outline of the thesis

6.1. Background

Promoted MoS₂ catalyst has been used for long time, and actually it has been working very well in industrial HDS units. Despite extensive research efforts to elucidate the active site of HDS and reaction mechanisms, it is still under debate. The legislation of sulfur content in transportation fuels has been more and more strict due to the demand to reduce exhaust emissions. “Sulfur-free ”(less than 10 ppm) fuels have started to be produced and will become the standard all over the world in the near future. So, the conversion level should be more than 99.9% for diesel HDS. This changes the fuel processing technology to a chemical field. It means that although diesel consists of a huge variety of compounds, the final purification level need to be treated is in molecular level. In this situation, we need to understand the characteristics of catalysts, such as NiMo, CoMo, and NiW under realistic conditions. Not only the intrinsic HDS activity, but also the inhibiting effect by competitive adsorption needs to be taken into account. The aim of this work is to contribute to a better understanding for ultra deep diesel HDS and utilization of catalysts in a cost effective way.

6.2. Layout of the thesis

In Chapter 2, preliminary tests to establish experimental methods for measuring HDS activities will be discussed. Thiophene in a continuous microreactor (gas phase), (4,6-dimethyl) dibenzothiophene in a batch reactor (liquid phase) and real diesel in a trickle flow reactor will be tested. Several aspects for ranking of activities are examined and in the following chapters, the activity testing methods described in this chapter are adopted.

In Chapter 3, so-called type I and type II NiMo catalysts will be characterized by various techniques such as XRD, TPR, TPS, Laser Raman spectroscopy, and SO₂ adsorption. The active metals in the oxidic state and sulfidic state are investigated to evaluate the active phase interaction with the support. The dispersion and morphology of type I and type II active phase with the metal loading below and above monolayer surface coverage will be discussed.

In Chapter 4, the ranking of catalytic activities of several NiMo catalysts will be performed using various model compounds: thiophene (TH), tetrahydrothiophene (ThTH), dibenzothiophene (DBT) and 4,6-dimethyldibenzothiophene (4,6-DMDBT). So-called type I and type II NiMo catalysts with Mo loading from below to above monolayer coverage will be tested and the reaction pathways of HDS reaction such as hydrogenation (HG) and direct desulfurization pathway (DDS) will be discussed. The differences of susceptibility for NiMo and CoMo catalysts to H₂S will be included. Finally, the relation of structures and activities will be generalized.

In Chapter 5, the influence of the feed properties of diesel fuel will be discussed. The important parameters of feed properties for ultra deep HDS will be chosen using a datamining method. Especially, the nitrogen compound inhibition effect on HDS will be evaluated in realistic bench scale testing.

In Chapter 6, simultaneous hydrodesulfurization of dibenzothiophene (DBT) and hydrodenitrogenation (HDN) of carbazole was carried out in order to evaluate mutual inhibiting effects on NiMo catalysts in comparison to a CoMo catalyst. The inhibition for the direct

desulfurization (DDS) and the hydrogenation (HG) pathways in HDS of DBT will be discussed. Moreover, the inhibition of the intermediate of HDN reaction will be evaluated. The susceptibility to inhibition by nitrogen compounds will be discussed on CoMo or NiMo and type I or type II catalysts. An inhibition mechanism will be suggested with characteristics of the reaction pathways of catalysts.

In Chapter 7, W addition effects on NiMo catalyst will be tested as new highly active catalysts for ultra deep HDS of diesel. Moreover, titanium oxide addition on support for improving the interaction between metals and support will be evaluated using model HDS reaction such as (4,6-dimethyl) dibenzothiophene in liquid phase. Finally, experiments with real diesel in the trickle flow reactor will be carried out to confirm the results obtained, for practical applications.

In Chapter 8, a better understanding for ultra deep diesel HDS and utilization of catalysts in cost effective way will be proposed, summarizing all chapters. Conceivable process schemes and combinations of catalysts will be discussed.

References

- [1] <http://autoalliance.org/archives>, World-wide fuel charter, December 2002.
- [2] <http://www.dieselnets.com/standards>, accessed March 2004. 36.
- [3] H.Mahzoul, P.Gilot, J.F.Brilhac, and B.R.Stanmore, *Topics in Catalysis*, **16** (2001) 293.
- [4] Kiuru, L., Klavers K., World refining January/February 2004, 36.
- [5] <http://www.arb.ca.gov/regact/ulsd2003>, accessed March 2004.
- [6] <http://www.env.go.jp/council/07air/y071-19a.html>, accessed March 2004.
- [7] I.V.Babich and J.A.Moulijn, *Fuel*, **82** (2003) 607.
- [8] K.G.Knudsen, B.H.Cooper, and H.Topsoe, *Applied Catalysis A-General*, **189** (1999) 205.
- [9] C.Song, *Catalysis Today*, **86** (2003) 211.
- [10] Y.Yoshimura, M.Toba, H.Farag, and K.Sakanishi, *Catalysis Surveys from Asia*, **8** (2004) 47.
- [11] H.Topsoe, R.Candia, N.-Y.Topsoe, and B.S.Clausen, *Bull.Soc.Chim.Belg.*, **93** (1984) 783.
- [12] H.Topsoe and B.S.Clausen, *Catal.Rev.-Sci.Eng.*, **26** (1984) 395.
- [13] Y.Okamoto, K.Ochiai, M.Kawano, and T.Kubota, *Journal of Catalysis*, **222** (2004) 143.
- [14] M.Sun, J.Adjaye, and A.E.Nelson, *Applied Catalysis A: General*, **263** (2004) 131.
- [15] S.Helveg, J.V.Lauritsen, E.Laegsgaard, I.Stensgaard, J.K.Norskov, B.S.Clausen, H.Topsoe, and F.Besenbacher, *Physical Review Letters*, **84** (2000) 951.
- [16] J.V.Lauritsen, S.Helveg, E.Laegsgaard, I.Stensgaard, B.S.Clausen, H.Topsoe, and E.Besenbacher, *Journal of Catalysis*, **197** (2001) 1.
- [17] J.V.Lauritsen, M.V.Bollinger, E.Laegsgaard, K.W.Jacobsen, J.K.Norskov, B.S.Clausen, H.Topsoe, and F.Besenbacher, *Journal of Catalysis*, **221** (2004) 510.
- [18] J.V.Lauritsen, M.Nyberg, R.T.Vang, M.V.Bollinger, B.S.Clausen, H.Topsoe, K.W.Jacobsen, E.Laegsgaard, J.K.Norskov, and F.Besenbacher, *Nanotechnology*, **14** (2003) 385.
- [19] J.V.Lauritsen, M.Nyberg, J.K.Norskov, B.S.Clausen, H.Topsoe, E.Laegsgaard, and F.Besenbacher, *Journal of Catalysis*, **224** (2004) 94.
- [20] R.Candia, O.Sørensen, J.Villadsen, N.-Y.Topsoe, B.S.Clausen, and H.Topsoe, *Bull.Soc.Chim.Belg.*, **93** (1984) 763.
- [21] J.A.R.Van Veen, E.Gerkema, A.M.Van der Kraan, and A.Knoester, *J.Chem.Soc., Chem.Comm.* 1987) 1684.
- [22] S.M.A.M.Bouwens, F.B.M.Vanzon, M.P.Vandijk, A.M.Van der Kraan, V.H.J.Debeer, J.A.R.Vanveen, and D.C.Koningsberger, *Journal of Catalysis*, **146** (1994) 375.
- [23] T.Shimizu, K.Hiroshima, T.Honma, T.Mochizuki, and M.Yamada, *Catal.Today*, **45** (1998) 271.
- [24] Y.Ohta, T.Shimizu, T.Honma, and M.Yamada, *Stud.Surf.Sci.Catal.*, **127** (1999) 161.
- [25] A.Griboval, P.Blanchard, E.Payen, M.Fournier, and J.L.Dubois, *Catalysis Today*, **45** (1998) 277.
- [26] J.L.G.Fierro, A.L.Agudo, N.Esquivel, and R.L.Cordero, *Appl.Catal.*, **48** (1989) 353.
- [27] R.C.Ryan, R.A.Kemp, J.A.Smegal, D.R.Denley, and G.E.Spinnler, *Stud.Surf.Sci.Catal.*, **50** (1989) 21.
- [28] J.Ramirez, V.M.Castano, C.Leclercq, and A.L.Agudo, *Applied Catalysis A-General*, **83** (1992) 251.

- [29] J.A.R. Van Veen, H.A. Colijn, P.A.J.M. Hendriks, and A.J. Van Welsenens, *Fuel Proc. Tech.*, **35** (1993) 137.
- [30] R. Iwamoto, N. Kagami, and A. Iino, *Journal of the Japan Petroleum Institute*, **48** (2005) 237.
- [31] R. Iwamoto, N. Kagami, Y. Sakoda, and A. Iino, *Journal of the Japan Petroleum Institute*, **48** (2005) 351.
- [32] D. Nicosia and R. Prins, *Abstracts of Papers of EuropaCat-VI*, **A1.064** (2003)
- [33] D. Nicosia and R. Prins, *Journal of Catalysis*, **234** (2005) 414.
- [34] D. Nicosia and R. Prins, *Journal of Catalysis*, **231** (2005) 259.
- [35] D. Nicosia and R. Prins, *Journal of Catalysis*, **229** (2005) 424.
- [36] T. Fujikawa, H. Kimura, K. Kiriya, and K. Hagiwara, *Catalysis Today*, **111** (2006) 188.
- [37] Y. Okamoto, A. Maezawa, and T. Imanaka, *J. Catal.*, **120** (1989) 29.
- [38] S. Dzwigaj, C. Louis, A. Breyse, M. Cattenot, V. Belliere, C. Geantet, M. Vrinat, P. Blanchard, E. Payen, S. Inoue, H. Kudo, and Y. Yoshimura, *Applied Catalysis B-Environmental*, **41** (2003) 181.
- [39] K. Segawa, K. Takahashi, and S. Satoh, *Catalysis Today*, **63** (2000) 123.
- [40] Y. Saih and K. Segawa, *Catalysis Surveys from Asia*, **7** (2003) 235.
- [41] H.R. Reinhoudt, A.D. van Langeveld, P.J. Kooyman, R.M. Stockman, R. Prins, H.W. Zandbergen, and J.A. Moulijn, *Journal of Catalysis*, **179** (1998) 443.
- [42] M.J. Vissenberg, Y. van der Meer, E.J.M. Hensen, V.H.J. de Beer, A.M. van der Kraan, R.A. van Santen, and J.A.R. van Veen, *J. Catal.*, **198** (2001) 151.
- [43] J. Ramirez and A. Gutierrez-Alejandre, *Catal. Today*, **43** (1998) 123.
- [44] S. Eijssbouts, L.C.A. van den Oetelaar, and R.R. van Puijenbroek, *Journal of Catalysis*, **229** (2005) 352.
- [45] A.I. Dugulan, M.W.J. Craje, and G.J. Kearley, *Journal of Catalysis*, **222** (2004) 281.
- [46] N. Koizumi, M. Yamazaki, S. Hatanaka, and M. Yamada, *Catal. Today*, **39** (1997) 33.
- [47] M. Yamada, N. Koizumi, and M. Yamazaki, *Catal. Today*, **50** (1999) 3.
- [48] R. Prada Silvy, F. Delannay, F. Delannay, and B. Delmon, *Applied Catalysis*, **46** (1989) 113.
- [49] W. Qian, S. Yamada, A. Ishihara, M. Ichinoseki, and T. Kabe, *Sekiyu Gakkaishi-Journal of the Japan Petroleum Institute*, **44** (2001) 225.
- [50] H. Topsøe, B.S. Clausen, F.E. Massoth, J.R. Anderson, and D. Bougeard, *Catalysis Science and Technology*, **Vol. 11** (1996).
- [51] R. Shafi and G.J. Hutchings, *Catalysis Today*, **59** (2000) 423.
- [52] M.J. Girgis and B.C. Gates, *Ind. Eng. Chem. Res.*, **30** (1991) 2021.
- [53] M. Vrinat, *Appl. Catal.*, **6** (1983) 137.
- [54] J. Leglise, L. Finot, J.N.M. van Gestel, and J.C. Duchet, *Stud. Surf. Sci. Catal.*, **127** (1999) 51.
- [55] J. Leglise, J.N.M. van Gestel, L. Finot, J.C. Duchet, and J.L. Dubois, *Catal. Today*, **45** (1998) 347.
- [56] H. Topsøe, B.S. Clausen, N.Y. Topsøe, J.K. Nørskov, C.V. Ovesen, and C.J.H. Jacobsen, *Bull. Soc. Chim. Belg.*, **104** (1995) 283.
- [57] X.L. Ma and H.H. Schobert, *Journal of Molecular Catalysis A-Chemical*, **160** (2000) 409.
- [58] J. Kraus and M. Zdrzil, *Reaction Kinetics and Catalysis Letters*, **6** (1977) 475.
- [59] E.J.M. Hensen, M.J. Vissenberg, V.H.J. De Beer, J.A.R. Van Veen, and R.A. Van Santen, *J. Catal.*, **163** (1996) 429.
- [60] P. Michaud, J.L. Lemberon, and G. Perot, *Applied Catalysis A: General*, **169** (1998) 343.

- [61] C.Aubert, R.Durand, P.Geneste, and C.Moreau, *Journal of Catalysis*, **97** (1986) 169.
- [62] D.D.Whitehurst, H.Farag, T.Nagamatsu, K.Sakanishi, and I.Mochida, *Catalysis Today*, **45** (1998) 299.
- [63] V.Lamure-Meille, E.Schulz, M.Lemaire, and M.Vrinat, *Applied Catalysis A: General*, **131** (1995) 143.
- [64] D.D.Whitehurst, T.Isoda, and I.Mochida, *Advances in Catalysis*, **42** (1998) 345.
- [65] S.Cristol, J.F.Paul, E.Payen, D.Bougeard, F.Hutschka, and S.Clemendot, *Journal of Catalysis*, **224** (2004) 138.
- [66] X.Ma, L.Sun, and C.Song, *Prepr.Pap.-Am.Chem.Soc.Div.Fuel.Chem.*, **42** (2003) 522.
- [67] I.Isoda, X.Ma, and I.Mochida, *Sekiyu Gakkaishi*, **37** (1994) 375.
- [68] A.Borgna, E.J.M.Hensen, J.A.R.van Veen, and J.W.Niemantsverdriet, *Journal of Catalysis*, **221** (2004) 541.
- [69] T.Kabe, Y.Aoyama, D.H.Wang, A.Ishihara, W.H.Qian, M.Hosoya, and Q.Zhang, *Appl.Catal.A: Gen.*, **209** (2001) 237.
- [70] J.Ancheyta-Juarez, E.Aguilar-Rodriguez, D.Salazar-Sotelo, G.Marroquin-Sanchez, G.Quiroz-Sosa, and M.Leiva-Nuncio, *Applied Catalysis A-General*, **183** (1999) 265.
- [71] M.Egorova and R.Prins, *Journal of Catalysis*, **225** (2004) 417.
- [72] E.Lecrenay, K.Sakanishi, and I.Mochida, *Catalysis Today*, **39** (1997) 13.
- [73] T.C.Ho, *Catal.Rev.-Sci.Eng.*, **30** (1988) 117.
- [74] T.Koltai, M.Macaud, A.Guevara, E.Schulz, M.Lemaire, R.Bacaud, and M.Vrinat, *Applied Catalysis A-General*, **231** (2002) 253.
- [75] T.Isoda, S.Nagao, X.L.Ma, Y.Korai, and I.Mochida, *Applied Catalysis A-General*, **150** (1997) 1.
- [76] T.Kabe, K.Akamatsu, A.Ishihara, S.Otsuki, M.Godo, Q.Zhang, and W.H.Qian, *Industrial & Engineering Chemistry Research*, **36** (1997) 5146.

2

Testing of HDS catalysts

Abstract

In this chapter, preliminary tests to establish experimental methods for measuring HDS activities were carried out. Two model HDS reactions were chosen, viz the HDS of thiophene and of 4,6-dimethyl-dibenzothiophene. Thiophene HDS was tested in a micro flow reactor at atmospheric pressure while 4,6-dimethyl-dibenzothiophene HDS was carried out in a high-pressure batch type reactor. Also diesel fuel was used as reactant in a high-pressure micro flow reactor. Several aspects for ranking of activities were examined and in following chapters, the activity testing methods described in this chapter are adopted. Especially for high-pressure micro flow reactor studies, dilution with silicon carbide (SiC) is essential to provide reliable data for deep desulfurization for diesel fuel.

1. Introduction

To evaluate HDS activity, several testing methods are applied, depending on the purpose and the stages for R&D. The most common one is the thiophene HDS, because of its convenience. However, the reaction mixture is in the gas phase and mostly at atmospheric pressure, totally different from the conditions for the HDS of diesel fuel. A more realistic model compound is dibenzothiophene (DBT), tested in the liquid phase and at high pressure. Although commercial units consist of fixed bed reactors, batch type reactors are also used, especially for kinetic studies.

In this chapter, three kinds of testing methods will be introduced, HDS of thiophene in a micro flow reactor at atmospheric pressure, HDS of 4,6-dimethyldibenzothiophene (4,6-DMDBT) using a high-pressure autoclave, and HDS of diesel fuel in a high-pressure micro flow reactor.

In preliminary work, several aspects that could be important in the activity measurements for each testing procedure have been studied. For thiophene HDS, the effect of mild presulfiding temperature programmed patterns was investigated to see if they provide different effect on the type I and type II catalysts. Moreover, the H₂S partial pressure was varied, in order to establish a potential relation with the ranking of activity for type I and type II catalysts.

For HDS of 4,6-DMDBT in the liquid phase, several presulfiding agents have been investigated to see if DMDS (dimethyldisulfide) works properly.

Moreover, for HDS of diesel fuel in deep HDS range, the procedure for the high-pressure microflow reactor needs to be investigated. There are several conceivable aspects important in the evaluation of the activity in deep HDS range. One of them is the so-called dilution technique in which small inert particles, e.g. SiC, are added. Moreover, the particle size of catalyst could be important, and catalysts were crushed, sieved and tested. It has been reported that testing of crushed catalyst is acceptable for fundamental studies in which intraparticle diffusion limitation in general have to be avoided [1]. Our experimental conditions were checked from this point of view.

2. Experimental

2.1. Preparation of NiMo type I and type II catalysts

NiO-MoO₃/Al₂O₃ catalysts were prepared via liquid phase pore volume impregnation. High purity γ -Al₂O₃ samples in the form of 1.5 mm extrudates (Surface area by BET: 200 m²/g, Pore volume by Hg intrusion method: 0.8 cm³/g) were impregnated using aqueous solutions containing the required amount of Ni and Mo, according to the literature [2]. The least amount of phosphoric acid was added to dissolve nickel carbonate and molybdenum trioxide stably, stirring at 80 °C for 3 hours and in consequence, the molar ratio of P to Mo was 1/7.

In the case of type I, after the supports had been impregnated by the metal solution, they were dried at 120 °C for 16 hours and calcinated at 500 °C for 4 hours. While in type II, triethylene glycol was added into the metal solution with a ratio of 6 wt% per weight of support, and only the drying step was applied. For high metal loading catalyst preparation, catalysts were impregnated twice (second impregnation was carried out after a drying step following first

impregnation), as the stability of the metal solution became worse at a higher metal concentration.

The composition of catalyst was measured by INAA (Instrumental Neutron Activation Analysis). Specific surface area and pore volume of alumina support were measured by the nitrogen adsorption method (BET). Two different metal loading catalysts were prepared; high and low loading with 5, 10 Mo atom per nm², respectively. All catalysts were prepared to have the same molar ratio of Ni to Mo. The results of elemental analysis are shown in Table 1.

The nomenclature of type I / type II in this work is based on the catalyst preparation method described above. The MoO₃ loading of high loading catalysts was above the monolayer coverage, as it was reported as approximately 4.6 atoms per nm² [3, 4]. The structures of high metal loading catalysts will be discussed in chapter 3 and chapter 4.

Table 1. Composition of the NiMo and CoMo catalysts.

	Co/Mo, or Ni/Mo molar ratio	Mo loading (atom / nm ²)
NiMo type I low loading	0.34	5.1
NiMo type II low loading	0.34	5.2
NiMo type I high loading	0.35	10.3
NiMo type II high loading	0.35	10.5

2.2. Thiophene HDS activity measurement

The activity for gas-phase thiophene (TH) HDS was tested in a micro flow reactor at atmospheric pressure. The schematic diagram of the reactor set-up is shown in Fig. 1. The reproducibility of the test has been established previously [5]. The catalyst particles were crushed and sieved (75~125 μm). The amount of catalyst particles were 200 mg, and were diluted with 320 mg of SiC particles (120 μm). The sample was packed in a glass reactor tube between glass wool plugs. As a presulfiding treatment, the catalyst was exposed to the gas mixture, containing H₂S, H₂ and Ar (5, 50, and 45 vol.%) at a total flow rate of 60 ml/min.

As it was reported that for type II catalyst, mild presulfiding leads to higher activity [6], two kinds of the temperature programmed sulfiding procedures were applied; for the standard method: 30 min at room temperature, increased of 5 K /min to 400 °C, followed by isothermal stage at 400 °C for 2 h; for the mild method: 30 min at room temperature, increased of 2 K /min to 250 °C, followed by an isothermal stage at 250 °C for 1 h, again increased 2 K/min to 370 °C, followed by an isothermal stage at 370 °C for 1 h. After presulfiding, the temperature was set at 350 °C and purged by He for 5 min, then reaction was started to expose the catalyst into a flow of the reaction mixture (5.0 vol.% TH, balance H₂) at a flow rate of 100 ml/min. To test the influence of H₂S for the reaction, a reaction mixture of 200 ml/min, containing 5.0 vol.% TH, balance H₂/Ar (1:1), and a reaction mixture of 200 ml/min, containing 5.0 vol.% TH, balance H₂/Ar containing 10 % of H₂S mixture (1:1) were fed. The reaction products were taken on-line and analysed using a FID gas chromatograph with a fused silica column. The pseudo first order rate constants were obtained from the reactant conversion, which can be calculated from the peak areas of the GC analysis.

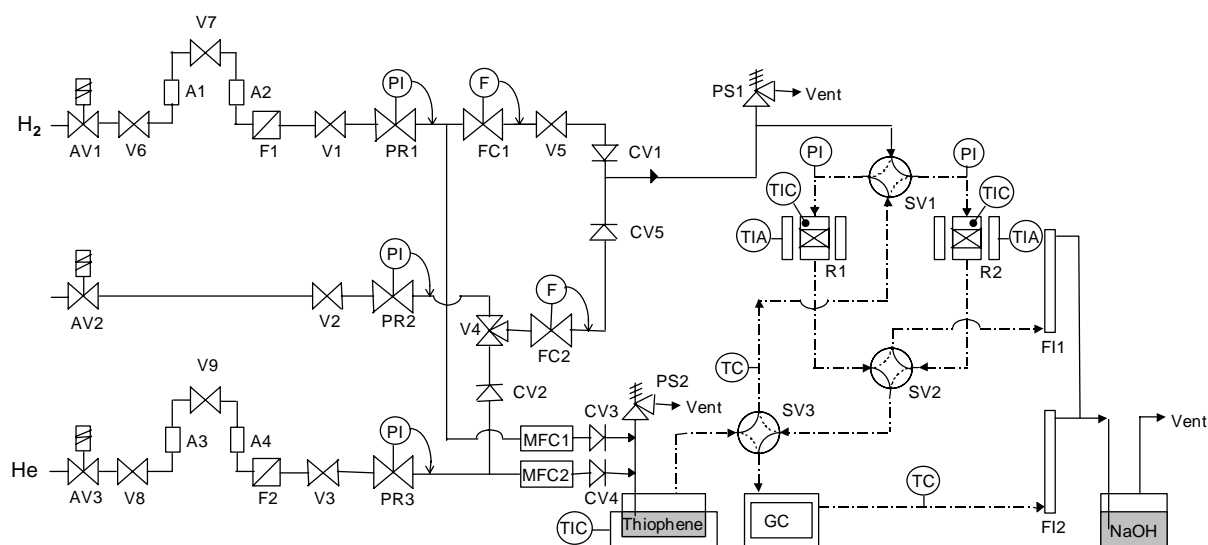


Figure 1. Schematic flow diagram of the dual reactor thiophene HDS set-up.

2.3. Dibenzothiophene HDS activity measurement

The activity for liquid-phase HDS of 4,6-DMDBT was determined in a batch reactor at 350 °C and 5 MPa total pressure in balance hydrogen. The schematic diagram of the reactor set-up (a 250 ml swinging-capillary autoclave reactor) is shown in Fig. 2. The reactant liquid (4,6-DMDBT in tetradecane) was filled in the liquid injection vessel mounted on the autoclave, starting the reaction at a well-defined time.

Catalysts were crushed and sieved properly before the test, to satisfy the criteria for avoiding mass transfer limitations [7]. 200 mg of catalyst with the particle size fraction between 125 and 250 μm was placed in the reactor. Before the reaction, catalysts were presulfided at 250 °C for 1 h and at 370 °C for 2 h, in the liquid phase containing an excess amount of dimethyldesulfide (0.4 ml) in tetradecane (60 ml) with respect to the required amount of sulfur for the formation of NiS and MoS₂. DMDS is known to decompose into H₂S and methane below 250°C. The autoclave was pressurized with hydrogen at 2.4 MPa before presulfiding. Eventually the total pressure of the autoclave during presulfiding at 370 °C was about 5.5 MPa.

The inhibiting effect of H₂S is strong for HDS reactions. To mimic commercial reactor conditions, DMDS was added in the liquid phase reactions to adjust the H₂S pressure to a constant level (0.75 bar). This also provided the condition that the effect of self-produced H₂S was minimized. After presulfiding and cooling down, the sulfiding gases were discarded through the ZnO bed vessel and the appropriate amount of DMDS was added in the autoclave. The system was purged with H₂. Then the autoclave was pressurized with hydrogen at 2.4 MPa.

The autoclave was heated up to the reaction temperature and the reaction mixture was quickly injected from the liquid injection vessel into reactor by opening the interconnecting valve. The final sulfur concentration of the feed in the reaction was 350 ppm. Then the total pressure was pressurized to be 5 MPa, and the stirring speed was set to be 2200 rpm according to the previous study [8], triggering the reaction.

After flushing the sampling line with very small amount of liquid in the reactor, about 150 μl of samples were taken at well-defined time. Gas chromatography with a FID detector was used for quantitative analysis of products. In liquid phase reaction, inert hydrocarbon (0.2 wt% octadecane) was added as the internal standard in the feed for GC analysis.

To see the effect of presulfiding agents, several methods were tested. Gas presulfiding by H_2S , H_2 and Ar (5, 50, and 45 vol.%) at a total flow rate of 60 ml/min at atmospheric pressure was carried out, using a special catalyst cell mounted on the autoclave. The following temperature programmed sulfiding programs were applied: increased at 5 K/min to 250 $^\circ\text{C}$, followed by an isothermal stage at 250 $^\circ\text{C}$ for 1 h, again increased at 5 K/min to 370 $^\circ\text{C}$, followed by an isothermal stage at 370 $^\circ\text{C}$ for 1 h. The cell has a small sieve which can be turned by hand to drop the catalysts. After presulfiding the catalyst particles were dropped into the reaction solvent in the autoclave without air exposure. For liquid presulfiding, DMDS (dimethyldisulfide), Sulfrzol 54 [9] (commercial product as commonly available for presulfiding) and DBT (dibenzothiophene) were tested as sulfiding agents.

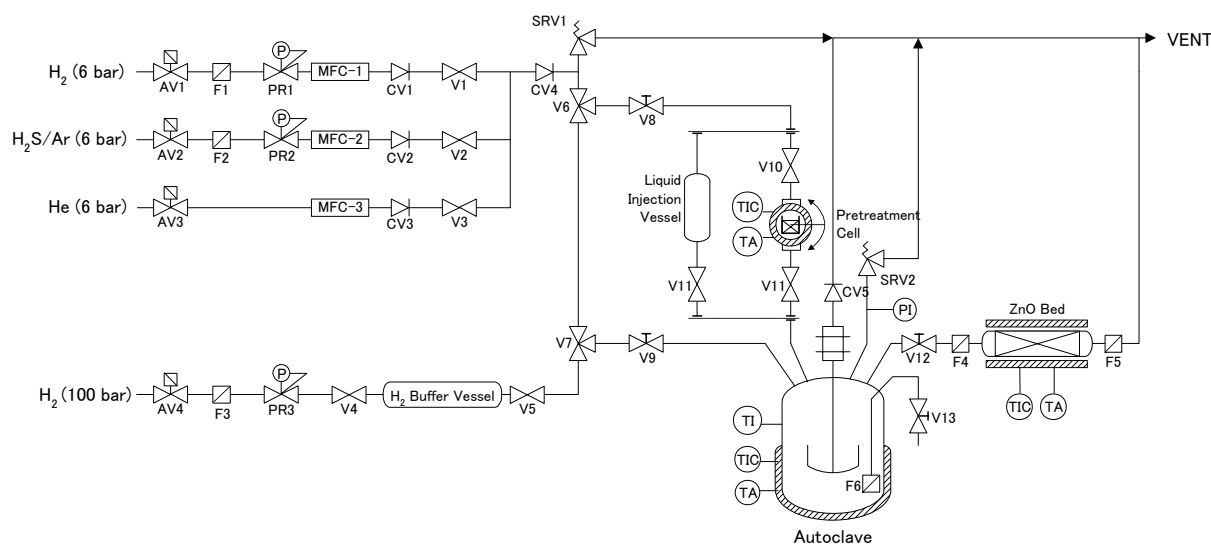


Figure 2. Schematic flow diagram of batch type autoclave reactor.

2.4. High-pressure fixed bed micro flow reactor for diesel HDS activity measurement

For diesel HDS a high-pressure fixed bed micro flow reactor was used. The schematic diagram of the reactor set-up is shown in Fig. 3. The catalyst bed was diluted with inert particles SiC with an average diameter of 120 μm to prevent bypassing of the feed. The rest of the reactor tube was filled with coarse and fine particles of SiC [10]. Feed was charged by a high-pressure pump and hydrogen was fed by micro flow controller. The total pressure was controlled at 5 MPa by the back pressure controller. A mixture of hydrogen and feed oil was charged into the reactor and separated in the high-pressure liquid level controlled separator. An auto sampling system was used and the liquid product was stored in the bottle. The gas stream was treated in H_2S scrubber with a NaOH aqueous solution. The catalyst volume filled in the reactor was 7.5 cm^3 , and LHSVs were varying from 2 to 6 h^{-1} and temperature range was from 320 $^\circ\text{C}$ to 370 $^\circ\text{C}$.

Hydrogen flow rate to oil feed rate was set to be $330 \text{ m}^3_{\text{H}_2} / \text{m}^3_{\text{oil}}$ (293 K, 1 bar). Feed properties of straight run light gas oil are shown in Table 2. Before the reaction, catalysts were presulfided at 5 MPa and 250 °C for 4 h and at 300 °C for 6 h, using a liquid flow rate of LHSV 2 h^{-1} with straight run gas oil and DMDS (sulfur concentration was adjusted to be 2.5 wt%). After feed was switched to the straight run light gas oil, samples were taken at regular intervals. H_2S in the liquid sample was stripped with nitrogen flow equipped in the auto sampling system. Gas chromatography with a SCD detector was used for quantitative analysis of sulfur compounds. The standard solutions were prepared, diluting diesel with heptadecane. The quantitative standard line was measured in each measuring day.

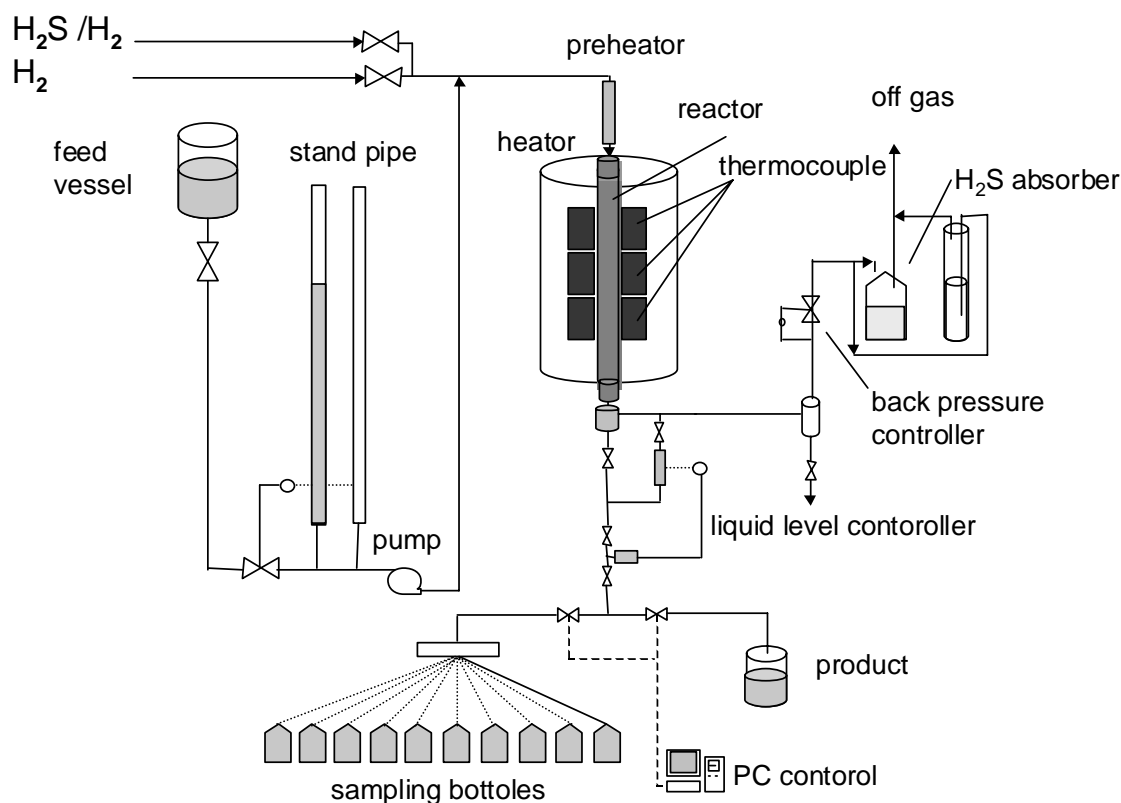


Figure 3. Schematic flow diagram of high pressure fixed bed micro flow reactor.

Table 2. Feed properties of diesel for high-pressure fixed bed micro flow reactor

Density	at 15 °C	g/cc	0.8542
Sulfur		wt%	0.84
Composition (HPLC)	1-ring Aromatics	vol%	16.2
	2-ring Aromatics	vol%	9.9
	≥3-ring Aromatics	vol%	1.3
Distillation (ASTM D86)	IBP vol%	°C	233
	5 vol%	°C	273
	10 vol%	°C	281
	20 vol%	°C	291
	30 vol%	°C	299
	40 vol%	°C	307
	50 vol%	°C	316
	60 vol%	°C	326
	70 vol%	°C	338
	80 vol%	°C	353
	90 vol%	°C	370
	95 vol%	°C	380
	FBP vol%	°C	387
Nitrogen		ppm	124
Cetane Index			54.2

3. Results and discussion

3.1. Thiophene HDS activity measurement

In Fig. 4, the effect of mild presulfiding on the activity of thiophene HDS was tested on type I and type II catalysts in comparison with the standard presulfiding. Activity is deteriorated significantly for initial 120 min, and it becomes stable after around 360 min. In all catalysts, the activity with the mild presulfiding procedure is higher, especially at low time-on-stream (≤ 2 min). The ranking of the catalysts is the same, regardless of the presulfiding procedures. We applied mild presulfiding after that, as it provides higher activity. The difference can be explained as follows. As the final temperature of the standard method is higher, and the rate of increasing temperature is faster, in the case of the standard sulfiding procedure more sintering of active phases is to be expected than in the case of mild presulfiding.

To compare the effect of H_2S addition under the same condition, a dilution with Ar was applied for H_2 balance gas, using the same flow rate of Ar as H_2 . As shown in Fig. 5, rate constants did not change significantly: a slightly higher value is observed with Ar. Generally thiophene HDS kinetics is described as Langmuir-Hinshelwood type equation 1, supposing first-order reaction for reactant:

$$r_{Th} = k_{Th} \frac{K_{Th} C_{Th} K_{H_2} P_{H_2}}{1 + K_{Th} C_{Th} + K_{H_2S} P_{H_2S} + K_{H_2} P_{H_2}} \quad , \quad (1)$$

where r_{Th} , k_{Th} are reaction rate and reaction rate constant of thiophene, and K_{Th} , K_{H_2} , K_{H_2S} , are the adsorption constant of thiophene, H_2 , H_2S , and p_{H_2} , p_{H_2S} , C_{Th} , are the partial pressure of H_2 , H_2S and concentration of thiophene, respectively.

It has been reported that the reactant and H_2S adsorption constants are much larger than that of H_2 [11] and, as a consequence, equation 1 simplifies to equation 2:

$$r_{Th} = k_{Th} \frac{K_{Th} C_{Th} K_{H_2} p_{H_2}}{1 + K_{Th} C_{Th} + K_{H_2S} p_{H_2S}} \quad (2)$$

Moreover, it was reported that the adsorption constant of H_2S is much higher than that of thiophene at atmospheric pressure, 350 °C [12]. So, equation 2 reduces to equation 3

$$r_{Th} = k_{Th} \frac{K_{Th} C_{Th} K_{H_2} p_{H_2}}{K_{H_2S} p_{H_2S}} \quad (3)$$

Therefore, it is not surprising that when the positive effect of increasing the H_2 pressure balances the negative influence of increasing the H_2S pressure, dilution with Ar has apparently no effect on the rate constant. In Fig. 5, the negative influence of increasing the H_2S pressure by self produced H_2S during the HDS reaction was reduced by the dilution with Ar: a slightly higher value is observed with Ar.

In agreement with this equation the activities were retarded significantly with H_2S (see Fig. 6). However, the ranking of catalysts holds, regardless of H_2S partial pressure. Without H_2S , the deactivation tends to be larger in the catalysts with higher activity. With H_2S , the deactivation seems to be smaller for all catalysts. This observation supports the conclusion that the cause of the deactivation for thiophene HDS is sulfur deficiency by H_2 [13].

From these results we decided to use the initial activity without H_2S in ranking of catalysts in the following chapters.

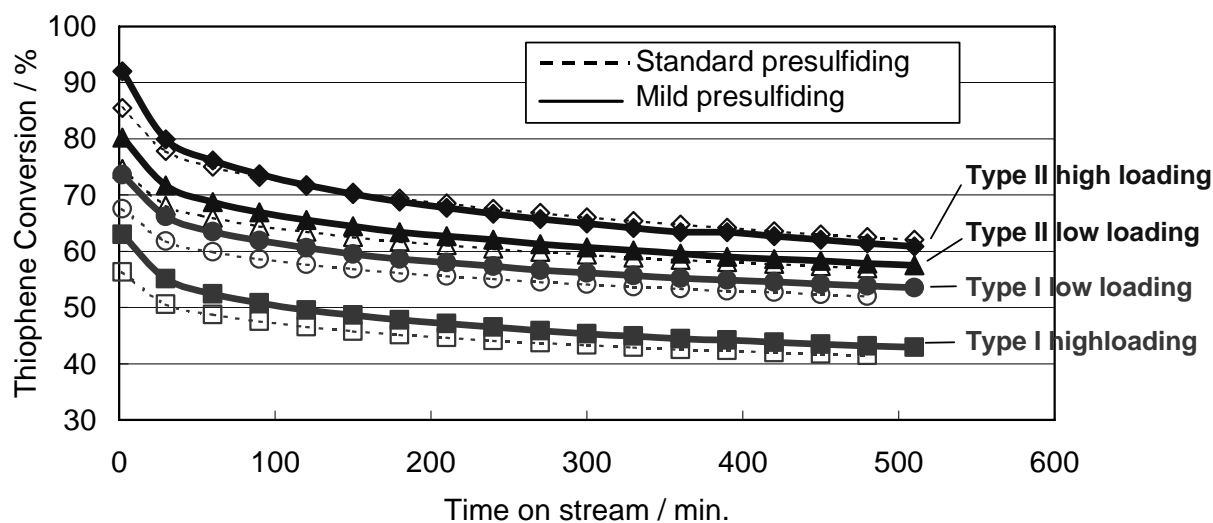


Figure 4. Mild presulfiding effect on thiophene HDS activity of NiMo catalysts

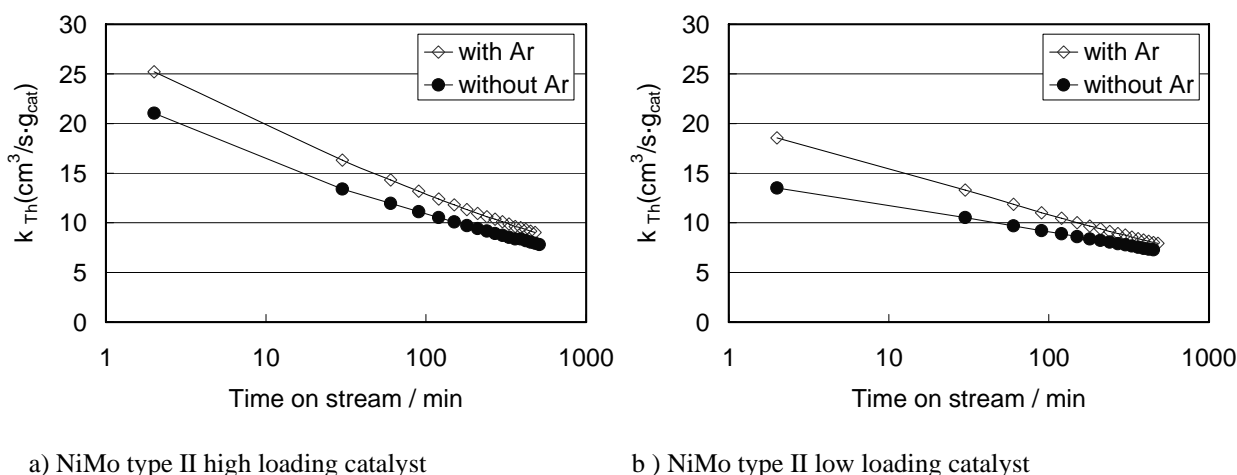


Figure 5. Effect of dilution with Ar on thiophene HDS activity of NiMo catalysts

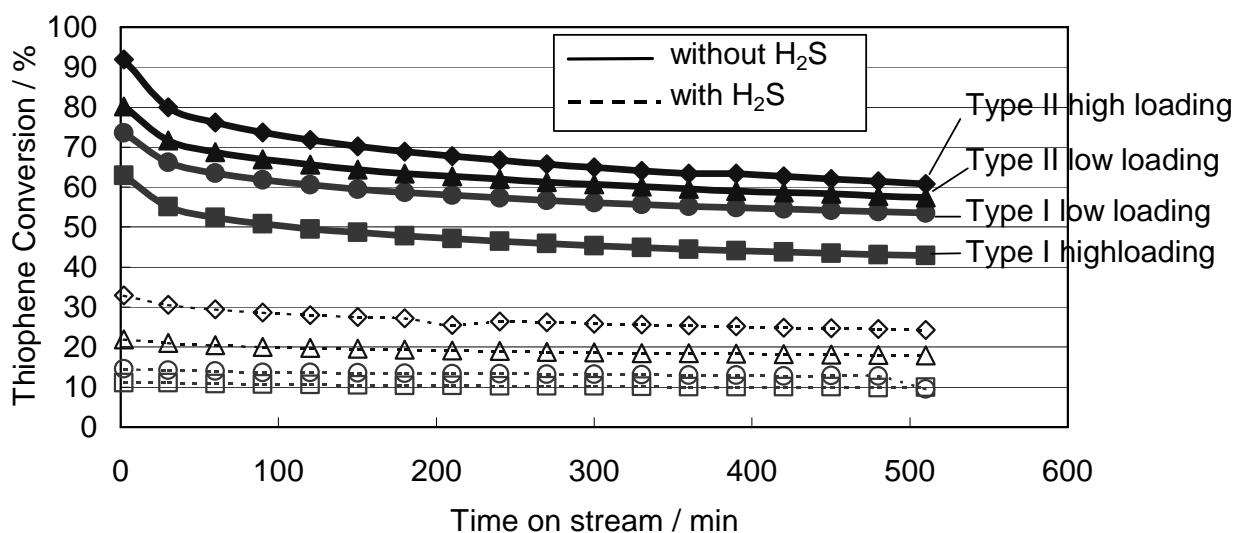


Figure 6. Ranking of thiophene HDS activity between with and without H_2S .

3.2. Dibenzothiophene HDS activity measurement

Several presulfiding methods were tested to see the difference of activity for 4,6-DMDBT HDS. From Fig. 7 it can be concluded that the difference of activities between the case of gas presulfiding at atmospheric pressure and of liquid presulfiding by DMDS at high pressure was not very significant. The slightly lower activity by gas-presulfiding might be due to the sintering as the heat by sulfiding is removed more effectively by liquid phase than by gas phase.

Among liquid presulfiding by sulfiding agents, there was not so much difference between DMDS and Sulfrzol 54, while DBT showed much less activity. The reason is that the sulfur atom in DBT is not used effectively at presulfiding. This agrees with literature [14], sulfur atoms of -SH or -S-S- are easily converted during sulfiding with H_2 , in contrast with sulfur in thiophene-rings.

As DMDS sulfiding is more commonly applied in liquid phase HDS, this sulfiding procedure is followed in our works for liquid phase reactions.

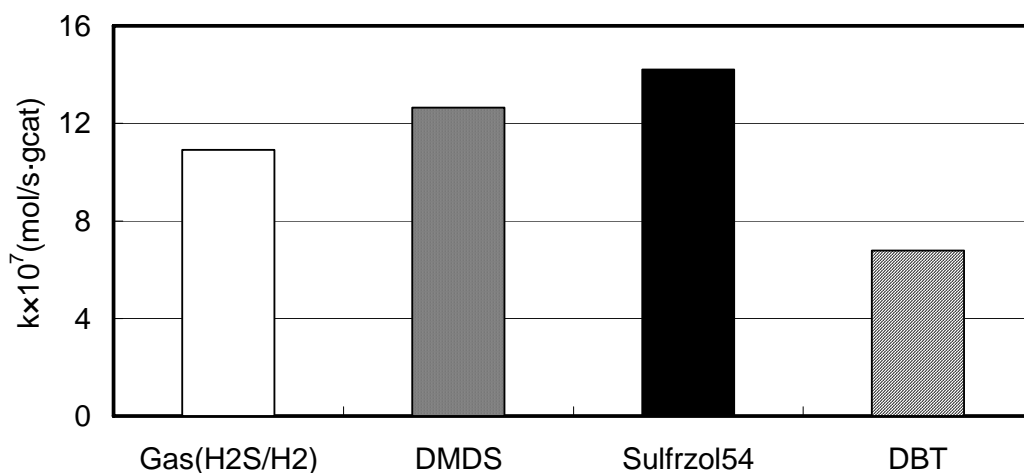


Figure 7. Presulfiding effect on 4,6-DMDBT HDS activity (NiMo type II high loading catalyst, Gas: gas phase presulfiding, DMDS, Sulfrzol54 and DBT: liquid phase presulfiding in tetradecane)

3.3. High-pressure fixed bed micro flow reactor for diesel HDS activity measurement

To check if we can get reasonably accurate data for ranking of catalyst activity in the deep HDS range, catalysts filling procedures were tested.

In catalyst testing at high conversion, axial dispersion should be minimized. An often used criterion is provided by equation 4:

$$Pe = \frac{L_b \nu_L}{D_{ax}} = \frac{L_b}{d_p} Bo > 8 \cdot n \cdot \ln\left(\frac{1}{1-X}\right), \quad (4)$$

where Pe , Bo are Peclet number, Bodenstein number, L_b , d_p is length of reactor and particle diameter, n is reaction order, ν_L is superficial fluid velocity, D_{ax} is effective diffusivity in axial direction, and X is conversion.

In small trickle bed reactors, according to a global correlation between Bo and Re established by Gierman [15], substituting $Bo = 0.04$ in equation 4 yields:

$$\frac{L_b}{d_p} > 200 \cdot n \cdot \ln\left(\frac{1}{1-X}\right), \quad (5)$$

From this equation, it is clear that a higher conversion requires longer bed length and smaller particle diameter. It is known that the apparent reaction order observed is around 1 to 1.6 for the deep HDS of diesel, and especially in ultra deep desulfurization, can be assumed to be equal to 1 while the feed is regarded as a single component (the most refractory compound). The minimum bed length at 0.1 mm of particle size calculated by the criteria is shown in Fig. 8. When the conversion is 0.99, corresponding to 100 ppm of product sulfur using the feed shown in Table 2, the length is calculated as approx. 8 cm.

It has been reported that when the catalyst bed voids are filled with small inert particles like SiC, the hydrodynamics will be largely dictated by the packing of the fine inert particles [16]. As

the particle size of SiC in our experiment was 0.1mm and the catalyst bed height was 7 cm (catalyst volume 7.5 cm³, SiC volume is 4 cm³, respectively), the condition of the first run was in the boundary of good regime when HDS conversion is 0.99 (product sulfur is 100 ppm).

First, the dilution technique was applied and the catalysts were filled as extrudate without crushing. However as the Arrhenius plots show in Fig. 9, the data scattering was rather large. Therefore, pseudo cold packing tests to see the situation in the tubes by several filling methods were carried out.

In Run-1, all catalyst particles were packed, and subsequently SiC was added under gently tapping. In Run-2, the catalyst and SiC were filled dividedly in four portions. In Run-3, the catalysts were crushed and sieved, so that the particle sizes were from 0.25 to 0.5 mm. Pictures for the three situations are shown in Fig. 10. Moreover, pictures of the situation by pouring water from the top of the tubes were taken and shown in Fig. 11.

The actual situation in the reactor in Run-1 could not be observed, however from the cold packing observation it is clear that if the catalysts were filled in one time, it is not so easy to fill the voids of the catalysts with SiC after that. In Run-2, the catalysts voids could be filled with SiC in a packed situation. Fig. 11 shows that when the voids are not filled with SiC, maldistribution of the liquid in case of down flow has to be expected. Even in Run-2 several small air pockets still remained near the wall. In Run-3 the catalyst extrudates were crushed into smaller size of particle, and the wetting of particle seemed to be easily achieved.

The results of activity testing of Run-1, Run-2, and Run-3 are shown in Fig. 12. Firstly, smaller scattering of data in Run-2 and Run-3 is observed than in Run-1. This is probably due to inhomogeneous packing and, associated herewith, poor reproducibility. Therefore, when the catalyst extrudates are diluted with SiC, a proper filling method is crucial.

For Run-3 the linearity is held in 50 ppm range of product sulfur content, while in Run-2 it was held only up to 100 ppm. There are two possible causes to explain it. Firstly the occurrence of internal mass transfer limitation could be important for Run-2, because of the large particle size compared to that in Run-3. To check this the Thiele modulus (equation 9) can give a good indication. This was calculated as follows. It has been reported that the diffusivity can be estimated by the following equations [17] [18].

$$\text{Wilke -Chang: } D_{L,i} = \frac{7.4 \times 10^{-8} \cdot M_{wb}^{0.5} T}{\eta_b \cdot V_{s,i}^{0.6}}, \quad (6)$$

$$D_{eff} = \frac{\varepsilon_p \cdot D_{L,i}}{\tau_p} \cdot F(\lambda) \quad (7)$$

$$\text{with } F(\lambda) = (1 - \lambda)^Z, Z = 4 \quad \text{for } \lambda \leq 0.2$$

where, M_{wb} : the solvent average molecular weight (g/mol), T : temperature(K), V_{si} is the average molar volume at normal boiling point (cm³/mol), η_b : solvent viscosity (mPa·s) and $D_{L,i}$ is molecular diffusivity in solvent (cm²/s). M_{wb} , η_b were calculated to be 246, 0.18 (623 K, 5 Mpa) by process simulator II (SIMSI) using feed properties in Table 2. $D_{L,i}$ was calculated to be 1.2×10^{-4} (cm²/s) by equation 4. ε_p , τ_p , is the catalyst porosity, tortuosity, respectively (0.7, 3

were used). λ is the ratio of molecular to the catalyst pore diameter (0.13 was used). D_{eff} is the diffusion constant; in our experiment it was calculated to be 1.4×10^{-9} (m^2/s).

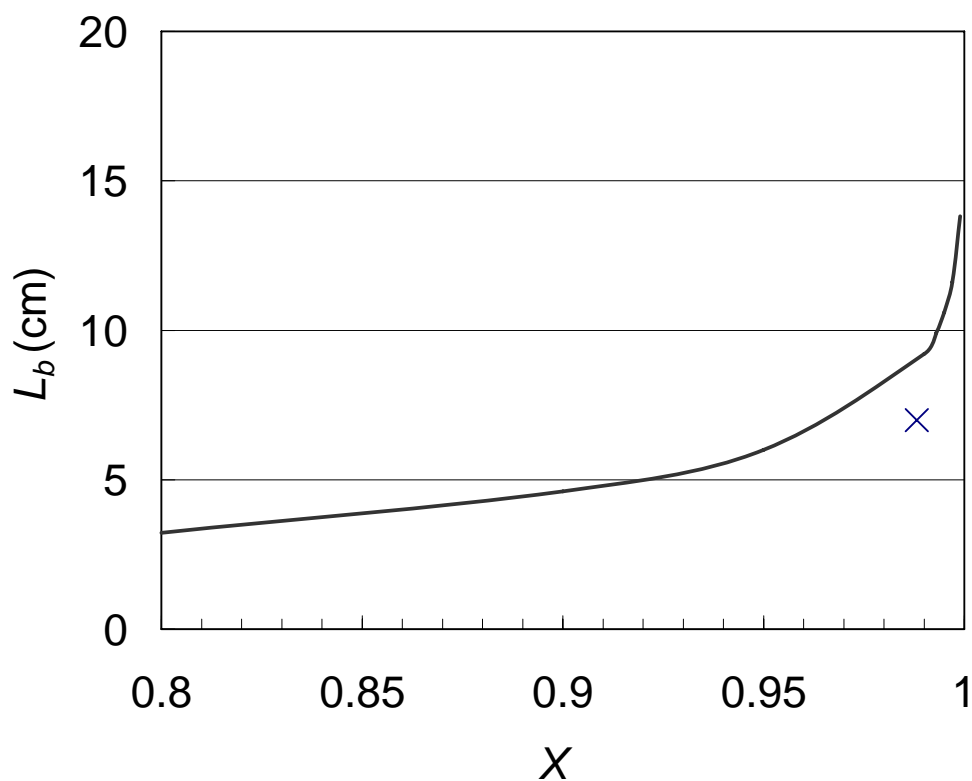


Figure 8. Trickle bed reactor criteria for bed length and catalyst particle size. \times : Bed length of Run-1 in our experiment.

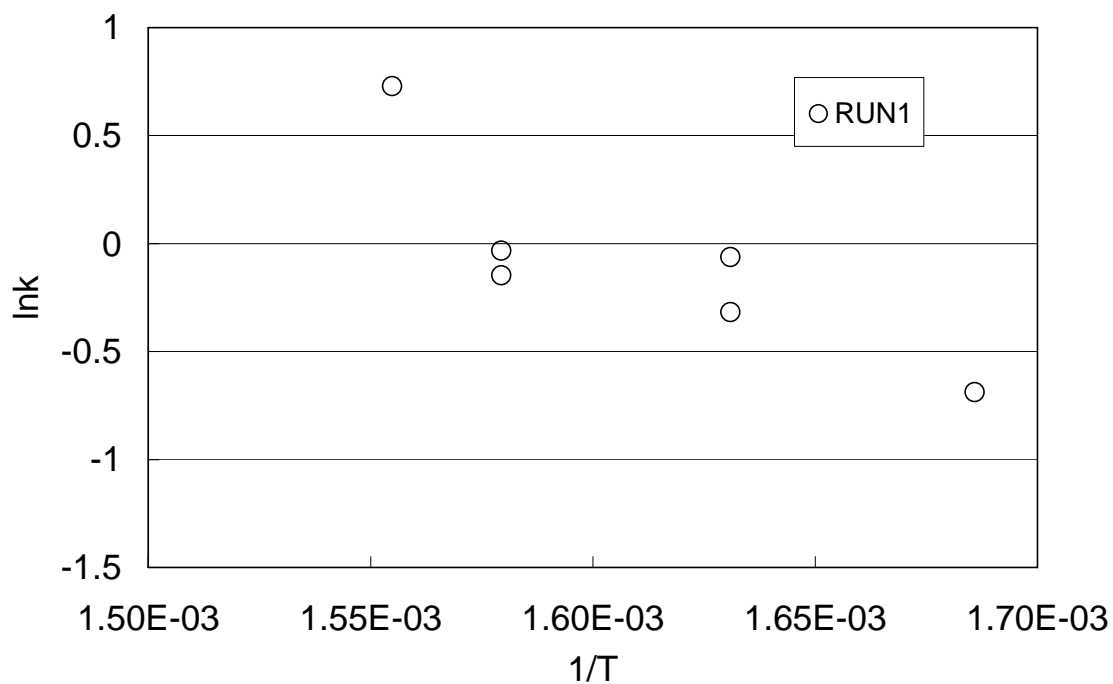


Figure 9. Results of HDS activity test of Run-1

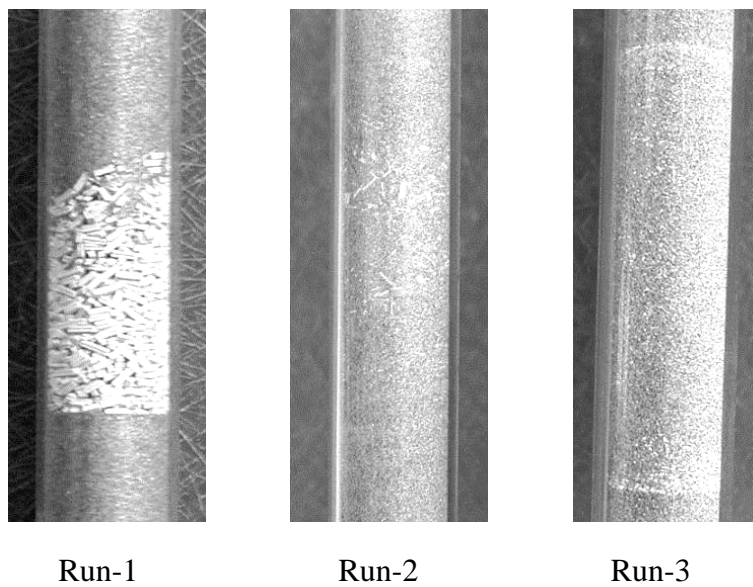


Figure 10. Pictures of cold packing tests

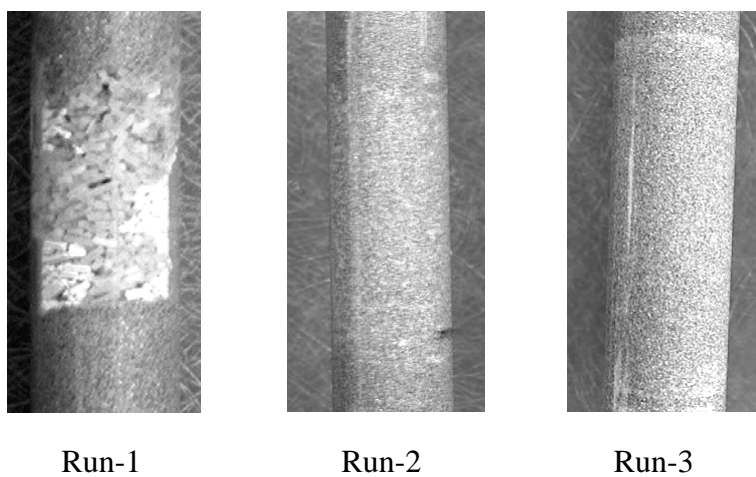


Figure 11. Pictures of cold packing tests after pouring water

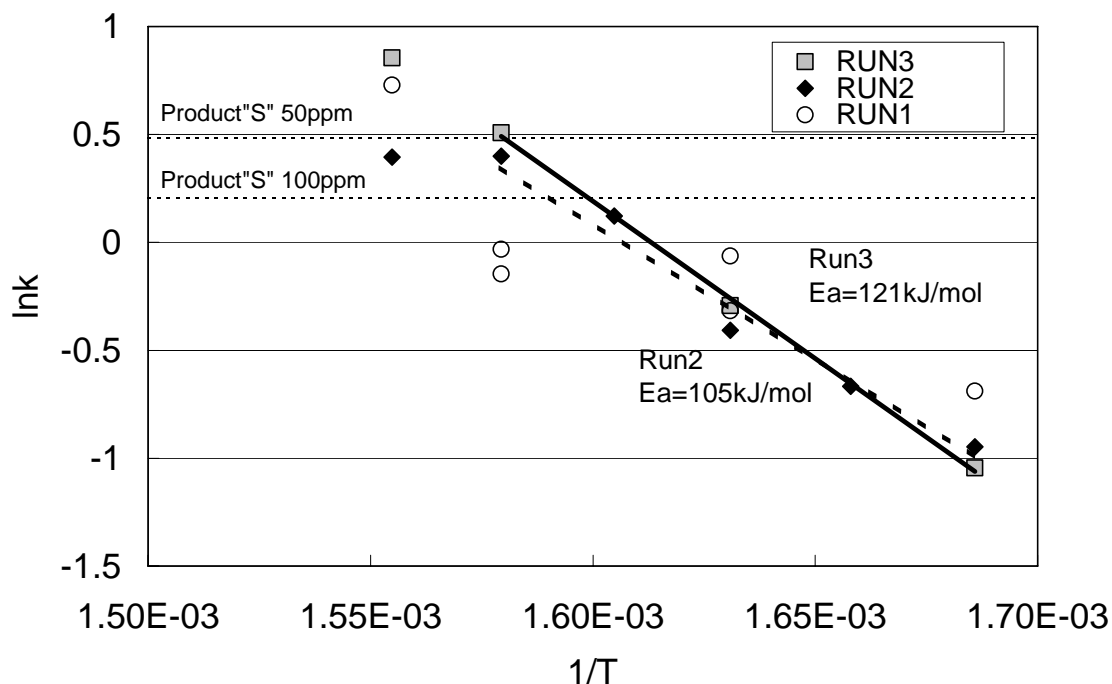


Figure 12. Arrhenius plots for HDS activity tests

The rate constant can be calculated from the following equation, assuming n th pseudo order reaction.

$$k = \frac{LHSV}{n-1} \times \left(\frac{1}{C_p^{n-1}} - \frac{1}{C_f^{n-1}} \right), \quad (8)$$

where $LHSV$: space hour velocity (h^{-1}), n : reaction order (1.3 from our data, varying $LHSV$), and C_p , C_f are the concentrations of sulfur in product and feed.

The Thiele modulus is defined as:

$$\phi = L \sqrt{\frac{k_{v,p}}{D_{eff}}}, \quad (9)$$

where L is diffusion length (0.3 to 0.4 mm of the catalyts).

Thiele modulus was approx. 0.38 in our experimental conditions, corresponding to a catalyst effective factor exceeding 0.95. From this estimation, it is concluded that the reaction was not carried out under internal mass transfer limitations.

The second possible reason is suggested by the cold flow packing observations. In Run-2 the extrudates still seem to have some relatively large voids between the SiC particles. That might cause bypassing of the liquid flow, and this can be the reason that the product sulfur could not reach below 50 ppm.

From these considerations, we decided to apply Run-3 method for the high-pressure micro flow reactor to test the activity in deep desulfurization range below 100 ppm.

4. Conclusions

In this chapter, preliminary tests to establish experimental methods were carried out. For model HDS reactions, thiophene HDS was tested in a micro flow reactor at atmospheric pressure. For DBTs HDS, a high-pressure batch type reactor was applied. Presulfiding agent and method were tested and the proper methods were chosen as the standard methods for the following chapters.

In HDS for diesel fuel, a high-pressure micro flow reactor was tested. To establish the testing method, several aspects were checked and in following chapters, the activity testing methods described in this chapter will be adopted. The proper filling method with dilution of Silicon Carbide can provide reliable data for ultra deep desulfurization for diesel fuel.

Acknowledgements

Bas M. Vogelaar is appreciated for his advising for the testing equipments.

References

- [1] S.T.Sie, *Revue de l'Institute Français du Pétrole*, **46** (1991) 501.
- [2] D.Nicosia and R.Prins, *Journal of Catalysis*, **229** (2005) 424.
- [3] A.L.Diaz and M.E.Bussell, *Journal of Physical Chemistry*, **97** (1993) 470.
- [4] I.E.Wachs, *Catalysis Today*, **27** (1996) 437.
- [5] Van der Zijden T.F., B.M.Vogelaar, A.D.van Langeveld, J.A.Moulijn, and S.Eijsbouts, Master thesis, Delft University of Technology, Delft, The Netherlands, 2003)
- [6] S.M.A.M.Bouwens, F.B.M.Vanzon, M.P.Vandijk, A.M.Van der Kraan, V.H.J.Debeer, J.A.R.Van veen, and D.C.Koningsberger, *Journal of Catalysis*, **146** (1994) 375.
- [7] H.R.Reinhoudt, C.H.M.Boons, A.D.van Langeveld, J.A.R.van Veen, S.T.Sie, and J.A.Moulijn, *Appl.Catal.A: Gen.*, **207** (2001) 25.
- [8] J.P.Janssens, PhD.Thesis, Delft University of Technology, Delft, The Netherlands, 1996)
- [9] <http://www.lubrizol.com/RefineryOilField/default.asp>, accessed August 2005.
- [10] B.M.Vogelaar, PhD thesis, Delft University of Technology, Delft, The Netherlands, 2005)
- [11] B.M.Vogelaar, N.Kagami, A.D.van Langeveld, S.Eijsbouts, and J.A.Moulijn, *Prepr.Pap.-Am.Chem.Soc.Div.Fuel Chem.*, **48** (2003) 548.
- [12] A.Borgna, E.J.M.Hensen, J.A.R.van Veen, and J.W.Niemantsverdriet, *Journal of Catalysis*, **221** (2004) 541.
- [13] B.M.Vogelaar, P.Steiner, A.D.van Langeveld, S.Eijsbouts, and J.A.Moulijn, *Appl.Catal.A: Gen.*, **251** (2003) 85.
- [14] R.Prada Silvy, F.Delannay, F.Delannay, and B.Delmon, *Applied Catalysis*, **46** (1989) 113.
- [15] H.Gierman, *Applied Catalysis*, **43** (1988) 277.
- [16] S.T.Sie, *Deactivation and Testing of Hydrocarbon-processing Catalysts*, ACS Symposium Series, **634** (1996) 6.
- [17] C.R.Wilke and P.Chang, *Aiche Journal*, **1** (1955) 264.
- [18] M.C.Tsai, Y.W.Chen, and C.Li, *Ind.Eng.Chem.Res.*, **32** (1993) 1603.

3

Characterization of NiMo type I and type II catalysts -The effect of metal loading-

Abstract

In this chapter, so-called type I and type II NiMo catalysts are characterized by various techniques such as XRD, TPR, TPS, Laser Raman spectroscopy, and SO₂ adsorption. The results agree with the conclusion that the type II active phase has weaker interaction with the support, which originates from their oxidic precursors. Moreover, all results are consistent with the assumption that type II active phase consists of several stacked layers of MoS₂ slabs or edge-bonded layers, and type I active phase is like a single slab. The high dispersion of type II active phase can be maintained at higher loading than the type I active phase.

1. Introduction

So-called type II active phase was proposed as highly active phase species in CoMo or NiMo/Al₂O₃ catalysts [1]. The idea is that type II active phase has a weaker interaction with the support than type I and type II active phase consists of more stacking MoS₂ slabs than type I. It was also reported that the different HDS activity of those phases depends on these morphologies [2].

This work will show that the two phases (I and II) behave quite differently at increasing loading for HDS activity. Type II active phase has been studied for long time but the effect of metal loading is not reported in the open literature. An explanation will be given based on activity-structure relationships.

So-called type I and type II NiMo catalysts were prepared varying Mo loading from below to above monolayer coverage. For the characterization, the prepared catalysts were examined by XRD (X-ray diffraction), TPR (temperature programmed reduction), TPS (temperature programmed sulfidation), and Raman spectroscopy.

To investigate the formation of crystalline phases of supported metal oxides, one of the useful techniques is XRD. If XRD bands are observed, it is clear that a crystalline phase has been formed by aggregation of metals loaded. Raman spectroscopy can be also one of the powerful techniques to characterize especially metal oxide species on alumina. The IR bands of the dehydrated surface metal oxide on alumina are not detectable below 1000 cm⁻¹ because of the IR absorption of the alumina support. However, these bands can be detected in the corresponding Raman spectra [3]. It has been reported that Raman is very sensitive to the appearance of the microcrystalline metal oxide particles since their Raman cross sections are usually orders of magnitude greater than that of the surface metal oxide species [4]. TPR can be also useful to investigate if metals have been supported as the same species.

To study transformation of oxidic catalyst precursors into active sulfided metals, TPS is applicable. The sulfiding behaviour can be informative with respect to the interaction between metals and support. From the consumption of H₂S, quantitative data of the degree of sulfiding are obtained.

After sulfiding, morphology of type I and type II phases has been investigated by chemisorption of SO₂. It has been reported that SO₂ does not adsorb on NiO or MoO₃ but only on alumina. The amount of SO₂ adsorption was measured on CoMo/Al₂O₃ before and after presulfiding, varying the metal loading. SO₂ chemisorption decreased at increasing metal loading. SO₂ adsorbs on hydroxyl groups and NO adsorbs only on the CUS (coordinative unsaturated site). This is nicely shown from IR spectroscopy. So, fortunately, SO₂ chemisorption can be used for quantifying the number of OH groups, even when NO is present [5]. Therefore, it is applicable to evaluate bare surface ratio on alumina unoccupied by metal sulfides. The amounts of SO₂ adsorption on presulfiding NiMo type I and type II catalysts have been measured, varying metal loading of catalyst.

2. Experimental

2.1. Preparation of NiMo type I and type II catalysts

NiO-MoO₃/Al₂O₃ catalysts (type I and type II) had been prepared via liquid phase pore volume impregnation using aqueous solutions containing Ni and Mo, according to the literature.

In the case of type I, after the supports had been impregnated by the metal solution, they were dried at 120 °C for 16 hours and calcinated at 500 °C for 4 hours. While in type II, only the drying step was applied (see Chapter 2).

The composition of catalyst was measured by INAA (Instrumental Neutron Activation Analysis). Specific surface area of alumina support was measured by nitrogen adsorption method (BET). Two different metal loading catalysts were prepared; high and low loading with 5, 10 Mo atom per nm², respectively. All catalysts were prepared to have the same molar ratio of Ni or Co to Mo. The results of elemental analysis are shown in table 1.

Table 1. Composition of the NiMo catalysts

	NiO (wt%)	MoO ₃ (wt%)	Ni/Mo molar ratio	Mo loading (atom / nm ²)
NiMo type I	1.8	10.1	0.34	2.5
	3.2	18.2	0.34	5.1
	5.5	30.0	0.35	10.3
NiMo type II	1.8	10.1	0.34	2.5
	3.3	18.6	0.34	5.2
	5.6	30.6	0.35	10.5

2.2. Activity measurement

The activity for gas-phase thiophene (TH) HDS was tested in a micro flow reactor at 350 °C and atmospheric pressure and a flow rate of reaction mixture of 100 ml/min, containing 5.0 vol.% TH in balance H₂. 200 mg of catalyst was diluted with SiC particles. The activity for liquid-phase DBT was determined in a batch reactor at 350 °C and 5 MPa total pressure in balance hydrogen. Catalysts were crushed and sieved properly before the test and the amount of catalyst placed in the reactor was 100 mg. Before the reaction, catalysts were presulfided at 370 °C. The feed consisted of DBT in hexadecane and sulfur concentration in feed was 350 ppm. The inhibiting effect of H₂S is strong for HDS reactions. To mimic commercial reactor conditions, dimethyldisulfide (DMDS) was added in the liquid phase reactions to adjust the H₂S pressure to constant level (1.5 bar). This also provided the condition that the effect of self-produced H₂S was minimized. Gas chromatography with a FID detector was used for quantitative analysis of products. In liquid phase reaction, inert hydrocarbon (0.2 wt% octadecane) was added as the internal standard in the feed for GC analysis (see Chapter 2).

2.3. Characterization

XRD analysis was adapted for the characterization of the oxide precursor of active metals. A conventional powder diffractometer was employed to determine crystalline phases, using 40 kV, 50 mA, Cu-K α radiation. In particular, XRD was applied to investigate the crystalline formation at increasing the metal loading.

Raman spectroscopy was also applied for characterization of the oxide precursor of active metals. The schematic diagram is shown in Fig. 1. A Renishaw Ramanscope System 2000 instrument was linked to a Leica microscope, using a 514 nm, 20 mW Ar⁺ laser. To investigate the sample without the exposure to moisture in the air, a Linkam THMS600 flow cell was used

(see Fig. 2). After the catalysts had been heated and dried in the cell in the flow of the dry air at 150 °C for 4 h and cooled down to the room temperature, the spectra were recorded in a flow of nitrogen. To make the surface of the sample flat [4], the catalysts were well crushed in an agate grinder, and pressed into a flat pellet, applying a pressure of 5 GPa during 30 seconds.

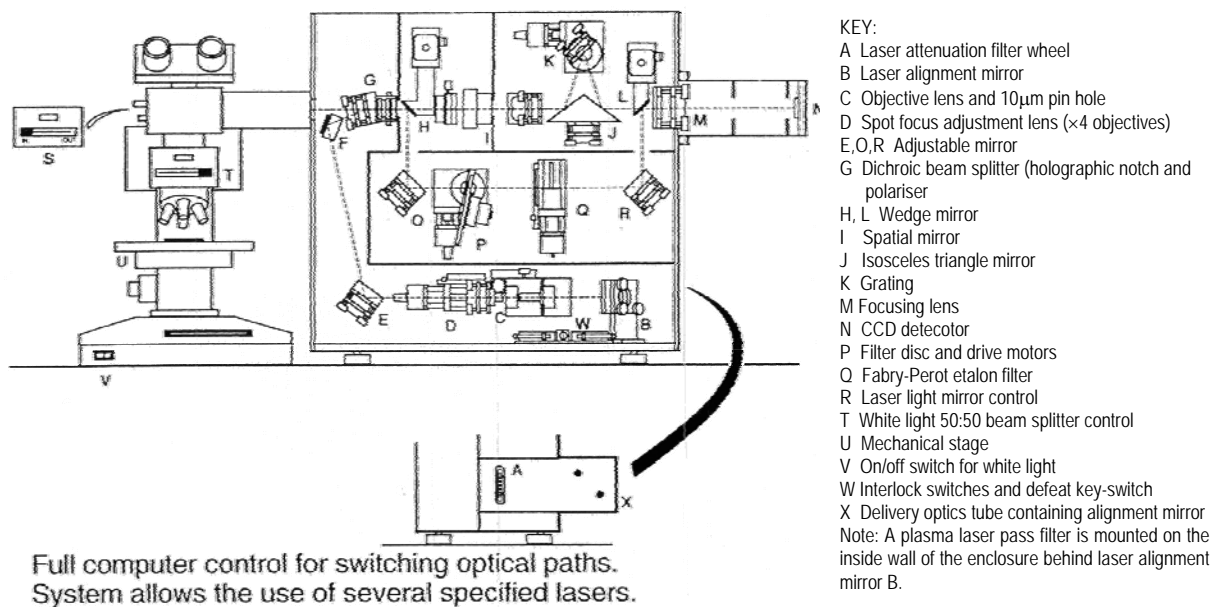


Figure 1. Schematic diagram of Laser Raman set-up

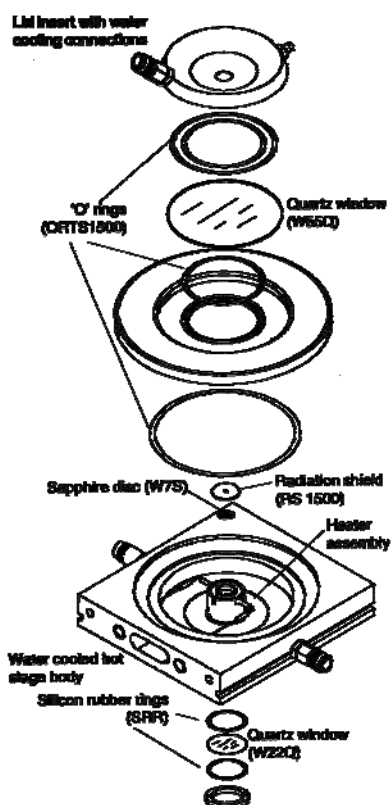


Figure 2. Schematic diagram of the heated sample in-situ cell

TPR was performed for the characterization of the reducibility of oxide precursor and identification of the oxidic phases of active metals. The catalyst particles were crushed and sieved (75~125 μm). The catalyst particles were diluted with SiC particles (120 μm). The sample was filled in a quartz reactor tube between quartz wool plugs. As a pre-treatment, the sample was dried at 150 $^{\circ}\text{C}$ for 4 h in a flow of He. The catalyst was exposed to the gas mixture, containing H_2 and Ar (2.5 and 27.5 vol.%) at a total flow rate of 30 ml/min. After the base line of TCD was stabilized at room temperature, the temperature program was started, and the reactor was heated to 1000 $^{\circ}\text{C}$ in a linear temperature program (10 K/min), subsequently kept at 1000 $^{\circ}\text{C}$ for 30 min.

TPS was carried out for the characterization of the transformation from oxidic precursor to sulfidic phase. The schematic diagram is shown in Fig. 3. The same size of reactor and catalyst particles as in TPR were used. As a pre-treatment, the sample was dried at 150 $^{\circ}\text{C}$ for 4 h in a flow of Ar. The catalyst was exposed to the sulfiding mixture, containing H_2S , H_2 and Ar (3.3, 25.0, 71.7 vol.%, respectively) at a total flow rate of 30 ml/min. After 0.5 h at room temperature, the temperature program was started, and the reactor was heated to 1000 $^{\circ}\text{C}$ in a linear temperature program (10 K/min), subsequently kept at 1000 $^{\circ}\text{C}$ for 30 min.

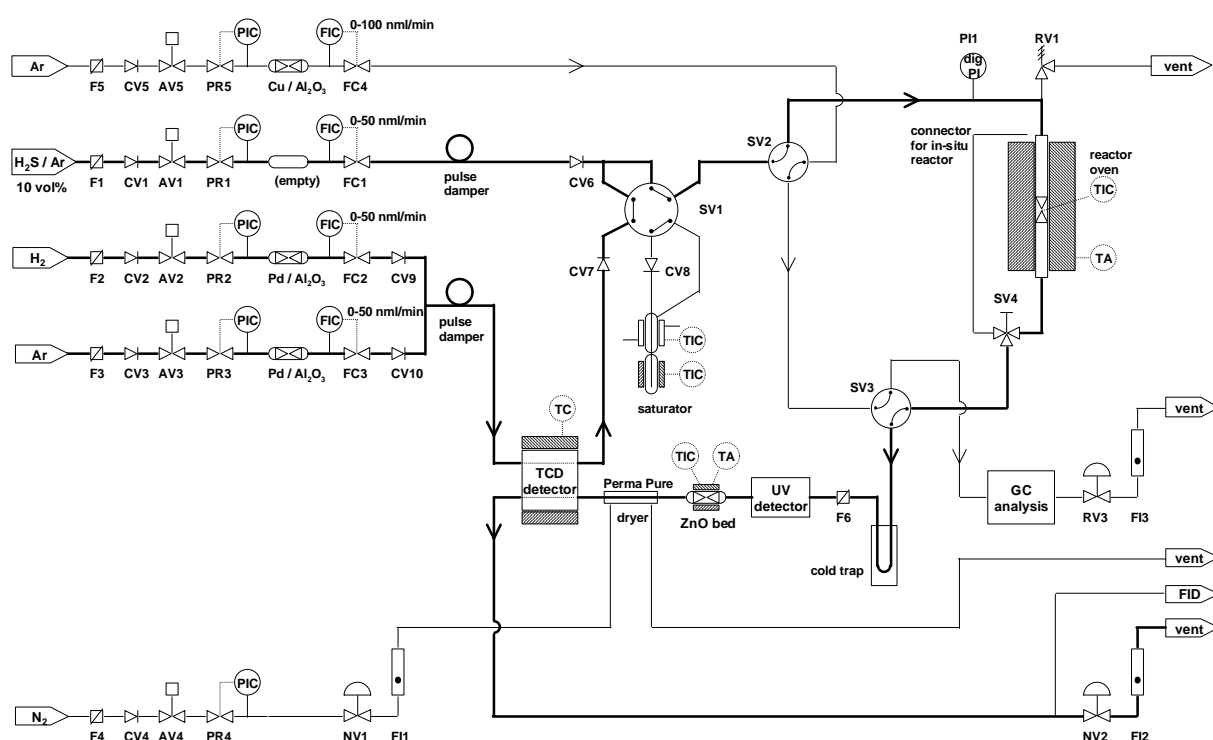


Figure 3. Schematic diagram of TPS set-up

SO_2 adsorption amount was measured by the static method. Before the adsorption, catalysts were presulfided at 250 $^{\circ}\text{C}$ for 1 h and at 370 $^{\circ}\text{C}$ for 2 h, in the liquid phase containing excess amount of dimethyldesulfide corresponding with the amount required for the transformation of the oxidic precursors into NiS and MoS_2 . The catalysts were washed with toluene and ethyl alcohol with decantation after every washing step. The sample was placed in an adsorption cell,

and evacuated at 200 °C for 2 h. SO₂ was admitted, at increasing the pressure from 0 to 1 bar. The temperature was controlled constantly at 35 °C. After desorbing by the vacuum evacuation, physisorption was measured at increasing the pressure of SO₂ again. The chemisorption data was obtained by the subtraction of the physisorption from the total adsorption, determined by vacuum evacuation.

3. Results and discussion

3.1. Metal loading effect on HDS activity

The effect of active metals loading on the thiophene, and DBT HDS activities for both NiMo type I and type II catalysts is shown in Fig. 4. It is remarkable that at increasing loading, type II catalyst activities both for thiophene and DBT HDS increased almost linearly, while this was not the case in type I catalyst. The difference in behaviour is probably related to the dispersion of the active phase. In the next paragraph, the formation of crystallites due to the aggregation of active phase is investigated.

Compared to type I catalysts, type II catalysts showed higher activity for thiophene at low metal loading. On the other hand, type I catalyst shows higher activity than type II for DBT HDS at low metal loading. These results agree with the literature [6]. This will be investigated later in chapter 4.

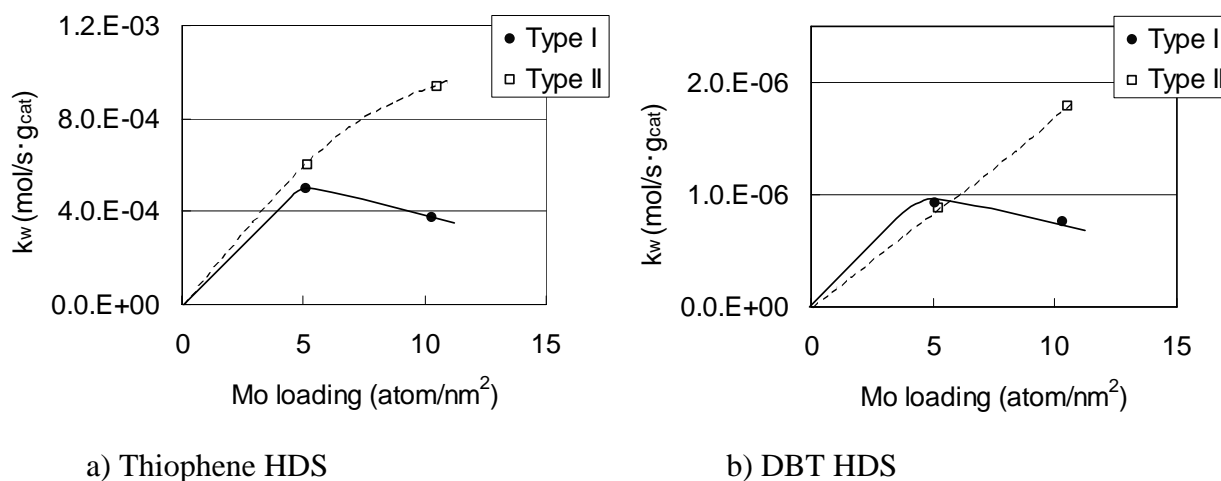


Figure 4. HDS activities of NiMo type I and type II catalysts at increasing metal loading

3.2. Formation of crystalline material

XRD, TPR and Raman spectra were used for the characterization of the oxidic catalyst precursor, especially concerning their aggregation.

The results of XRD analysis for type I and type II catalysts with Mo loading above and below monolayer coverage are shown in Fig. 5. Both type II catalysts and the low loading type I are very dispersed and do not exhibit bands suggesting crystalline phases. Only type I high loading catalyst shows well-defined bands, viz., at 23.4 ° and 27.6 °, 26.7 °; they are assigned to formation of crystals of MoO₃, NiMoO₄, respectively [7, 8]. For the assignment of NiMoO₄,

laser Raman spectroscopy is useful to distinguish between α -NiMoO₄ and β -NiMoO₄; this is investigated later in this paragraph.

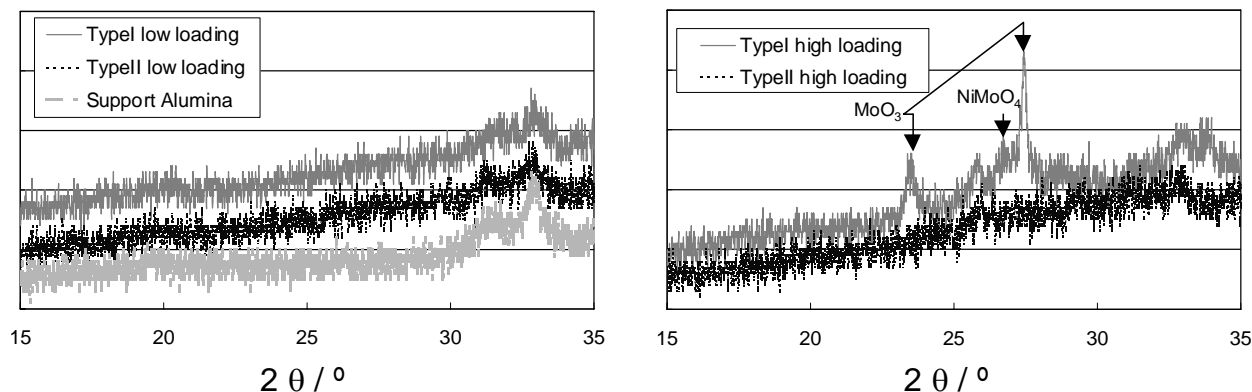


Figure 5. XRD analysis for NiMo type I and type II catalysts

In the TPR spectra of NiMo/Al catalysts, (see Fig. 6) two main peaks are observed, in agreement with literature where also two peaks are reported, a low- and a high-temperature peak, associated mainly with the reduction of Mo⁶⁺ bilayer/multilayer and Mo⁶⁺ monolayer species, respectively [9]. As in our catalysts the Ni to Mo ratio is low (see table 1) and the stoichiometry of reduction for Ni is one (for Mo it is three), it is not surprising that we do not see a clear Ni contribution in the TPR patterns. As expected, at increasing loading both type I and type II catalysts show higher hydrogen consumption in the low-temperature peak. But the type I high loading catalyst exhibits this behaviour much more than the others. Moreover, the peak in the lower-temperature of type I high loading catalyst shifted around +70 °C higher at 500 °C. It could correspond to NiMoO₄ crystalline formation, as the inhibition of Mo reduction by Co in case of co-impregnated CoO-MoO₃/ Al₂O₃ was reported [10], probably due to the formation of CoMoO₄ crystallites, reducing at about 555 °C [9]. So, it can be suggested that the type I high loading catalyst has large crystals in the oxidic precursor before presulfiding.

In Fig. 7, results of Raman spectroscopy under ambient conditions are shown. Mo₈O₂₆⁴⁻ (Mo=O Raman band at 958-960 cm⁻¹) and Mo₇O₂₄⁶⁻ (Mo=O Raman band at 946-951 cm⁻¹) are observed in both of NiMo type I and type II high loading catalysts [11]. From careful inspection it is clear that the high loading type I catalyst shows a Raman shift assigned to aggregated microcrystalline MoO₃ species at 815-820 cm⁻¹ band [3]. Recently it has been reported that the structure of surface species is strongly affected by the degree of hydration [12]. Raman spectra in in-situ cell after drying in dried air at 150 °C are shown in Fig. 7. In agreement with literature, dehydration shortens the terminal M=O bond and generally shifts this vibration to above 1000 cm⁻¹. The Raman shift assigned to aggregated microcrystalline MoO₃ species is now clearly observed. For microcrystalline NiMoO₄, it was reported that β -NiMoO₄ shows a 705 cm⁻¹ band. The absence of this band suggests that β -NiMoO₄ is absent, in agreement with the literature [13].

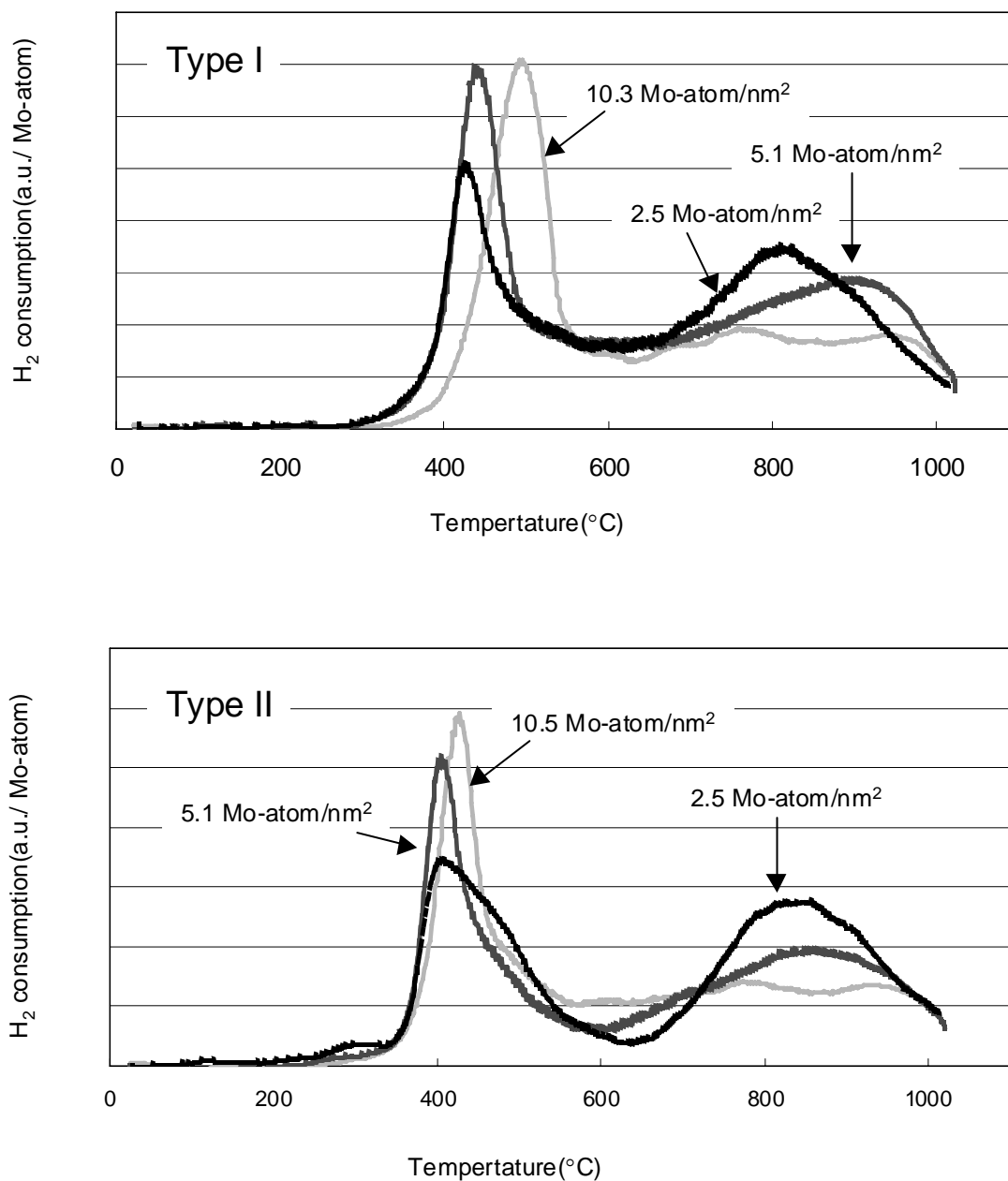


Figure 6. TPR spectra of NiMo type I and type II catalysts varying metal loading.

From these observations it is concluded that at high loading type I active phase forms an aggregated phase on the support alumina, probably a mixture of MoO₃ and α -NiMoO₄. It is remarkable that only type II active phase can achieve higher metal dispersion above monolayer surface coverage.

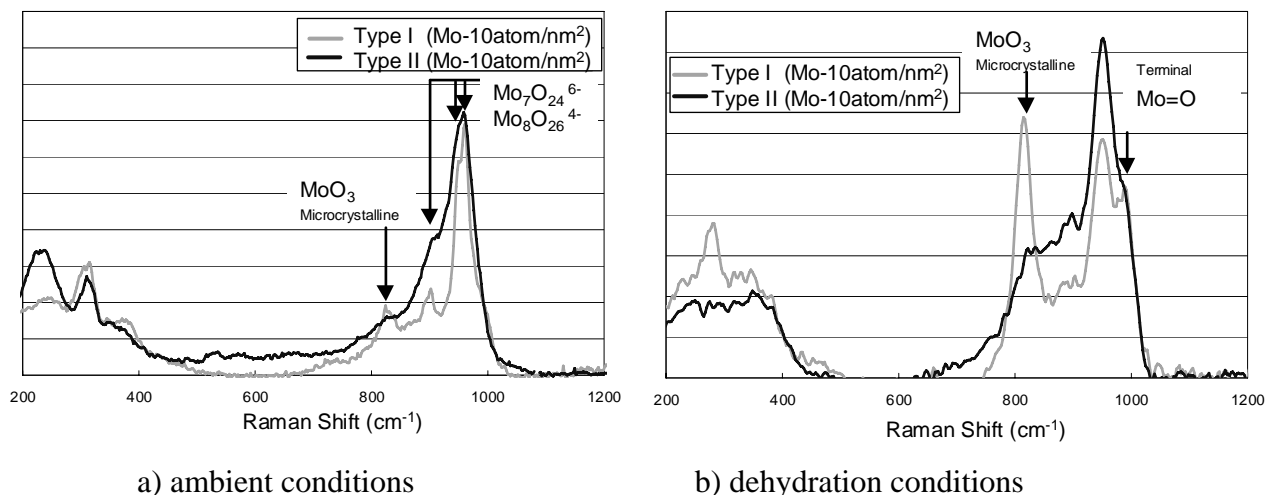
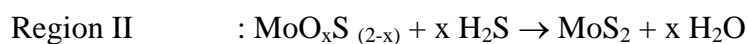
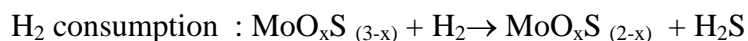
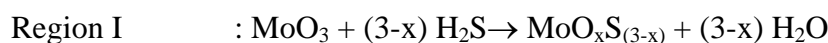


Figure 7. Raman spectra of NiMo type I and type II high loading catalysts

3.3. Metal and support interaction and morphology

To study the transformation of oxidic catalyst precursors into active sulfided metals, TPS technique is one of the powerful techniques.

In TPS, we observe two regions for the H₂S consumption. The first H₂S consumption peak (region I) is observed at lower temperature from RT to about 280 °C, the second is observed at higher temperature from 280 °C to 500 °C approximately. H₂ consumption is observed in between region I and II. From these observations, it has been concluded that the transformation from oxidic to sulfided phase mainly takes place in three steps as follows [14]. Firstly in region I, O-S exchange in MoO₃ occurs without H₂ consumption. Next H₂ is consumed sharply to reduce Mo(VI) to Mo(IV). Thirdly in region II, O-S exchange without H₂ consumption occurs, eventually forming MoS₂.



At increasing loading, the type I catalysts show higher H₂S consumption in region II than in region I (Fig. 8). It is likely that at low loading the active phase can disperse highly on support, resulting in easier sulfiding at lower temperature. The highest loading type I exhibits a higher H₂S consumption in region II, and H₂ consumption is occurring not only in the sharp peak after region I but also in region II. This could be attributed to the formation of crystalline phases as described above in TPR measurement, corresponding to the shift of the first peak in the lower-temperature to higher temperature.

At low loading, the type II catalysts show higher H₂S consumption in region I. This trend can be explained by the dispersion of active metal phase. Again, at low loading the active phase can be highly dispersed on support, resulting in higher H₂S consumption at lower temperature. However, it is interesting that the H₂S consumption in region I for type II is much more extended

than for type I (see Fig. 8); at every metal loading type II catalysts show easier sulfiding than type I. These results provide a simple interpretation about the strength of interaction between support and active metal precursor. The interaction of support and metal precursor is weaker in type II than type I, resulting in easily sulfiding of type II active phase at lower temperature.

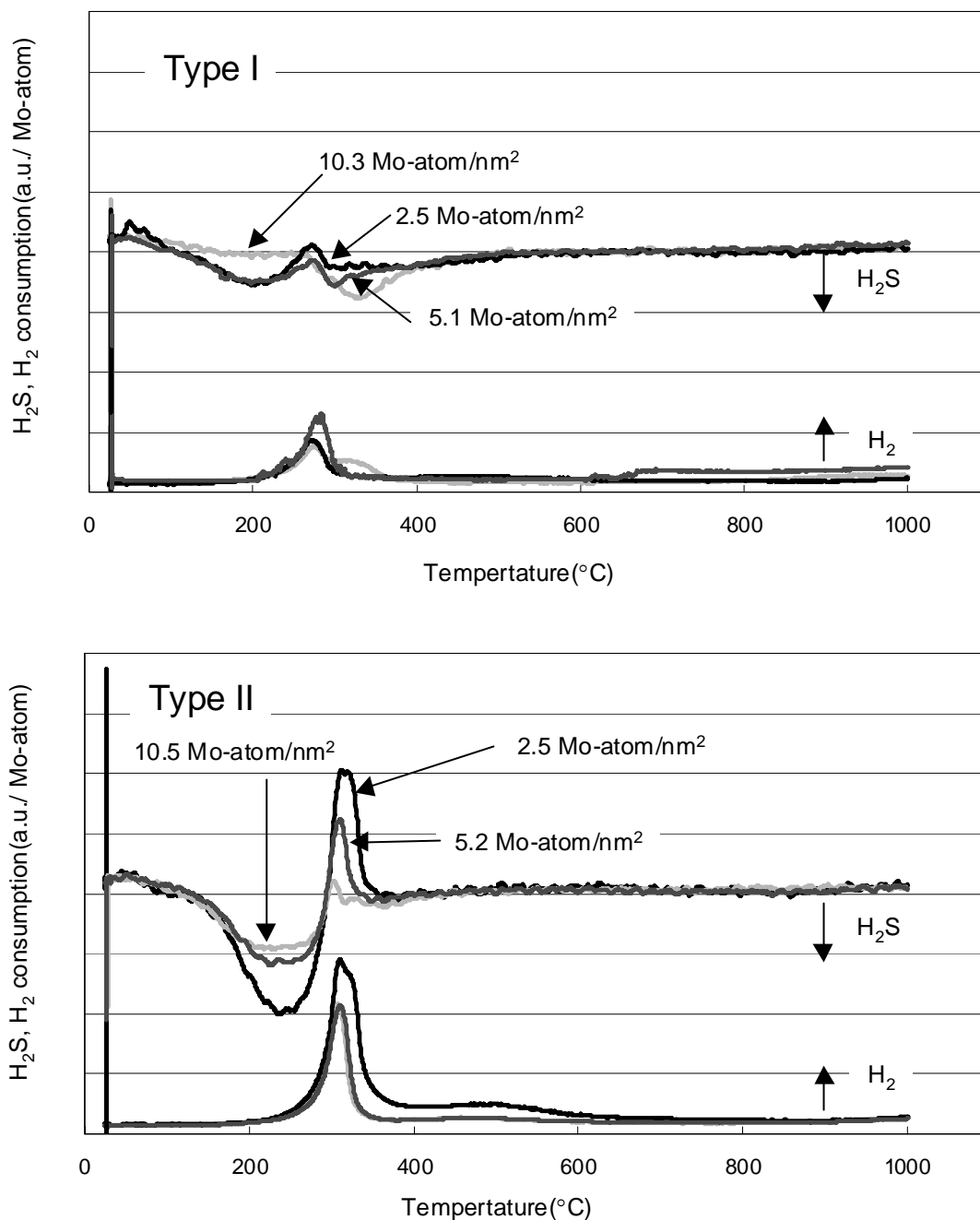


Figure 8. TPS spectra of NiMo type I and type II catalysts varying metal loading.

Moreover, from the integration of the H_2S consumption and the metal loading, the relative sulfiding ratio can be calculated, and the results are shown in table 2. Except for the highest loading type I and the lowest loading type II, all show full sulfiding, assuming that type I low

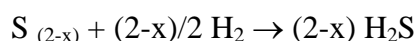
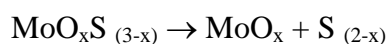
loadings catalysts are fully sulfided from the literature [14]. The observation that type I high loading catalyst is not completely sulfided confirms the earlier conclusion of the presence of relatively large crystallites. The reason is not so clear but for the type II lowest loading catalyst, the less total consumption of H₂S is due to the large release of H₂S during reduction.

Table 2. Relative H₂S consumption of the NiMo catalysts

	Mo(atom/nm ²)	H ₂ S consumption/ Mo atom*
Type I	2.5	104
	5.1	100
	10.3	86
Type II	2.5	(80)
	5.2	96
	10.5	104

* normalized type I Mo 5.1 atom/nm² as 100

For the hydrogen consumption, type II catalysts show the peak at higher temperature than type I. It has been suggested that the following reaction steps can be observed before H₂ consumption.



In type II, the hydrogen consumption is retarded because of the first reaction step, and the second reaction step corresponds to the sharp H₂S release with the hydrogen consumption. And this sharp H₂S release is observed more in low loading catalysts. From the literature [14], it was suggested that the wet catalysts show these reactions and this effect is explained tentatively by catalysis of O-S exchange by Brønsted acid sites on alumina. Therefore, it is not surprising that the type II catalyst with the lowest loading which has higher bare surface area of alumina and has some moisture because of catalyst preparation method (without calcinations after impregnation) shows the largest H₂S release. Moreover, compared with type I catalysts, type II catalysts have been pretreated less severely (the calcinations steps were avoided), suggesting a more hydrophilic character.

After loading metals on a support alumina, part of the support will be occupied by the metals. From the results of adsorption of SO₂, the free area of the surface on the support can be evaluated.

In Fig. 9, the chemical uptake of SO₂ against the SO₂ pressure is shown for the various catalysts. Below 0.5 bar the adsorption isotherm looks like a kind of Langmuir type. Above 0.5 bar, another type of adsorption seems to be occurring. It has been reported that SO₂ adsorbs on the basic OH groups on alumina, probably corresponding to the Langmuir type adsorption isotherm. At high SO₂ pressure SO₂ might adsorb on neutral OH groups. The SO₂ uptake is obtained from V value at 0.13 bar calculated by fitting Langmuir isothermal equation ($P/V = P/a + 1/ab$), using the data at SO₂ pressures below 0.5 bar.

In Fig. 10, the results of SO₂ uptake on catalysts varying metal loadings are shown. The SO₂ uptake on support is 0.3 mmol/g_{Al₂O₃}, measured after dipping into heptadecane solvent and

washing with toluene. The amount is $0.9 \text{ SO}_2 \text{ molecule/nm}^2$, while the amount of OH groups on $\gamma\text{-Al}_2\text{O}_3$ dehydrated at 773 K was reported as 4.5 OH/nm^2 [15]. The difference is probably due to the fact that SO_2 adsorbs on basic OH groups selectively. In the literature, SO_2 uptake measured by pulse method is $0.5 \text{ mmol/g}_{\text{Al}_2\text{O}_3}$ [16], in reasonable agreement with our results.

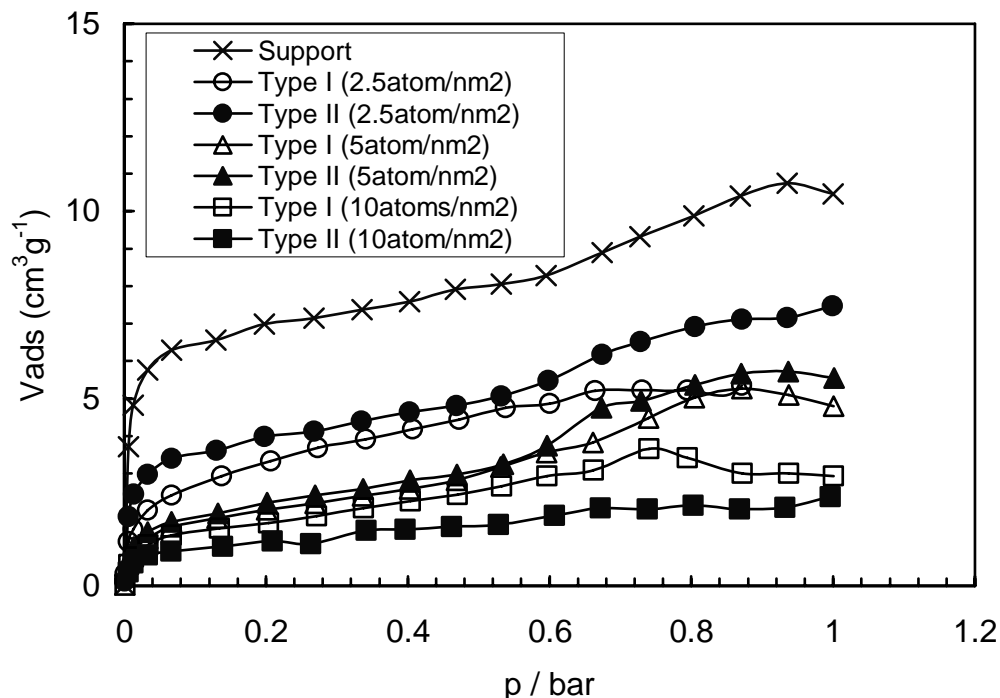


Figure 9. SO_2 Uptake on the NiMo catalysts after sulfiding.

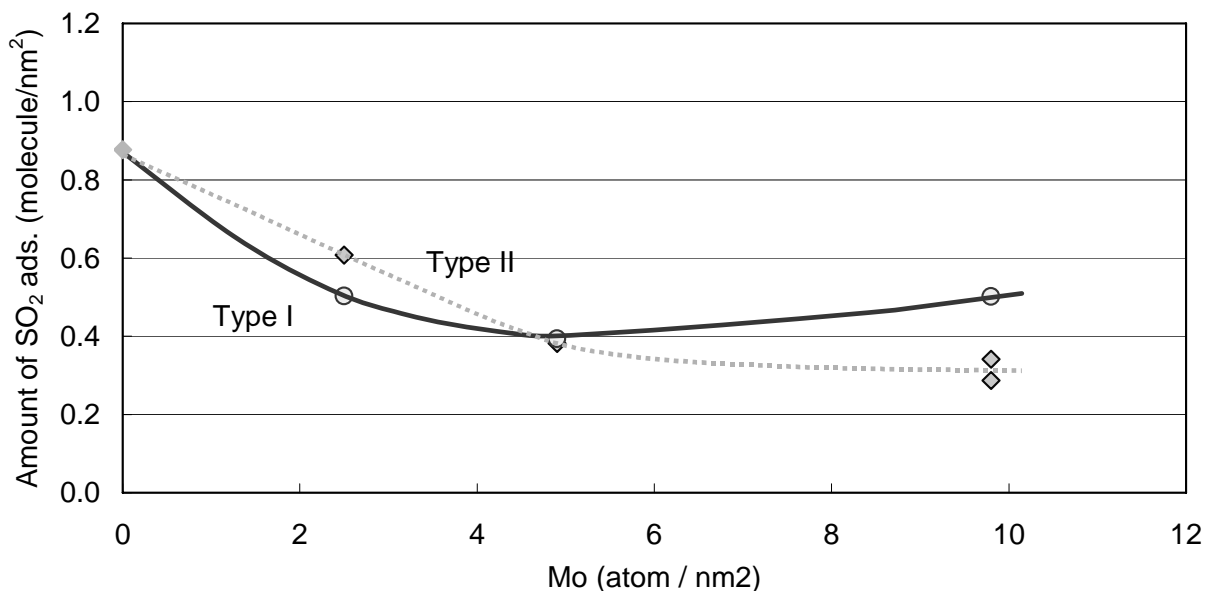


Figure 10. SO_2 Uptake on the NiMo catalysts varying Mo loading

As we expected, the SO_2 uptake corresponding to unoccupied area on support by active metals decreases sharply in an early stage at increasing loading, in both NiMo type I and type II

catalysts. It is logical that the SO₂ uptake becomes almost constant at Mo loadings above monolayer coverage except the highest loading type I. The monolayer surface coverage of MoO₃ was reported as approximately 4.6 atoms per nm² [3, 17]. The reason of decline of uptake in NiMo type I above monolayer coverage is probably that NiMo aggregates significantly, resulting in crystalline formation in agreement with the results from the other characterization techniques.

It is interesting that the SO₂ uptake in type II catalyst is higher than in type I at Mo loadings below monolayer coverage. It can be interpreted that the type I active phase occupies larger surface area on support than type II.

From those observations, the morphologies of type I and type II active phase are suggested to be as follows. At first sight, if the interaction of support and type II metal phase is weaker than type I, type II is expected to have a lower dispersion than type I. However, at higher loadings this is not correct. A simple model can illustrate this. For example, if type II active phase consists of two stacked slabs that have equal slab lengths of type I active phase, the dependency of the amount of accessible edge sites against metal loading is given in Fig. 11a. The observation that the SO₂ uptake in type II catalyst is higher than in type I at Mo loadings below monolayer coverage, is consistent with this model.

However, this is not the case at Mo loading above monolayer coverage. This could be explained as follows. Both SO₂ and Mo occupy OH groups on alumina and preferably occupy basic OH groups. However, SO₂ adsorbs more selectively on basic OH groups and does not adsorb on acidic OH groups, than Mo does. At increasing Mo loading, Mo probably prefers to occupy basic OH group first during impregnation in both type I and type II cases. However, after the calcination step in case of type I preparation, Mo could react with other OH groups than basic OH group. Therefore, below the monolayer coverage, the basic OH groups have been occupied completely by Mo, resulting in earlier saturation of SO₂ on type I catalysts. At high loading type II is more dispersed than type I and, as a consequence, the SO₂ uptake for type I exceeds that of type II.

In type I (based on the preparation method with calcination) high loading, it is clear that NiMo aggregates significantly, resulting in crystalline formation in agreement with the results from all characterization techniques. However, it is not easy to discuss the morphology after presulfiding. Since the surface area is not enough to accommodate Mo as a monolayer above monolayer surface coverage, some part of the aggregated species must be stacking like type II (not based on the preparation method, but on the morphology described above). It could be a very low-dispersed type II phase, although its TPS and TPR spectra showed significantly different features from type II catalysts (without calcination).

So, type II catalysts at high loading exhibit a relatively large dispersion as shown in Fig. 11a. Another possibility of the MoS₂ orientation on support was suggested as edge-bonded active phases. It was pointed out that it is difficult to distinguish between edge-bonded active phase and basal bonded, i.e. planar bonding of MoS₂ to the support by HRTEM, as the conventional supports have the artefacts associated with porous structure. In a study using γ -Al₂O₃ thin films it has been reported that both of them are observed [18]. As shown in Fig. 11b, this would not change the conclusion that the combination of high loading and high dispersion exists for type II catalysts, in agreement with all our results.

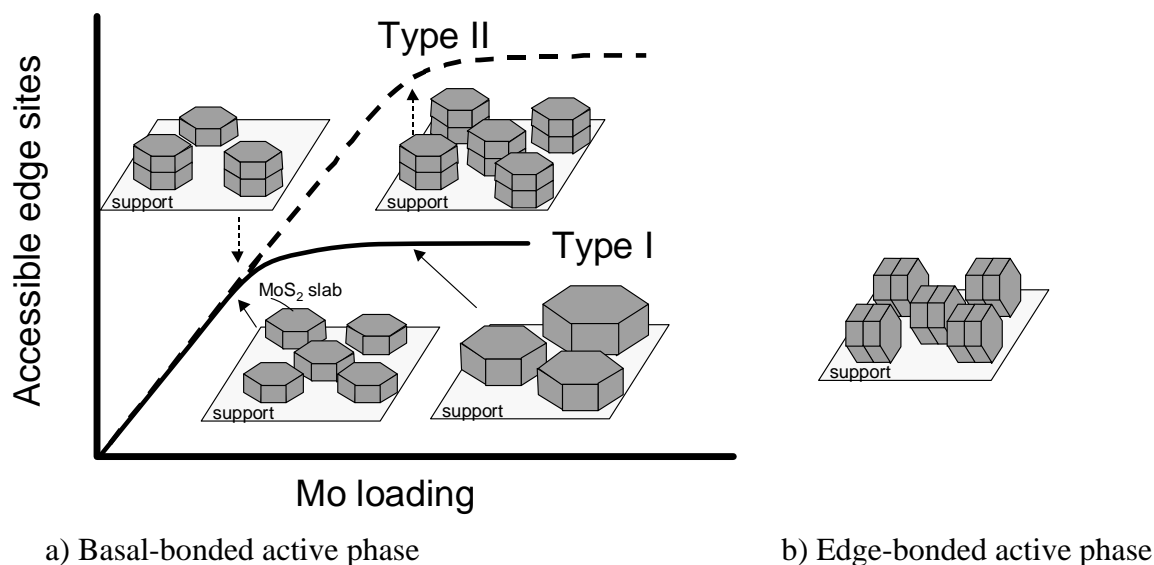


Figure 11. Possible models of morphology of MoS₂ in type I and type II active phase

4. Conclusions

Type I and type II NiMo catalysts have been characterized by various techniques such as XRD, TPR, TPS, Laser Raman spectroscopy, and SO₂ adsorption. At increasing Mo loading above monolayer surface coverage, type I active phase forms some aggregated crystallites on the support alumina, probably a mixture of MoO₃ and α -NiMoO₄. It is remarkable that type II active phase can achieve relatively high metal dispersion above monolayer surface coverage.

It is suggested that the type II active phase has weaker interaction with the support, which originated from their oxidic precursors. At low loading, both type I and type II active phase can be highly dispersed, although probably type I is more like a single phase highly dispersed species because of stronger interaction with support than type II. On the other hand, type I active phase forms aggregated microcrystalline at increasing loading, while the high dispersion of type II active phase can be maintained, existing as the specific morphology because of weaker interaction with support. All results are consistent with the assumption that the type II active phase consists of several stacked layers of MoS₂ slabs or edge-bonded layers, and type I active phase is like a single slab.

Acknowledgements

Johan C. Groen is appreciated for the analysis of SO₂ adsorption.

References

- [1] R.Candia, O.Sørensen, J.Villadsen, N.-Y.Topsøe, B.S.Clausen, and H.Topsøe, *Bull.Soc.Chim.Belg.*, **93** (1984) 763.
- [2] S.M.A.M.Bouwens, F.B.M.Vanzon, M.P.Vandijk, A.M.Vanderkraan, V.H.J.Debeer, J.A.R.Van Veen, and D.C.Koningsberger, *Journal of Catalysis*, **146** (1994) 375.
- [3] I.E.Wachs, *Catalysis Today*, **27** (1996) 437.
- [4] I.E.Wachs and L.L.Murrell, *Journal of Catalysis*, **90** (1984) 150.
- [5] M.Yamazaki, H.Magara, N.Koizumi, and M.Yamada, *Catalyst Deactivation 1999*, **126** (1999) 155.
- [6] J.A.R.Van Veen, H.A.Colijn, P.A.J.M.Hendriks, and A.J.Van Welsenens, *Fuel Proc.Tech.*, **35** (1993) 137.
- [7] Jorge Laine and Kerry C.Pratt, *Industrial & Engineering Chemistry Fundamental*, **20** (1981) 1.
- [8] J.L.Brito and J.Laine, *Applied Catalysis*, **72** (1991) L13.
- [9] P.Arnoldy, M.C.Franken, B.Scheffer, and J.A.Moulijn, *J.Catal.*, **96** (1985) 381.
- [10] K.S.Chung and F.E.Massoth, *J.Catal.*, **64** (1980) 332.
- [11] H.C.Hu, I.E.Wachs, and S.R.Bare, *Journal of Physical Chemistry*, **99** (1995) 10897.
- [12] G.Mestl, *J.Mol.Catal.A: Chem.*, **158** (2000) 45.
- [13] P.Dufresne, E.Payen, J.Grimblot, and J.P.Bonnelle, *J.Phys.Chem.*, **85** (1981) 2344.
- [14] P.Arnoldy, J.A.M.Van den Heijkant, G.D.De Bok, and J.A.Moulijn, *J.Catal.*, **92** (1985) 35.
- [15] H.Knozinger and P.Ratnasamy, *Catal.Rev.-Sci.Eng.*, **17** (1978) 31.
- [16] M.Yamazaki, H.Magara, N.Koizumi, and M.Yamada, *Abstracts of 28th Annual meeting of the Japan Petroleum Institute*, **A08** (1998)
- [17] A.L.Diaz and M.E.Bussell, *Journal of Physical Chemistry*, **97** (1993) 47.
- [18] Y.Sakashita and T.Yoneda, *Journal of Catalysis*, **185** (1999) 487.

4

Reaction pathways on NiMo/Al₂O₃ catalysts for hydrodesulfurization of diesel fuel

Abstract

Ranking of catalytic activities of several NiMo catalysts was performed using various model compounds: thiophene (TH), tetrahydrothiophene (ThTH), dibenzothiophene (DBT) and 4,6-dimethyldibenzothiophene (4,6-DMDBT). Type I and type II differ most at high loading. Higher loading type I catalyst shows lower DDS activity and only slightly increased HG activity. Higher loading Type II phase shows higher DDS and extremely high hydrogenation (HG) activity and, as a consequence, high HDS activity for TH and 4,6-DMDBT.

In order to be able to generalize the results a CoMo catalyst was included in the study. The results at first sight are not fully consistent. Although this catalyst shows a low HG activity in HDS of DBT, it shows a relatively high activity in HDS of 4,6-DMDBT. Two reaction schemes were examined, one of them taking into account a dehydrogenation step. Although a dehydrogenation step could occur substantially, under our experimental conditions, the main cause of ranking differences is the difference of susceptibility for NiMo and CoMo catalysts to H₂S.

The contents of this chapter was published as:

N. Kagami, B. M. Vogelaar, A. D. van Langeveld and J. A. Moulijn, *Applied catalysis A*. **293** (2005) 11.

1. Introduction

For a sustainable society deep desulfurization of transport fuels is crucial. It is not surprising that environmental legislation has become more and more strict. Some refineries in the world have already started producing ultra low sulfur diesel (less than 50 ppm) and in the near future environmental regulation will become very strict, probably less than 10 ppm.

In principle, many improvements for hydrotreating processes are conceivable. On the one hand, chemical engineering solutions, and on the other hand, the development and selection of advanced catalysts suggest themselves [1]. The latter is the subject of this paper. In modern catalyst development it is important to fundamentally elucidate the relation between catalyst structure and reaction mechanism. Historically, thiophene often has been a model compound in HDS research, because of its convenience. However, thiophene is exceptionally reactive and, as a consequence, its use as model compound is not straightforward. Dibenzothiophene and its derivatives, especially so-called β -substituted DBTs, are more refractory and therefore more appropriate model compounds for the evaluation of the HDS activity in deep diesel desulfurization [2-4].

It has been found that the so-called type II NiMoS (or CoMoS) phase has a higher activity for thiophene HDS than the so-called type I [5, 6]. For catalyst design such a conclusion is of major importance. However, this has not been unequivocally proven to hold for DBT HDS [7-9]. This work will show that the two phases (type I and II) behave quite differently for TH and DBT. An explanation will be given based on activity-structure relationships and evaluation of different reaction rates on the level of the elementary steps of each pathway for HDS of various model sulfur compounds.

It has been reported that sulfur compounds react through two pathways, viz., the so-called direct desulfurization (DDS) and the hydrogenation (HG) pathway [10-12]. In HDS of thiophene, it is almost impossible to discriminate between those pathways from product yields, as butadiene produced via DDS pathway is rapidly hydrogenated to butene and butane, the product of HG. On the other hand, in HDS of DBT and 4,6-DMDBT, both pathways can be distinguished as the consecutive hydrogenation of (substituted) biphenyls is very slow [13],[14], especially under H_2S rich conditions [15, 16]. As a representative reaction for DDS in the gas phase, HDS of tetrahydrothiophene (ThTH) could be applicable, as it has been proposed to be one of the most important intermediates for HDS of TH [17, 18]. In order to assess the potential of using ThTH as a model compound, the ranking of TH and ThTH is informative.

There are several dominant factors determining the ranking of HDS catalysts. First of all, more complete pathways could be taken into account, for instance including dehydrogenation steps in the HG pathway [19]. A priori, a thermodynamic analysis can indicate if such a scheme is reasonable. Unfortunately, there are only a few reports discussing detailed thermodynamics in DBT and 4,6-DMDBT HDS reactions [13, 16, 20]. Next important factor is the susceptibility of catalysts to H_2S adsorption. It is well known that H_2S inhibits HDS reaction significantly for (substituted) DBT, especially with respect to the DDS pathway [15, 21-23]. However, few reports are available to discuss about the consequences for the ranking of the HDS catalysts.

To elucidate the properties of catalysts for reaction pathways, we carried out ranking tests using various model compounds: TH, ThTH, DBT and 4,6-dimethyldibenzothiophene. We

focused on NiMo catalysts, but for comparison we included a CoMo catalyst. The influence of the presence of H₂S was taken into account explicitly. In order to get an indication of the possible contribution of dehydrogenation steps a thermodynamic analysis was carried out.

2. Experimental

2.1. Activity measurement Catalyst preparation

NiO-MoO₃/Al₂O₃ catalysts (type I and type II) and CoMo/Al₂O₃ (type I) were prepared via the conventional liquid phase pore filling method. High purity γ - Al₂O₃ in the form of 1.5 mm extrudates were impregnated using aqueous solutions containing the required amount of Ni and Mo, according to the literature [24]. In the case of type I, after the supports had been impregnated by the metal solution, they were dried at 120 °C for 16 hours and calcinated at 500 °C for 4 hours. While in type II, only the drying step was applied (see Chapter 2).

The composition of catalyst was measured by INAA (Instrumental Neutron Activation Analysis). Specific surface area of alumina support was measured by nitrogen adsorption method (BET). Two different metal loading catalysts were prepared; high and low loading with 5, 10 Mo atom per nm², respectively. All catalysts were prepared to have the same molar ratio of Ni or Co to Mo. The results of elemental analysis are shown in Table 1.

For the characterization, the prepared catalysts were examined by XRD (X-ray diffraction), TPS (temperature programmed sulfidation), and Raman spectroscopy to study the transformation of oxidic catalyst precursors into active sulfided metals (see Chapter 3).

Table 1. Composition of the NiMo and CoMo catalysts.

	Co/Mo, or Ni/Mo molar ratio	Mo loading (atom / nm ²)
NiMo type I low loading	0.34	5.1
NiMo type II low loading	0.34	5.2
NiMo type I high loading	0.35	10.3
NiMo type II high loading	0.35	10.5
CoMo type I low loading	0.33	5.2

2.2. Activity measurements

Before the reaction, catalysts were presulfided at 370 °C. All activity tests were carried out at 350 °C, a typical temperature for the HDS of diesel fuel. The activity for gas-phase TH and tetrahydrothiophene (ThTH) HDS was tested in a micro flow reactor at atmospheric pressure and a flow rate of reaction mixture of 100 ml/min, containing 5.0 vol.% TH in balance H₂ (total flow rate 175 ml/min for 5.0 vol.% ThTH). The amount of catalyst was 200 mg for TH HDS and 15 mg for ThTH HDS, respectively, diluted with SiC particles. The activity for liquid-phase DBT and 4,6-DMDBT HDS was determined in a batch reactor at 5 MPa total pressure in balance hydrogen. Catalysts were crushed and sieved properly before the test, to satisfy the criteria for avoiding mass transfer limitations [9]. The amount of catalyst placed in the reactor was 100 mg for DBT HDS and 200mg for 4,6-DMDBT HDS, respectively. The feed consisted of DBT in hexadecane and 4,6-DMDBT in tetradecane. In both cases sulfur concentration in feed was 350

ppm. The inhibiting effect of H_2S is strong for HDS reactions. To mimic commercial reactor conditions, dimethyldisulfide (DMDS) was added in the liquid phase reactions to adjust the H_2S pressure to constant level (1.5 bar). This also provided the condition that the effect of self-produced H_2S was minimized. Gas chromatography with a FID detector was used for quantitative analysis of products. In liquid phase reaction, inert hydrocarbon (0.2 wt% octadecane) was added as the internal standard in the feed for GC analysis.

3. Results

3.1. Ranking of NiMo catalysts activities, using various sulfur compounds

It is well known that cyclic sulfur compounds react through two pathways, so-called DDS and HG, and that the ratio of DDS to HG depends on the reactant molecules, the catalysts properties and the reaction conditions. Reaction pathways of the reactants applied are shown in Scheme 1. The numbers refer to the values of the quasi-first order rate constants for a high-loading NiMo catalyst under industrial conditions. It is possible to discriminate from the product distribution between DDS and HG in DBT and 4,6-DMDBT, but not in TH because of the fast hydrogenation of butadiene. Therefore, ThTH, the intermediate of HG pathway, was also tested to represent DDS reaction in gas phase conditions. Fig. 1 shows the pseudo first order rate constants for the catalysts and model compounds studied.

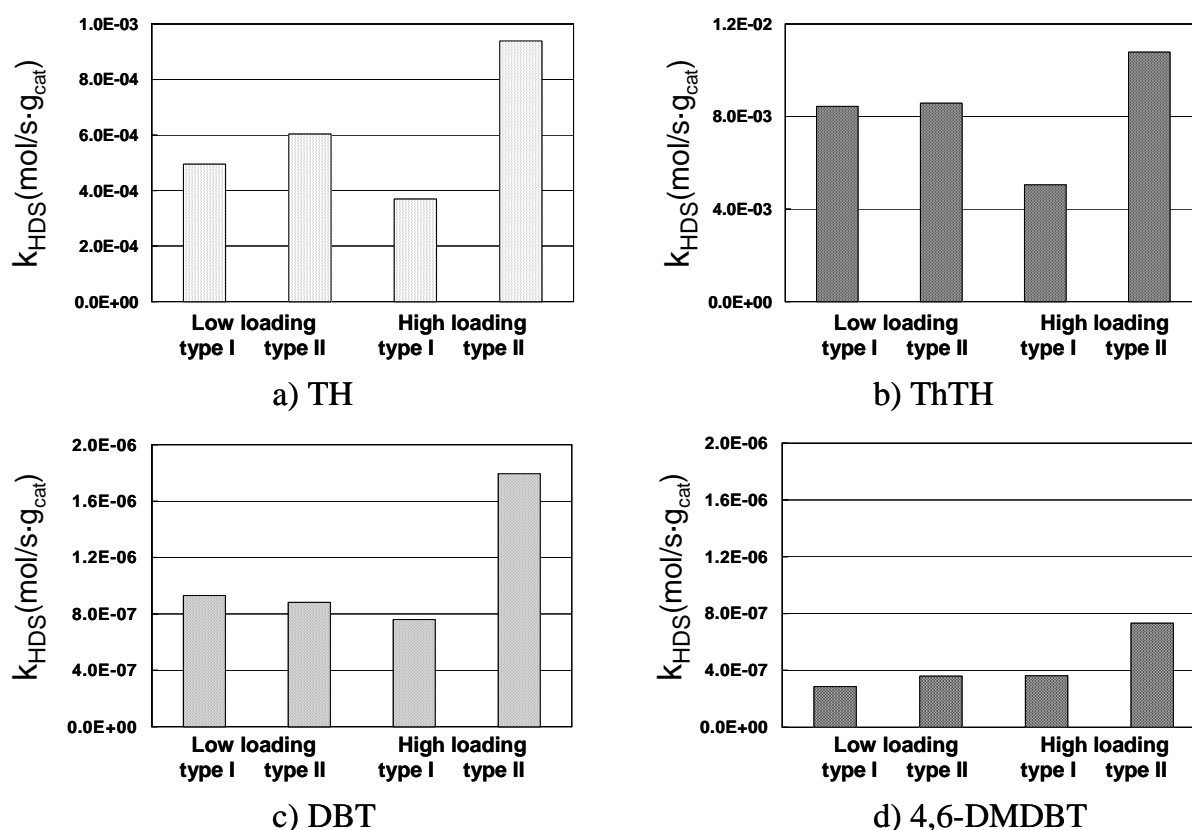
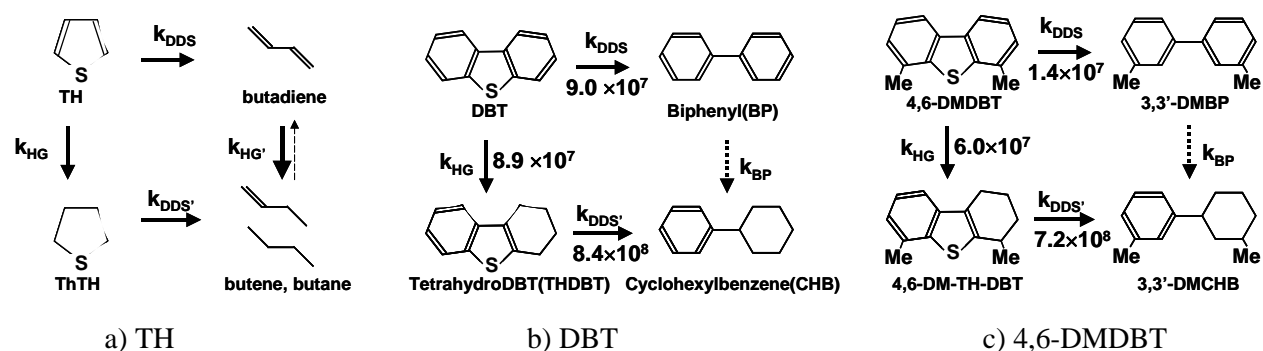


Figure 1. Ranking of NiMo catalysts for HDS of TH, ThTH, DBT and 4,6-DMDBT
a), b) 350 °C, 1 bar. c), d) 350 °C, 50 bar ($p_{\text{H}_2\text{S}}$: 1.5 bar).

At low metal loading, compared to type I, type II catalyst shows higher activity for TH and 4,6-DMDBT, but this is not the case for DBT. These rankings are in agreement with literature [7]. It is noteworthy that the type II catalyst activity in all cases increases with metal loading, while this is not the case for type I activity; this will be discussed later.

In gas phase reaction conditions, the reactivity of ThTH is extremely high, around 15 times, higher than TH, in agreement with literature [25, 26]. These results imply that the HG pathway might be dominant for TH. Only a trace amount of TH was detected in ThTH HDS, so the reverse reaction of ThTH to TH can be neglected.

In liquid phase reaction, 4,6-DMDBT is around 3 times more refractory than DBT. In these cases, we can discriminate well between the DDS and HG rate as shown in Scheme 1 b), c). (Substituted) biphenyl and (substituted) cyclohexylbiphenyl were observed showing the reaction pathways of DDS and HG, respectively. Moreover, (substituted) tetrahydro-DBT was observed, supporting the reaction scheme. A very small amount of (substituted) hexahydro-DBT was observed, but neglected in the kinetic analysis.



Scheme 1. Reaction pathways of HDS of TH, DBT and 4,6-DMDBT (NiMo high-loading Type II catalyst, 350 °C, 50 bar ($p_{\text{H}_2\text{S}}$: 1.5 bar))

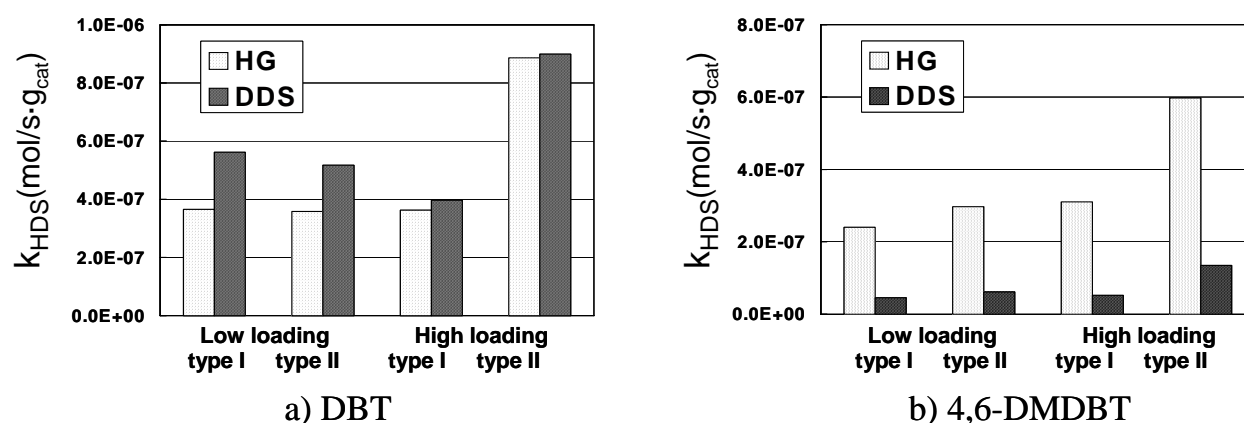


Figure 2. DDS vs HG pathways of NiMo catalysts for HDS of DBT and 4,6-DMDBT a), b) 350 °C, 50 bar ($p_{\text{H}_2\text{S}}$: 1.5 bar)

Table 2. Rate constants ($k \times 10^7$ (mol/s·g_{cat})) for reaction pathways for HDS of DBT and 4,6-DMDBT on NiMo catalysts.

a) DBT

	k_{HDS}	k_{DDS}	k_{HG}	$k_{\text{DDS}'}$	$k_{\text{HG}}/k_{\text{DDS}}$	$k_{\text{DDS}'}/k_{\text{DDS}}$	$k_{\text{DDS}'}/k_{\text{HG}}$
NiMo type I low loading	9.3	5.6	3.7	36	0.65	6.5	10
NiMo type II low loading	8.8	5.2	3.6	48	0.69	9.4	14
NiMo type I high loading	7.6	4.0	3.6	33	0.91	8.4	9.2
NiMo type II high loading	18	9.0	8.9	84	0.99	9.3	9.4

b) 4,6-DMDBT

	k_{HDS}	k_{DDS}	k_{HG}	$k_{\text{DDS}'}$	$k_{\text{HG}}/k_{\text{DDS}}$	$k_{\text{DDS}'}/k_{\text{DDS}}$	$k_{\text{DDS}'}/k_{\text{HG}}$
NiMo type I low loading	2.9	0.46	2.4	27	5.3	59	11
NiMo type II low loading	3.6	0.62	3.0	34	4.8	56	12
NiMo type I high loading	3.6	0.52	3.1	32	5.9	62	10
NiMo type II high loading	7.3	1.4	6.0	72	4.4	53	12

Pseudo first order rate equations were adopted and rate constants of each step were given by numerically fitting, using least square method; the values for high-loading NiMo are shown in Scheme 1 b), c). The rate constants of DDS and HG pathways on NiMo catalysts for DBT and 4,6-DMDBT are shown in Fig. 2 and Table 2. On the one hand, for DBT, both the DDS and the HG pathways are kinetically significant for all catalysts, while DDS is slightly more important than HG under our experimental conditions. On the other hand, for 4,6-DMDBT, the HG pathway is dominant for all catalysts ($k_{\text{HG}}/k_{\text{DDS}}$ 4 to 6). The consecutive DDS rates in HG pathways are approximately 10 times higher than the HG rates.

3.2. Comparison with CoMo catalyst

Fig. 3 shows the comparison of the reaction rate constants of NiMo and CoMo catalysts at low loading. The CoMo catalyst shows slightly lower activity than NiMo for HDS of TH, ThTH, and DBT, but slightly higher activity in HDS of 4,6-DMDBT. Especially the HG activity for DBT is relatively low on the CoMo catalyst.

Table 3 shows the rate constants for the individual steps for the HDS of DBT and 4,6-DMDBT on CoMo catalyst. Again, $k_{\text{HG}}/k_{\text{DDS}}$ is low for DBT, but not for 4,6-DMDBT. In the latter case it is even higher than that of NiMo catalysts (Table 2). It is striking that $k_{\text{DDS}'}/k_{\text{HG}}$ is enhanced on CoMo in comparison to NiMo catalysts for both DBT and 4,6-DMDBT HDS.

It is reported that usually NiMo shows higher HG selectivity than CoMo [27-29]. At first sight it is surprising that HG selectivity of CoMo is relatively high in 4,6-DMDBT HDS. The major differences of the literature and our work are the experimental conditions, viz., temperature and H₂S pressure. [27] and [28] were performed at lower temperature 310-320 °C than our condition (350 °C) and H₂S was not added (our experiment: H₂S 1.5 bar). In the literature [29], temperature was 340 °C and H₂S pressure was 0.5 bar. The authors did not discuss this point, but the difference of HG selectivity on NiMo and CoMo catalysts in 4,6-

DMDBT HDS was rather small. To elucidate the consistency, the possible occurrence of dehydrogenation reactions and susceptibility to H₂S were investigated.

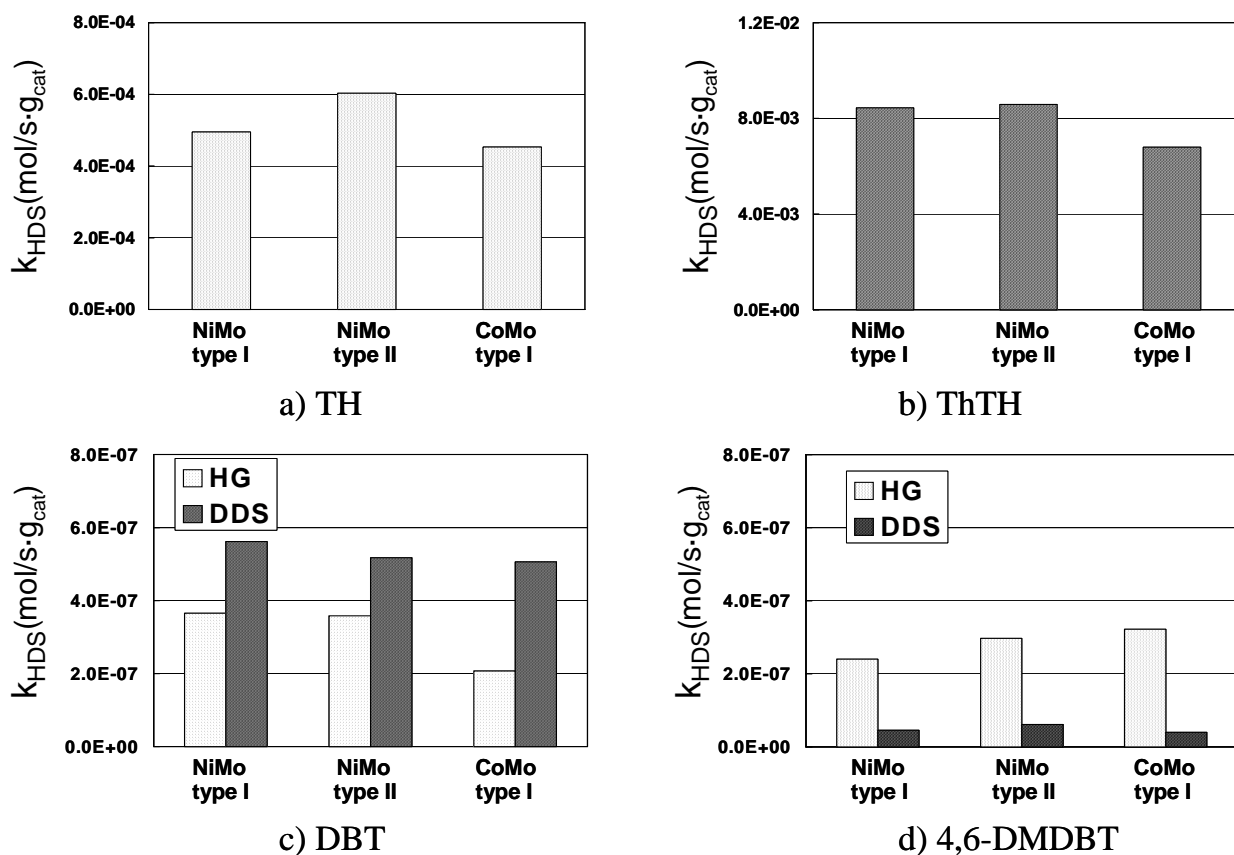


Figure 3. Comparison of low-loading NiMo and CoMo catalysts for HDS of TH, ThTH, DBT and 4,6-DMDBT

Table 3. Rate constants ($k \times 10^7$ (mol/s.g_{cat})) for reaction pathways of HDS of DBT and 4,6-DMDBT on CoMo catalyst.

a) DBT HDS

	k_{HDS}	k_{DDS}	k_{HG}	$k_{DDS'}$	k_{HG}/k_{DDS}	$k_{DDS'}/k_{DDS}$	$k_{DDS'}/k_{HG}$
CoMo type I low loading	7.1	5.1	2.1	36	0.41	7.1	17

b) 4,6-DMDBT HDS

	k_{HDS}	k_{DDS}	k_{HG}	$k_{DDS'}$	k_{HG}/k_{DDS}	$k_{DDS'}/k_{DDS}$	$k_{DDS'}/k_{HG}$
CoMo type I low loading	3.6	0.40	3.2	59	8.0	148	18

3.3. H₂S inhibiting effect

In recent reports the difference of susceptibility to H₂S of CoMo and NiMo for 4,6-DMDBT HDS reactions has been highlighted [30, 31]. CoMo shows less susceptibility to H₂S, and as a consequence, it shows higher activity than NiMo at H₂S > 0.3 bar. H₂S partial pressure in our experimental condition was much higher (1.5 bar). However, an opposite trend was also reported [15]. It was suggested that the DDS pathway is more inhibited by H₂S than the HG pathway, and

that would suggest that CoMo catalyst could suffer more from inhibition by H₂S [32]. Therefore, literature is contradictory and experimental data is needed.

The activities of CoMo and NiMo catalysts without H₂S addition were tested at 350 °C for HDS of 4,6-DMDBT to check their susceptibility to H₂S. The results are shown in Fig. 4 and Table 7. It is clear that without H₂S addition, the NiMo catalyst shows higher HDS activity than the CoMo catalyst. However, the NiMo catalyst is more inhibited by H₂S, whereas the CoMo stays almost constant with addition of H₂S at 1.5 bar. The main difference of CoMo and NiMo regards the susceptibility of HG pathway to H₂S. The rate constant k_{HG} of CoMo catalyst is not retarded by H₂S, but rather significantly enhanced.

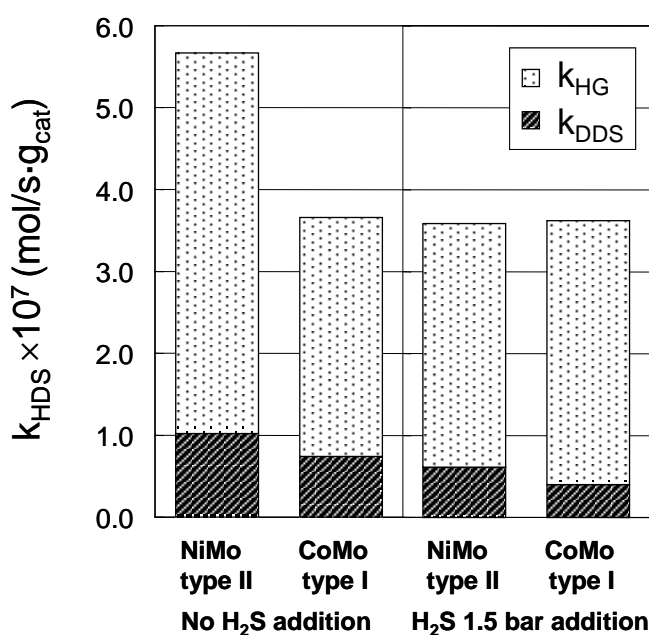


Figure 4. Susceptibility to H₂S of NiMo and CoMo low loading catalysts for HDS of 4,6-DMDBT

4. Discussion

4.1. Reactivity of various sulfur compounds and ranking of NiMo catalysts activities

The main difference between DBT and 4,6DMDBT is in the DDS step, as shown in Fig. 2 and Fig. 3. This can be explained by the strong steric hindrance of the two methyl groups in the coordination of sulfur on the active sites, needed for DDS [32]. In contrast, DDS of the hydrogenated intermediates occurs relatively fast. The opposite effects of steric hindrance and the electron density on sulfur atom in the molecule could explain that the difference between DBT and 4,6-DMDBT is small after hydrogenation. Compared with DBT and 4,6-DMDBT, the steric restrictions of the hydrogenated intermediates are reduced. By the two methyl groups the electron density on sulfur atom is increased, which strengthens the coordination of the molecule to the active site [33].

Fig. 5 shows the relative rate constants of NiMo catalysts normalized with respect to type I low loading catalyst activity. It is striking that ranking based on TH is similar to that based on 4,6-DMDBT. It is obvious that catalysts with higher HG activity show higher HDS activity for

TH and especially for 4,6-DMDBT in NiMo catalysts. This suggests that TH reacts also mainly via the HG pathway. In literature support for this can be found [34]. Recently, a mechanism of TH via HG pathway has been proposed in a theoretical study, using molecular simulation [35]. According to the literature, the most stable coordination geometry of thiophene is flat adsorption configuration (η^5 -bondings), and after ring is saturated, hydrogenolysis occurs. This supports that HG pathway could be the main pathway. However, it is under discussion as it has been observed by IR that the initial steps are $\eta^1(\text{S})$ adsorption of thiophene at the surface of sulfided Mo/Al₂O₃, where as C-S bonds are significantly weakened [36].

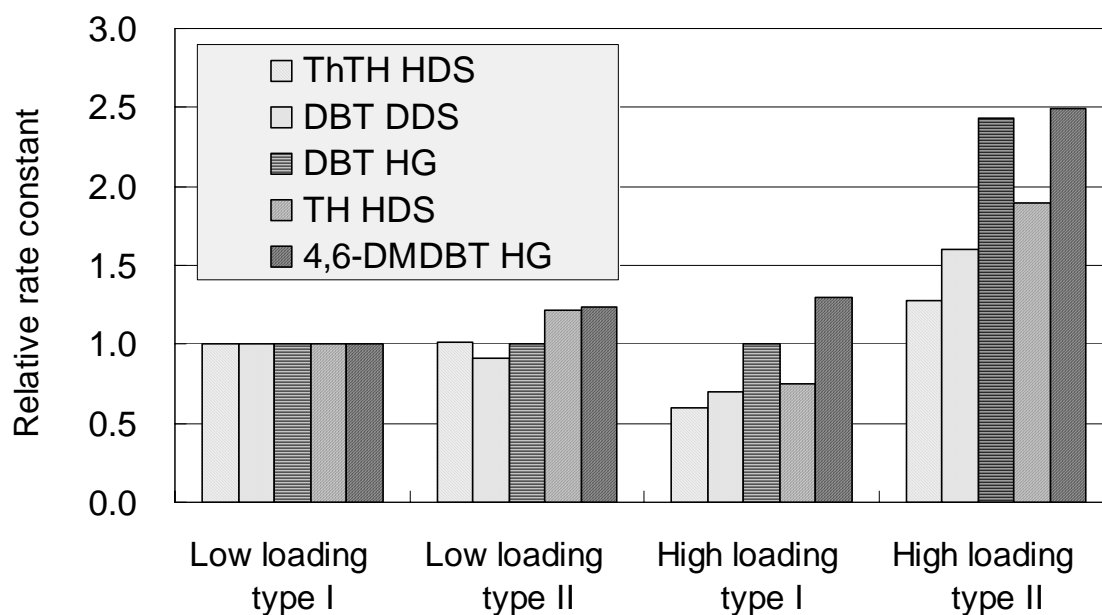


Figure 5. Ranking of NiMo catalysts in terms of the DDS and HG pathways (TH, ThTH: 350 °C, Pressure 1bar. DBT, 4,6-DMDBT: 350 °C, Pressure 50 bar ($p_{\text{H}_2\text{S}}$:1.5 bar))

ThTH HDS activity behaves similarly to DBT DDS. The interpretation is that both reactions are DDS reactions. This observation can be correlated with structure data from literature. It is reported for unpromoted MoS₂ alumina catalysts, that single layer catalyst shows relatively high HDS activity for ThTH and multilayer shows high HDS activity for TH [26]. Moreover, it has been proposed that type II active phase consists of stacked slabs of MoS₂ and type I is more like single phases present on the alumina support [37, 38]. Mostly the edge and corner of MoS₂ slabs are believed to host the active sites for HDS reaction. Type II active phase, protruding from support surface can have much space in the edges of MoS₂ slabs, without the interference of support surface. Therefore, it is likely that such active phases can provide more opportunities for a cyclic sulfur molecule to adsorb in the flat configuration that might be the first step of HG pathway. In summary, it is tentatively concluded that the higher stacking active phase shows higher HG selectivity, although further investigation is necessary to prove it. The trend that higher stacking is more favorable for TH HDS than for ThTH HDS is consistent with this conclusion.

As shown in Fig 1, type II catalyst exhibits increasing activity at increasing metal loading, while this is not the case for type I catalyst. To examine this observation, several characterization techniques were applied (see Chapter 3). The monolayer surface coverage of MoO_3 was reported as approximately 4.6 atoms per nm^2 [39, 40]. For the high metal loading catalysts, the metal loading exceeds the monolayer surface coverage. In XRD, only the high loading type I catalyst shows the bands assigned as MoO_3 or NiMoO_4 [41]. In Raman spectroscopy, again the high loading type I catalyst shows the Raman shift assigned to aggregated microcrystalline MoO_3 species [40].

From these observations, it is concluded that above monolayer surface coverage type II active phase can achieve higher metal dispersion, while type I active phase forms aggregated crystals on the support alumina. Probably, type II active phase consists of stacked slabs, and is weakly bonded to the support. TPS measurements were carried out to get information about the strength of interaction between support and active metal precursor. It was found that type II active phase is easily presulfurized at relatively low temperature in TPS. This confirms that the interaction of support and metal precursor is weaker in type II than type I [42].

At first sight, if the interaction of support and type II metal phase is weaker than type I, type II is expected to have lower dispersion than type I. However, a simple model can explain this counterintuitive observation. For example, if type II active phase consists of two stacked slabs that have equal slab lengths of type I active phase, the dependency of the amount of accessible edge sites against metal loading is given in Fig. 6 a). So, it is not surprising that type II catalysts at high loading exhibit a relatively large dispersion.

Another possibility of the MoS_2 orientation on support was suggested as edge-bonded active phases [43]. As shown in Fig. 6 b) this would not change the conclusion that the combination of high loading and high dispersion exists for type II catalysts.

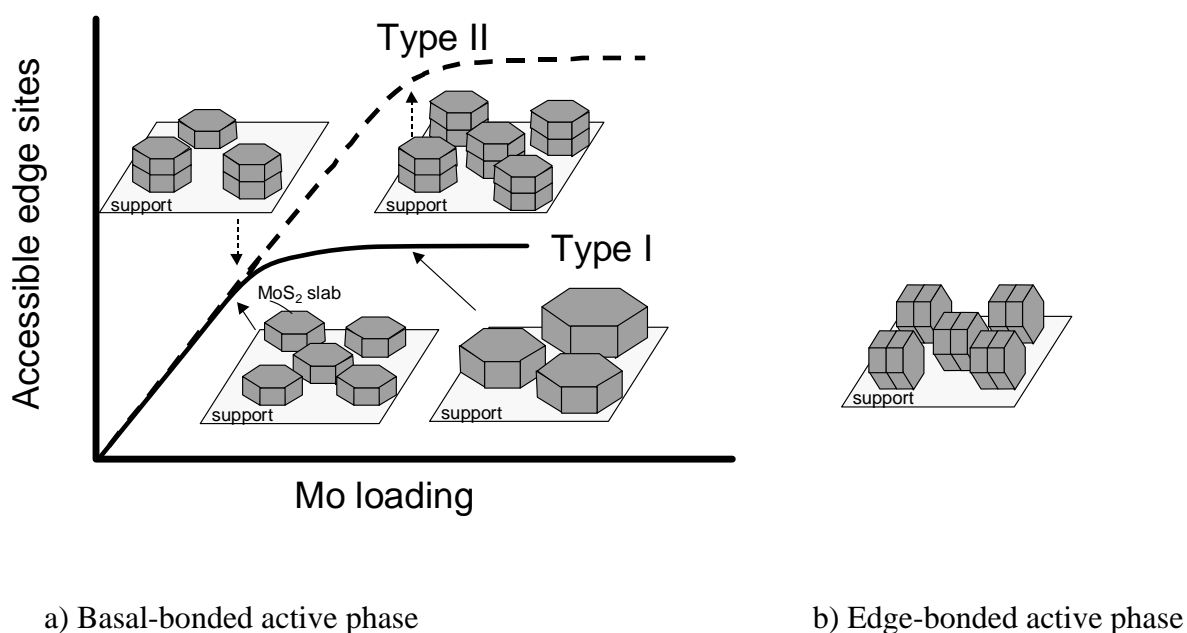
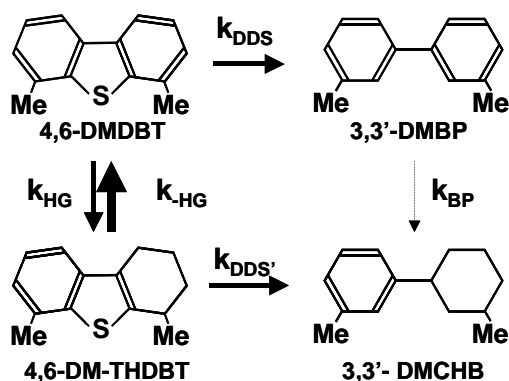


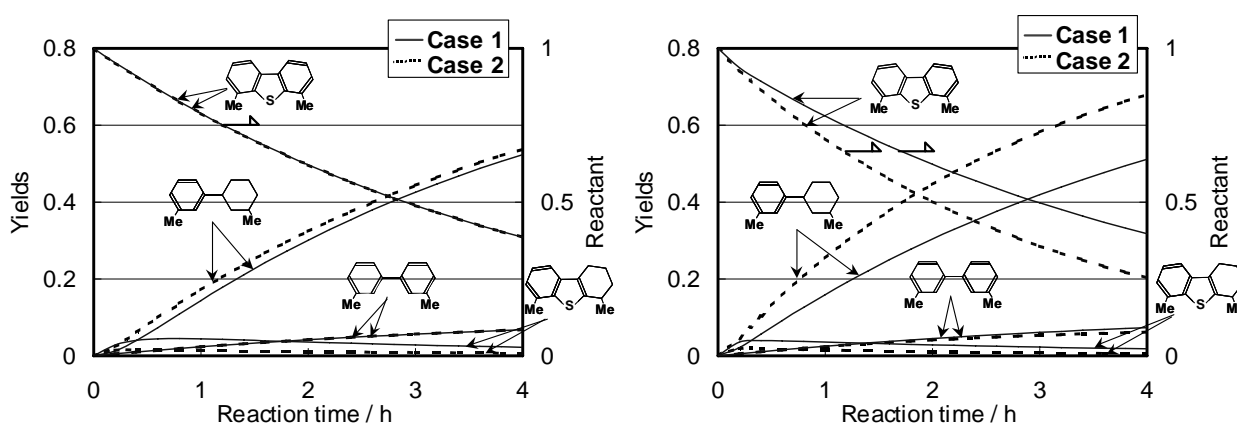
Figure 6. Possible models of morphology of MoS_2 in type I and type II active phase

4.2. The possible impact of dehydrogenation reactions

The incorporation of a dehydrogenation step as shown in Scheme 2 could be important. As already mentioned, the rate of consecutive DDS (k_{DDS}) in HG pathway is relatively enhanced on CoMo in comparison to NiMo. In principle, it has to be expected that the kinetic importance of the consecutive DDS rate is dependent on the incorporation of a dehydrogenation step. To check if this is the case under our conditions a simple kinetic modeling was performed. Results are shown in Fig. 7 a), b). The overall k_{HDS} in case 1 of a) and b) was kept equal in order to allow a proper comparison. In case 2 the DDS step following the hydrogenation step is increased with a factor 2-3. If the dehydrogenation step is not taken into account (Fig. 7 a), the increase of the consecutive DDS reaction hardly affects the rate of conversion of 4,6-DMDBT. On the other hand, in Fig. 7b), when the dehydrogenation step is incorporated into the scheme, the increase of the consecutive DDS rate results in a gain of 50 % for the rate of HDS of 4,6-DMDBT. In summary, an increase of k_{DDS} competing with the rate of dehydrogenation, could significantly increase the rate of conversion for 4,6-DMDBT.



Scheme 2. Reaction pathways for the HDS of 4,6-DMDBT, taking into account the dehydrogenation of the hydrogenated intermediate



a) Without k_{HG} ($C_{\text{DBT}}(t_0) = 1$)

Case1: k_{DDS} 0.03, k_{HG} 0.2, $k_{\text{DDS}'}$ 4, k_{BP} 0.

Case2: k_{DDS} 0.03, k_{HG} 0.2, $k_{\text{DDS}'}$ 10, k_{BP} 0.

b) With k_{HG} ($C_{\text{DBT}}(t_0) = 1$)

Case1: k_{DDS} 0.03, k_{HG} 0.4, k_{HG} 5, $k_{\text{DDS}'}$ 5, k_{BP} 0.

Case2: k_{DDS} 0.03, k_{HG} 0.4, k_{HG} 5, $k_{\text{DDS}'}$ 15, k_{BP} 0.

Figure 7. The effect of the incorporation of a dehydrogenation step for the HDS of 4,6-DMDBT

A thermodynamic analysis is a convenient way to investigate if such a scheme can be realistic, in advance. Thermodynamics equilibrium data for DBTs and intermediates in HDS is available from literature [20]. Figure 8 gives data for 3 MPa (based on theoretical calculations) and 5 MPa (by extrapolation applying the van't Hoff equation of the 3 MPa data) hydrogen pressure. The equilibrium molar fraction of tetrahydro-DBT is around 60% and 4,6-DM-tetrahydro-DBT is around 8 % at 350 °C. Therefore, from a thermodynamic point of view, it is expected that the dehydrogenation step does not have to be considered in DBT HDS, but this is not the case for 4,6-DMDBT HDS.

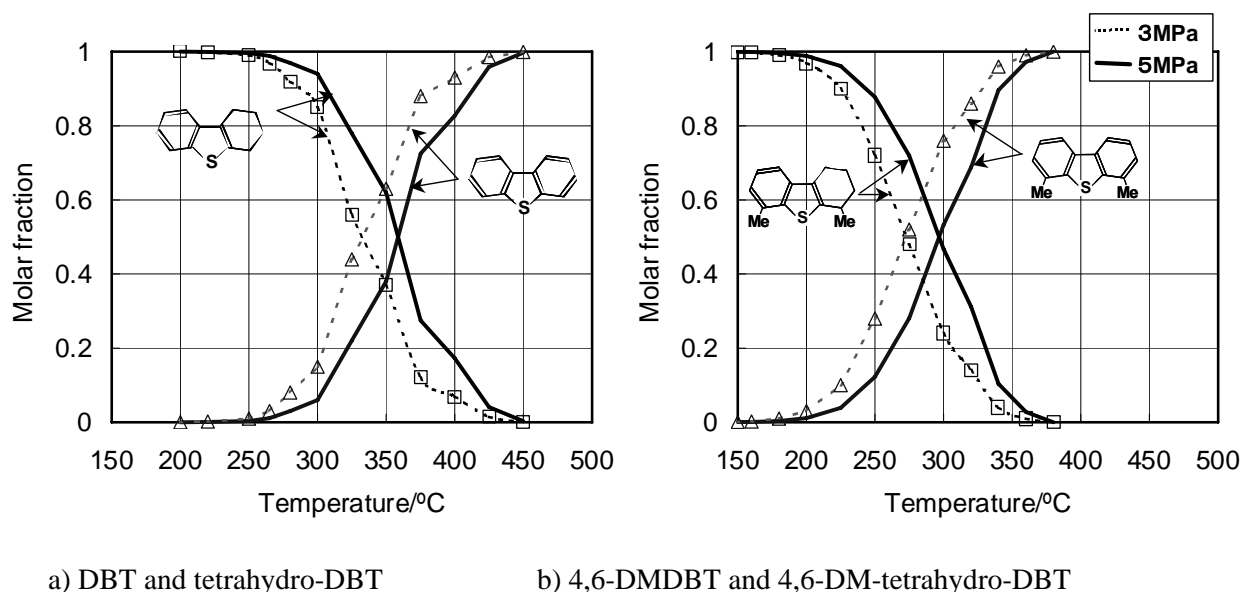


Figure 8. Thermodynamic equilibrium of (substituted) DBT and (substituted) tetrahydro-DBT

In Scheme 2 the dehydrogenation step (k_{HG}) is now included. In the regression analysis the ratio of k_{HG}/k_{-HG} was kept constant as the equilibrium molar ratio of 4,6-DM-tetrahydro-DBT to 4,6-DMDBT. The consecutive hydrogenation reaction (k_{BP}) of dimethylbiphenyl is also taken into account. First, k_{BP} was set free. Next, to give the same degree of freedom as in Scheme 1, from the literature [20], $k_{BP} / (k_{HG} + k_{DDS})$ was kept as a constant, viz., at 0.015. Fig. 9 a), b) compares the numerically fitting quality of these two cases for 4,6-DMDBT. The selectivity vs conversion is taken to check for the best model, as the sensitivity of selectivity plots is higher than the yield plots. All catalysts show the same tendency in fitting quality. The plots of selectivity vs conversion for DBT HDS in Scheme 1 are shown in Fig. 10. The fitting quality is high enough to discuss the reaction pathways, as the mean error (root mean square error) of the numerically fitting is rather low, see Table 4.

The values for the mean error for the two cases of Scheme 2 do not differ much. Careful inspection of the results shows that the profile of the fitting lines for 3,3'-DMBP is informative: at higher conversion Scheme 2 with k_{BP} free leads to a decreasing and Scheme 2 with $k_{BP} / (k_{HG} + k_{DDS}) = 0.015$ to an increasing trend with conversion. The experimental data indicates that the latter is preferred and in the subsequent analysis Scheme 1 is compared with Scheme 2 with $k_{BP} / (k_{HG} + k_{DDS}) = 0.015$.

The ratio of $k_{\text{DDS}}/k_{\text{HG}}$ is higher in CoMo than NiMo for 4,6-DMDBT HDS. It should be noted that k_{DDS} and k_{HG} are in the same order of magnitude. In this situation, higher k_{DDS} can enhance the relative contribution of the HG pathway, competing with dehydrogenation pathway. In this way, differences between CoMo and Ni Mo might be explained.

In summary, the model considering the reverse reaction (k_{HG}) could describe the pathways for 4,6-DMDBT HDS. The rate of k_{DDS} is relatively high for CoMo, leading to relatively high activity for 4,6-DMDBT HDS. Therefore, there is a possible significant contribution of dehydrogenation reactions. However, it remains unclear if this contribution is a major factor for the ranking of NiMo and CoMo catalysts. Hence, the activities under the conditions that thermodynamically the dehydrogenation reaction cannot be significant are informative. As the HG reaction is exothermic, the equilibrium of HG is increased at decreasing temperature. Tests at lower temperature (300 °C) were carried out for NiMo and CoMo catalysts, where the equilibrium of dehydrogenated intermediate is about 60% (Fig. 8 b). Table 6 shows the rate constants by numerically fitting in Scheme 1 without the dehydrogenation step.

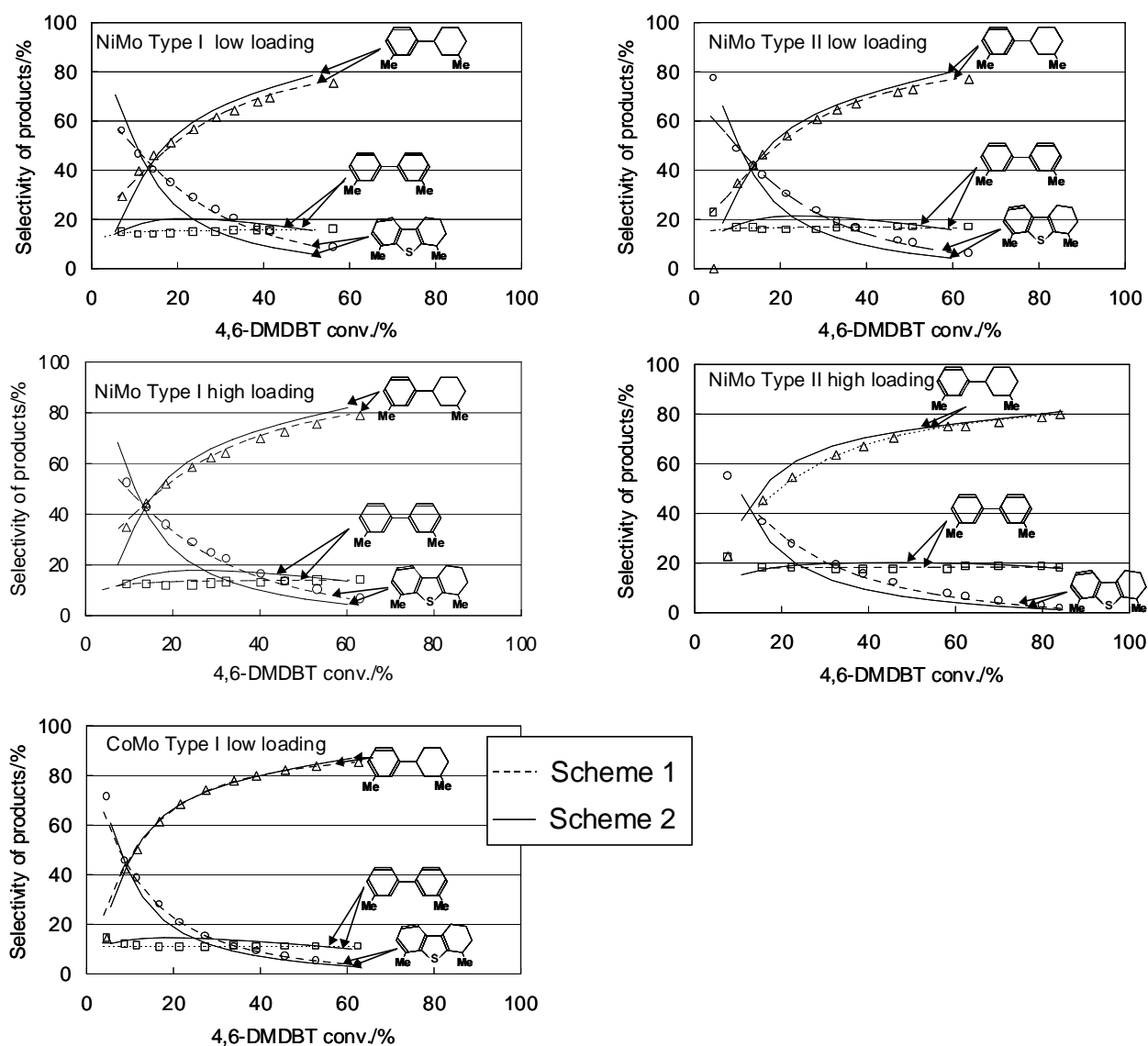


Figure 9 a). Selectivity vs conversion by numerically fitting in Scheme 1 and Scheme 2 (k_{BP} free) for 4,6-DMDBT HDS

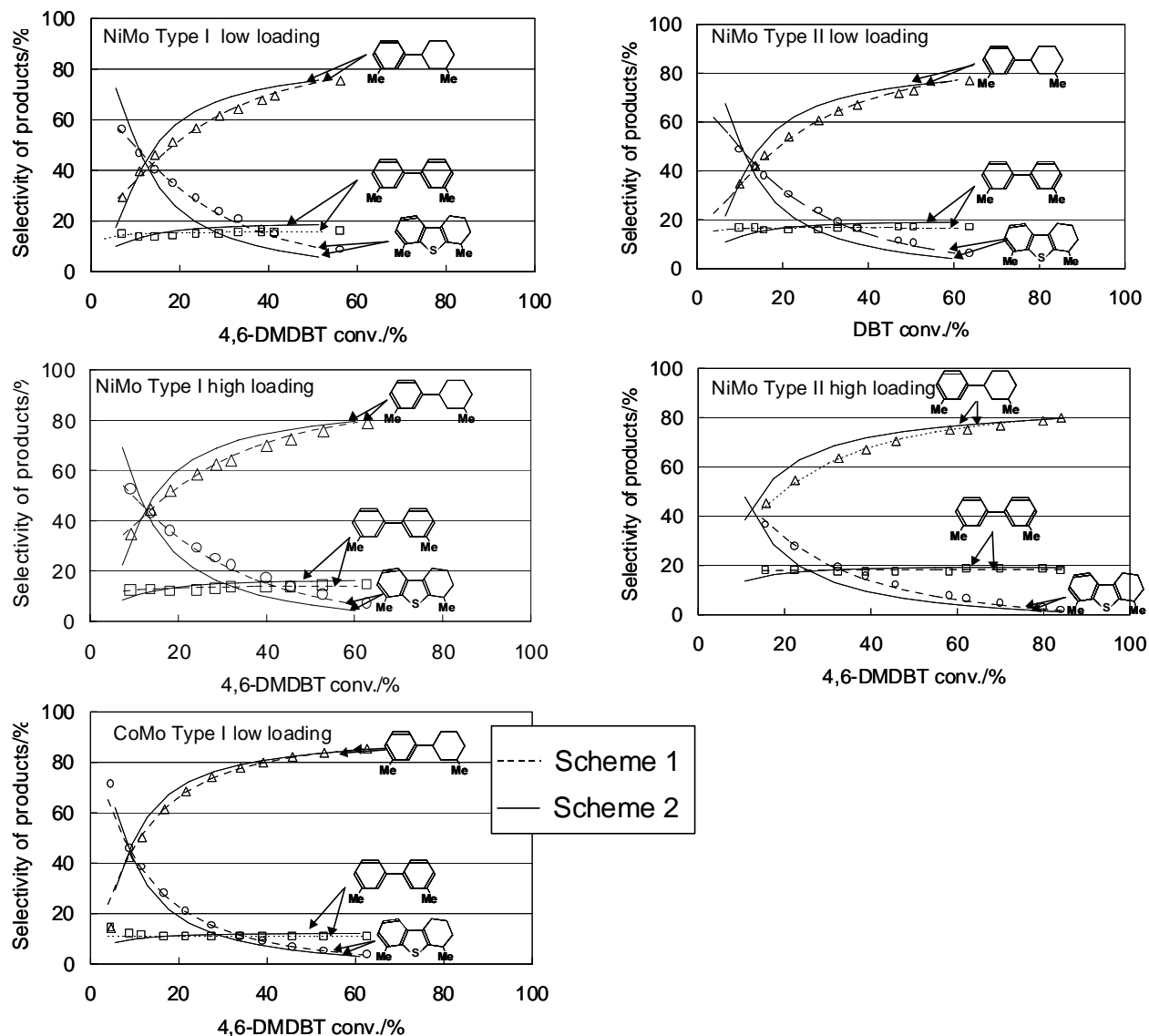


Figure 9 b). Selectivity vs conversion by numerically fitting in Scheme 1 and Scheme 2 ($(k_{BP}/(k_{HG} + k_{DDS})=0.015)$) for 4,6-DMDBT HDS

Comparing to the data at higher temperature (350 °C), higher HG/DDS ratios are observed at low temperature (300 °C). So, these data suggest that there is a possible involvement of dehydrogenation reactions at high temperature (350 °C). Does this explain the relatively high activity of CoMo catalysts for HDS of 4,6-DMDBT? In fact not, because at low temperature the impact of dehydrogenation should be relatively low but the data in Table 6 shows that at both temperatures NiMo and CoMo catalysts behave very similarly (e.g., k_{DDS}/k_{HG} are temperature independent). In HDS of 4,6-DMDBT at low temperature, CoMo shows higher activity not only because k_{DDS} is high but also because k_{HG} is high. So, a possible contribution of dehydrogenation is minor for the ranking of NiMo and CoMo catalyst.

Then these results brought us to examine the susceptibility by H_2S on NiMo and CoMo catalysts.

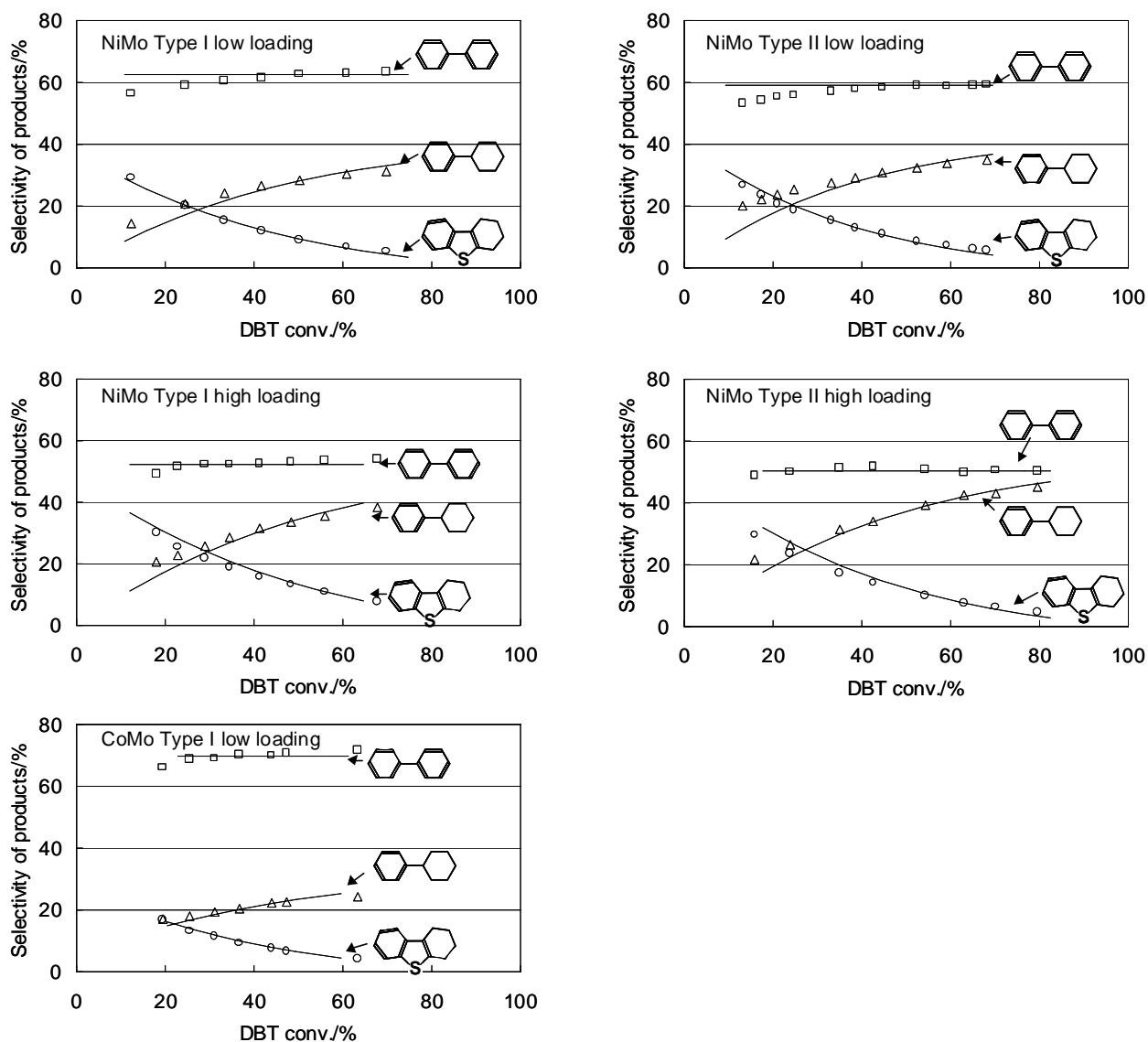


Figure 10. Selectivity vs conversion by numerically fitting in Scheme 1 for DBT HDS

Table 4. Mean error of the numerically fitting.

	4,6-DMDBT HDS			DBT HDS
	Scheme 1	Scheme 2a	Scheme 2b	Scheme 1
NiMo type I low loading	0.009	0.016	0.017	0.027
NiMo type II low loading	0.008	0.016	0.017	0.009
NiMo type I high loading	0.007	0.015	0.016	0.013
NiMo type II high loading	0.011	0.017	0.017	0.012
CoMo type I low loading	0.003	0.009	0.010	0.010

Table 5. Rate constants ($k \times 10^7$ (mol/s·g_{cat})) according to Scheme 2 for NiMo and CoMo catalysts for 4,6-DMDBT HDS.Scheme 2a: k_{BP} free (but k_{BP}/k_{HG} constant)

	k_{DDS}	k_{HG}	$k_{DDS'}$	k_{HG}/k_{DDS}	$k_{DDS'}/k_{DDS}$	$k_{DDS'}/k_{HG}$	$k_{DDS'}/k_{HG}$	k_{HG}	k_{BP}
NiMo type I low loading / Scheme 2	0.75	4.2	32	5.6	42	7.6	0.66	48	4.2
Ratio of Scheme 2/ Scheme 1	1.7	1.7	1.2	1.1	0.7	0.68	-	-	-
NiMo type II low loading / Scheme 2	0.97	7.7	40	8.0	42	5.2	0.45	89	4.1
Ratio of Scheme 2/ Scheme 1	1.6	2.6	1.2	1.6	0.7	0.45	-	-	-
NiMo type I high loading / Scheme 2	0.83	10	41	12	49	4.1	0.35	115	3.9
Ratio of Scheme 2/ Scheme 1	1.6	3.2	1.3	2.0	0.8	0.39	-	-	-
NiMo type II high loading / Scheme 2	1.6	17	95	10	59	5.7	0.49	191	1.4
Ratio of Scheme 2/ Scheme 1	1.2	2.8	1.3	2.3	1.1	0.48	-	-	-
CoMo typeI low loading / Scheme 2	0.64	5.9	64	9.3	100	11	0.94	68	4.2
Ratio of Scheme 2/ Scheme 1	1.6	1.8	1.1	1.2	0.7	0.59	-	-	-

Scheme 2b: $k_{BP}/(k_{DDS}+k_{HG}) = 0.015$ case (but k_{BP}/k_{HG} constant)

	k_{DDS}	k_{HG}	$k_{DDS'}$	k_{HG}/k_{DDS}	$k_{DDS'}/k_{DDS}$	$k_{DDS'}/k_{HG}$	$k_{DDS'}/k_{HG}$	k_{HG}	k_{BP}
NiMo type I low loading / Scheme 2	0.52	6.5	36.4	12.6	70	5.6	0.49	74.9	0.103
Ratio of Scheme 2/ Scheme 1	1.1	2.7	1.4	2.4	1.2	0.50	-	-	-
NiMo type II low loading / Scheme 2	0.67	8.3	46.0	12.3	68	5.6	0.48	95.3	0.132
Ratio of Scheme 2/ Scheme 1	1.1	2.8	1.3	2.5	1.2	0.48	-	-	-
NiMo type I high loading / Scheme 2	0.58	9.9	46.0	17	80	4.6	0.40	113.9	0.154
Ratio of Scheme 2/ Scheme 1	1.1	3.2	1.4	2.9	1.3	0.45	-	-	-
NiMo type II high loading / Scheme 2	1.43	17.3	96.9	12.1	68	5.6	0.49	198.5	0.275
Ratio of Scheme 2/ Scheme 1	1.1	2.9	1.4	2.7	1.3	0.47	-	-	-
CoMo typeI low loading / Scheme 2	0.44	6.3	68.5	14.4	156	11	0.94	72.6	0.099
Ratio of Scheme 2/ Scheme 1	1.1	2.0	1.2	1.8	1.1	0.59	-	-	-

Table 6. Rate constants ($k \times 10^7$ (mol/s·g_{cat})) for the HDS of 4,6-DMDBT according to Scheme 1 on NiMo and CoMo catalysts at 300 and 350 °C.

	Temp.	k_{HDS}	k_{DDS}	k_{HG}	$k_{DDS'}$	k_{HG}/k_{DDS}	$k_{DDS'}/k_{DDS}$	$k_{DDS'}/k_{HG}$
NiMo TypeII Low loading	350	3.6	0.62	3.0	34	4.8	56	12
NiMo TypeII Low loading	300	0.76	0.049	0.71	8.3	14	169	12
CoMo Type I Low loading	350	3.6	0.40	3.2	59	8.0	148	18
CoMo Type I Low loading	300	0.9	0.023	0.86	17.9	37	772	21

4.3. Susceptibility to H₂S

In Fig. 4, a higher susceptibility to H₂S is observed on NiMo than CoMo catalyst in HDS of 4,6-DMDBT. It is not important to incorporate the dehydrogenation for assessing the ranking of the catalyst activities. However, for the discussing the rates for each reaction pathways; HG and DDS, it is worthwhile to take the dehydrogenation into account. To assess the inhibiting effect

by H₂S on the separate steps in the DDS and the HG pathways, the apparent rate constants according to Scheme 2 in which the reverse pathway of dehydrogenation (k_{HG}) is included are shown in Table 7. In the case of Scheme 2, k_{HG} of CoMo catalyst without H₂S addition is much lower than of NiMo. As discussed in 4.2, Scheme 2 is a more realistic case to discuss not only total HDS rate but also each reaction pathways.

Table 7. Rate constants ($k \times 10^7$ (mol/s·g_{cat})) according to Scheme 2, on NiMo and CoMo low loading catalysts ($k_{BP}/(k_{DDS}+k_{HG}) = 0.015$ case) for 4,6-DMDBT HDS.

	H ₂ S (bar)	k_{HDS}	k_{DDS}	k_{HG}	$k_{DDS'}$	k_{HG}/k_{DDS}	$k_{DDS'}/k_{DDS}$	$k_{DDS'}/k_{HG}$
NiMo type II low loading / Scheme 2	0	5.7	1.1	14.5	73	13	68	5.0
NiMo type II low loading / Scheme 2	1.5	3.6	0.67	8.3	46	12	68	5.6
CoMo typeI low loading / Scheme 2	0	3.7	0.75	4.2	103	5.5	136	25
CoMo typeI low loading / Scheme 2	1.5	3.6	0.44	6.3	68	14	156	11

Table 8. Ratio of rate constants with and without H₂S for 4,6-MDBT HDS in Scheme 2.

	k_{DDS}	k_{HG}	$k_{DDS'}$
NiMo type II low loading	0.63	0.57	0.63
CoMo typeI low loading	0.58	1.51	0.67

Table 8 shows the ratio of rate constants with H₂S to those without H₂S. It is clearly shown that k_{HG} of CoMo catalyst is increased by H₂S, whereas the other rates are retarded significantly.

For the NiMo catalysts all the ratios of rate constants with and without the presence of H₂S show almost the same value (approx. 0.6). At first sight this is surprising as the DDS pathway is dominant in HDS of DBT but not in that of 4,6-DMDBT. However, the reason why DDS and HG are evenly inhibited on NiMo catalyst could be explained from comparison with the results in the literatures [29, 31]. At increasing H₂S pressure, there is a sharp decrease of the ratio of DDS /HG at the early stage, then it slows down at H₂S > 0.25 bar. In our batch reaction, the self-produced H₂S accumulates in the reactor and it will reach 0.4 bar at a conversion 100 %. Taking into account the dehydrogenation step of Scheme 2, it is not surprising that DDS/HG ratio is almost constant irrespective of H₂S addition in our experimental conditions.

Although the difference of structure between NiMoS and CoMoS is not fully clear and further investigations are necessary to elucidate it, recent DFT calculation studies have suggested that nickel prefers to incorporate into the metal edge and cobalt in the S-edge of MoS₂ slabs under typical sulfiding conditions [44, 45]. It is likely that the metal edge where Ni is incorporated in would be more easily adsorbed by H₂S than S-edge where Co is incorporated in.

In summary, the main difference of the NiMo and CoMo is the susceptibility of the HG step to H₂S. Although there is a minor contribution on the reverse pathway of dehydrogenation (k_{HG}) and HG selectivity is slightly affected by the incorporation of reaction scheme, the high HG activity with H₂S of CoMo cannot be explained by it. Basically, the equilibrium of the first step

in HG pathway is not completely achieved, and the contribution of consecutive DDS (k_{DDS}) is minor and is not an independent rate-determining step.

The difference of susceptibility to H_2S is the main cause of the relatively high activity of CoMo catalyst for HDS of 4,6-DMDBT in comparison to NiMo catalysts under realistic conditions (Total press. 5 MPa, Temp. 350 °C, H_2S 1.5 bar).

5. Conclusions

ThTH HDS activity behaves similarly to DBT DDS, because direct desulfiding is the major process in both cases. The HG pathway is the main pathway both in HDS of TH and 4,6-DMDBT. The consecutive DDS step in the HG pathway is important for the CoMo catalyst, but not for NiMo catalysts.

Dehydrogenation reactions might be important for 4,6-DMDBT HDS under our experimental conditions. However, this effect could not explain fully the relatively high activity of CoMo catalysts for HDS of 4,6-DMDBT. The main reason is the relatively low susceptibility to H_2S of CoMo catalysts.

At increasing metal loading, type II active phase can achieve high metal dispersion above monolayer surface coverage, while type I active phase forms aggregated crystals on the alumina support. A simple geometric model based on a relatively high stacking rate for type II explains this. It is tentatively concluded that the higher stacking type II active phase shows a relatively high HG selectivity. The difference in activity of type I and II is explained by the difference in hydrogenation activity and dispersion.

Acknowledgement

The authors are grateful to Dr. Sonja Eijsbouts for stimulating discussions on this report to publish this work.

References

- [1] I.V.Babich and J.A.Moulijn, *Fuel*, **82** (2003) 607.
- [2] M.Houalla, D.H.Broderick, N.K.Nag, A.V.Sapre, V.H.J.De Beer, B.C.Gates, and H.Kwart, *J.Catal.*, **61** (1980) 523.
- [3] T.Kabe, A.Ishihara, and H.Tajima, *Ind.Eng.Chem.Res.*, **31** (1992) 1577.
- [4] X.Ma, K.Sakanishi, and I.Mochida, *Ind.Eng.Chem.Res.*, **33** (1994) 218.
- [5] R.Candia, O.Sørensen, J.Villadsen, N.-Y.Topsøe, B.S.Clausen, and H.Topsøe, *Bull.Soc.Chim.Belg.*, **93** (1984) 763.
- [6] H.Topsøe and B.S.Clausen, *Appl.Catal.*, **25** (1986) 273.
- [7] J.A.R.Van Veen, H.A.Colijn, P.A.J.M.Hendriks, and A.J.Van Welsenens, *Fuel Proc.Tech.*, **35** (1993) 137.
- [8] H.R.Reinhoudt, R.Troost, A.D.van Langeveld, J.A.R.van Veen, S.Sie, and J.A.Moulijn, *J.Catal.*, **203** (2001) 509.
- [9] H.R.Reinhoudt, C.H.M.Boons, A.D.van Langeveld, J.A.R.van Veen, S.T.Sie, and J.A.Moulijn, *Appl.Catal.A: Gen.*, **207** (2001) 25.
- [10] M.Vrinat, *Appl.Catal.*, **6** (1983) 137.
- [11] M.J.Girgis and B.C.Gates, *Ind.Eng.Chem.Res.*, **30** (1991) 2021.
- [12] R.Shafi and G.J.Hutchings, *Catalysis Today*, **59** (2000) 423.
- [13] C.Aubert, R.Durand, P.Geneste, and C.Moreau, *Journal of Catalysis*, **97** (1986) 169.
- [14] P.Michaud, J.L.Lemberton, and G.Perot, *Applied Catalysis A: General*, **169** (1998) 343.
- [15] V.Lamure-Meille, E.Schulz, M.Lemaire, and M.Vrinat, *Applied Catalysis A: General*, **131** (1995) 143.
- [16] D.D.Whitehurst, H.Farag, T.Nagamatsu, K.Sakanishi, and I.Mochida, *Catalysis Today*, **45** (1998) 299.
- [17] J.Kraus and M.Zdrazil, *Reaction Kinetics and Catalysis Letters*, **6** (1977) 475.
- [18] E.J.M.Hensen, M.J.Vissenberg, V.H.J.deBeer, J.A.R.vanVeen, and R.A.vanSanten, *Journal of Catalysis*, **163** (1996) 429.
- [19] M.Daage and R.R.Chianelli, *Journal of Catalysis*, **149** (1994) 414.
- [20] H.Farag, D.D.Whitehurst, K.Sakanishi, and I.Mochida, *Catalysis Today*, **50** (1999) 49.
- [21] I.Isoda, X.Ma, and I.Mochida, *Sekiyu Gakkaishi*, **37** (1994) 375.
- [22] T.Kabe, Y.Aoyama, D.H.Wang, A.Ishihara, W.H.Qian, M.Hosoya, and Q.Zhang, *Appl.Catal.A: Gen.*, **209** (2001) 237.
- [23] B.M.Vogelaar, N.Kagami, A.D.van Langeveld, S.Eijsbouts, and J.A.Moulijn, *Abstracts of Papers of the American Chemical Society*, **226** (2003) U533.
- [24] D.Nicosia and R.Prins, *Journal of Catalysis*, **229** (2005) 424.
- [25] D.L.Sullivan and J.G.Ekerdt, *Journal of Catalysis*, **178** (1998) 226.
- [26] W.P.Boone and J.G.Ekerdt, *Journal of Catalysis*, **193** (2000) 96.
- [27] T.Isoda, X.Ma, and I.Mochida, *Abstracts of Papers of the American Chemical Society*, **208** (1994) 59.
- [28] T.Kameoka, T.Sato, Y.Yoshimura, H.Shimada, N.Matsubayashi, and A.Nishijima, *Sekiyu Gakkaishi*, **37** (1994) 497.

- [29] F.Bataille, J.L.Lemberton, P.Michaud, G.Perot, M.Vrinat, M.Lemaire, E.Schulz, M.Breysse, and S.Kasztelan, *Journal of Catalysis*, **191** (2000) 409.
- [30] E.Lecrenay, K.Sakanishi, and I.Mochida, *Catalysis Today*, **39** (1997) 13.
- [31] M.Egorova and R.Prins, *Journal of Catalysis*, **225** (2004) 417.
- [32] K.G.Knudsen, B.H.Cooper, and H.Topsoe, *Applied Catalysis A-General*, **189** (1999) 205.
- [33] D.D.Whitehurst, T.Isoda, and I.Mochida, *Advances in Catalysis*, **42** (1998) 345.
- [34] H.Topsoe, B.S.Clausen, N.Y.Topsoe, J.K.Nørskov, C.V.Ovesen, and C.J.H.Jacobsen, *Bull.Soc.Chim.Belg.*, **104** (1995) 283.
- [35] X.L.Ma and H.H.Schobert, *Journal of Molecular Catalysis A-Chemical*, **160** (2000) 409.
- [36] P.Mills, S.Korlann, M.E.Bussell, M.A.Reynolds, M.V.Ovchinnikov, R.J.Angelici, C.Stinner, T.Weber, and R.Prins, *J.Phys.Chem.A*, **105** (2001) 4418.
- [37] S.M.A.M.Bouwens, F.B.M.Vanzon, M.P.Vandijk, A.M.Van der Kraan and D.C.Koningsberger, *Journal of Catalysis*, **146** (1994) 375.
- [38] E.J.M.Hensen, P.J.Kooyman, Y.van der Meer, A.M.van der Kraan, V.H.J.de Beer, J.A.R.van Veen, and R.A.van Santen, *J.Catal.*, **199** (2001) 224.
- [39] A.L.Diaz and M.E.Bussell, *Journal of Physical Chemistry*, **97** (1993) 470.
- [40] I.E.Wachs, *Catalysis Today*, **27** (1996) 437.
- [41] J.L.Brito and J.Laine, *Applied Catalysis*, **72** (1991) L13.
- [42] N.Kagami, B.M.Vogelaar, A.D.van Langeveld, and J.A.Moulijn, *Preprint of ICC 13th, Paris*, **P1-193** (2004).
- [43] Y.Sakashita and T.Yoneda, *Journal of Catalysis*, **185** (1999) 487.
- [44] H.Schweiger, P.Raybaud, and H.Toulhoat, *Journal of Catalysis*, **212** (2002) 33.
- [45] M.Sun, A.E.Nelson, and J.Adjaye, *Journal of Catalysis*, **226** (2004) 32.

5

Application of datamining method (ID3) to data analysis for ultra deep hydrodesulfurization of straight-run light gas oil -Determination of effective factor of the feed properties to reaction rate of HDS -

Abstract

Six kinds of straight run light gas oils were tested under various conditions in high pressure fixed bed reactor. First the formula of the corrected WAT (weight average temperature) normalized to the standard conditions was made by trial and error method, using the parameters chosen by the information of literature. Next the analysis of datamining method (ID3) and correlation coefficient were applied. This method is very unique and useful to evaluate the validity of the chosen parameters. The valid parameters of feed properties were density (SpGr), nitrogen content, and the temperature of 90 % distillation (T90) under our experimental conditions.

The contents of this chapter was published as:
N. Kagami, R. Iwamoto and T. Tetsuji, Fuel. **84** (2005) 279.

1. Introduction

In recent years, much attention has been focused on the deep hydrodesulfurization (HDS) of diesel fuel oil because environmental legislation has become more and more strict. Some refineries in the world have already started producing ultra low sulfur diesel below 50ppm and further regulation will be probably less than 10ppm in the near future. The countermeasures for the ultra deep desulfurization are to apply novel highly active and stable catalysts, and to optimize the operation condition of HDS process. Hence, it becomes more important to estimate the reaction temperature accurately to meet the target of sulfur at various conditions using various feedstocks. Because the production of the lower sulfur diesel than the correct targeted sulfur makes the catalyst life shorter [1] and it also consumes excess amount of hydrogen. The establishment of the accurate corrected WAT (weight average temperature) is very important for the management of the diesel production and the schedule on catalyst replacement to meet the catalyst run length.

It is well known that corrected WAT is used to evaluate the catalyst life. Corrected WAT is the required average temperature of catalyst beds to meet the targeted sulfur level of product at a certain operation condition using a certain feed properties. It is a function of the operation condition parameters such as temperature, LHSV, hydrogen pressure, hydrogen-oil ratio and the feed properties. Operation condition parameters can be normalized from the formula based on n-order (pseudo) reaction kinetics and Arrhenius plots through tuning the constants. These operation parameters can be varied independently using bench tests. However, it is almost impossible with a real feed to vary just one property independently. Therefore, the suitable selection of key parameters of feed properties may be difficult in the case of real feed.

The formula of the corrected WAT normalized to the standard from various feed properties was made by trial and error method somehow, using the parameters chosen by the information of literature [2]. However, we still need a convenient way to evaluate the validity of the chosen parameters.

Recently, datamining methods tend to be used more commonly in data processing field. Datamining is one of the technologies for building knowledge-based systems by inductive inference from examples. Therefore, it can also be the method to search the valuable information from large data sets. In datamining methods, the classification analysis called ID3 (Iterative Dichotomiser) is applicable.

ID3 algorithm was suggested by J.R Quinlan [3] and extended to deal with numerical values [4]. Using entropy of information that shows the degree of chaotic state, ID3 establishes the importance of the parameter automatically.

In this work, ID3 was applied to evaluate the validity of the chosen parameters of various feed properties for the corrected WAT normalized to the standard.

2. Experimental Method

2.1. Catalyst and Pretreatment

One hundred cubic centimeters of commercial catalyst of CoMo type catalyst was filled in a high-pressure micro-flow reactor. Before the evaluation of straight-run light gas oil (SRLGO),

the catalyst was presulfided in situ at 250 °C for 2 h and then 300 °C for 2 h in stream of dimethyl-disulfide/SRLGO/hydrogen mixture (sulfur content, adjusted as 2.5 wt%).

2.2. Bench test

Bench tests were carried out using high-pressure micro-flow reactor. Table 1 shows the operation condition parameters such as temperature, LHSV, hydrogen pressure, and hydrogen to oil ratio (HTO). The temperature of the catalyst bed was kept constant through the reactor by using multiple heating blocks. Thermocouples were located in the center of the catalyst bed. In these range of the operation conditions, the results of sulfur content of the product were from 500 ppm to 5 ppm.

Table 1. The operation and standard conditions of bench tests

		Operation range	Standard condition
LHSV	h ⁻¹	1.0 - 2.0	1.5
Hydrogen pressure	MPa	3.5 - 5.0	5.0
Hydrogen to oil ratio	m ³ _{H₂} /m ³ _{Oil}	250 - 1000	250
Temperature	°C	330 - 370	-

Table 2. Feed properties of various straight-run gas oil

			FEED A	FEED B	FEED C	FEED D	FEED E	FEED F
Density	at 15° C	g/cc	0.8605	0.8483	0.8525	0.8516	0.8517	0.8440
Sulfur		wt%	1.36	1.34	1.2	1.33	1.18	1.09
Composition (HPLC)	Saturate	vol%	70.8	73.9	74.6	73.5	72.8	76.4
	1-ring Aroma	vol%	13.7	14.2	14	14.4	14.0	12.7
	2-ring Aroma	vol%	7.0	6.9	7.4	9.8	10.6	6.6
	≥3-ring Aroma	vol%	8.5	5.0	4.0	2.3	2.6	4.3
Distillation (ASTM D-86)	IBP	° C	188	181	194	194	211	183
	5VOL%	° C	266	224	239	241	260	231
	10VOL%	° C	280	244	256	257	271	248
	20VOL%	° C	296	265	273	273	281	266
	30VOL%	° C	303	280	283	285	287	277
	40VOL%	° C	312	291	293	295	294	287
	50VOL%	° C	321	301	302	303	301	295
	60VOL%	° C	331	312	313	314	309	304
	70VOL%	° C	343	325	326	327	318	313
	80VOL%	° C	356	342	340	343	329	324
	90VOL%	° C	374	363	360	363	344	339
95VOL%	° C	389	383	377	380	357	351	
EP	° C	395	390	383	388	360	361	
Viscosity	at 30° C	mm ² /S	7.4	5.2	5.5	5.6	5.4	4.6
ASTM Color		-	0.5	0.3	0.2	0.2	0.2	0.1
Nitrogen		ppm	190	120	180	110	110	77
Basic nitrogen		ppm	59	37	64	32	36	27
Cetane Index		-	57.6	55.7	55.4	56.2	57.5	57.1

2.3. Analysis of feeds and products

Six kinds of SRLGO from Middle East crude were tested in high-pressure micro-flow reactor. The various properties of feedstocks were measured as shown in Table 2. Density, sulfur content, boiling points, total nitrogen content, basic nitrogen content, aromatics contents

were measured by oscillation u-tube method for density, X-ray fluorescence method for sulfur content, standard test method for distillation of petroleum products at atmospheric pressure (ASTM D86) for boiling points, chemiluminescence method for total nitrogen content, potentiometric titration for basic nitrogen content [5], high performance liquid chromatography for aromatics contents, respectively.

The sulfur content of product was also measured by oxidative micro-coulometric titration methods. The product oils were stripped by nitrogen to remove the H₂S in the liquid before the measurement.

Definition for entropy of information

Entropy $E_n = \sum p_n (\sum -p_i \log_2 p_i)$
 p_n : Probability for all data, p_i : Probability for each case(i)
 (If $p_i = 0$, $-p_i \log_2 p_i = 0$)

At Step 0, $\sum p_n = 1$, $E_n = I(i) = \sum -p_i \log_2 p_i$

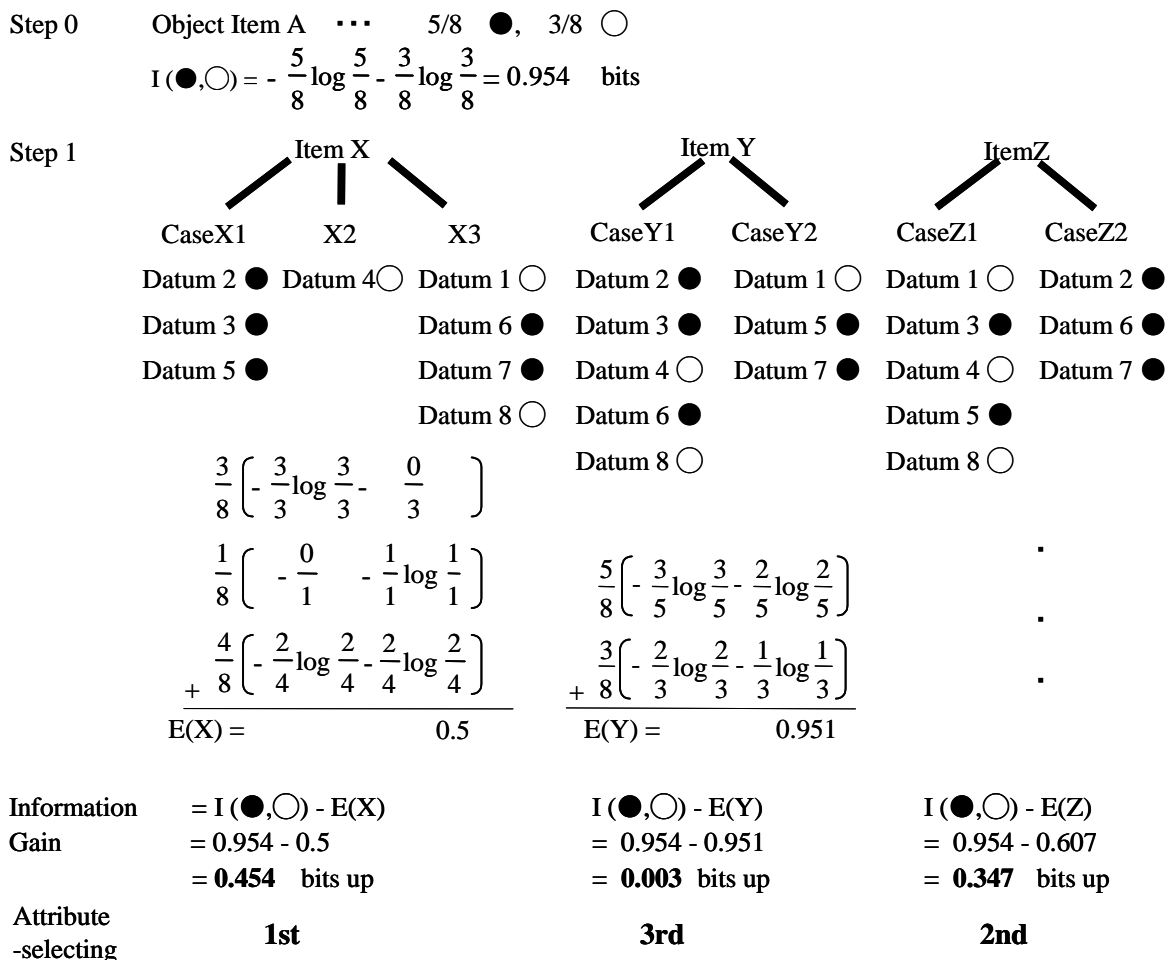


Figure 1. Outline algorithm of ID3 (Iterative Dichotomiser).

2.4. ID3 data analysis

ID3 software package (XpertRule (Lascombe and Company, Ltd.)) were used for the analysis from the data of bench tests. Figure 1 shows the algorithm of ID3. A classification rule was expressed as a decision tree. The relationship between object Item A and attribute Items X, Y, Z was examined using the entropy of information. First, in step 0, the entropy of the object item (I) was calculated. Next object item was distributed according to the attribute items, and in each case the entropy (E (X), E (Y), E (Z), ...) was calculated as shown in step 1. Finally the subtracted values of I – E (X or Y or Z ...) were taken as information gains. And the largest information gain means that the information of the item become less chaotic. Therefore, Item X was selected as first attribute and this routine was reiterated. In this way, ID3 can select the simplest decision tree.

As described above, ID3 is quite useful as we can get the ranking of effective parameters very easily.

3. Results and Discussion

3.1. Corrected WAT method for operation condition

Operation condition parameters can be corrected independently, because each operation parameter can be varied independently using the same feed. It is well known that corrected WAT is used to evaluate the catalyst activity and its deactivation rate. The reaction temperature under the normalized conditions can be calculated as follows [6] (Arrhenius; equation (1), nth-order reaction; equation (2), hydrogen to oil ratio (HTO); equation(3), hydrogen pressure; equation(4)).

$$\ln k = \ln A - \frac{Ea}{RT}, \quad \ln k' = \ln A - \frac{Ea}{RT'}, \quad \ln k'' = \ln A - \frac{Ea}{RT''} \quad (1)$$

$$k = \frac{LHSV}{n-1} \times \left(\frac{1}{S_p^{n-1}} - \frac{1}{S_f^{n-1}} \right) \quad (2)$$

$$k' = k \times \left(\frac{HTO_p}{HTO_s} \right)^\alpha \quad (3)$$

$$\ln k'' = \ln k' \times \left(\frac{HP_p}{HP_s} \right)^\beta \quad (4)$$

Nomenclature:

k, k', k'' : rate constant [h^{-1}], A : frequency factor [h^{-1}], Ea : activation energy [cal/mol]

k, k' and k'' correspond to normalized temperature T, T' and T'' , respectively in eq.1.

R : gas constant [$1.987 \text{ cal/mol}\cdot\text{K}$],

T : temperature [K], T' : normalized temperature at a certain HTO,

T'' : normalized temperature at a certain hydrogen pressure.

n : reaction order [-]

S_f : feed sulfur concentration [ppm], S_p : product sulfur concentration [ppm]

$LHSV$: liquid hourly space velocity (volumetric feed rate to catalyst bed volume)[h^{-1}]

HTO : hydrogen rate to oil rate [$\text{m}^3_{\text{H}_2} / \text{m}^3_{\text{oil}}$ (293 K, 1 bar)],

HP: hydrogen pressure [MPa]

α , β : constants for hydrogen to oil ratio and for hydrogen pressure

Suffix "s": value at a certain standard condition

Suffix "p": practical value (actual condition).

For the normalizing of temperature, Arrhenius equation (1) was used and activation energy (E_a) could be tuned as the constant. And for the LHSV (liquid hourly space velocity) n th-order (pseudo) reaction equation (2) was applied and n could be tuned as the constant. Hydrogen pressure and hydrogen to oil ratio effects also should be normalized. These effects on the ultra deep desulfurization of diesel were reported [1]. These parameters were normalized by using the function just for the fitting independently, and the formula as equation (3) and equation (4) were fitted well.

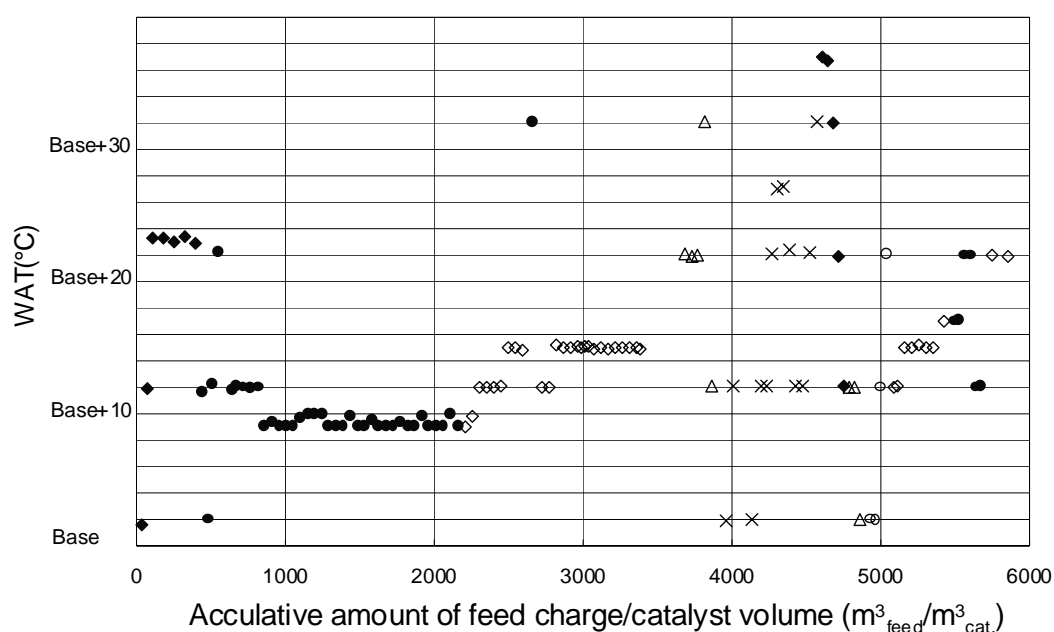


Figure 2. Actual operation WAT vs accumulative feed throughput: (◆) feed A; (●) feed B; (◇) feed C; (△) feed D; (×) feed E; (○) feed F.

Figure 2 shows the actual WAT vs accumulative amount of feed throughput. The corrected WAT normalized to the standard operation condition in Table 1 are shown in Figure 3. The data using the same kind of feed are shown as the same symbols. After the normalization of operation condition parameters, the data scattering range became small. However, the scattering is still over 15 °C, depending on the properties of feedstock.

3.2. Deactivation pattern of catalyst during desulfurization of the gas oil

The WAT during the deep desulfurization of the gas oil could be regarded to increase linearly with time on stream as shown in the literature [7,8]. When LHSV were changed, accumulative amount of feed throughput per catalyst volume must be better to use instead of time on stream, to evaluate the deactivation behaviour of catalyst.

In Figure 3, it appears that the data using the same kind of feedstock have the same increasing slope. It could be concluded that the movement of WAT due to the deactivation of catalyst is a straight line against the accumulative amount of feed throughput per catalyst volume.

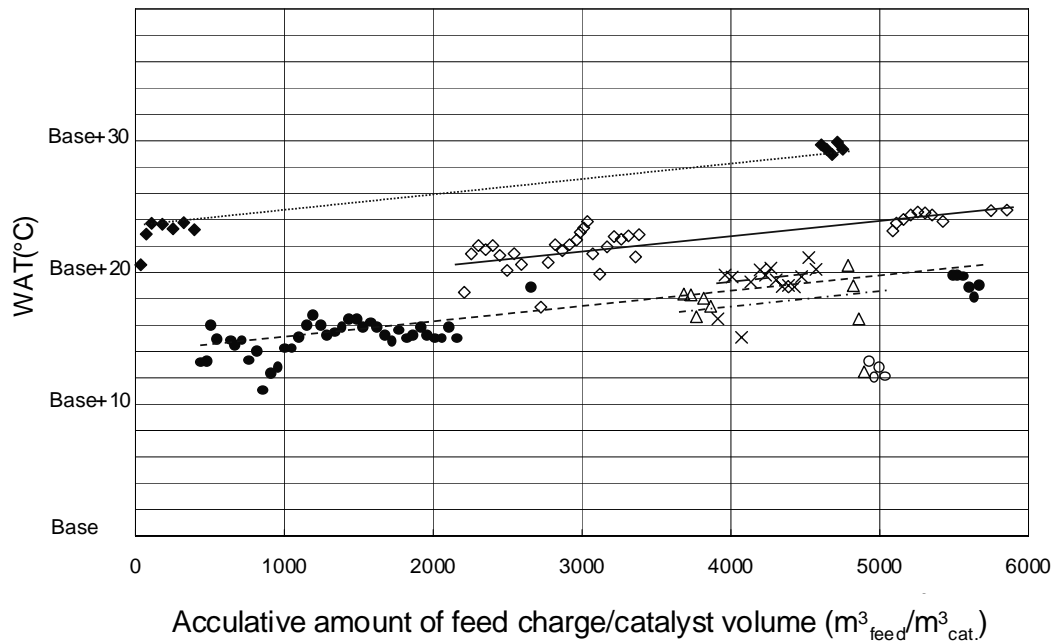


Figure 3. Corrected WAT normalized by operation conditions. (◆) feed A; (●) feed B; (◇) feed C; (△) feed D; (×) feed E; (○) feed F.

3.3. Corrected WAT method for feed properties by trial and error method

Corrected WAT method for feed properties was reported in the case of residue hydrodesulfurization reaction [6]. However, using the same method, the parameters of feed properties should be properly chosen in the ultra deep hydrodesulfurization of SRLGO.

Recently, the inhibition of HDS reaction by nitrogen compounds was evaluated [9,10,11], especially in deep range of HDS.

Moreover, it is well known that the heavy sulfur compounds (dibenzothiophene (DBT) type sulfur compounds, especially 4,6-substituted DBT) have lower activity than light sulfur compounds such as benzothiophenes in HDS for diesel fuel [12].

Therefore, the following parameters of feed properties were chosen for WAT normalized feed properties as follows.

$$\ln A' = \ln A + a \cdot \ln\left(\frac{SpGr'}{SpGr}\right) + b \cdot \ln\left(\frac{N'}{N}\right) + c \cdot \ln\left(\frac{T90'}{T90}\right) \quad (5)$$

" $SpGr$ " is density of feedstock and it was also used to estimate residue hydrodesulfurization reaction. " N " is the total content of nitrogen compounds. And " $T90$ " is the temperature of 90 % distillation (ASTM D-86), which reflects heaviness of the feedstock.

The trial and error method was used to determine the constant value of a , b , c in equation (5). For instance, the properties of "Feed E" were used as the standard feed to normalize WAT, as it showed the average reactivity in our feedstocks. As mentioned above, assuming the

movement of WAT as a straight line against the accumulative amount of feed throughput, the least square method was applied and the standard error of all data was minimized by optimizing each constant values. In this way, the values of constants were determined, and the results of WAT normalized by operation conditions and feed properties are shown in Figure 4. The data scattering range of WAT became much smaller (approx. 4 °C) than the one normalized only by operation condition parameters. Moreover, the slope of the line shown in Figure 4 is almost the same as those shown in Figure 3. Therefore, the corrected WAT obtained from this trial and error method is proved to be reasonable.

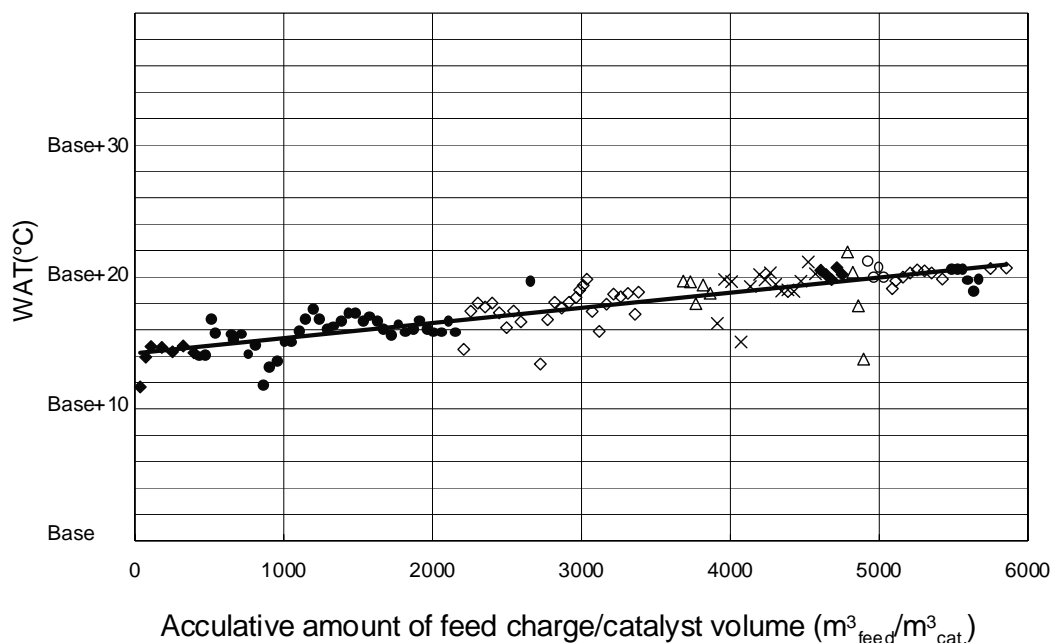


Figure 4. Corrected WAT normalized by operation conditions and feed properties: (◆) feed A; (●) feed B; (◇) feed C; (△) feed D; (×) feed E; (○) feed F.

3.4. Confirmation of the effectiveness of parameters of feed properties by data mining (ID3)

As described above, corrected WAT for feed properties was obtained. However, The question whether the parameters of feed properties chosen for normalization of the WAT are the best or not still remains. To evaluate the validity of the chosen parameters, one of the useful methods is ID3.

It was reported that PLS method was applied to find mutually uncorrelated latent variables (LVs) concerning to the correlation of feed properties and reactivity for HDS of middle distillates [13]. Basically PLS is to deal with the dimension of the problem and to select a minimum number of such LVs with minimal loss of information. The feedstocks in the report were full of variety including gas oil, light gas oil and heavy gas oil. As the data were taken under the same operation condition, the product sulfur may not be in the same range of deep desulfurization. In our study, the feedstocks are all SRLGO with various properties, and sulfur contents in products were below 500 ppm and mostly less than 50 ppm. In such a small variation, ID3 may be very convenient method to find the ranking of key parameters easily. However, ID 3 is not the method that deals with the dimension of the problem. In order to select the valid

parameters, they should be independent with each other. In our study, the correlation analysis was simply applied. The parameters were lumped if their correlation coefficient is above 0.9.

As Figure 5 shows, each difference between the plots of corrected WAT normalized by operation condition parameters and the calculated deactivation line was examined. The data of subtraction from the corrected WAT normalized by operation conditions to the line was taken as object item 'A' and, 'A' was examined by the feed properties parameters, items X, Y, Z, etc. Operation parameters were also used to convince that the normalization by them is enough. Table 3 shows the data analysis sheet to examine. As described above, two methods were applied in this analysis. The one applied method is ID3, and the other is the correlation coefficient for the analysis. As object item 'A' should not be continuum but step number for the ID3 analysis, the subtraction was classified per 2 °C.

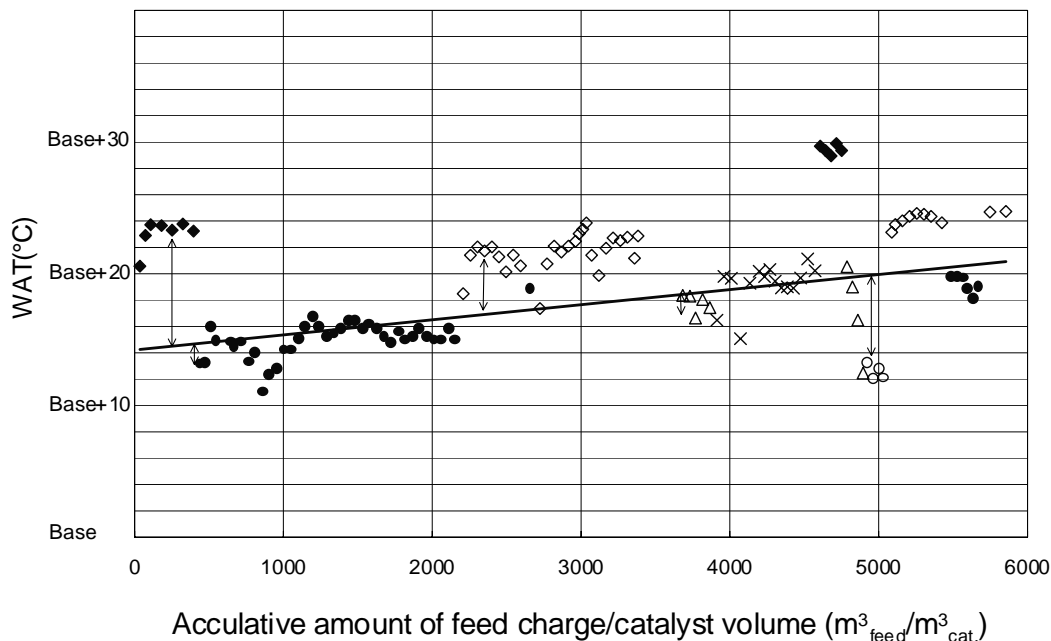


Figure 5. Tentative corrected WAT deactivation line (—) and corrected WAT normalized by operation conditions: (◆) feed A; (●) feed B; (◇) feed C; (△) feed D; (×) feed E; (○) feed F.

Table 4 shows the results of the analysis. The effective parameters for classification were arranged in small order of increasing entropy (Class I to XII), using ID3 method. Clearly, the smaller the entropy is, the more effective the parameter is. As mentioned above, the correlation coefficient analysis was used, and the parameters having correlation coefficient above 0.9 mutually are shown as the same pattern-code. The operative parameters such as WAT, LHSV, hydrogen pressure, and hydrogen to oil ratio are ranked in lesser effective parameters for classification. It proved that the normalization by operation condition parameters is fully corrected.

Table 3. Data analysis sheet for ID3

A	X	Y	Z				...				
Subtraction (WAT(1) - tentative performance line)	Feed name	Density	Sulfur	Composition				WAT	LHSV	HTO	HP
				Saturate	1ring Aroma	2ring Aroma					
.
.
.	number
.	of data
.	---120
.
.

Table 4. The ranking of entropies obtained by ID3 analysis

Ranking of entropy (step 1, E(X,Y...))	Parameters for classification					
I	Type of feed
II	Density	Nitrogen	Basic nitrogen	.	.	.
III	Saturate	1-ring Aroma.	T50vol%.	T60vol%.	T70vol%.	Viscosity
IV	Feed Sulfur	T80vol%..	T90vol%...	T95vol%...	EP.	.
:	:	:	:	:	:	:
VII	Accumulative amount of feed
VIII	WAT
IX	LHSV
X	Product Sulfur
XI	HTO
XII	HP

The most effective parameter is type of feed, and it shows that the feed properties parameters normalization is necessary to be carried out.

The second ranking parameters are density, total nitrogen, and basic nitrogen. The correlation coefficient of nitrogen and basic nitrogen is higher, and it means that they had a monotonic relation. Although it was not unequivocally proven, basic nitrogen compounds such as acridines have been known to have rather high reactivity than non-basic compounds such as carbazoles [14]. In the early stage of catalyst bed, the former are easily removed, and the latter can inhibit HDS reaction in deep range. Hence, total nitrogen content was selected.

The third effective ranking parameters which do not have higher correlation coefficient with each other were saturate (Sa) and 1-ring aromatics. They will be investigated later.

The fourth were feed sulfur, T90 vol%, T95vol%, and EP, as the feed sulfur has already been used to calculate the reaction rate constant. T90 vol%, T95 vol%, and EP could be considered to be the same parameter and as a consequence, T90 vol% was taken. These parameters can reflect the amount of refractory sulfur species such as 4,6-dimethyldibenzothiophene, although the analysis of sulfur species is needed to make it clear.

In Table 4, the parameters determined by trial and error method were shown in the bold type. As a consequence, all of them are validated by ID3 and correlation coefficient analysis.

As described above, the feed property parameter of the saturate (S_a) and 1-ring aromatics could be the possible parameters to obtain the better method of WAT normalized feed properties. Those parameters could represent the amount of aromatics. It was generally accepted that the aromatic compounds inhibit HDS reaction substantially [15-17]. As SRLGO does not contain any olefin, total aromatics content ($100-S_a$) should be taken here, and the following eq.6 was applied. Constant values were determined by minimizing the standard error of all data.

$$\ln A' = \ln A + a \cdot \ln\left(\frac{SpGr'}{SpGr}\right) + b \cdot \ln\left(\frac{N'}{N}\right) + c \cdot \ln\left(\frac{T90'}{T90}\right) + d \cdot \ln\left(\frac{100 - Sa'}{100 - Sa}\right) \quad (6)$$

Table 5 shows the minimized standard error of all data using equation (5) and equation (6). No change of standard error shows that WAT is not affected by total aromatics. It is probably because the content of the total aromatics of 6 kinds of SRLGO were not so different. However, it might be expected that if LCO (light cyclic oil from cracking units) is blended as the feed, the parameter of the total amount of aromatics should be examined again, as LCO contains extremely high amount of aromatic compounds.

Table 5. The effect of total aromatics on the standard error of the corrected WAT

Equation	Selected parameters of feed prperties	Standard error / °C
5	SpGr, Total Nitrogen, T90	1.27
6	SpGr, Total Nitrogen, T90, Total Aromatics	1.27

4. Conclusions

The bench HDS tests were carried out using six feed stocks of straight light gas oil that have different properties, under various conditions (WAT, LHSV, hydrogen to oil ratio, hydrogen pressure,) for the target below 500 ppm sulfur in product.

The formula of the corrected WAT (weight average temperature) normalized to the standard condition was made by trial and error method, using the parameters chosen by the information of literature. However, these parameters of feed properties should be examined to see if they are the best or not.

The application through the analysis of datamining method (ID3) and correlation coefficient can be the unique and effective, because the validity of the chosen parameters for the corrected WABT is easily convinced.

Under our experimental conditions, the valid parameters of feed properties were density (SpGr), nitrogen content, and the temperature of 90 % distillation (T90).

Acknowledgement

The authors are grateful to Prof. Jacob A. Moulijn for his comments on this report to publish this work.

References

- [1] K.G.Knudsen, B.H.Cooper, H.Topsoe, *Applied Catalysis A: General*, **189** (1999) 205.
- [2] S.G.Laredo, R.H.De los, C.D.Luis, C.M.Jesus, *Applied Catalysis A: General*, **207** (2001) 103.
- [3] J.R.Quinlan, *Machine Learning*, **1(1)** (1986) 81.
- [4] Araki, Kojima, *Jinkou Chinou Gakkaishi*, **7(6)** (1992) 992.
- [5] I.Okuno, D.R.Latham, W.E.Haines, *Analytical Chemistry*, **37** (1965) 54.
- [6] Y.Miyauchi, T.Hashiguchi, N.Kimbara, K.Fujita, *Abstracts of Papers of the American Chemical Society, Div. of Petroleum Chemistry*, **210** (1995) 111.
- [7] L.A.Gerritsen, K.Vogt, A.Huismans, Summary at the ERTC in Berlin in November 1998. Options to meet future European diesel demand and specifications. ERTC Berlin, November 1998. (*Catalyst Courier* 37 - September 1999, <http://www.akzonobel-catalysts.com/home.htm>)
- [8] T.Fujikawa, O.Chiyoda, M.Tsukagoshi, K.Idei, S.Takehara, *Catalysis Today*, **45** (1998) 307.
- [9] D.D.Whitehurst, K.G.Knudsen, I.V.Nielsen, P.Wiwel, P.Zeuthen, *Abstracts of Papers of the American Chemical Society, Div. of Petroleum Chemistry*, **219** (2000a) 23.
- [10] D.D.Whitehurst, K.G.Knudsen, P.Wiwel, P.Zeuthen, *Abstracts of Papers of the American Chemical Society, Div. of Petroleum Chemistry*, **219** (2000b) 24.
- [11] P.Zeuthen, K.G.Knudsen, D.D.Whitehurst, *Catalysis Today*, **65** (2001) 307.
- [12] R.Shafi, G.J.Hutchings, *Catalysis Today*, **59** (2000) 423.
- [13] T.C. Ho, *Applied Catalysis A-General*, **244(1)** (2003) 115.
- [14] T.Koltai, M.Macaud, A.Guevara, E.Schulz, M.Lemaire, R.Bacaud, M.Vrinat, *Applied Catalysis A-General* **231** (2002) 253.
- [15] T.Isoda, S.Nagao, X.L.Ma, Y.Korai, I.Mochida, *Applied Catalysis A-General*, **150** (1997) 1.
- [16] T.Kabe, K.Akamatsu, A.Ishihara, S.Otsuki, M.Godo, Q.Zhang, W.H.Qian, *Industrial & Engineering Chemistry Research*, **36** (1997) 5146.
- [17] D.D.Whitehurst, H.Farag, T.Nagamatsu, K.Sakanishi, I.Mochida, *Catalysis Today*, **45** (1998) 299.

6

Modeling of inhibition of deep hydrodesulfurization by competitive adsorption of carbazole

Abstract

Simultaneous hydrodesulfurization (HDS) of dibenzothiophene (DBT) and hydrodenitrogenation (HDN) of carbazole was carried out in order to evaluate mutual inhibiting effects on NiMo catalysts in comparison to a CoMo catalyst. Carbazole significantly inhibits not only both the direct desulfurization (DDS) and the hydrogenation (HG) pathways in HDS of DBT, but also the HDN reaction itself. For HDS of DBT the HG pathway is more strongly inhibited by carbazole than the DDS pathway. Tetrahydrocarbazole was added in order to evaluate the influence of the hydrogenation of carbazole that occurs simultaneously with HDS. Compared to carbazole, tetrahydrocarbazole retards HDS of DBT more significantly, probably because of its stronger basicity. The type II high metal loading catalyst is inhibited the most by carbazole, probably related to its high HG activity.

The contents of this chapter is in preparation to be published as:

Narinobu Kagami, Bas M. Vogelaar, Rob J. Berger and Jacob A. Moulijn, in preparation.

1. Introduction

With respect to diesel-exhaust emissions more and more stringent legislation is formulated for transportation fuels. Generally speaking, the reasons to decrease the content of sulfur in fuel is (i) reduction of acid rain and (ii) preventing sulfur poisoning of deNO_x and combustor catalysts that contain noble metals, e.g., in order to reduce NO_x and PM (particulate matter). Some refineries in the world have already started producing ultra low sulfur diesel (less than 50 ppm) and in the near future environmental regulation will become very strict, probably requiring fuels with less than 10 ppm sulfur.

Promoted molybdenum catalysts have been the work-horses in HDS processes. Under industrial conditions for hydrotreatment of diesel fuel, HDS reaction takes place simultaneously with HDN (hydrodenitrogenation) and HDA (aromatics hydrogenation) reactions. It is generally accepted that HDS is inhibited by nitrogen compounds and polyaromatics [1-3]. Especially nitrogen compounds inhibit HDS reaction significantly in deep HDS [4]. Although it is not completely clear which nitrogen compound inhibits the most for ultra deep HDS, recent studies suggest that the refractory alkylcarbazoles that survive the early stage of the hydrotreatment process are the major inhibitors in deep desulfurization [5].

In the feed of straight run light gas oil, typical nitrogen content is from 100-500 ppm [6]; three types of nitrogen compounds are present, viz., non-heterocycles, heterocycles with 6-membered rings (6MR), and heterocycles with 5-membered rings (5MR). We do not have to consider non-heterocycles, viz., anilines and aliphatic amines, as they undergo HDN quickly. An important role of basicity suggests itself. The nitrogen compounds are very different in this respect. 6MR pyridinic species are basic and 5MR pyrrole species are non-basic or rather acidic [7]. The ratio of the content of basic to non-basic nitrogen compounds is 0.2-0.3.

Generally the inhibiting effect of basic nitrogen compounds is reported to be the strongest. However, non-basic nitrogen compounds such as carbazole are also reported to be comparable strong inhibitors for HDS. It is noteworthy that non-basic pyrolic type nitrogen compounds transform into strong basic compound by hydrogenation [7].

A systematic study on the reactivity of nitrogen compounds over NiMo catalysts was recently reported [8]. The reaction rate of carbazole appeared to be two orders of magnitude lower than that of acridine for the first benzene ring hydrogenation step and to be of the same order of magnitude as the reaction rate of 4,6-dimethyldibenzothiophene. In deep HDS remaining nitrogen compounds could well be strong inhibitors. Moreover, this work concerns the simultaneous HDS and HDN reaction in order to assess the mutual inhibition. There are only a few reports discussing this [9] using model compounds testing, as in a testing both of sulfur and nitrogen compounds must be detectable during the reaction. From these considerations, it was decided to focus on carbazole for this investigation.

Little work has been published about the susceptibility to nitrogen compounds for different classes of HDS catalysts [10]. For catalyst selection this information is crucial. In this work, a systematic investigation is presented regarding the susceptibility for nitrogen compounds on NiMo and CoMo, so-called type I and type II, and metal loading effects. For HDS of diesel range fuels, dibenzothiophene (DBT) is informative. It reacts via two pathways, the so-called direct desulfurization (DDS) and the hydrogenation (HG) pathway [11-13]. The difference of

nitrogen compound inhibiting effect between DDS and HG might have a large impact on the selection of the optimal catalyst and the understanding of the reactivity of various feedstocks. As type I high loading catalysts showed lower activity due to lower dispersion of active phase, it is not included in this work (see Chapter 3 and 4).

From these considerations it was decided to study the HDS of DBT, while varying the content of added carbazole. Various NiMo catalysts were tested and compared with a representative CoMo catalyst. The influence of the transformation during HDS of non-basic pyrolic type nitrogen was investigated by using tetrahydrocarbazole, the hydrotreated (strongly basic) intermediate in HDN of carbazole.

2. Experimental

2.1. Catalyst preparation

NiO-MoO₃/Al₂O₃ (type I and type II) and CoMo/Al₂O₃ (type I) catalysts were prepared via conventional liquid phase pore filling method. A high purity γ -Al₂O₃ in the form of 1.5 mm extrudates were impregnated using aqueous solutions containing the required amount of Ni and Mo, according to the literature. In the case of type I, after the supports had been impregnated by the metal solution, they were dried at 120 °C for 16 hours and calcinated at 500 °C for 4 hours. While in type II, only the drying step was applied. In the case of high metal loading catalyst preparation, catalysts were impregnated in two steps (second impregnation was carried out after a drying step, following the first impregnation), as the stability of the metal solution became worse at a higher metal concentration (see Chapter 2).

The composition of catalyst was measured by INAA (Instrumental Neutron Activation Analysis). Specific surface area of support alumina was measured by nitrogen adsorption method (BET). Two different metal loading catalysts were prepared; low and high loading with 5, 10 Mo atoms per nm², respectively. All catalysts were prepared to have the same molar ratio of Ni or Co to Mo. The results of element analysis are shown in Table 1.

Table 1. Composition of NiMo and CoMo catalysts

	NiO or CoO (wt%)	MoO ₃ (wt%)	Co/Mo, or Ni/Mo molar ratio	Mo loading (atom / nm ²)
NiMo type II low loading	3.4	19.2	0.34	5.2
NiMo type I low loading	3.3	18.8	0.34	5.1
NiMo type II high loading	5.6	30.6	0.35	10.5
CoMo type I low loading	3.3	19.2	0.33	5.2

2.2. Activity measurements

Before the reaction, catalysts were presulfided at 370 °C and about 5.5 MPa total pressure in balance hydrogen. All activity tests were carried out at 350 °C and 5 MPa total pressure in balance hydrogen, a typical condition for diesel fuel HDS reaction. The HDS activities for DBT simultaneously with HDN of carbazole were tested in a batch reactor, varying the content of carbazole. Catalysts were crushed and sieved properly before the test, to satisfy the criteria for avoiding mass transfer limitations [14]. The feed consisted of DBT, carbazole and the solvent

consisting of a mixture of hexadecane (90 vol%) and xylene (10 vol%) added for increasing the solubility of carbazole [9]. The Sulfur concentration in feed was 350 ppm and nitrogen concentrations were varied from 0 to 40 ppm. To mimic commercial conditions in the latter part of reactor, dimethyldisulfide (DMDS) was added in the liquid phase reactions to adjust the H₂S pressure to a constant level (1.5 bar). This also provided the condition that the effect of self-produced H₂S was minimized. Gas chromatography with a FID detector was used for quantitative analysis of products. In liquid phase reaction, inert hydrocarbon (0.2 wt% octadecane) was added as the internal standard in the feed for GC analysis (see Chapter 2).

3. Results

3.1. Inhibiting effect of carbazole for HDS of DBT

It is well known that carbazole does not react via the direct denitrogenation (DDN) pathway, in other words, hydrogenolysis of C-N can only occur after full saturation of the ring. To confirm this, carbazole was hydrogenated over the catalysts studied. In Fig. 1, the yields are plotted vs reaction time for low loading type II NiMo. As expected, no biphenyl product is observed. Tetrahydrocarbazole is observed as the first intermediate, confirming the importance of the hydrogenation (HG) pathway. Bicyclohexyl is the main N-free product, showing that tetrahydrocarbazole hydrogenolysis via perhydrocarbazole is fast. Cyclohexylbenzene is produced in a later stage, by dehydrogenation of bicyclohexyl. In Scheme 1, the reaction pathways of carbazole in literature [15] are shown, in agreement with our results. In Scheme 2, the reaction pathway of carbazole HDN is simplified, lumping the yields of bicyclohexyl and cyclohexylbenzene. Since HDS was the real objective for fitting the dataset of HDN, pseudo first order rate equations were adopted for analysis of HDN results. Rate constants of each step were estimated by numerically fitting using least square method according to the following equation (available in the package Scientist).

$$r_{CZ} = -\frac{V_L}{W} \frac{dC_{CZ}}{dt} = k_1[C_{CZ}] - k_{-1}[C_{TC}] \quad , \quad (1)$$

$$r_{TC} = -\frac{V_L}{W} \frac{dC_{TC}}{dt} = k_{-1}[C_{TC}] - k_1[C_{CZ}] + k_2[C_{TC}] \quad , \quad (2)$$

where V_L is the total liquid volume (L), W the catalyst weight (g_{cat}), k_1 , k_{-1} , k_2 are the rate constant (L/g_{cat}/h) of pathways according to Scheme 2, $[C_{CZ}]$, $[C_{TC}]$ are the concentration (mol/L) of carbazole and tetrahydrocarbazole, respectively. In Fig. 2a the yields vs reaction time are plotted for carbazole HDN; in contrast with Fig. 1 the lines are the result of modeling.

In HDS of a mixture of DBT and carbazole, we can discriminate between the DDS and HG pathways of DBT HDS in Scheme 3, as for carbazole DDN that might lead to biphenyl does not take place. Overall HDS and DDS rates have been calculated from the conversion of DBT and the yield of biphenyl, respectively. The difference between the HDS and the DDS rates corresponds to the HG rate. Pseudo first order rate equations were adopted and rate constants of each step were estimated by numerically fitting using the least square method. In Fig. 2 the

yields vs reaction time are plotted for HDS of DBT. Fig. 2b represents HDS of DBT without the addition of carbazole, Fig. 2c gives the analogous data for low concentration carbazole (N 12.5 ppm), and Fig. 2d for high concentration of carbazole (N 40 ppm). As shown in the figures, the carbazole could be detected sufficiently accurately to obtain the reaction rate.

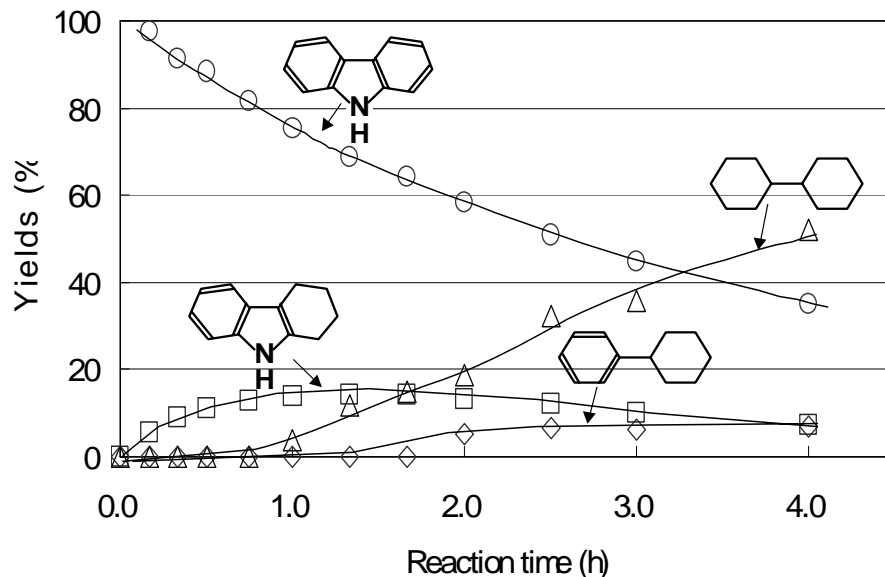
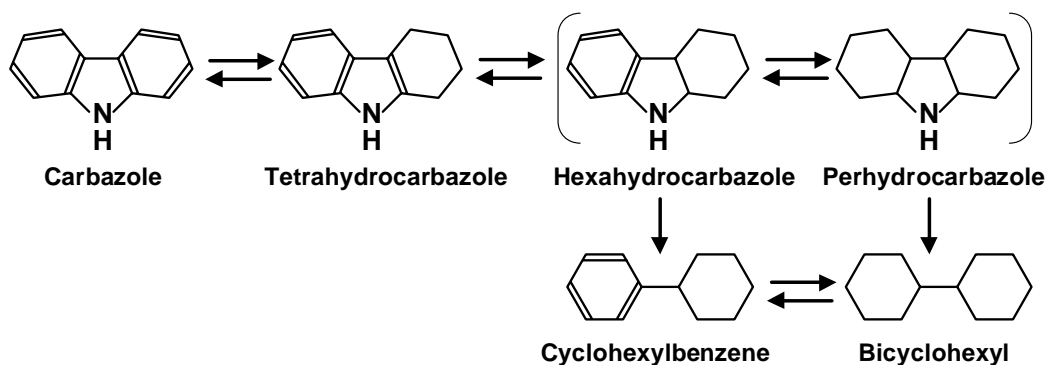
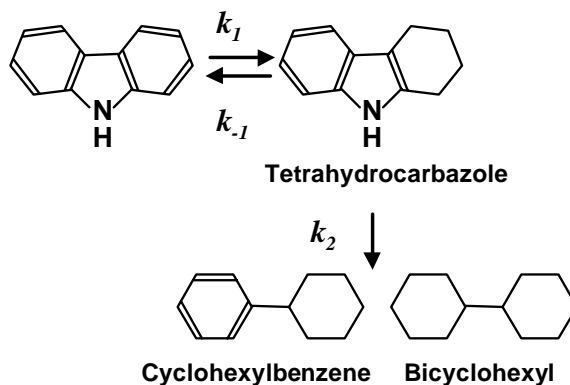


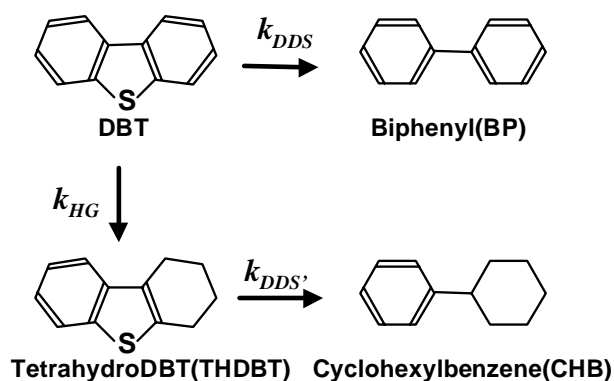
Figure 1. Product yields vs reaction time for HDN of carbazole on NiMo catalyst (NiMo type II low loading catalyst, H_2 5 MPa, H_2S 1.5 bar, 350 °C). Lines are drawn to guide the eye.



Scheme 1. Reaction pathways for the HDN of carbazole (ref: [16])



Scheme 2. Simplification of reaction pathways for the HDN of carbazole



Scheme 3. Reaction pathways for the HDS of dibenzothiophene (DBT)

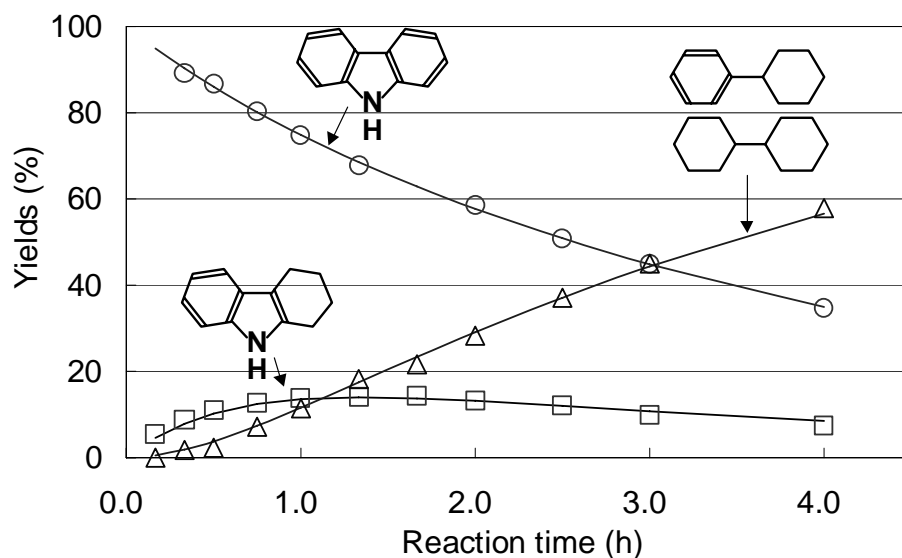


Figure 2a. Product yields vs reaction time for HDN of carbazole on NiMo catalyst (NiMo type II low loading catalyst, H_2 5 MPa, H_2S 1.5 bar, 350 °C, no DBT present. Pseudo-first-order kinetics, Scheme 2).

Next, the influence of the presence of xylene, that was added to improve the solubility of carbazole, on HDS of DBT was tested. Table 2 gives the results. Overall k_{HDS} (sum of k_{DDS} and k_{HG} , according to Scheme 3) are shown. All catalysts show the same degree of activity drop (approx. 20 %). Moreover, the effect on the selectivity is shown. Inhibiting effects of xylene on the HG and on the DDS are almost even, while there is slight difference for the various catalysts.

In Fig. 3, the inhibiting effect of carbazole for HDS of DBT is shown. The activities for HDS of DBT are plotted vs the amount of carbazole added. A very small content of carbazole such as 10 ppm is enough to retard the HDS reaction significantly, by approx. 30%. The HDS activity decreases sharply with increasing carbazole concentration at low carbazole concentrations and slower at higher carbazole concentrations. In Fig. 4, the ratio of HG/DDS pathway for HDS of DBT on various catalysts is plotted vs the amount of carbazole added.

k_{HG}/k_{DDS} is decreased gradually at increasing the addition of carbazole for all catalysts. It is clear that compared to the DDS pathway the HG pathway is more inhibited by carbazole.

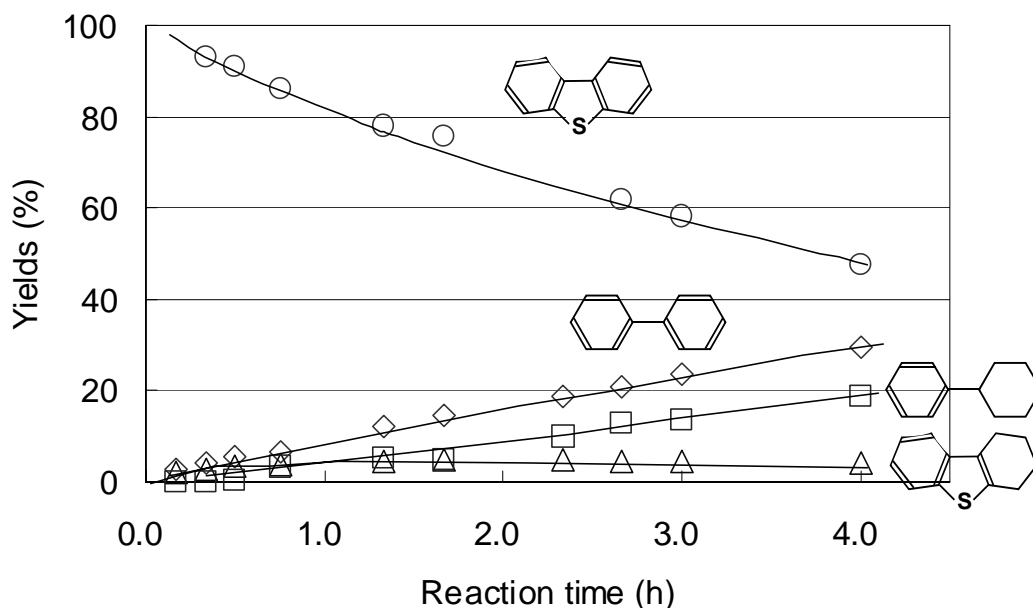


Figure 2b. Product yields vs reaction time for HDS of DBT without carbazole on NiMo catalyst (NiMo type II low loading catalyst, H_2 5 MPa, H_2S 1.5 bar, 350 °C. Pseudo-first-order kinetics, Scheme 3).

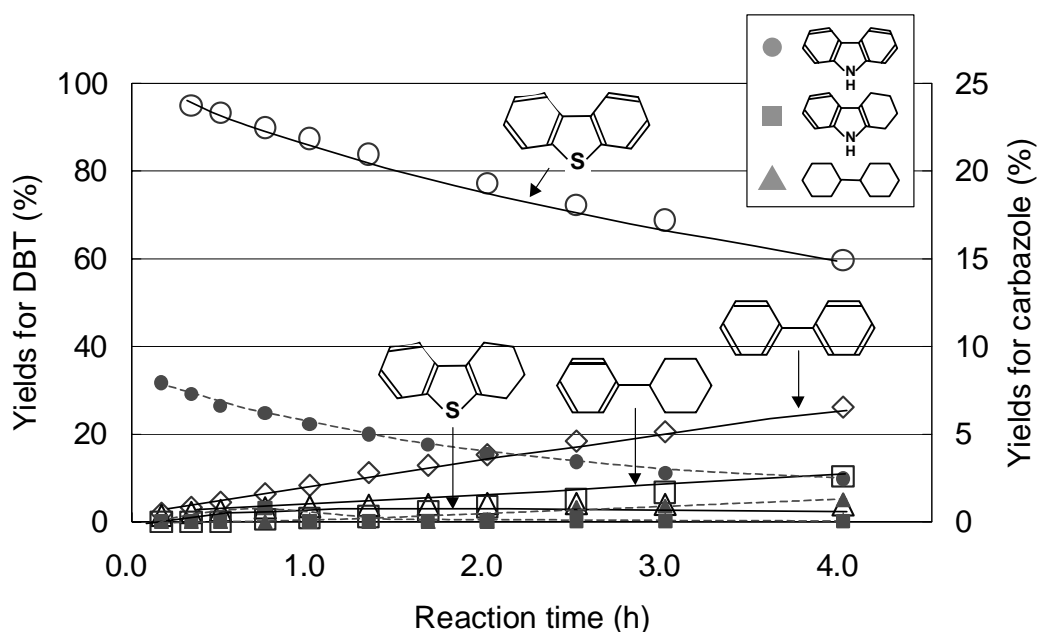


Figure 2c. Product yields vs reaction time for HDS of DBT in the presence of low concentration carbazole (N 12.5 ppm) on NiMo catalyst (NiMo type II low loading catalyst, H_2 5 MPa, H_2S 1.5 bar, 350 °C. Pseudo-first-order kinetics, Scheme 3). The molar yields are based on the initial amount of moles of DBT.

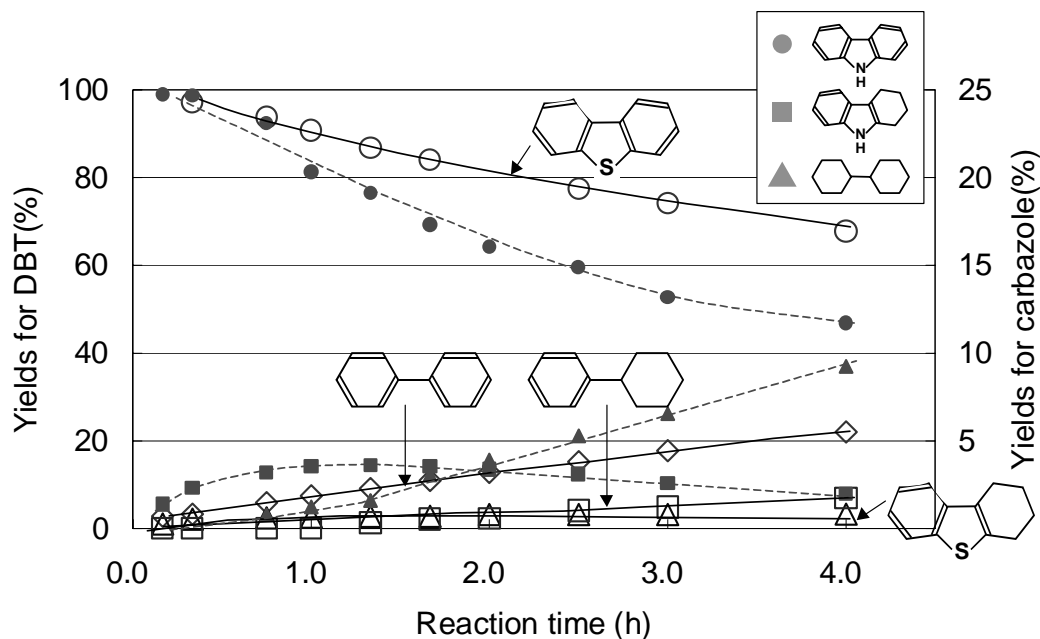


Figure 2d. Product yields vs reaction time for HDS of DBT in the presence of high concentration carbazole (N 40 ppm) on NiMo catalyst (NiMo type II low loading catalyst, H₂ 5 MPa, H₂S 1.5bar, 350 °C. Pseudo-first-order kinetics, Scheme 3). The molar yields are based on the initial amount of moles of DBT.

Table 2. Effect of addition of xylene to solvent for HDS of DBT (Pseudo-first-order kinetics in Scheme 3, Rate constant (L/g_{cat}·h))

	Solvent	k_{HDS}^*	k_{DDS}	k_{HG}	$k_{DDS'}$	k_{HG}/k_{DDS}	$k_{HDS}(xylene)/k_{HDS}(no\ xylene)$
NiMo type II low loading	Hexadecane	0.37	0.22	0.15	2.07	0.69	0.81
	Hexadecane/Xylene=90/10	0.30	0.17	0.13	1.97	0.79	
NiMo type I low loading	Hexadecane	0.40	0.24	0.16	1.55	0.65	0.79
	Hexadecane/Xylene=90/10	0.31	0.18	0.13	1.75	0.71	
NiMo type II high loading	Hexadecane	0.76	0.38	0.38	3.58	0.99	0.81
	Hexadecane/Xylene=90/10	0.62	0.33	0.29	3.97	0.87	
CoMo type I low loading	Hexadecane	0.30	0.22	0.09	1.55	0.41	0.84
	Hexadecane/Xylene=90/10	0.26	0.20	0.06	1.66	0.29	

* $k_{HDS} = k_{DDS} + k_{HG}$

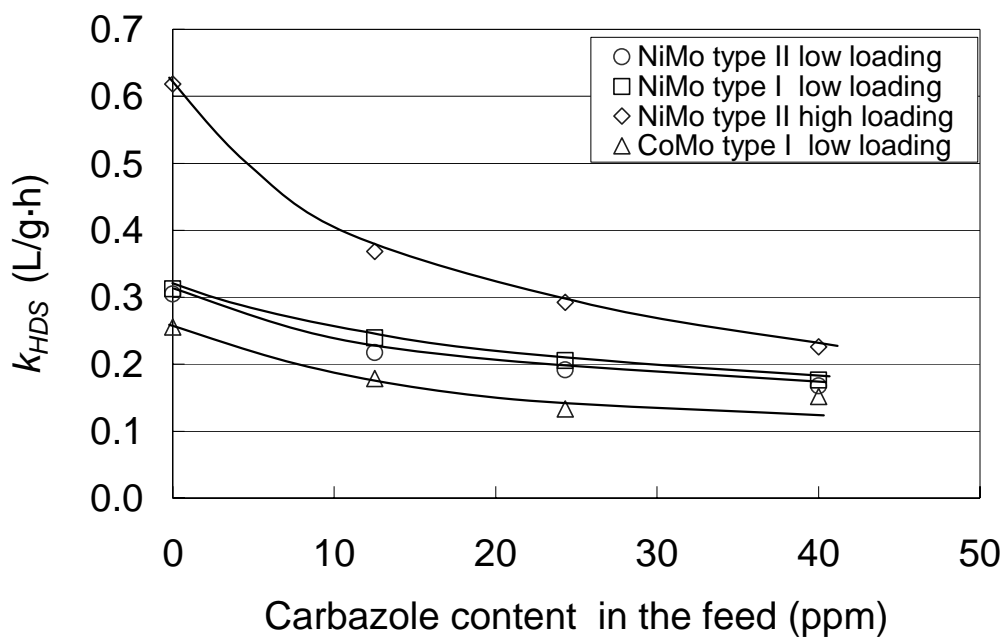


Figure 3. Carbazole inhibiting effects for HDS of DBT on various catalysts (H_2 5 MPa, H_2S 1.5 bar, 350 °C. Pseudo-first-order kinetics, $r_{HDS} = k_{HDS} \cdot [C_{DBT}]$). Lines are drawn to guide the eye.

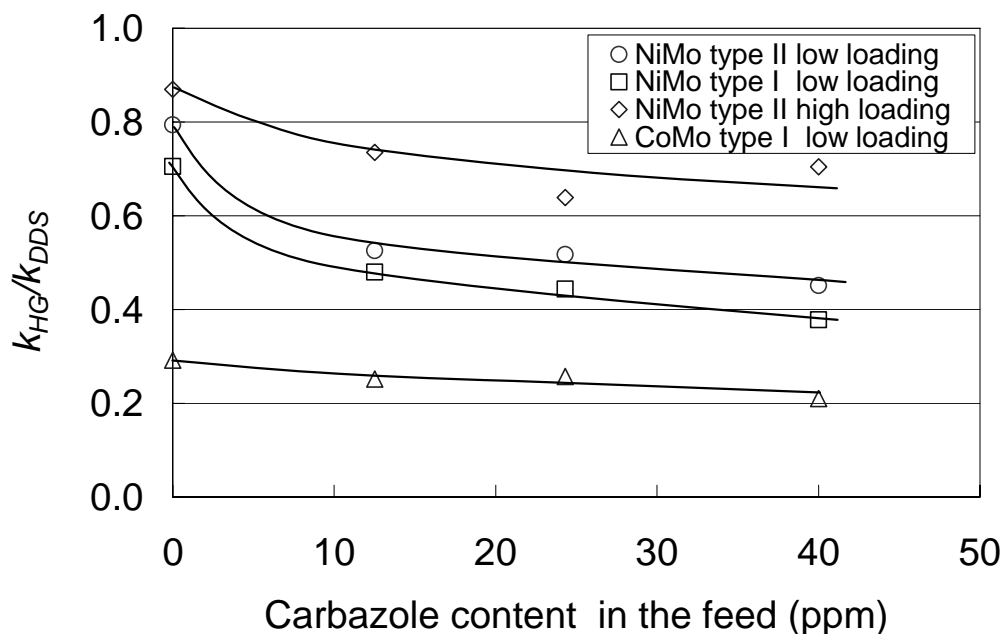


Figure 4. Carbazole inhibiting effect on ratio of HG/DDS rates in HDS of DBT on various catalysts (H_2 5 MPa, H_2S 1.5 bar, 350 °C. Pseudo-first-order kinetics, Scheme 3). Lines are drawn to guide the eye.

3.2. Comparison of the catalysts

In Fig. 5, the HDN activity ranking at varying carbazole content of the feed is shown for the catalysts studied. Rate constants $k_{\text{carbazole}}$ is calculated assuming Pseudo-first-order kinetics ($r_{\text{HDN}} = k_{\text{carbazole}} \cdot [C_{\text{carbazole}}]$). The catalyst with a high HG activity for HDS of DBT (see Table 2) shows also high activity for HDN of carbazole. This is not unexpected as carbazole reacts via the HG pathway; the result suggests that the HG steps are slower than the consecutive hydrogenolysis of C-N bond. The drop in HDN activity at increasing amounts of carbazole could be explained by Langmuir-Hinshelwood kinetics.

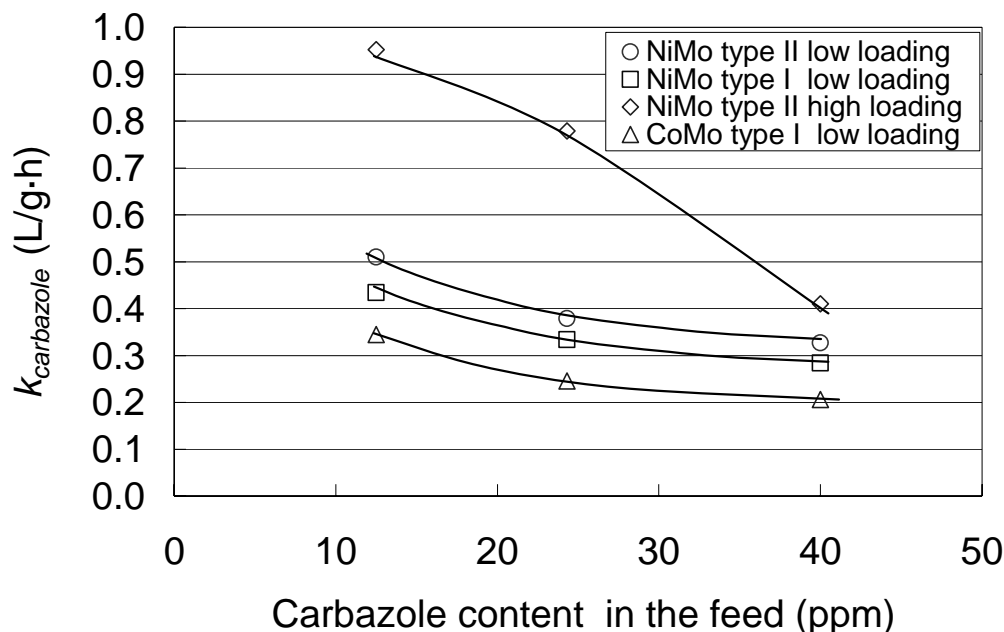


Figure 5. Carbazole self-inhibiting effect during HDS of DBT on various catalysts (H_2 5 MPa, H_2S 1.5 bar, 350 °C. Pseudo-first-order kinetics, $r_{\text{HDN}} = k_{\text{carbazole}} \cdot [C_{\text{carbazole}}]$). Lines are drawn to guide the eye.

In Table 3, the influence of DBT on the rate of HDN of carbazole is shown. The influence is very small although the molar ratio of DBT to carbazole in the feed is approx. 4. The observation that the rate of HDN of carbazole is hardly influenced by the presence of DBT whereas for the HDS of DBT carbazole does inhibit strongly suggests that the adsorption of carbazole is much stronger than that of DBT.

Table 3. The influence of the presence of DBT on the rate of HDN of Carbazole (N: 40 ppm, NiMo type II low loading. $r_{\text{HDN}} = k_{\text{carbazole}} \cdot [C_{\text{carbazole}}]$, Rate constant (L/g_{cat}·h))

	$k_{\text{carbazole}}$
Without DBT	0.35
With DBT (S: 350ppm)	0.33

In Fig. 6, the ratio of $k_{carbazole}$ to k_{HDS} is shown for increasing concentration of carbazole in the feed. This ratio decreases against the amount of carbazole added for all catalysts. It can be explained by the difference of reaction pathways of DBT and carbazole. DBT reacts via both the DDS and the HG pathways, whereas carbazole reacts only via the HG pathway. As already shown in Fig. 4, the HG pathways are inhibited more than the DDS pathways by carbazole.

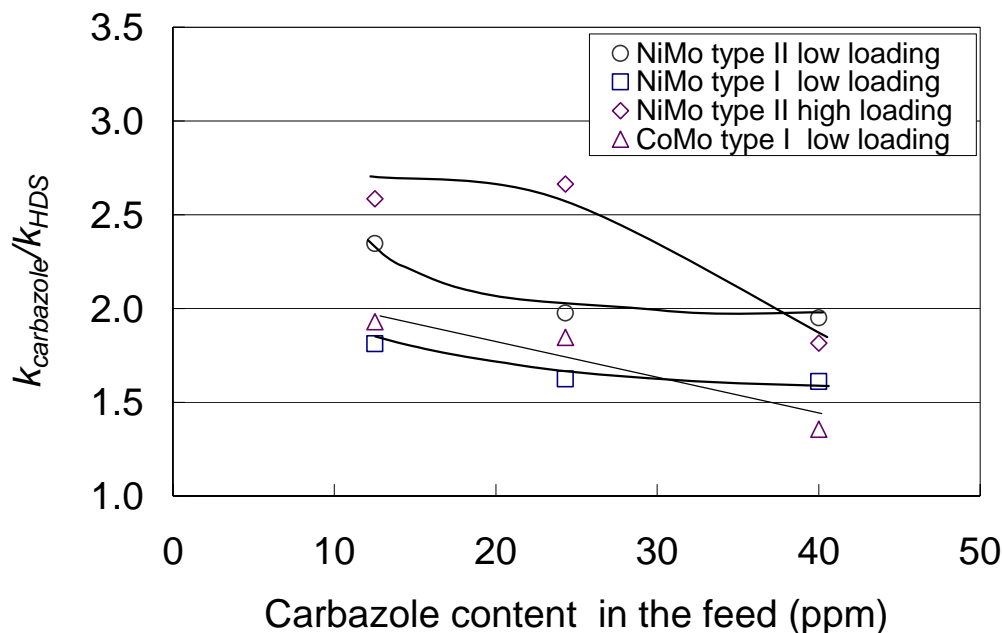


Figure 6. Ratio of carbazole and DBT rate constants vs the initial carbazole content in the feed (NiMo type II low loading catalyst, H_2 5 MPa, H_2S 1.5 bar, 350 °C. Pseudo-first-order kinetics, HDN according to $r_{HDN} = k_{carbazole} \cdot [C_{carbazole}]$, HDS according $r_{HDS} = k_{HDS} \cdot [C_{DBT}]$). Lines are drawn to guide the eye.

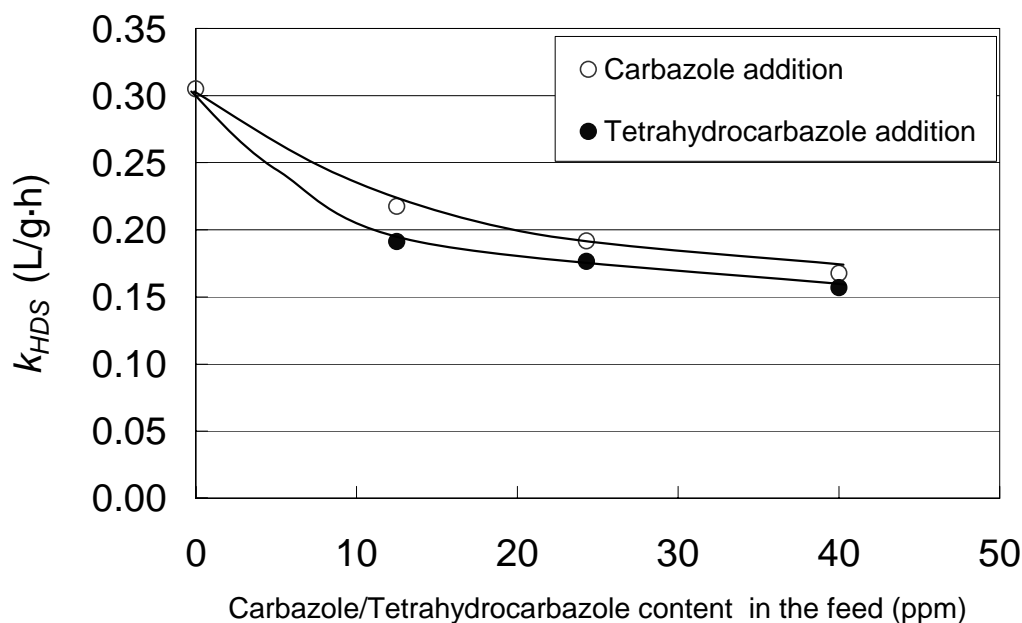


Figure 7. Carbazole and tetrahydrocarbazole inhibiting effects for HDS of DBT (NiMo type II low loading catalyst, H_2 5 MPa, H_2S 1.5 bar, 350 °C. Pseudo-first-order kinetics, $r_{HDS} = k_{HDS} \cdot [C_{DBT}]$). Lines are drawn to guide the eye.

3.3. Comparison between addition of carbazole and tetrahydrocarbazole in HDS of DBT

In Fig. 7, the inhibiting effects of carbazole and tetrahydrocarbazole during HDS of DBT on NiMo type II low loading catalyst are compared. Tetrahydrocarbazole appears to be a little stronger inhibitor than carbazole.

In Fig. 8, the ratio of k_{HG}/k_{DDS} for HDS of DBT is plotted vs initial amount of carbazole or tetrahydrocarbazole. Again the ratio of k_{HG}/k_{DDS} is decreased at increasing initial amount of these nitrogen compounds added. This supports the conclusion that the HG pathway is inhibited more than the DDS.

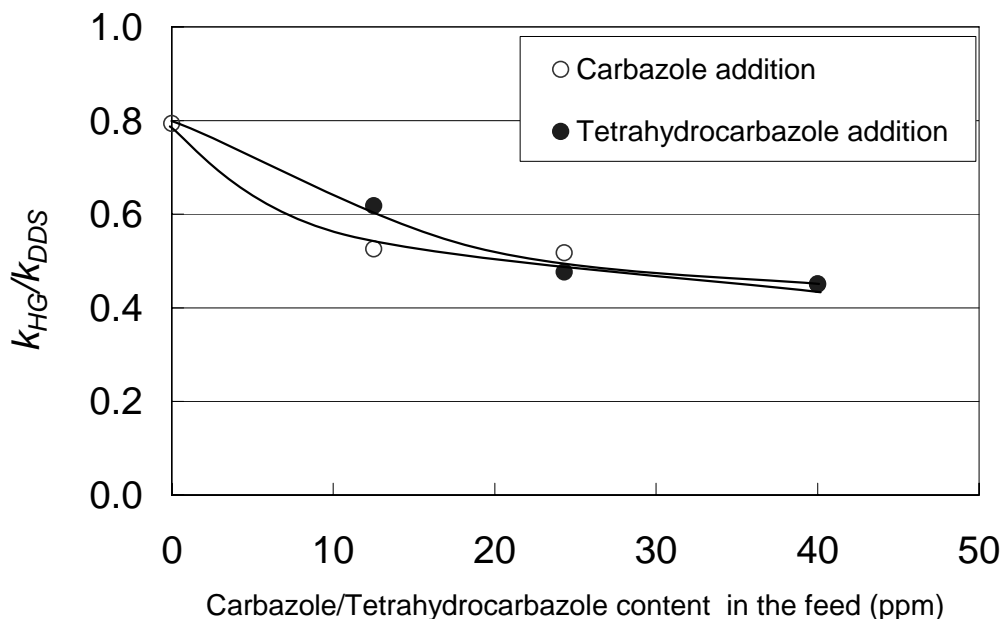


Figure 8. Carbazole and tetrahydrocarbazole inhibiting effects on the ratio of HG/DDS rate constants in HDS of DBT (NiMo type II low loading catalyst, H_2 5 MPa, H_2S 1.5 bar, 350 °C. Pseudo-first-order kinetics, Scheme 3). Lines are drawn to guide the eye.

4. Discussion

4.1. Modeling of the reaction kinetics

As shown in Fig. 8, compared to the DDS pathway the HG pathway is more inhibited by nitrogen compounds. This observation brought us to the presumption that the DDS and the HG reactions are occurring on different types of active sites. Using the Langmuir-Hinshelwood type equation in which all the organic compounds and H_2S produced are assumed to be competitively adsorbed on the two different catalytic sites, the reaction rate of DBT (r_{HDS}) is:

$$r_{HDS} = r_{DDS} + r_{HG} = \frac{N_{DDS} \cdot k_{DDS} K_{DDS,DBT} C_{DBT}}{1 + K_{DDS,DBT} C_{DBT} + K_{DDS,H_2S} C_{H_2S} + K_{DDS,CZ} C_{CZ} + K_{DDS,TC} C_{TC}} \cdot f_{DDS}(H_2) + \frac{N_{HG} \cdot k_{HG} K_{HG,DBT} C_{DBT}}{1 + K_{HG,DBT} C_{DBT} + K_{HG,H_2S} C_{H_2S} + K_{HG,CZ} C_{CZ} + K_{HG,TC} C_{TC}} \cdot f_{HG}(H_2) \quad (3)$$

where N is the number of active sites, k_{DDS} , k_{HG} is the rate constants of the DDS pathway, HG pathway according to Scheme 3, respectively, K_{DBT} , K_{H_2S} , K_{CZ} , K_{TC} are the adsorption constant of DBT, H_2S , carbazole, tetrahydrocarbazole, respectively, C_{DBT} , C_{H_2S} , C_{CZ} , C_{TC} , the concentration of DBT, H_2S , carbazole, tetrahydrocarbazole, respectively, and $f_{DDS}(H_2)$ and $f_{HG}(H_2)$ are the terms for hydrogen adsorption that can be regarded as constant under our excess H_2 conditions. The shape of this rate equation is in agreement with the reaction orders of approximately one for DBT and H_2 and minus one for H_2S , as reported by Vogelaar [16] for the DDS reaction in the HDS of DBT.

Based on the experimental results obtained, the kinetic model for both the DDS and the HG can be simplified,

$$K_{DBT} \leq K_{H_2S} \quad (4)$$

$$K_{CZ} \approx K_{TC} \equiv K_N, \quad (5)$$

$$K_{CZ} \gg K_{DBT}, \quad (6)$$

equation (3) reduces to:

$$r_{HDS} = r_{DDS} + r_{HG} = -\frac{V_L}{W} \frac{dC_{DBT}}{dt} = \frac{k'_{DDS} C_{DBT}}{1 + K'_{DDS,N} C_{CZ} + K'_{DDS,N} C_{TC}} + \frac{k'_{HG} C_{DBT}}{1 + K'_{HG,N} C_{CZ} + K'_{HG,N} C_{TC}}, \quad (7)$$

where k'_{DDS} , k'_{HG} is the relative rate constants (L/g_{cat}/h) of the DDS pathway, HG pathway according to Scheme 3, respectively, $K'_{DDS,N}$, $K'_{HG,N}$ are the relative adsorption constant (L/mol) of carbazole/tetrahydrocarbazole, C_{DBT} , C_{CZ} , C_{TC} , the concentration (mol/L) of DBT, carbazole, tetrahydrocarbazole, respectively.

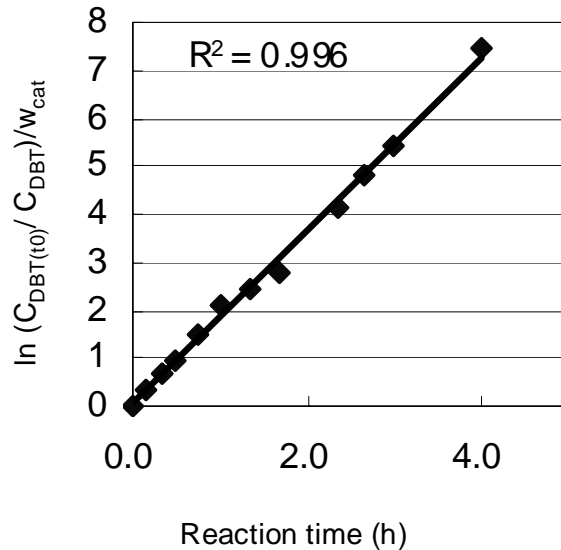


Figure 9. $\ln(C_{DBT(t)}/C_{DBT(0)})$ vs reaction time for HDS of DBT (NiMo type II low loading catalyst, H_2 5 MPa, H_2S 1.5 bar, 350 °C. Pseudo-first-order kinetics, $r_{HDS} = k_{HDS} \cdot [C_{DBT}]$).

This major simplification is based on the following reasoning. Without the presence of carbazoles, apparent first-order behaviour of DBT HDS was observed under our experimental conditions, since we obtained a linear dependency, plotting $\ln(C_{DBT(t)}/C_{DBT})$ vs reaction time [17], see Fig. 9. The high R^2 shows that the conclusion is statistically justified. This observation leads to a simple interpretation. It was reported that the adsorption constant of H_2S is higher than DBTs as shown in equation (4) [18]. Therefore, due to the excess H_2S (DMDS was added, decomposing to H_2S approx. 10 times more than initial concentration of DBT before reaction starts), the term $K_{DBT}C_{DBT} \ll K_{H_2S}C_{H_2S}$ is satisfied and that $K_{H_2S}C_{H_2S}$ will be almost independent of DBT conversion. As shown in Fig. 7, the inhibiting effect of tetrahydrocarbazole is only slightly different from that of carbazole, leading to the simplification given in equation (5). From the data in Table 3, it was concluded that the adsorption constant of carbazole is much higher than that of dibenzothiophene. This leads to equation (6). After neglecting $K_{DBT}C_{DBT}$ vs. $K_{H_2S}C_{H_2S}$ and assuming C_{H_2S} to be constant, both numerator and denominator in both terms in equation (3) can be divided by $1 + K_{DDS,H_2S}C_{H_2S}$, $1 + K_{HG,H_2S}C_{H_2S}$, respectively, equation (3) reduces to equation (7).

From the experiments in which the amount of carbazole and tetrahydrocarbazole was varied, the relative adsorption constants of nitrogen compounds for the DDS ($K'_{DDS,N}$) and the HG ($K'_{HG,N}$) pathways could be obtained numerically using least square method (equation (1), (2) and (7)).

4.2. Quality of fitting results

In Fig.10, fitting results for HDS of DBT on NiMo type II low loading in the presence of carbazole and tetrahydrocarbazole are shown, varying their concentration. In the case that tetrahydrocarbazole was added as initial nitrogen compound, the reverse dehydrogenation has been observed directly, producing carbazole. From data of NiMo type II low loading for HDS of DBT in addition of carbazole and tetrahydrocarbazole (see Fig.10 a, 10b), the k_1 , k_{-1} and k_2 in equation (1) and (2) were calculated numerically, corresponding to the simplified Scheme 2. Table 4 shows the relative adsorption constants for the NiMo type II low loading and the rate constants. The quality of fitting of the DBT molar fractions is high, and that of the carbazoles molar fraction is reasonable.

In both cases of HDN of carbazole and tetrahydrocarbazole, the simulated curves deviate to lower values than the actual at increasing their concentration, probably due to self-inhibition, in agreement with the results in Fig. 5. However, it is hard to draw more detailed conclusions as the concentrations of products from carbazole were quite low.

Table 4. Relative adsorption constant of $K_{DDS,N}$, $K_{HG,N}$ on addition of carbazoles on NiMo type II low loading catalyst (by equation (7), the standard deviations are shown in parentheses)

HDS of DBT (L/g _{cat} ·h)			Relative adsorption constant (L/mol)		HDN of carbazole (L/g _{cat} ·h)		
k'_{DDS}	k'_{HG}	$k'_{DDS'}$	$K'_{DDS,N}$	$K'_{HG,N}$	k_1	k_{-1}	k_2
0.14	0.10	1.13	266	1438	0.44	0.30	0.63
(0.002)	(0.003)	(0.060)	(23)	(112)	(0.023)	(0.032)	(0.024)

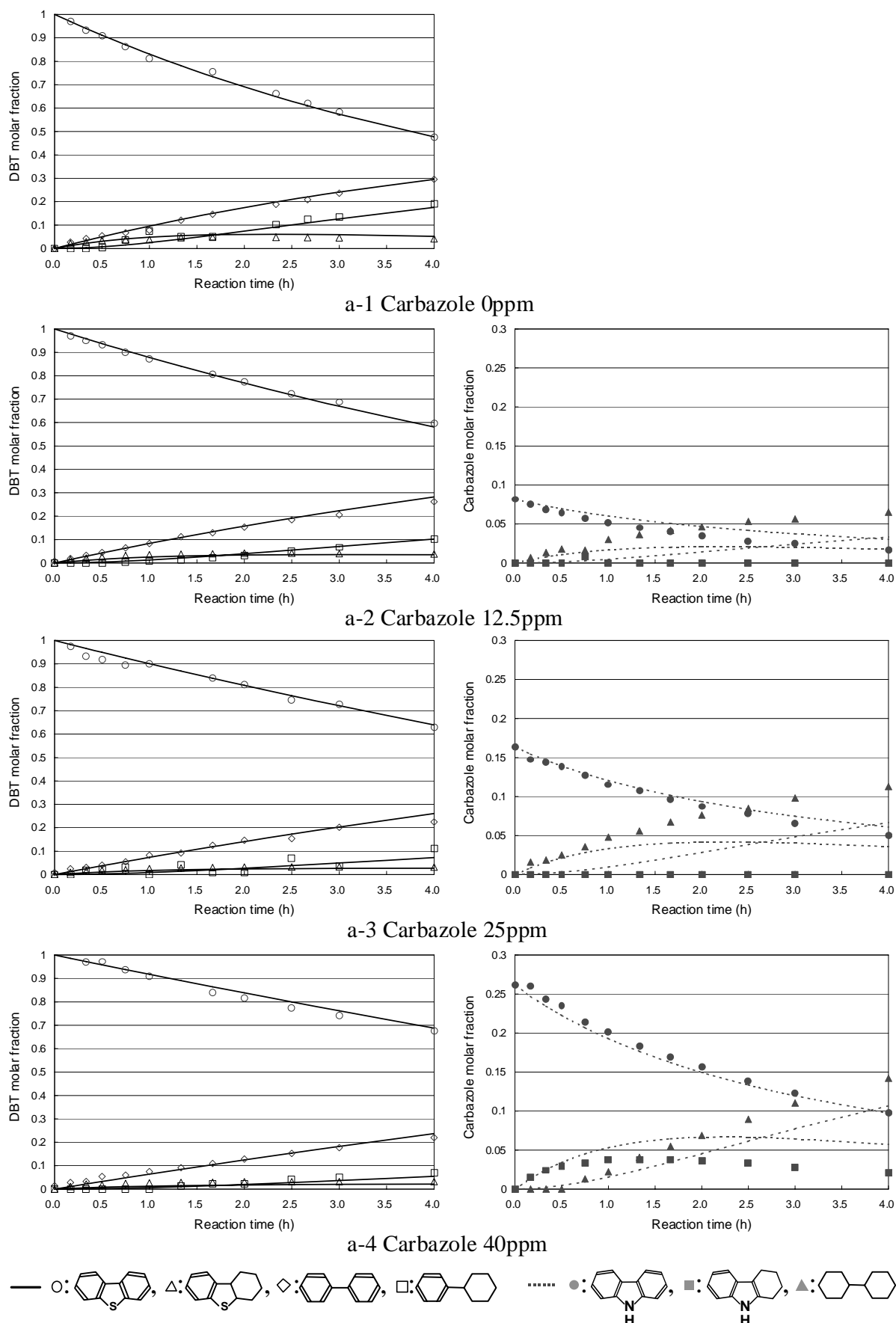


Figure 10a. Fitting results for HDS of DBT in the presence of carbazole on NiMo type II low loading (H_2 5 MPa, H_2S 1.5 bar, 350 °C, HDN/HDS according to Scheme 2/Scheme 3).

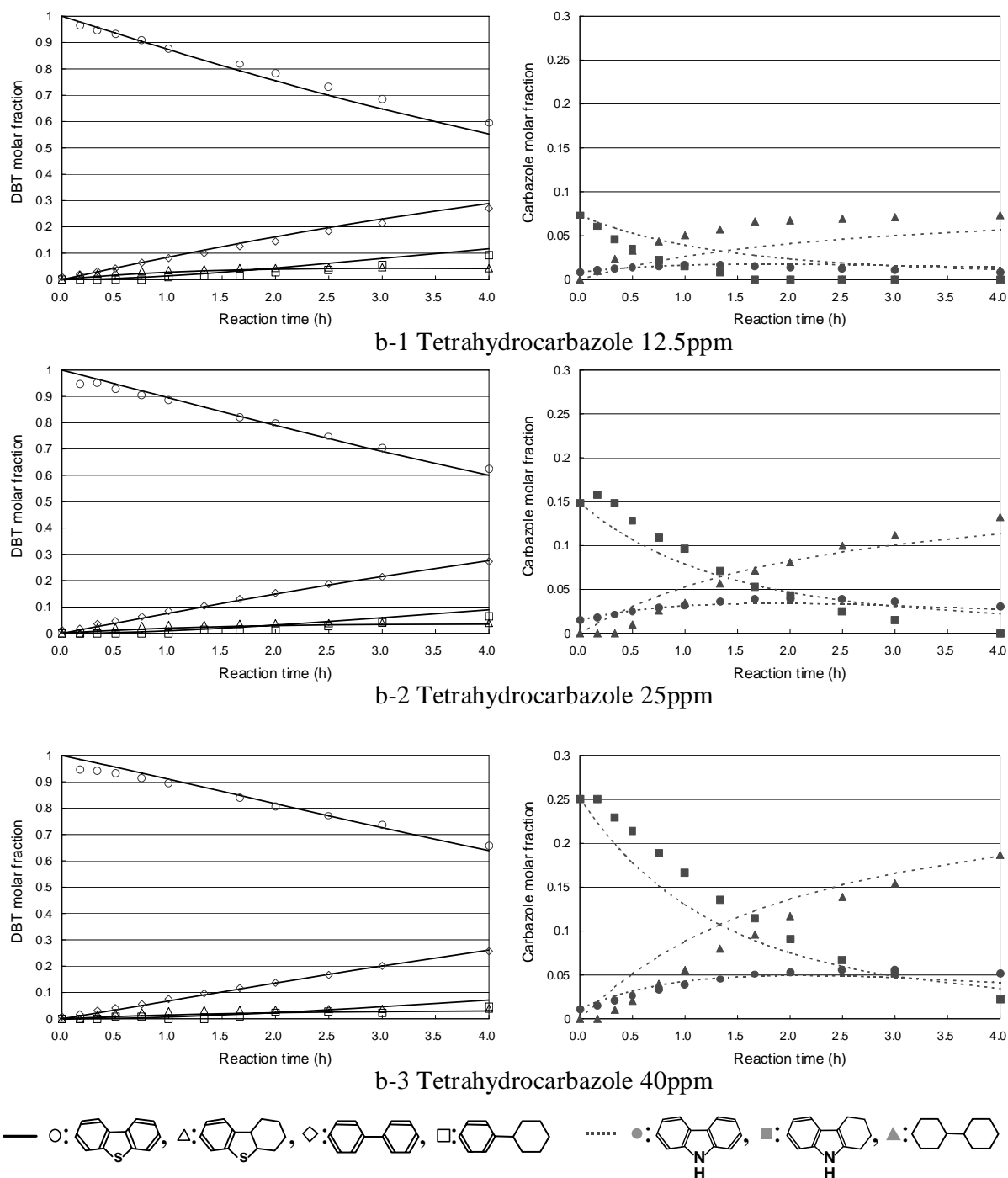


Figure 10b. Fitting results for HDS of DBT in the presence of tetrahydrocarbazole on NiMo type II low loading (H_2 5 MPa, H_2S 1.5 bar, 350 °C. HDN/HDS according to Scheme 2/ Scheme 3).

The dataset of Fig 10a and 10b was used for fixing the ratio k_{-1}/k_1 . To check the validity of Scheme 2, we applied the ratio k_{-1}/k_1 for fitting the data of the HDN of carbazole without DBT. As shown in Table 5 and Fig. 11, the fitting quality is almost the same as in Fig. 2a (the sum of squared deviations of the fits shown in Fig. 11 and 2a were 0.00188 and 0.00177, respectively). Therefore, it is reasonable that for the fitting the ratio of k_{-1}/k_1 , the data set of DBT HDS with carbazole and tetrahydrocarbazole addition is used. And after that the data set of HDN of

carbazole without DBT was applied for fitting k_2/k_1 , as this dataset is the most suitable to get the proper ratio of the rate constants of HDN pathways of carbazole.

The ratios k_1/k_1 and k_2/k_1 obtained for the NiMo type II low loading, which are shown in Table 5, are assumed to be the same for the other catalysts tested, having similar active sites and exhibiting a similar reaction mechanism. Therefore these ratios are used in the fitting the data for HDS of DBT in addition of carbazole on all the catalysts. The fitting results are shown in Fig. 12a-c. Again, the quality of fitting of the DBT molar fractions is high, and that of the carbazoles molar fraction is reasonable. Moreover, the simulated curves of HDN deviate to lower values at increasing concentration of the nitrogen compounds, probably due to self-inhibition. Table 6 shows the relative adsorption constants for the various catalysts and the rate constants corresponding to the simplified scheme.

The values of the adsorption constants confirm that the inhibiting effect of carbazole and tetrahydrocarbazole on the HG pathway is higher than that on the DDS pathway for all catalysts, which is in agreement with the results in Fig. 4. Moreover, the type II high loading catalyst is inhibited most significantly, which was expected since this catalyst exhibits the highest HG activity. However, compared with the type II low loading catalyst, the increase of adsorption constant is also significant for the DDS. In Fig. 3, at large nitrogen addition, the activity of type II high loading catalysts is not so much higher any more. Therefore, the nitrogen concentration in feedstocks will be an important factor to investigate for the application of the type II high loading catalyst.

4.3. Comparison between tetrahydrocarbazole and carbazole inhibiting effects

To see the difference of inhibiting effects of tetrahydrocarbazole and carbazole, equation (8) was applied, instead of equation (7):

$$r_{HDS} = r_{DDS} + r_{HG} = \frac{k'_{DDS} C_{DBT}}{1 + K'_{DDS,CZ} C_{CZ} + K'_{DDS,TC} C_{TC}} + \frac{k'_{HG} C_{DBT}}{1 + K'_{HG,CZ} C_{CZ} + K'_{HG,TC} C_{TC}} \quad , \quad (8)$$

It means that the assumption that $K_{CZ} = K_{TC}$, i.e. equation (5), was not used.

From the experiments in which the amount of carbazole and tetrahydrocarbazole were varied, the relative adsorption constants for the DDS ($K'_{DDS,CZ}$, $K'_{DDS,TC}$) and the HG ($K'_{HG,CZ}$, $K'_{HG,TC}$) pathways could be obtained numerically using the least square method. The fitting quality in Table 7 is the same as that in Table 4 (the sum of squared deviation of the fits in Table 4 and 7 were 0.111 and 0.108, respectively). As shown in Table 7, the inhibiting effect of tetrahydrocarbazole on HG pathway is stronger than that of carbazole. This is probably related to the higher basicity of tetrahydrocarbazole. Literature gives support to this conclusion. The proton affinity and gas basicity data of cyclic nitrogen compounds, shown in Table 8 [19], clearly show that tetrahydrocarbazole is more basic than carbazole itself. Analogously, also hydrogenated intermediates of carbazole are likely to show more basicity than carbazole.

Table 5. Rate constants of HDN of carbazole without DBT on NiMo type II low loading catalyst (H_2 5 MPa, H_2S 1.5 bar, 350 °C. Pseudo-first-order kinetics, by equation (1),(2), Rate constant ($L/g_{cat}\cdot h$)).

k_1	k_{-1}	k_2
0.40	0.27	1.66

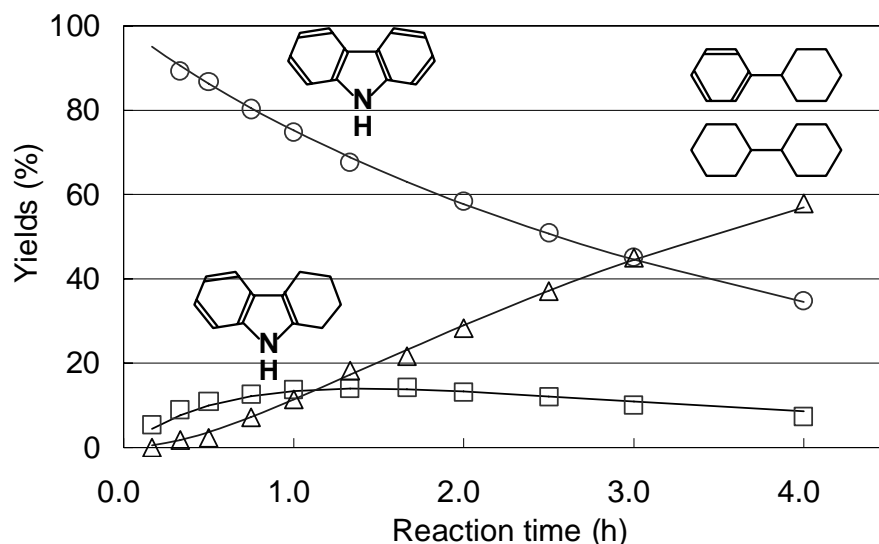
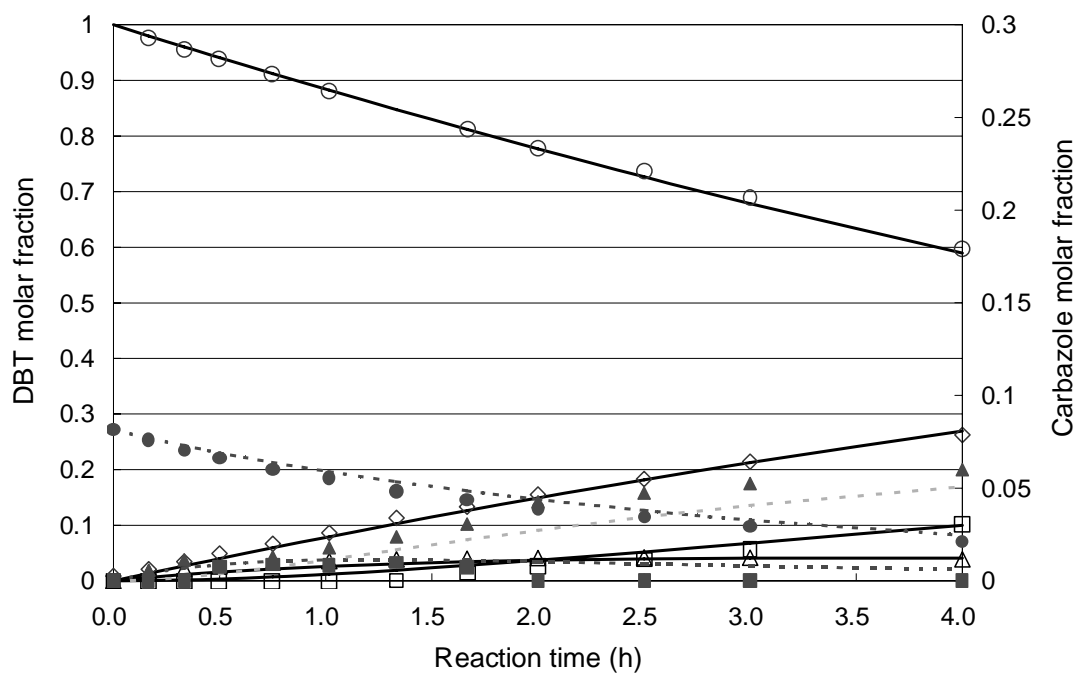


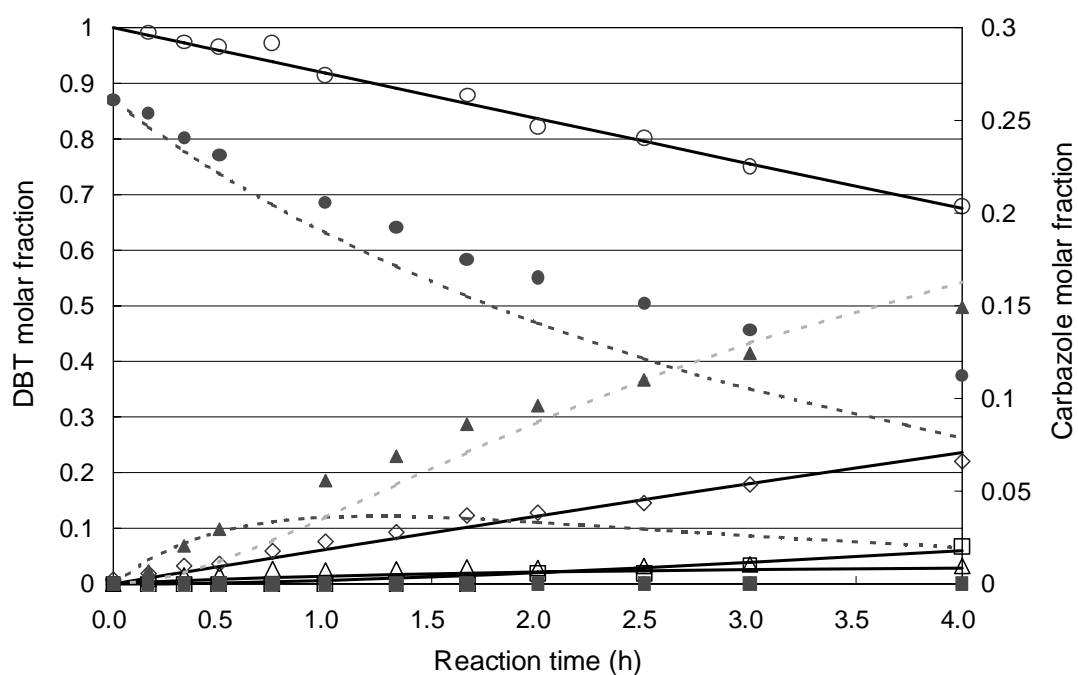
Figure 11. Product yields vs reaction time for HDN of carbazole on NiMo catalyst (NiMo type II low loading catalyst, H_2 5 MPa, H_2S 1.5 bar, 350 °C, no DBT present. Pseudo-first-order kinetics, Scheme 2)

Table 6. Rate constant of HDS of DBT and HDN of carbazole, and relative adsorption constant of $K_{DDS,N}$, $K_{HG,N}$ on addition of carbazoles on various catalysts (by equation (7), the standard deviations are shown in parentheses)

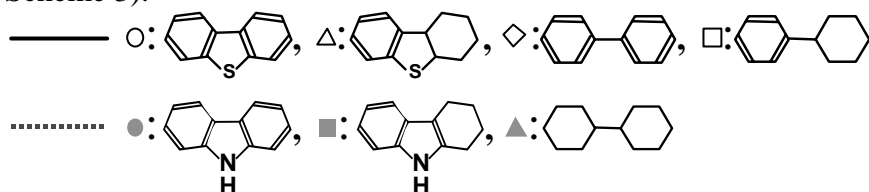
	HDS of DBT ($L/g_{cat}\cdot h$)			Relative adsorption constant (L/mol)		HDN of carbazole ($L/g_{cat}\cdot h$)		
	k'_{DDS}	k'_{HG}	$k'_{DDS'}$	$K'_{DDS,N}$	$K'_{HG,N}$	k_1	k_{-1}	k_2
NiMo type II low loading	0.14 (0.002)	0.10 (0.002)	1.31 (0.063)	355 (24)	1158 (88)	0.42 (0.012)	0.29 -	1.76 -
NiMo type I low loading	0.12 (0.003)	0.09 (0.004)	1.02 (0.087)	236 (36)	1097 (151)	0.45 (0.017)	0.31 -	1.88 -
NiMo type II high loading	0.21 (0.004)	0.19 (0.004)	2.06 (0.112)	890 (47)	1703 (97)	0.59 (0.017)	0.40 -	2.46 -
CoMo type I low loading	0.17 (0.003)	0.05 (0.003)	0.92 (0.099)	389 (25)	1044 (176)	0.26 (0.010)	0.18 -	1.09 -

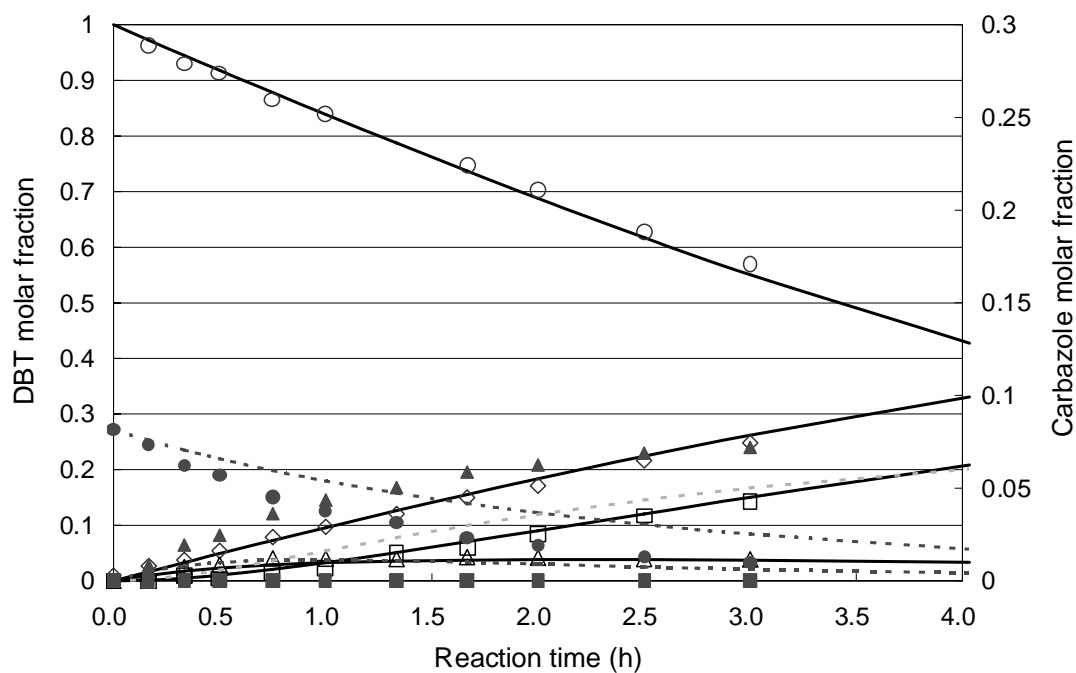


a-1. Carbazole 12.5 ppm

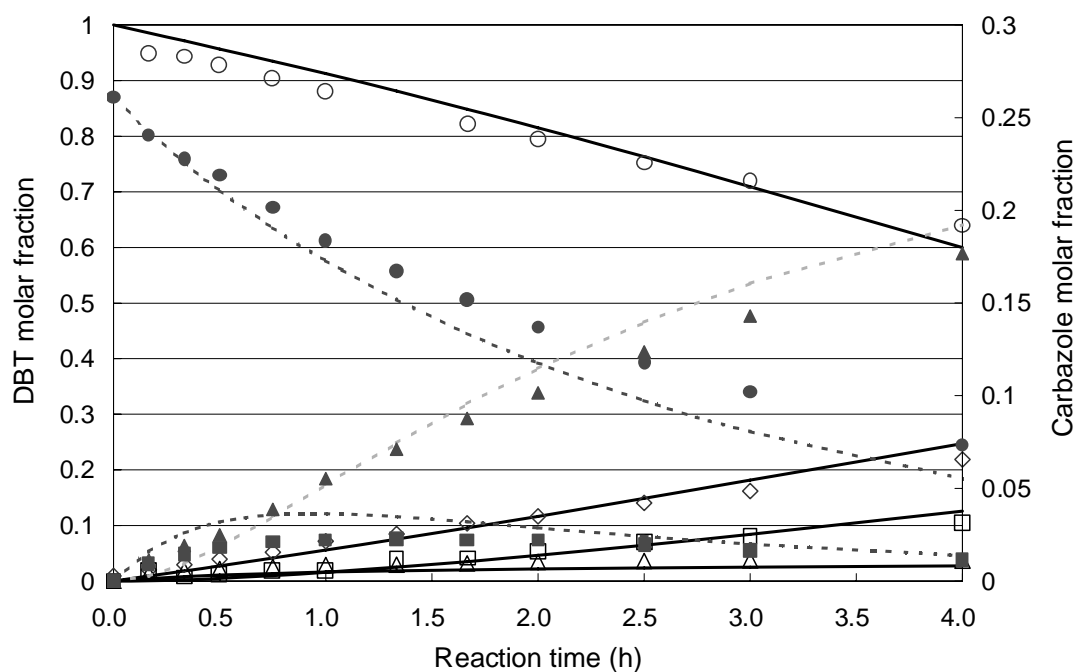


a-2. Carbazole 40ppm

 Figure 12a. Fitting results for HDS of DBT in the presence of carbazole on NiMo type I low loading (H_2 5 MPa, H_2S 1.5 bar, 350 °C. HDN according to Scheme 2, HDS according to Scheme 3).


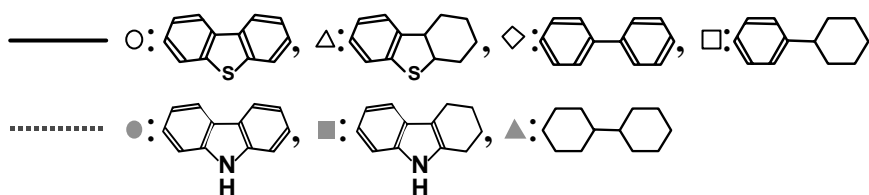


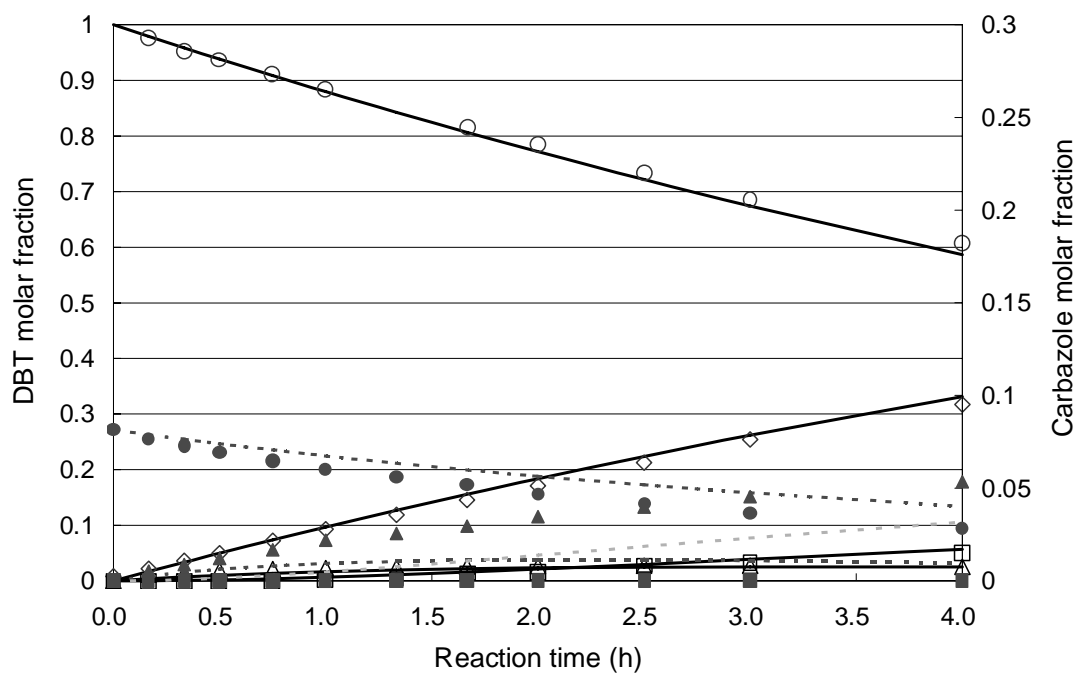
b-1. Carbazole 12.5 ppm



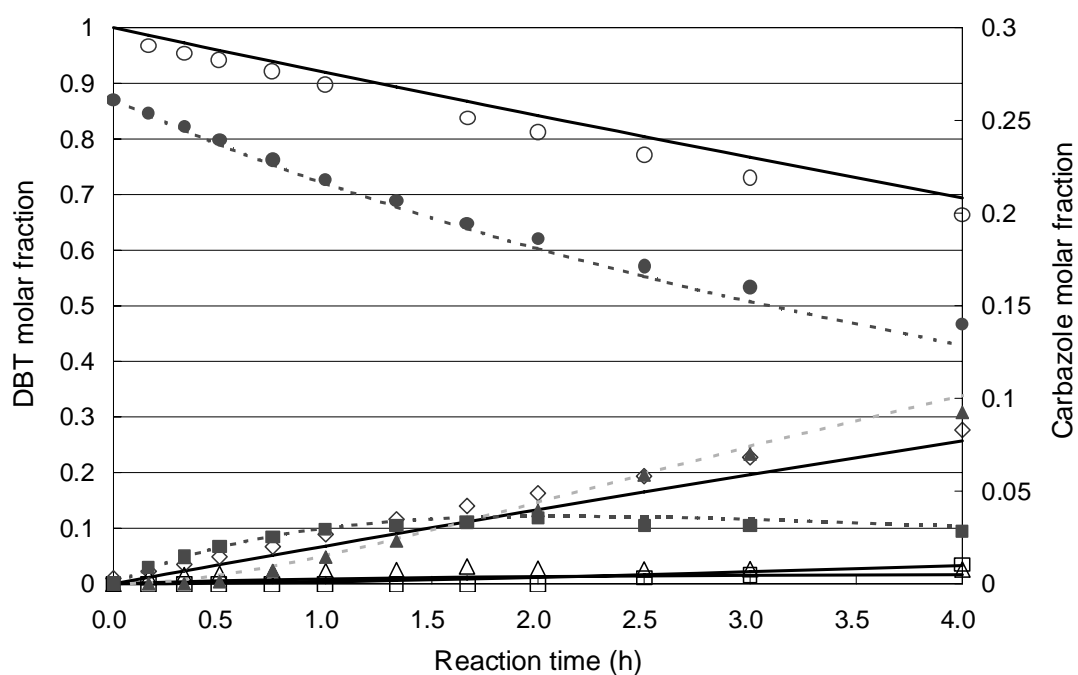
b-2. Carbazole 40 ppm

Figure 12b. Fitting results for HDS of DBT in the presence of carbazole on NiMo type II high loading (H_2 5 MPa, H_2S 1.5 bar, 350 °C. HDN according to Scheme 2. HDS according to Scheme 3).





c-1. Carbazole 12.5 ppm



c-2. Carbazole 40 ppm

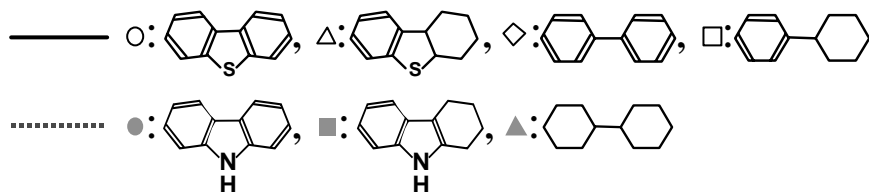
 Figure 12c. Fitting results for HDS of DBT in the presence of carbazole on CoMo type I low loading (H_2 5Mpa, H_2S 1.5bar, $350^\circ C$. HDS according to Scheme 3).


Table 7. Relative adsorption constant of $K_{DDS, N}$, $K_{HG, N}$ on addition of carbazole and tetrahydrocarbazole on NiMo type II low loading catalyst (by equation (8), the standard deviations are shown in parentheses)

HDS of DBT			Relative adsorption constant				HDN of carbazole		
k'_{DDS}	k'_{HG}	$k'_{DDS'}$	$K'_{DDS,CZ}$	$K'_{DDS,TC}$	$K'_{HG,CZ}$	$K'_{HG,TC}$	k_1	k_{-1}	k_2
0.14 (0.002)	0.11 (0.003)	1.15 (0.060)	306 (33)	226 (40)	593 (131)	2802 (326)	0.43 (0.022)	0.28 (0.031)	0.64 (0.024)

Table 8. The basicity of cyclic nitrogen compounds and their hydrogenated compounds

Nitrogen compound						
Proton affinity (kJ/mol)	875.9	948.7	934.1	957.9	929.5	954.6
Gas basicity (kJ/mol)	844.5	912.7	902.7	927.0	898.9	921.1

4. Conclusions

Carbazole inhibits not only both the DDS and the HG pathways in HDS of DBT significantly, but also the HDN reaction itself. The HG pathway for DBT HDS is more inhibited by carbazoles than the DDS pathway. Consequently, HDN is inhibited more than HDS by carbazole since HDN reaction occurs only after the hydrogenation of aromatic rings.

Tetrahydrocarbazole addition was applied to see the difference in inhibiting effect between before and after the hydrogenation during HDN of carbazole. The hydrogenated intermediate retards HDS of DBT more significantly than the original nitrogen compound, probably due to its stronger basicity.

The NiMo type II high loading catalyst is inhibited the most strongly. This was expected since the highest HG activity is retarded the most easily by carbazole.

References

- [1] D.D.Whitehurst, H.Farag, T.Nagamatsu, K.Sakanishi, and I.Mochida, *Catalysis Today*, **45** (1998) 299.
- [2] T.Kabe, K.Akamatsu, A.Ishihara, S.Otsuki, M.Godo, Q.Zhang, and W.H.Qian, *Industrial & Engineering Chemistry Research*, **36** (1997) 5146.
- [3] T.Isoda, S.Nagao, X.L.Ma, Y.Korai, and I.Mochida, *Applied Catalysis A-General*, **150** (1997) 1.
- [4] P.Zeuthen, K.G.Knudsen, and D.D.Whitehurst, *Catalysis Today*, **65** (2001) 307.
- [5] K.H.Choi, N.Kunisada, Y.Korai, I.Mochida, and K.Nakano, *Catalysis Today*, **86** (2003) 277.
- [6] H.Topsoe, B.S.Clausen, F.E.Massothe, J.R.Anderson, and D.Bougeard, *Catalysis Science and Technology*, **Vol. 11** (1996)
- [7] T.C.Ho, *Catalysis Reviews-Science and Engineering*, **30** (1988) 117.
- [8] T.Koltai, M.Macaud, A.Guevara, E.Schulz, M.Lemaire, R.Bacaud, and M.Vrinat, *Applied Catalysis A-General*, **231** (2002) 253.
- [9] G.C.Laredo, A.Montesinos, and J.A.los Reyes, *Applied Catalysis A: General*, **265** (2004) 171.
- [10] S.D.Sumbogo Murti, H.Yang, K.H.Choi, Y.Korai, and I.Mochida, *Applied Catalysis A: General*, **252** (2003) 331.
- [11] M.J.Girgis and B.C.Gates, *Ind.Eng.Chem.Res.*, **30** (1991) 2021.
- [12] M.Vrinat, *Appl.Catal.*, **6** (1983) 137.
- [13] R.Shafi and G.J.Hutchings, *Catalysis Today*, **59** (2000) 423.
- [14] H.R.Reinhoudt, C.H.M.Boons, A.D.van Langeveld, J.A.R.van Veen, S.T.Sie, and J.A.Moulijn, *Appl.Catal.A: Gen.*, **207** (2001) 25.
- [15] M.Nagai, Y.Goto, A.Irisawa, and S.Omi, *Journal of Catalysis*, **191** (2000) 128.
- [16] B.M.Vogelaar, N.Kagami, A.D.van Langeveld, S.Eijsbouts, and J.A.Moulijn, *Prepr.Pap.-Am.Chem.Soc.Div.Fuel Chem.*, **48** (2003) 548.
- [17] V.La Vopa and C.N.Satterfield, *Journal of Catalysis*, **110** (1988) 375.
- [18] T.Kabe, Y.Aoyama, D.H.Wang, A.Ishihara, W.H.Qian, M.Hosoya, and Q.Zhang, *Appl.Catal.A: Gen.*, **209** (2001) 237.
- [19] E.P.L.Hunter and S.G.Lias, *Journal of Physical and Chemical Reference Data*, **27** (1998) 413.

7

New highly active Ni-Mo catalyst for deep HDS of diesel

Abstract

In this chapter, W addition effects on NiMo catalyst are tested for HDS of DBT and 4,6-DMDBT, varying the molar ratio of W to Mo. For DBT HDS, the activity decreases at increasing W/Mo ratio, while for 4,6-DMDBT, the activity increases at low W-loading and decreases at higher W-loading ($W/(W+Mo) > 0.75$). Moreover, titanium oxide addition on alumina was tested. The NiMoW catalyst added titanium oxide was highly active for 4,6-DMDBT HDS, probably due to the synergy effects of W and titanium. The catalysts have been characterized by TPR, TPS and it is suggested that TiO_2 has less interaction with W than Al_2O_3 and co-existence with Mo enhances the sulfiding of W. The good performance of the new catalyst was confirmed for practical applications by carrying out HDS activity test using diesel fuel.

The contents of this chapter are patented in:

N. Kagami and J. A. Moulijn (Idemitsu Kosan Co.Ltd., Delft University of Technology), JP2005-262173, A(09//29/2005).

1. Introduction

To develop highly active catalysts for diesel ultra deep HDS, there are several conceivable ways to improve the activity of catalysts in desulfurization of the most refractory species such as β -substituted dibenzothiophene in diesel fuel [1].

First of all, the number of active sites can be increased by increasing the amount of active metal loading as much as possible, provided the dispersion of active metals is kept higher than the conventional catalyst at comparable metal loading. In Chapter 3 and 4, we reported that type II catalyst is promising because the active phase can exist as a higher dispersed state than the active phase of type I at loadings above monolayer surface coverage.

The second is to add isomerization activity to the catalyst in order to decrease the steric hindrance of the β -substituted DBT. However, generally, strong acidity is necessary for isomerization. For instance, the addition of Y-type zeolite has been studied catalyzing isomerization [2]. Due to high acidity, undesired hydrocracking might be occurring reducing the liquid yield, and catalyst deactivation might occur under the typical conditions for diesel hydrotreating. Furthermore, under deep desulfiding conditions N-compounds are usually present and because of their basic character they will block the strong acid sites.

The third is to optimize hydrogenation activity. It is expected that the steric hindrance of β -substituted groups is reduced after hydrogenation of the parent DBTs. An other effect is that the electron density of sulfur atom after the hydrogenation is higher than the parent one, resulting in higher reactivity [3]. In Chapter 4, type II NiMo catalysts appeared to be promising for the diesel in deep HDS range, probably due to their high hydrogenation activity.

It has been reported that NiW catalysts can be highly active for β -substituted DBT HDS [4]. Generally, NiW catalysts are known to be highly active for the hydrogenation of aromatics and they are often applied for the hydrofinishing of lubricant oil. To benefit from the high hydrogenation function of W, the exchange of W for Mo on type II of NiMo catalysts was investigated at high Mo loading, above monolayer surface coverage.

As a modification of support, titania has been reported as one of the effective components to increase the rate of HDS especially via the HG reaction pathway for 4,6-DMDBT [5]. Recently, it has been reported that W is more easily sulfided on TiO_2 than on Al_2O_3 , due to the weaker interaction with TiO_2 . NiW catalysts show higher activity in the case of titania support than in the case of alumina support [6, 7]. Therefore, the addition of TiO_2 to Al_2O_3 was investigated for a possible synergy effect with W addition on NiMo catalyst.

2. Experimental

2.1. Preparation of NiMo catalysts

NiO-MoO₃/Al₂O₃ catalysts were prepared via liquid phase pore volume impregnation using aqueous solutions containing the required amounts of Ni and Mo, according to the literature. After high purity γ -Al₂O₃ in the form of 1.5 mm extrudates had been impregnated by the solution, they were dried at 120 °C for 12 hours without calcinations (see Chapter 2).

NiO-MoO₃-WO₃/Al₂O₃ catalysts were prepared in the same way exchanging part of Mo to W, varying the W/(Mo+W) molar ratio from 0 to 1.0 at 0.25 intervals. The composition of

catalyst was measured by INAA (Instrumental Neutron Activation Analysis). In Table 1, the composition of the catalysts is shown.

For characterization of W exchange to Mo, three catalyst preparation procedures were applied, where the W/(Mo+W) molar ratio is 0.5: co-impregnation of NiMo and NiW, pre-impregnation of NiW followed by NiMo, and post-impregnation of NiW after NiMo impregnation. For the sequential procedure, the catalyst after the first impregnation was dried at 120 °C and, subsequently, the other impregnation was carried out and dried at 120 °C without calcination.

TiO₂ addition to the support alumina was carried out via liquid phase pore volume impregnation, using aqueous solution containing the various amounts of Ti. Titanium hydroxide gel was prepared from the precipitation of titanium tetrachloride and aqueous ammonia. The titanium tetrachloride was gradually dropwise added to the cooling demineralised water with cooling down with iced bath, producing colourless titanium hydroxide sol. Sequentially aqueous ammonia was gradually dropwise added, forming titanium hydroxide gel. The gel was washed and filtered in order to remove chloride ion. The titanium hydroxide was dissolved with ammonia and hydrogenperoxide aqueous solution and chelating was performed with citric acid at 50 °C, sequentially the mixture was heated up to 80 °C, according to the Japanese patent application JP2005-262173, A (09//29/2005). After the impregnation, the TiO₂-Al₂O₃ supports were dried and calcinated at 500 °C. In Table 2, the composition of the supports is shown. In the same way as the Al₂O₃ supported catalysts, NiO-MoO₃-WO₃/ TiO₂-Al₂O₃ catalysts were prepared.

Table 1 Composition of NiMoW catalysts

	Ni/(Mo+W) molar ratio	Mo loading (atom / nm ²)	W loading (atom / nm ²)
NiMoW(0)	0.35	10.5	0.0
NiMoW(25)	0.34	7.3	2.5
NiMoW(50)	0.33	5.0	4.6
NiMoW(75)	0.32	2.6	6.9
Pre-NiW-Mo(50)	0.32	4.9	4.6
Post-NiW-Mo(50)	0.32	4.9	4.7

Table 2 Composition of supports

Support	TiO ₂ (wt%)	TiO ₂ /(TiO ₂ +Al ₂ O ₃)
TiO ₂	0	0
TiO ₂ (3)-Al ₂ O ₃	3	2.6
TiO ₂ (4)-Al ₂ O ₃	4	3.5
TiO ₂ (5)-Al ₂ O ₃	5	4.3

2.2. Activity measurement

The activity for liquid-phase DBT was determined in a batch reactor at 5 MPa total pressure in balance hydrogen. Catalysts were crushed and sieved properly before the test, to satisfy the criteria for avoiding mass transfer limitations [8]. Before the reaction, catalysts were presulfided at 370 °C. The feed consisted of DBT in hexadecane. In both cases sulfur concentration in the

feed was 350 ppm. The inhibiting effect of H₂S is strong for HDS reactions. To mimic commercial reactor conditions, dimethyldisulfide (DMDS) was added in the liquid phase reactions to adjust the H₂S pressure to constant level (1.5 bar). This also provided the condition that the effect of self-produced H₂S was minimized. The activity for liquid-phase 4,6-dimethyldibenzothiophene (4,6-DMDBT) HDS was determined in the same way of DBT HDS. The feed consisted of 4,6-DMDBT in tetradecane and DMDS was added in the liquid phase reactions to adjust the H₂S pressure to constant level (0.75 bar). Gas chromatography with a FID detector was used for quantitative analysis of products. An inert hydrocarbon (0.2 wt% octadecane) was added as the internal standard in the feed for GC analysis.

A microflow reactor was used measure the activity for real feedstocks, straight run gas oil. The feed properties are shown in Table 3.

The same experimental methods as described in Chapter 2 were applied for these activity measurements.

Table 3 Feed properties of LGO

Density	at 15° C	g/cc	0.8542
Sulfur		wt%	0.84
Composition (HPLC)	1-ring Aromatics	vol%	16.2
	2-ring Aromatics	vol%	9.9
	≥3-ring Aromatics	vol%	1.3
Distillation (ASTM D86)	IBP vol%	° C	233
	5 vol%	° C	273
	10 vol%	° C	281
	20 vol%	° C	291
	30 vol%	° C	299
	40 vol%	° C	307
	50 vol%	° C	316
	60 vol%	° C	326
	70 vol%	° C	338
	80 vol%	° C	353
	90 vol%	° C	370
	95 vol%	° C	380
	FBP vol%	° C	387
Nitrogen		ppm	124
Cetane Index			54.2

2.3. Catalyst characterization

TPR measurements were performed for the characterization of the reducibility of oxide precursor and identification of the oxidic phases of active metals. Moreover, TPS measurements were carried out for the characterization of the transformation of oxidic precursor to sulfidic phase. In this chapter, these techniques were applied to investigate the effect of W exchange to Mo on NiMo. These techniques give information on the interaction between support and active metals. The effect of TiO₂ addition on Al₂O₃ in NiMo catalysts was also investigated. The same experimental methods as described in Chapter 3 were applied for TPR and TPS.

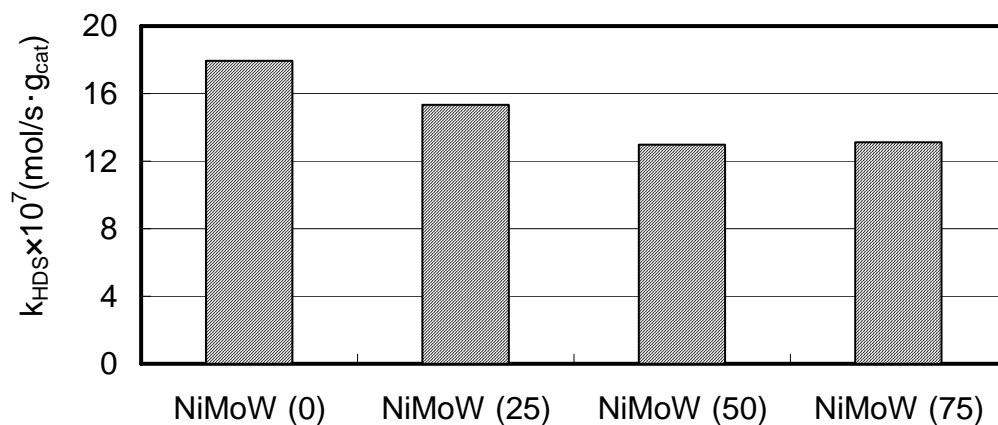


Figure 1 W exchanging effect on DBT HDS on co-impregnation NiMo/Al₂O₃.

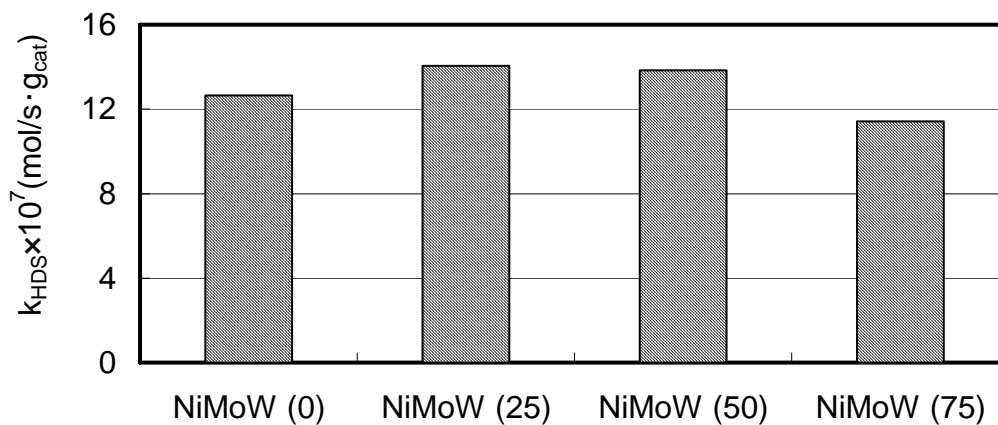


Figure 2 W exchanging effect on 4,6-DMDBT HDS on co-impregnation NiMo /Al₂O₃.

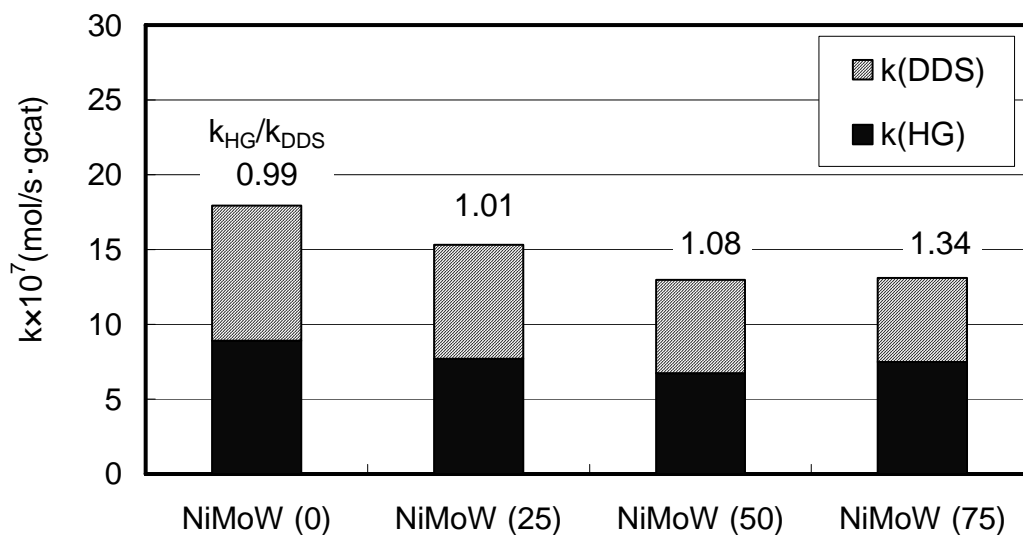


Figure 3 W exchanging effect on DDS and HG of DBT HDS on co-impregnation NiMo/Al₂O₃.

3. Results and discussion

3.1. HDS of DBT and 4,6-DMDBT

In Fig. 1, the effect of the addition of W on NiMo catalyst is shown. At increasing W/Mo ratio, the activity for DBT decreases. On the other hand in Fig. 2, it is remarkable that the activity for 4,6-DMDBT increases at low W/Mo ratio, whereas at high W/Mo ratio (0.75), it decreases. Recently, for W addition on NiMo catalyst it has been reported that thiophene HDS activity increases [9]. The authors explained this from the so-called Sabatier principle, that the metal (including promoter) -sulfur bonding energy could be optimal in the addition of W to NiMo.

Considering the results in Chapter 4, it can be concluded that the W effect is dominant for the HG reaction pathway. So, the effect of the addition of W should be more significant where the HG pathway is the more dominant. In agreement with this prediction, for the HDS of 4,6-DMDBT, where the HG pathway is relatively important, a positive effect is observed. In Fig.3, the selectivity of DDS and HG pathways for DBT HDS is shown. At increasing W, the DDS activity decreased in comparison to that of the HG step, explaining that in this case W exchange is unfavourable.

3.2. Titania addition to alumina support

In Fig. 4, the effect of TiO₂ addition is shown. At increasing TiO₂ loading, the activity increases. For 4,6-DMDBT, the increase is larger than for DBT. From these observations it is concluded that the addition of TiO₂ is effective both for the DDS and for the HG pathway.

The effect of TiO₂ saturates at 3 to 5 wt%. Several studies have been reported for the effect of TiO₂ for HDS activities. Segawa et al. reported that for MoO₃/Al₂O₃, TiO₂ addition by CVD on Al₂O₃ has a positive effect for the HDS of DBT [10]. Their IR results showed that the basic OH groups on γ -Al₂O₃ are reduced by the addition of TiO₂, in agreement with the point of zero charge to be 5-6 (pH), lower than that of γ -Al₂O₃ to be approx. 8. As our impregnation solution was acidic, where the basic OH groups would be primarily involved in the following reaction. The surface basic OH groups are forming positively charged sites by H⁺ adsorption. And molybdenum in anionic state is strongly interacting with the sites.



Therefore, the addition of TiO₂ to γ -Al₂O₃, lowering the point of zero charge, weaken the interaction between Mo in anionic state and the support. And it could enhance highly active type II phase formation, as it is suggested the type II phase have weaker interaction with support (see Chapter 3). However, at increasing loading of TiO₂ the specific surface area of the support decreases, and as a consequence also the dispersion of Mo decreases, resulting in a lower activity at high loading of TiO₂ to Al₂O₃.

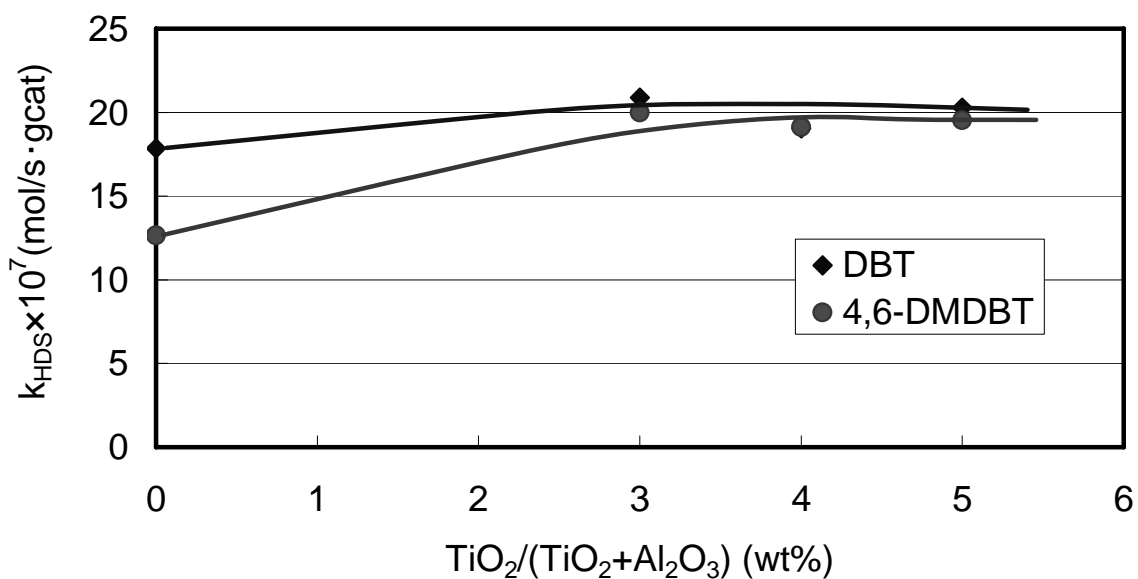


Figure 4. Effect of TiO₂ addition on DBT and 4,6-DMDBT HDS of co-impregnation NiMo/Al₂O₃.

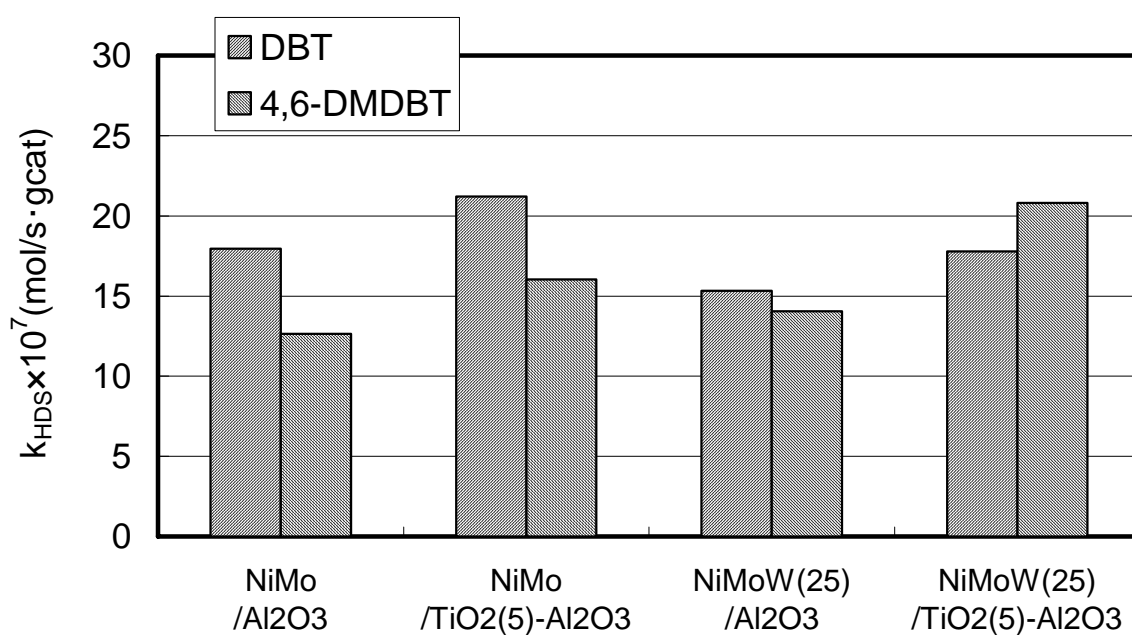


Figure 5. Effect of TiO₂ addition and W exchange on DBT and 4,6-DMDBT HDS of co-impregnation NiMo/Al₂O₃

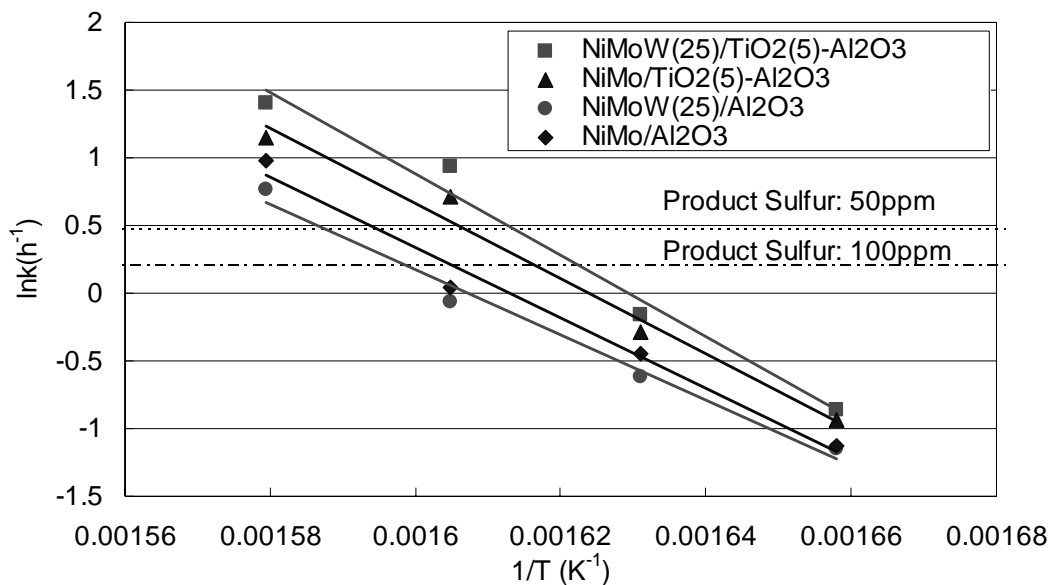


Figure 6. Activity test on co-impregnation NiMo/Al₂O₃ for diesel HDS

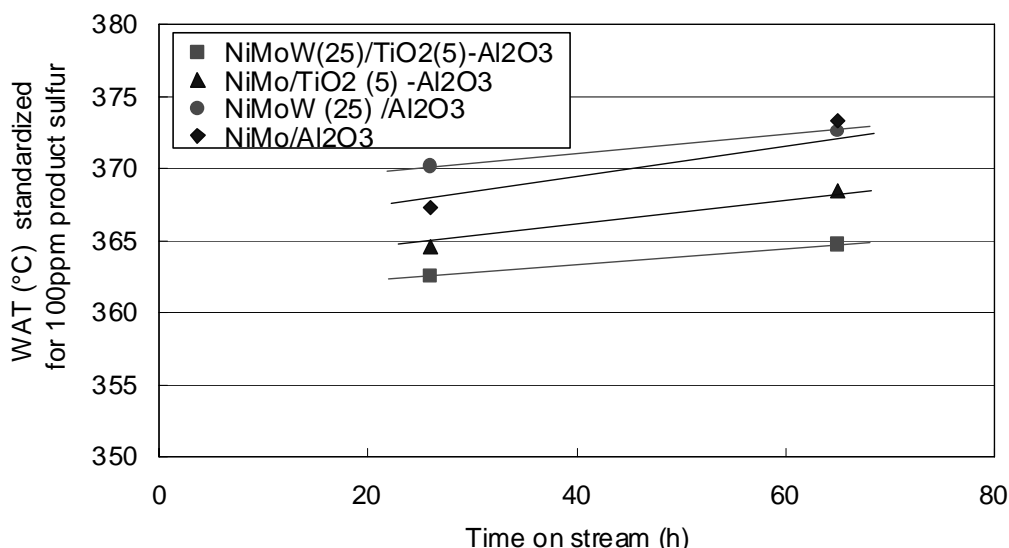


Figure 7. Stability of activity on co-impregnation NiMo/Al₂O₃.

Our positive effect of TiO₂ on NiMo/Al₂O₃ is in agreement with their study, although the catalyst preparation method was different. Our IR results also showed that the basic OH groups on γ -Al₂O₃ are reduced, and that the acid amount determined by differential heat adsorption by NH₃ above 120 kJ/mol increased by TiO₂ addition [11]. However, it should be noted that the effect of TiO₂ addition saturates at 3 wt% (0.4 mmol/g_{Al₂O₃}), corresponding to 1.2 atom/nm². It is slightly higher than the amount of basic OH group determined by SO₂ adsorption; 0.9 molecule/nm² (see Chapter 3). It is suggested that the effect of TiO₂ is to cover basic OH groups on alumina. Although the configuration of TiO₂ on alumina is not fully clear, it is likely that monolayer surface coverage of TiO₂ is much higher than 1.2 atom/nm², and has been reported to be 6.1 atom/nm² [10].

3.3. Synergy effect of titania and W on NiMo catalyst

To investigate a possible synergy of TiO₂ and W, supported NiO-MoO₃-WO₃ catalysts were prepared and tested for the HDS of DBT and 4,6-DMDBT. As shown in Fig. 5, the addition of TiO₂ is favourable for DBT, and very favourable for 4,6-DMDBT. It is also clear that W exchange is favourable for the HDS of 4,6-DMDBT, regardless of TiO₂ addition. This is not the case for HDS of DBT: W exchange is not favourable, but TiO₂ addition is.

The results were checked with real feedstock. The activity for diesel HDS was measured for NiO-MoO₃/Al₂O₃, NiO-MoO₃/TiO₂-Al₂O₃, NiO-MoO₃-WO₃/Al₂O₃ and NiO-MoO₃-WO₃/TiO₂-Al₂O₃. The results are shown in Fig. 6. TiO₂ addition substantially improves the HDS activity, and the synergy effect of TiO₂ and W addition is clearly observed, in agreement with the results of 4,6-DMDBT activity tests. For Al₂O₃ without TiO₂, W addition is not favourable. Probably, the reason is that the sulfur compounds in feed consist not only of 4,6-DMDBT, but also of DBT. For the latter W exchange is not positive, as already was shown in Fig. 5. Therefore, the effect of W addition depends on the composition of the feed. It is expected to be most effective in deep desulfurization when the most refractory 4,6-DMDBT determine the ranking of catalysts activity.

The stability of the catalyst activity has been tested for 200 hours. The normalized temperature to produce 100 ppm sulfur are presented in Fig. 7. At least for 200 hours, the synergy effect of TiO₂ and W has been observed.

3.4. Catalyst Characterization

In TPR spectra of NiMo and NiW catalyst (see Fig. 8, 9) two major peaks are observed, in agreement with the results in Chapter 3. As already mentioned, the low- and high-temperature peaks are associated with the reduction of Mo⁶⁺ bilayer/multilayer and Mo⁶⁺ monolayer species, respectively. For two reasons we do not see a clear contribution of Ni. First, the content is low (see Table 1). Second, the stoichiometry of the reduction equation predicts the consumption of 1 mol H₂/Ni, versus 3 mol H₂/Mo (W). The peak in the higher-temperature of NiW/Al catalysts is much larger than the one of NiMo/Al, in agreement with the literature. It is suggested that NiW is more like a single slab than NiMo. It is likely that the W has stronger interaction with support than Mo does. And the Mo+W loadings of these catalysts are almost twice as much as the monolayer coverage of Mo on alumina. Therefore, the increase of activity for HDS of 4,6-DMDBT by W addition is not likely to be explained by that W prefer to form type II structure than Mo. It has been reported that there is a general periodic trend that transition metal sulfides in the later row show higher HDN activity [12]. However, W and Mo do not follow this trend in the literature. It is probably because that W is difficult to be sulfided. In this work, the catalysts were prepared by a different method from the literature, promoted by Nickel, and were presulfided at high pressure. Eventually the active metals under our experimental condition were to be more easily presulfided than in the literature, resulting in the intrinsic higher HG activity of W. Recently, it was supported by Okamoto et. al that the turn over frequency of CoW could be higher than that of CoMo after properly presulfiding [13].

The spectra of TiO₂-Al₂O₃ catalysts where TiO₂/(TiO₂+Al₂O₃) is 5 wt% were also measured and are shown. In NiMo catalysts, the spectra of the catalyst with or without TiO₂ are almost the same. TiO₂-Al₂O₃ support was also measured (see Figure 8). TiO₂ can be reduced and it is

observed both in NiMo and NiW $\text{TiO}_2\text{-Al}_2\text{O}_3$ catalysts. In NiW catalysts, the spectra of the catalyst with TiO_2 shows a slightly lower temperature shift of the lower-temperature peak than the analogue without TiO_2 , although the effect evaluated by TPR is not so obvious. It is suggested that TiO_2 has less interaction with W than Al_2O_3 .

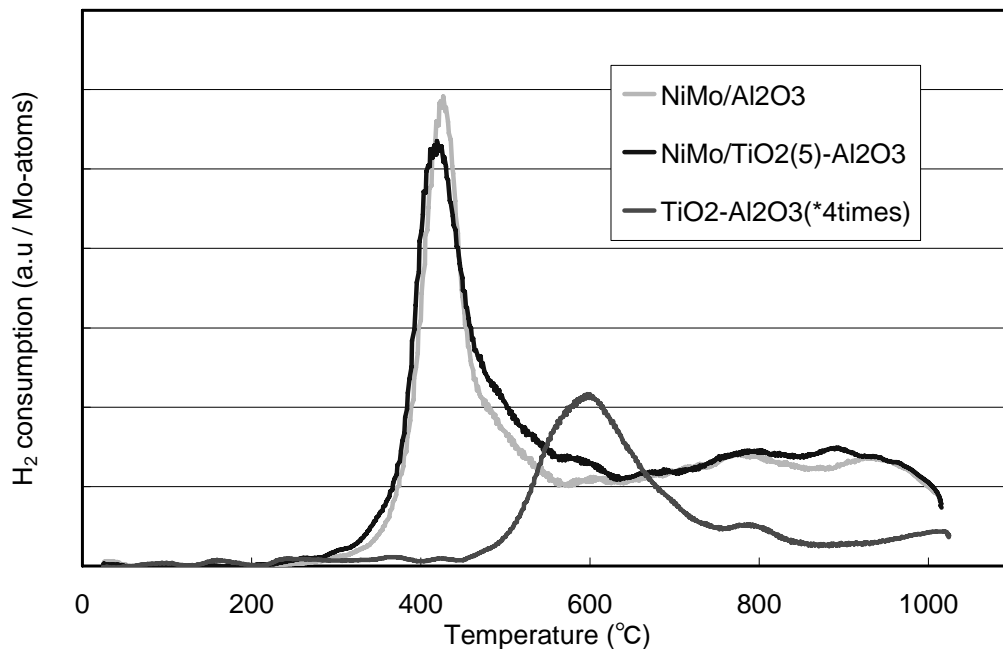


Figure 8. TiO_2 addition effect on TPR spectroscopy of $\text{NiMo}/\text{Al}_2\text{O}_3$

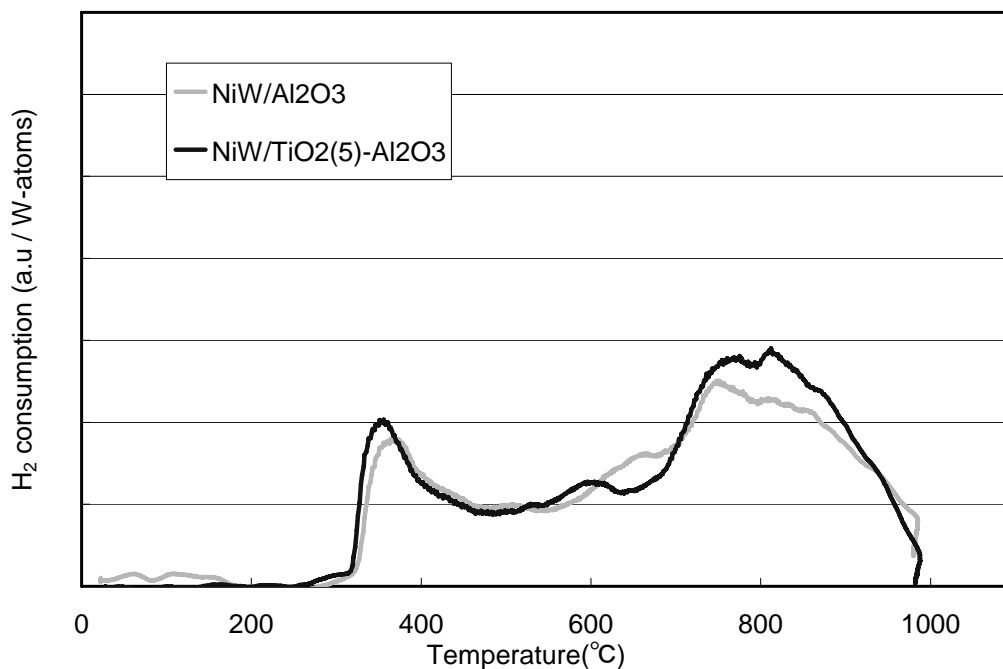


Figure 9. TiO_2 addition effect on TPR spectroscopy of NiW catalysts

In TPS spectra of NiMo and NiW catalyst (see Fig. 10, 11) we observed two regions for the H_2S consumption, in agreement with the results in Chapter 3. TPS spectra of NiW showed more H_2S consumption in region II (280 to 500 °C) than the one of NiMo. This is in agreement with

literature stating that NiW catalysts are not so easily sulfided and need higher temperature, around 550 °C [14]. This implies that the interaction of support and metal precursor in NiW is stronger than in NiMo, resulting in difficulty of the sulfiding. In both NiMo and NiW catalyst, the spectra of H₂S consumption by the catalyst with or without TiO₂ are almost the same. Only slight difference is that the spectra of the catalyst with TiO₂ show a slight shift of the low temperature peak towards lower temperature.

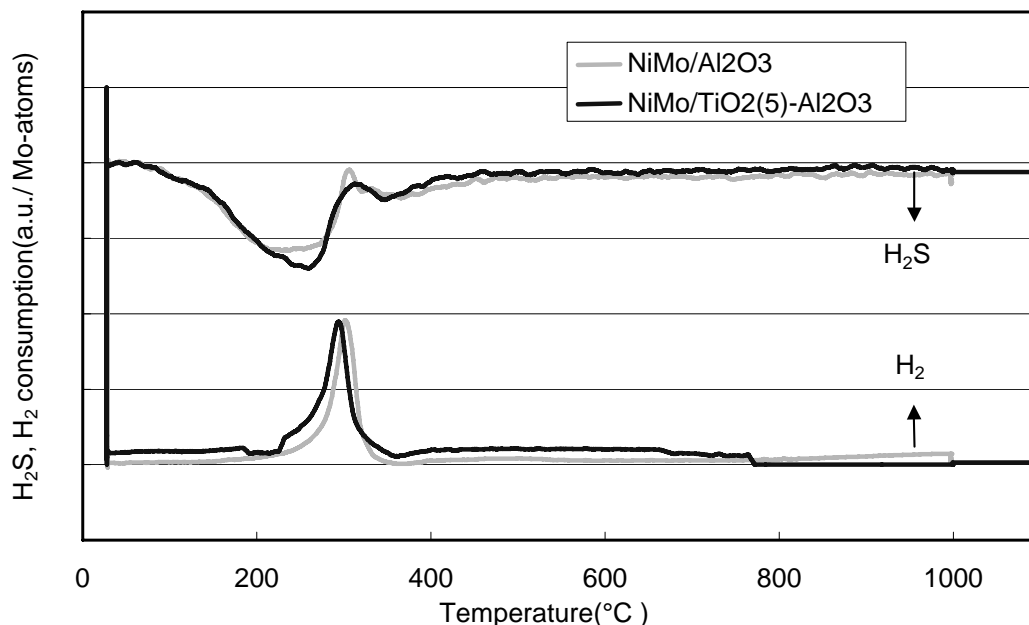


Figure 10. TiO₂ addition effect on TPS spectroscopy of NiMo catalysts

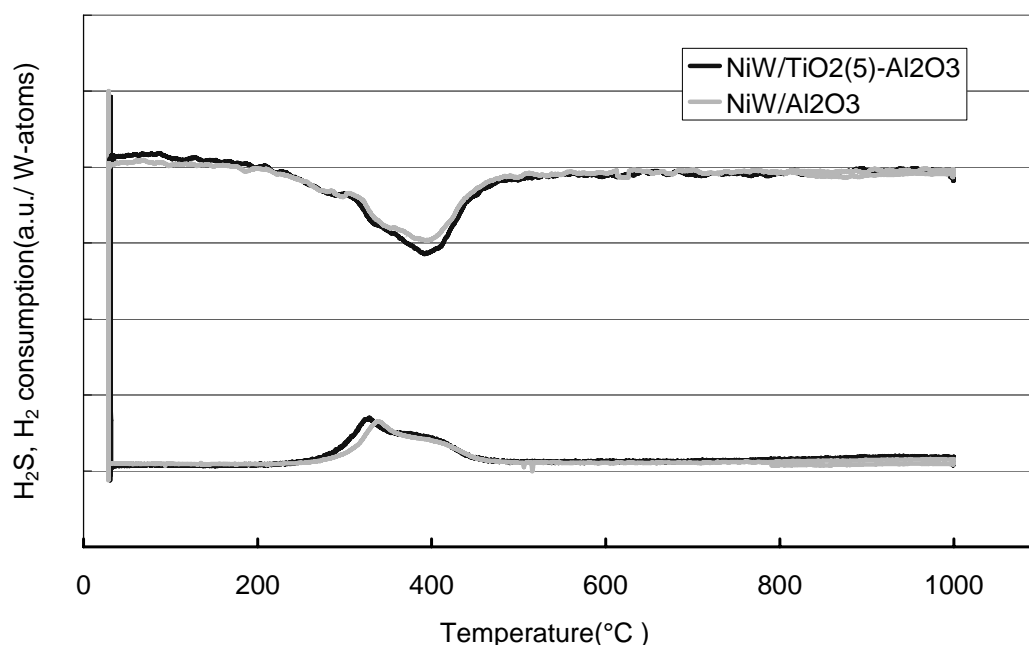


Figure 11. TiO₂ addition effect on TPS spectroscopy of NiW catalysts

To investigate the interaction of W with support in NiMo catalysts, co-impregnation of NiMo and NiW, pre-impregnation of NiW followed by NiMo, and post-impregnation of NiW

after NiMo impregnation was carried out. The results of TPR spectra for those three kinds of catalysts are shown in Fig. 12 and Fig. 13. Firstly as shown in Fig.12, co-impregnation catalyst shows a profile composed of the contribution of NiMo and NiW. High W/Mo ratio catalyst shows a larger high-temperature peak and the peak maximum is shifted from 950 °C to 770 °C. From the observation of the difference for the spectra of three kinds of catalysts in Fig.13, the spectra of pre-impregnation catalyst is more similar to the one of co-impregnation catalyst than the one of post-impregnation catalyst. It might imply that the adsorption of W precursor is stronger than the one of Mo. Therefore it is tentatively concluded that the W complex adsorbs on the support before the Mo complex does because it has stronger interaction with support.

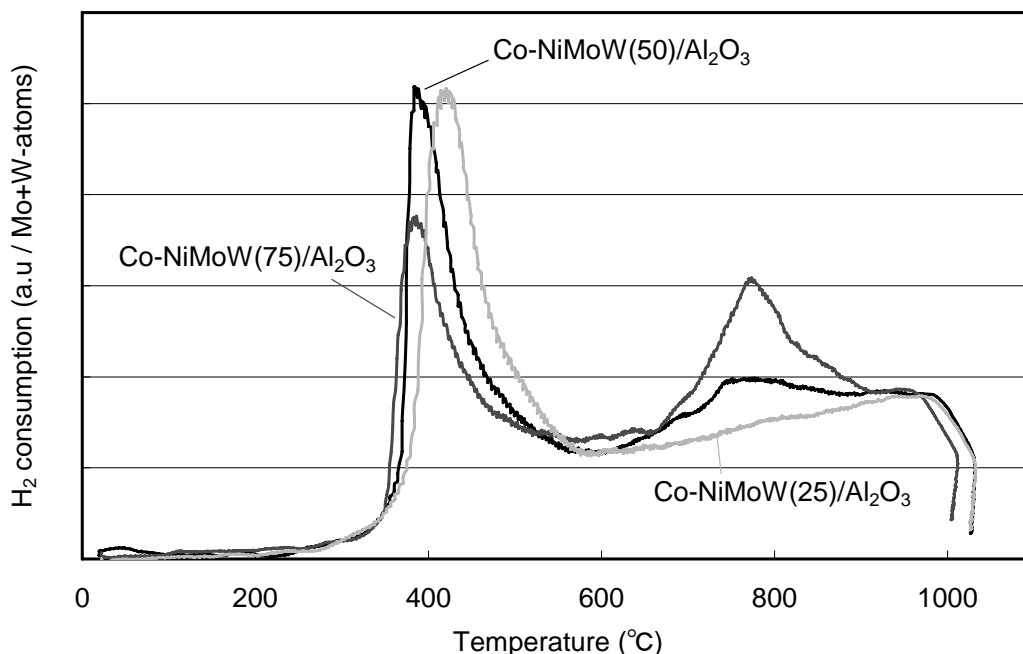


Figure 12. TPR spectra of co-impregnation NiMoW/Al₂O₃ catalysts at different W/Mo ratio.

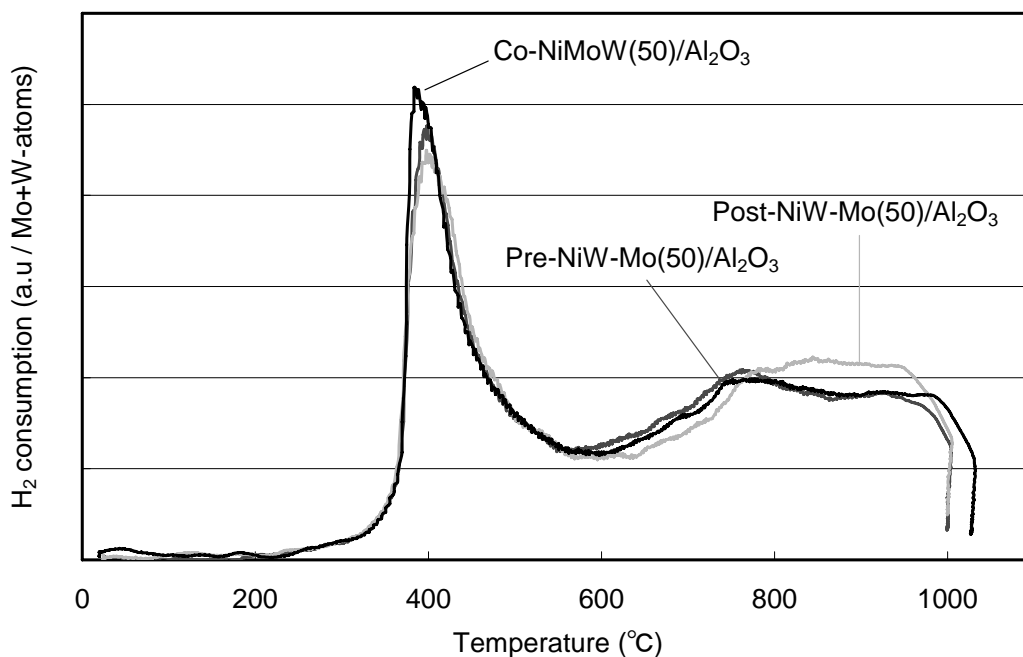


Figure 13. TPR spectra of three kinds of NiMoW/Al₂O₃ catalysts

Next, the results of TPS spectra for those three kinds of catalysts are shown in Fig. 14. All three catalysts show almost the same spectra regardless of the catalyst preparation procedures. Although W has a stronger interaction with support from the TPR results (Fig. 12), it is likely that co-existence of easier sulfiding Mo can enhance the sulfiding of W nearby it. Probably in three catalyst procedures, W and Mo can exist close to each other. As a consequence, the TPS spectra of those catalysts are almost the same.

This promoting effect on W sulfidation can be one of the reasons that NiMoW show a higher activity for 4,6-DMDBT HDS at an early stage of increasing the W ratio in NiMo catalysts.

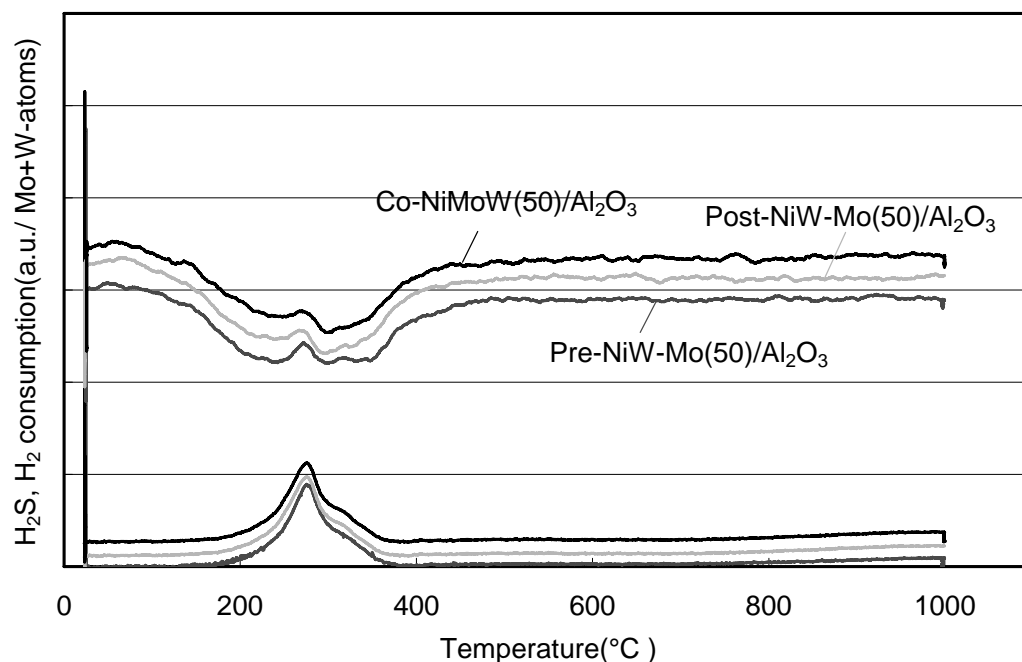


Figure 14. TPS spectra of three kinds of NiMoW/Al₂O₃ catalysts

4. Conclusion

The W exchange of Mo on NiMo catalyst has been tested. The activity for 4,6-DMDBT was increased at an early stage of increasing the W ratio, but for DBT the opposite was the case. From the characterization such as TPR and TPS measurement, co-existence with Mo can enhance the sulfiding of W.

The effect of TiO₂ addition on Al₂O₃ in NiMo has been investigated, varying the amount of TiO₂. At increasing TiO₂ on Al₂O₃, the activities of NiMo catalysts for DBT HDS increased. The activities for 4,6-DMDBT HDS were also increased, but more significantly.

NiMoW catalysts with the addition of TiO₂ showed higher HDS activity for DBT, and extremely higher HDS activity for 4,6-DMDBT than the catalysts without TiO₂ addition. A synergy effect of W exchange for Mo and TiO₂ addition on Al₂O₃ has been observed in NiMo catalysts. The synergy effect has been confirmed for a realistic feed, i.e., diesel.

References

- [1] C.Song, *Catalysis Today*, **86** (2003) 211.
- [2] T.Isoda, S.Nagao, Y.Korai, X.L.Ma, and I.Mochida, *Sekiyu Gakkaishi*, **41** (1998) 22.
- [3] D.D.Whitehurst, T.Isoda, and I.Mochida, *Advances in Catalysis*, **42** (1998) 345.
- [4] H.R.Reinhoudt, R.Troost, A.D.van Langeveld, S.T.Sie, J.A.R.van Veen, and J.A.Moulijn, *Fuel Processing Technology*, **61** (1999) 133.
- [5] Y.Saih and K.Segawa, *Catalysis Surveys from Asia*, **7** (2003) 235.
- [6] M.J.Vissenberg, Y.van der Meer, E.J.M.Hensen, V.H.J.de Beer, A.M.van der Kraan, R.A.van Santen, and J.A.R.van Veen, *J.Catal.*, **198** (2001) 151.
- [7] J.Ramirez and A.Gutierrez-Alejandre, *Catal.Today*, **43** (1998) 123.
- [8] H.R.Reinhoudt, C.H.M.Boons, A.D.van Langeveld, J.A.R.van Veen, S.T.Sie, and J.A.Moulijn, *Appl.Catal.A: Gen.*, **207** (2001) 25.
- [9] C.Thomazeau, C.Geantet, M.Lacroix, M.Danot, V.Harle, and P.Raybaud, *Preprint of ICC 13th, Paris*, **06-002** (2004)
- [10] K.Segawa, K.Takahashi, and S.Satoh, *Catalysis Today*, **63** (2000) 123.
- [11] H.Koshika, K.Inamura, Y.Suzuki, T.Hirano, N.Kagami, R.Iwamoto, and A.Iino, *33th Annual meeting of the Japan Petroleum Institute, Osaka*, **F02/P** (2003)
- [12] S.Eijsbouts, V.H.J.de Beer, and R.Prins, *Journal of Catalysis*, **109** (1988) 217.
- [13] A.Katou, T.Ebihara, T.Fujikawa, H.Koshika, K.Inamura, T.Ooba, T.Kubota, and Y.Okamoto, *Abstracts of 49th Annual meeting of the Japan Petroleum Institute*, (2006) 37.
- [14] H.R.Reinhoudt, A.D.Van Langeveld, P.J.Kooyman, R.M.Stockmann, R.Prins, H.W.Zandbergen, and J.A.Moulijn, *J.Catal.*, **179** (1998) 443.

8

Summary and evaluation

8.1. Introduction

For a sustainable society ultra deep desulfurization of transport fuels is crucial. It is not surprising that environmental legislation has become more and more strict. Some refineries in the world have already started producing sulfur free diesel (less than 10 ppm) and it will become the standard all over the world in the near future. In principle, many improvements for hydrotreating processes are conceivable. On the one hand, chemical engineering solutions, and on the other hand, the development and selection of advanced catalysts suggest themselves. The latter is the subject of this work.

Promoted MoS₂ catalysts have been work-horses in industrial HDS units. Although great efforts have been spent to elucidate the active site of HDS and reaction mechanisms, it is still under discussion. However, in modern catalyst development it is important to fundamentally elucidate the relation between catalyst structure and reaction mechanism. Especially for the production of sulfur free transportation fuels, the conversion level has reached more than 99.9% for diesel HDS. This changes the fuel processing technology to a chemical field. It means that although diesel contains huge variety of compounds, the final purification level is on a molecular level.

In this situation, we need to understand the characteristics of catalysts and reaction mechanisms, such as NiMo, CoMo, and NiW under realistic conditions. For the HDS activity the inhibiting effect by competitive adsorption needs to be taken into account. The aim of this work is to propose a better understanding of ultra deep diesel HDS, to contribute to the development of advanced catalysts, and to utilize catalysts in a cost effective way.

8.2. Reaction pathways of sulfur compounds and the ranking of catalysts

There are several important aspects regarding the catalytic reaction mechanism for ultra desulfurization of diesel. We considered promising ways for developing highly active catalysts, and investigated the effect of the active phases on catalyst such as type I or type II, NiMo or CoMo, and metal loading effect at below to above monolayer coverage.

Ranking of catalytic activities of several NiMo catalysts and a CoMo catalyst was performed using various model compounds: thiophene, tetrahydrothiophene, dibenzothiophene (DBT) and 4,6-dimethyldibenzothiophene (4,6-DMDBT). Thiophenes in gas phase (in a continuous microreactor), dibenzothiophenes in liquid phase (batch reactor) were tested in Chapter 4. Several aspects for ranking of activities were examined and in the following chapters, the activity testing methods described in Chapter 2 were adopted.

In Chapter 3, the dispersion and morphology of type I and type II active phase with the metal loading below and above monolayer surface coverage were discussed. So-called type I and type II NiMo catalysts were characterized by various techniques such as XRD, TPR, TPS, Laser Raman spectroscopy, and SO₂ adsorption. The active metals in oxidic state and sulfidic state were investigated to evaluate the active phase interaction with the support.

The results of characterization of catalysts and the ranking of catalytic activities, the relation between catalyst structure and reaction mechanism were discussed. It is well known that cyclic sulfur compounds react through two pathways, so-called direct desulfurization (DDS) and hydrogenation (HG), and that the ratio of DDS to HG depends on the reactant molecules, the

catalysts properties and the reaction conditions. From the ranking of catalyst activities, it is concluded that tetrahydrothiophene HDS activity behaves similarly to DBT DDS, because direct desulfiding is the major process in both cases. The HG pathway is the main pathway both in HDS of thiophene and 4,6-DMDBT (see Fig.1). The consecutive DDS step in the HG pathway is important for the CoMo catalyst, but not for NiMo catalysts.

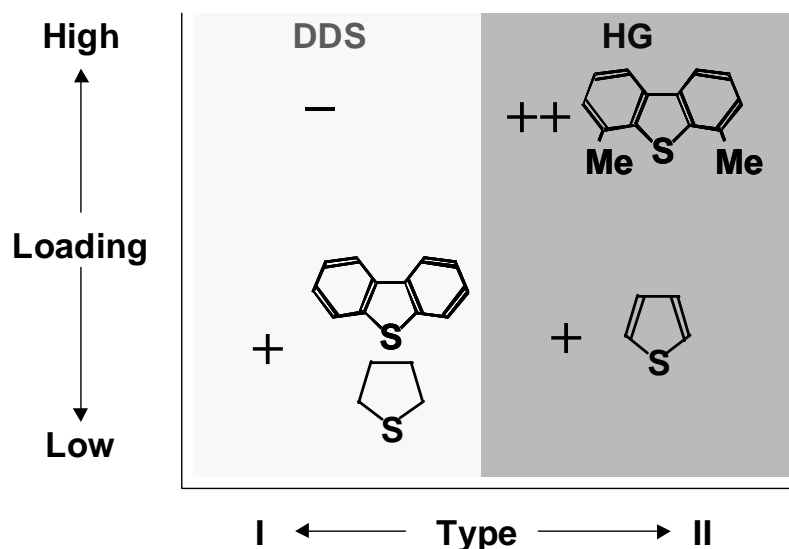


Figure 1. The effect of type I and type II active phase and metal loading on dominant reaction pathways of various sulfur compounds

Between type I and type II NiMo catalysts with Mo loading from below to above monolayer coverage, type I and type II differ most at high loading. Below monolayer surface coverage, type II active phase shows higher HG activity than type I. It is likely that type II active phase consists of higher stacking active phases, favoring the HG pathway. Consequently, type II catalyst shows higher HDS activity for thiophene and 4,6-DMDBT, as these sulfur compounds react mainly via the HG pathway. Above monolayer surface coverage type I active phase forms aggregated crystals on the support alumina, resulting in a low dispersion, whereas type II active phase can maintain high dispersion (see Fig.2). Higher loading type I catalyst shows lower DDS activity and only slightly increased HG activity. Higher loading Type II phase shows higher DDS and extremely high hydrogenation (HG) activity and, as a consequence, high HDS activity for TH and 4,6-DMDBT.

In order to be able to generalize the results, a CoMo catalyst was included in the study. At first sight it was surprising that CoMo catalyst showed a low HG activity in HDS of DBT, and it shows a relatively high activity in HDS of 4,6-DMDBT. Two reaction schemes were examined, one of those taking into account a dehydrogenation step. Although a dehydrogenation step could occur substantially, under our experimental conditions, the main cause of ranking differences is the difference of susceptibility for NiMo and CoMo catalysts to H_2S ; the relatively low susceptibility to H_2S of CoMo catalysts. Although the difference of structure between NiMoS and CoMoS is not fully clear and further investigations are necessary to elucidate it, recent DFT

calculation studies have suggested that nickel prefers to incorporate into the metal edge and cobalt in the S-edge of MoS₂ slabs under typical sulfiding conditions [1], [2]. It is likely that the metal edge where Ni is incorporated in would be more susceptible to H₂S adsorption than the S-edge where Co is incorporated in.

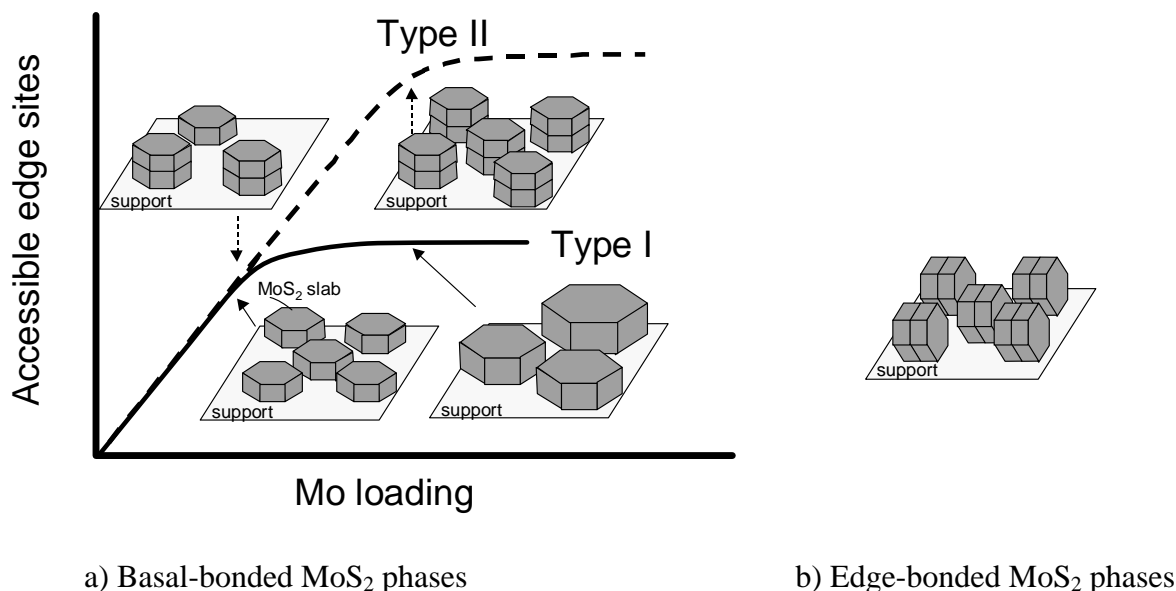


Figure 2. Schematic of type I and type II active phase model at increasing meal loading

8.3. Inhibiting effect of nitrogen compounds on deep HDS

It is generally accepted that HDS is inhibited by nitrogen compounds and polyaromatics. Especially nitrogen compounds inhibit HDS reaction significantly in deep HDS. However, it is not so clear which nitrogen compound inhibits the most for the ultra deep desulfurization reaction. Recently results have been published concerning both model reactions, using nitrogen compounds, and real feedstocks. In Chapter 5, bench scale HDS tests were carried out using six feed stocks of straight run light gas oil that have different properties, under various conditions for the target below 500 ppm sulfur in product. The important parameters of feed properties for ultra deep HDS were chosen using a datamining method. Especially, the nitrogen compound inhibiting effect on HDS was evaluated in realistic bench scale testing.

Little work has been published about the difference of susceptibility by nitrogen on catalysts properties (CoMo, NiMo, Mo, W, or additives). It will be crucial to choose the optimal catalyst or to establish the best catalysts combination, as nitrogen inhibition is significant especially for ultra deep desulfurization range.

In this work, simultaneous hydrodesulfurization of dibenzothiophene (DBT) and hydrodenitrogenation (HDN) of carbazole was carried out in order to evaluate mutual inhibiting effects on NiMo catalysts in comparison to a CoMo catalyst. Concerning the different susceptibility of catalyst to carbazole, CoMo catalyst is slightly more inhibited than NiMo, type II is more inhibited than type I, and the type II high metal loading catalyst is the most inhibited by carbazole, probably because of its high HG activity. Carbazole inhibits not only both the DDS

and the HG pathways in HDS of DBT significantly, but also the HDN reaction itself. The HG pathway for DBT HDS is more inhibited by carbazole than the DDS pathway. Consequently, HDN is inhibited more than HDS by carbazole since HDN reaction occurs only after the hydrogenation of rings.

The influence of the transformation during HDS of non-basic pyrolic type nitrogen was investigated by using tetrahydrocarbazole, the hydrotreated (strongly basic) intermediate in HDN of carbazole. Tetrahydrocarbazole addition was applied to see the difference of inhibiting effects between before and after the hydrogenation during HDN of carbazole. Hydrogenated intermediate retards HDS of DBT more significantly than the original nitrogen compound, probably because of its stronger basicity.

8.4. Development of highly active catalysts

To develop highly active catalysts for diesel ultra deep HDS, there are several conceivable ways to improve the activity of catalysts in desulfurization of the most refractory species such as β -substituted dibenzothiophene in diesel fuel.

First of all, the number of active sites can be increased by increasing the active metal loading as much as possible, provided the dispersion of active metals is kept higher than the conventional catalyst at comparable metal loading. In Chapter 3 and 4, we reported that type II catalyst is promising because the active phase can exist as a higher dispersed state than the active phase of type I at loadings above monolayer surface coverage.

The next is that the hydrogenation can be effective. One effect can be that the steric hindrance of β -substituted groups is weaker after the hydrogenation of the parent DBTs. The other effect is that the electron density of sulfur atom after the hydrogenation is higher than the parent one, resulting in higher reactivity. In Chapter 4, type II NiMo catalysts appeared to be promising for the diesel in deep HDS range.

It has been reported that NiW catalyst can be a highly active catalyst for β -substituted DBT HDS. Generally NiW catalysts are known to be highly active for the hydrogenation of aromatics and they are often applied for the hydrofinishing of lubricant oil. To benefit from the application of high hydrogenation function of W, the exchange of W for Mo on type II of NiMo catalysts was investigated at high Mo loading, above monolayer surface coverage.

As a modification of support, titania has been reported as one of the effective components to increase the HDS especially via the HG reaction pathway for 4,6-DMDBT. Recently, it has been reported that W is more easily sulfided on TiO₂ than on Al₂O₃, due to the weaker interaction with TiO₂. NiW catalysts show higher activity in the case of titania support than the case of alumina support. Therefore, the addition of TiO₂ to Al₂O₃ also was carried out to investigate a possible synergy effect of W addition on NiMo catalyst.

In this work the W exchange of Mo on NiMo catalyst has been tested. The activity for 4,6-DMDBT was increased at an early stage of increasing the W ratio, but for DBT the opposite was the case. From characterization studies such as TPR and TPS measurements, it was concluded that co-existence with Mo enhances the sulfiding of W. The effect of TiO₂ addition on Al₂O₃ in NiMo has also been investigated, varying the amount of TiO₂. At increasing TiO₂ on Al₂O₃, the

activities of NiMo catalysts for DBT HDS increased. The activities for 4,6-DMDBT HDS were also increased, but more significantly.

Moreover, we reported that NiMoW/Al₂O₃ catalysts with the addition of TiO₂ showed higher HDS activity for DBT, and extremely higher HDS activity for 4,6-DMDBT than the catalysts without TiO₂ addition. The synergy effect of W exchange for Mo and TiO₂ addition on Al₂O₃ has been observed in NiMo catalysts. The synergy effect has been confirmed for a realistic feed, i.e., diesel.

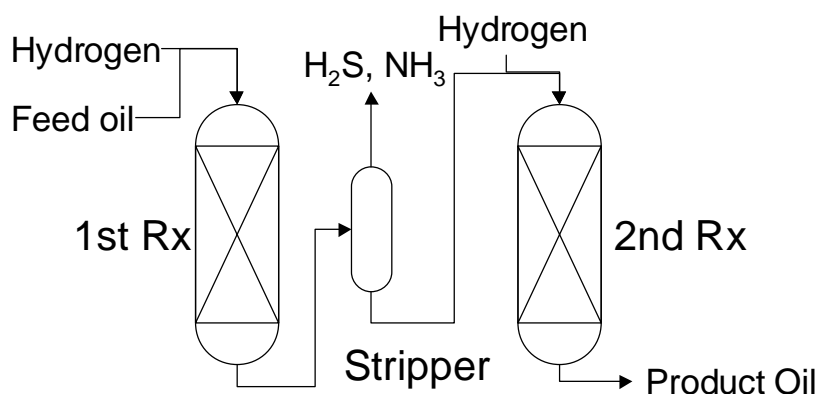
8.5. Conceivable process for ultra deep desulfurization of diesel

In Chapter 3 and Chapter 4, NiMo type II high loading catalyst is promising for ultra deep desulfurization of diesel, as it shows high hydrogenation activity, resulting in high activity for 4,6-DMDBT. Moreover, it was concluded that NiMo type II catalyst is especially highly active for 4,6-DMDBT without H₂S. From these results, a proposal of the process is shown in Fig. 3 a), containing a H₂S stripper between two HDS reactors to reduce H₂S pressure in the second reactor. For the second reactor, a NiMo type II high loading type catalyst is suggested, as after the first reactor, the refractory sulfur compound such as 4,6-DMDBT remains to be desulfurized. In Chapter 7, the NiMoW/TiO₂-Al₂O₃ was developed as a new more highly active HDS catalyst for 4,6-DMDBT, with especially enhanced hydrogenation activity. Therefore, this catalyst is a promising candidate for the catalyst in the second reactor. For future works, the susceptibility for H₂S of the NiMoW/TiO₂-Al₂O₃ and the long term stability should be investigated.

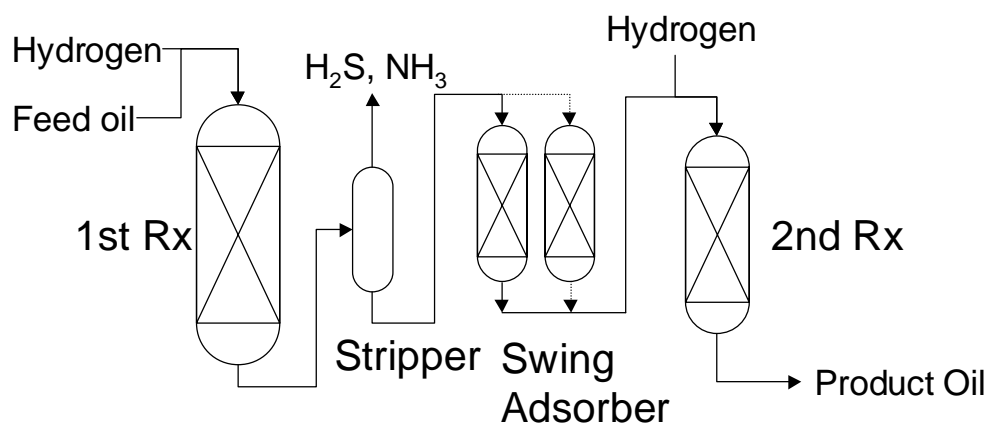
For the first reactor, the CoMo catalyst with higher DDS selectivity would rather be suggested, as its smaller hydrogen consumption than NiMo is beneficial. In Chapter 5 and Chapter 6, it was shown that the nitrogen inhibiting effect for HDS and especially for the hydrogenation pathway is significant. Regarding catalyst types, the NiMo type II high loading catalysts were retarded most significantly. Therefore, it may not be a good idea to apply NiMo type II high loading catalysts for the first reactor.

Concerning the reduction of the nitrogen compound inhibition, it is recommended that the NiMo type II high loading catalysts is situated in the second reactor. However, it is concluded that the most strong inhibiting nitrogen compound is the intermediate during HDN of carbazoles, after partial hydrogenation. This intermediate is believed to show higher basicity. A conceivable process for this inhibition is shown in Fig. 3 b); the intermediate stripper and sequentially swing adsorbers will reduce the basic nitrogen compound transformed in the first reactor. For instance, silica gel [3] and active carbon [4] could be applicable for the selective adsorption of these basic nitrogen compounds. However, the selectivity of the nitrogen adsorption without other hydrocarbons adsorption, the capacity of adsorption, and the regeneration of adsorbent are crucial for the next stage and need to be investigated.

For the second reactor our developed new highly active catalyst NiMoW/TiO₂-Al₂O₃ is one of the best choices, as it does not contain noble metals that are very expensive. It will be promising not only for the HDS activity but also for Cetane number improvement that is required as a high quality specification for diesel, as it has extremely high hydrogenation activity.



a) Two stage process with an intermediate stripper



b) Two stage process with an intermediate stripper and swing adsorbers

Figure 3. Conceivable processes and combination of catalysts for ultra deep desulfurization of diesel.

References

- [1] H.Schweiger, P.Raybaud, and H.Toulhoat, *Journal of Catalysis*, **212** (2002) 33.
- [2] M.Sun, A.E.Nelson, and J.Adjaye, *Journal of Catalysis*, **226** (2004) 32.
- [3] D.D.Whitehurst, K.G.Knudsen, I.V.Nielsen, P.Wiwel, P.Zeuthen, *Abstracts of Papers of the American Chemical Society, Div. of Petroleum Chemistry*, **219** (2000) 367.
- [4] Y.Sano, K.H.Choi, Y.Korai, and I.Mochida, *Applied Catalysis B: Environmental*, **53** (2004) 169.

Samenvatting en evaluatie

Inleiding

Ultra diepe ontzwaveling van brandstoffen is essentieel voor een duurzame samenleving. Het is daarom niet verrassend dat de milieuwetgeving steeds strikter is geworden. Verscheidene raffinaderijen in de wereld zijn reeds begonnen ‘zwavel vrije’ diesel (minder dan 10 ppm) te produceren, en dit zal in de nabije toekomst de norm over de hele wereld worden. In principe zijn vele verbeteringen voor hydrotreating processen denkbaar. Enerzijds dienen chemisch technologische oplossingen zich aan, en anderzijds wordt gewerkt aan de ontwikkeling en de selectie van geavanceerde katalysatoren. Het laatstgenoemde is het onderwerp van dit werk.

Gepromoteerde MoS₂ katalysatoren zijn altijd de werkpaarden in industriële HDS installaties geweest. Hoewel grote inspanningen zijn geleverd om de actieve plaatsen en de mechanismen van de HDS reactie nader toe te lichten, is momenteel nog steeds de discussie gaande. Toch is het voor de huidige katalysatorontwikkeling belangrijk de fundamentele relaties tussen katalysatorstructuur en reactiemechanisme op te helderen. Voor de productie van zwavelvrije brandstoffen (vooral diesel) ligt het HDS conversieniveau hoger dan 99,9%. Dit verschuift de technologie van brandstofverwerking meer en meer naar een chemisch gebied. Dit betekent dat, hoewel diesel een enorme verscheidenheid aan componenten bevat, het definitieve reinigingsniveau op een moleculair niveau ligt.

In deze situatie moeten wij de kenmerken van katalysatoren, zoals NiMo, CoMo, en NiW, en hun reactiemechanismen, onder realistische condities begrijpen. Voor de HDS activiteit moet het remmende effect door competitieve adsorptie in acht worden genomen. Het doel van dit werk is om tot een beter inzicht in ultra diepe diesel HDS te komen, tot de ontwikkeling van geavanceerde katalysatoren bij te dragen, en kennis te genereren die het mogelijk maakt om de katalysatoren op een rendabele manier te kunnen gebruiken.

Reactieroutes van zwavelverbindingen en het rangschikken van katalysatoren

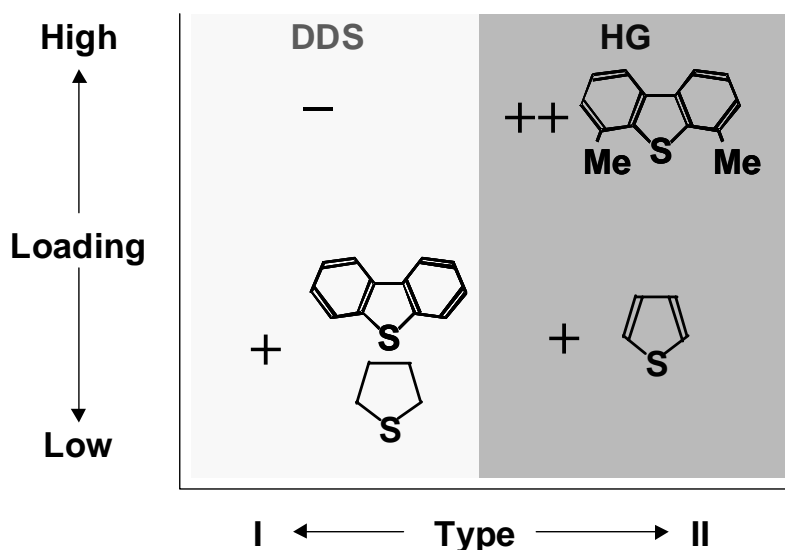
Er zijn verscheidene belangrijke aspecten van het katalytische reactiemechanisme aan de ultra diepe ontzwaveling van diesel. We beschouwden veelbelovende manieren om hoogst actieve katalysatoren te ontwikkelen, en onderzochten het effect van de actieve fasen op de katalysator, zoals type I of type II, NiMo of CoMo, en het effect van de metaalbelading onder of boven de monolaag bedekking.

Het rangschikken van katalytische activiteiten van verscheidene NiMo katalysatoren en een CoMo katalysator werd uitgevoerd met behulp van diverse modelcomponenten: thiofeen, tetrahydrothiofeen, dibenzothiofeen (DBT) en 4,6-dimethyldibenzothiofeen (4,6-DMDBT). Thiophenen werden getest in gasfase (in een continue microreactor) en dibenzothiophenen in vloeibare fase (batchreactor) in Hoofdstuk 4. Verscheidene aspecten voor het rangschikken van activiteiten werden onderzocht, en in de volgende hoofdstukken werden de activiteitstestmethoden toegepast zoals die in Hoofdstuk 2 worden beschreven.

In Hoofdstuk 3 werden de dispersie en de morfologie besproken van type I en type II actieve fase met een metaalbelading onder en boven monolaag oppervlaktebedekking. Zogenaamd type I en type II NiMo katalysatoren werden gekarakteriseerd door middel van diverse technieken zoals XRD, TPR, TPS, Raman Laser spectroscopie en SO₂ adsorptie. De actieve

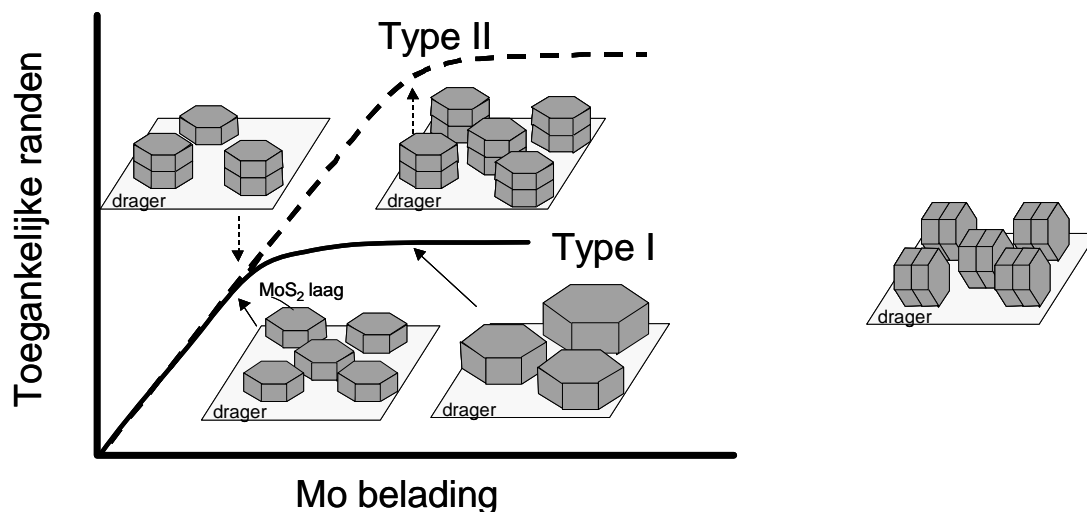
metalen in oxidische staat en sulfidische toestand werden onderzocht om de interactie van de actieve fase met de drager te evalueren.

De resultaten van katalysator karakterisering, het rangschikken van katalytische activiteiten en de relatie tussen katalysatorstructuur en reactiemechanisme werden besproken. Het is bekend dat de cyclische zwavelverbindingen via twee routes, zogenaamde directe ontzwaveling (DDS) en hydrogenering (HG) reageren, en dat de verhouding tussen DDS en HG afhangt van de reactant moleculen, de katalysatoreigenschappen en de reactiecondities. Uit de resultaten van het rangschikken van katalysatoractiviteiten, concluderen we dat de tetrahydrothiofeen HDS activiteit zich net zo gedraagt als DBT DDS, omdat de directe ontzwaveling het belangrijkste proces in beide gevallen is. De HG route is de belangrijkste route zowel in de HDS van thiophene als van 4,6-DMDBT (zie Fig.1). De DDS volgstep in de HG route is belangrijk voor de CoMo katalysator, maar niet voor NiMo katalysatoren.



Figuur 1. Het effect van type I en type II actieve fase en metaalbelading op dominante reactieroutes van diverse zwavelverbindingen

Tussen type I en type II NiMo katalysatoren met Mo belading van onder of boven monolaag bedekking, verschillen type I en type II het meest bij hoge belading. Onder monolaag oppervlaktebedekking toont de type II actieve fase een hogere HG activiteit dan type I. Het is waarschijnlijk dat de type II actieve fase uit structuren met een hogere stapeling bestaat, die de HG route bevorderen. Derhalve toont type II katalysator een hogere HDS activiteit voor thiophene en 4,6-DMDBT, aangezien deze zwavelcomponenten hoofdzakelijk via de HG route reageren. Boven monolaag oppervlaktebedekking vormt type I actieve fase geaggregeerde kristallen op de alumina drager, resulterend in een lage dispersie, terwijl de type II actieve fase een hoge dispersie kan handhaven (zie Fig.2). Hoger beladen type I katalysatoren vertonen een lagere DDS activiteit en slechts een licht verhoogde HG activiteit. De hoger beladen type II fase vertoont een hogere DDS en een uiterst hoge hydrogenerings (HG) activiteit, met als gevolg een hoge HDS activiteit voor Th en 4,6-DMDBT.

a) Grondvlakgebonden MoS₂ fasenb) Randgebonden MoS₂ fasen

Figuur 2. Schematisch model van type I and type II actieve fase bij toenemende metaalbelading

Om de resultaten te kunnen veralgemeniseren werd ook een CoMo katalysator in de studie opgenomen. Op het eerste gezicht was het verrassend dat de CoMo katalysator een lage HG activiteit in de HDS van DBT vertoonde, en een vrij hoge activiteit in de HDS van 4,6-DMDBT. Twee reactieschema's werden onderzocht, waarvan één met een dehydrogenatiestap rekening hield. Hoewel een dehydrogenatiestap onder onze experimentele omstandigheden zeker zou kunnen optreden, is de belangrijkste oorzaak voor verschillen in rangschikking het verschil in gevoeligheid van NiMo en CoMo katalysatoren voor H₂S: CoMo katalysatoren hebben een vrij lage gevoeligheid voor H₂S. Hoewel het verschil in structuur tussen NiMoS en CoMoS niet volledig duidelijk is en verdere onderzoeken noodzakelijk zijn om dit nader op te helderen, hebben de recente DFT berekeningsstudies gesuggereerd dat nikkel zich onder typische inzwavelingscondities bij voorkeur nestelt in de metallische rand, en kobalt in de zwavelrand van MoS₂ lagen [1], [2]. Het is waarschijnlijk dat de metaalrand waar Ni binnen wordt opgenomen vatbaarder zou zijn voor H₂S adsorptie dan de zwavelrand waar Co binnen wordt opgenomen.

Het remmende effect van stikstofverbindingen op diepe HDS

Het is algemeen aanvaard dat HDS wordt geremd door stikstofverbindingen en polycyclische aromaten. Vooral stikstofverbindingen remmen de HDS reactie beduidend in diepe HDS. Toch is het niet zo duidelijk welke stikstofverbindingen het meest de ultra diepe ontzwavelingsreactie remmen. Onlangs zijn de resultaten gepubliceerd over beide modelreacties, gebruik makend van stikstofverbindingen en echte voedingen. In Hoofdstuk 5 werden HDS testen uitgevoerd met zes voedingen van “straight run” lichte gasolie met verschillende eigenschappen, onder diverse condities, met als richtlijn lager dan 500 ppm zwavel in het product. De belangrijke parameters van voedingseigenschappen voor ultra diepe HDS werden gekozen met behulp van een geautomatiseerde gegevensverwerkingsmethode (data mining). Met

name werd het remmende effect van stikstofverbindingen op de HDS geëvalueerd in realistische testen.

Weinig werk is gepubliceerd over het verschil in gevoeligheid voor stikstof in relatie tot katalysatorseigenschappen (CoMo, NiMo, Mo, W, of additieven). Dit is essentieel om de optimale katalysator of de beste katalysatorcombinatie te kiezen, omdat stikstofremming vooral significant is in het ultra diepe ontzwavelingsbereik.

In dit werk werden gelijktijdige ontzwaveling van dibenzothiofeen (DBT) en denitrificatie (HDN) van carbazool uitgevoerd om synergetische remmende effecten te evalueren voor NiMo katalysatoren in vergelijking met een CoMo katalysator. Wat betreft de verschillende gevoeligheid van katalysatoren voor carbazool, is remming voor de CoMo katalysator iets meer dan voor NiMo, voor type II meer dan voor type I, en is de invloed van carbazool op de hoog beladen type II katalysator het grootst, waarschijnlijk vanwege zijn hoge HG activiteit. Carbazool remt niet alleen zowel de DDS als de HG route beduidend in de HDS van DBT, maar ook de HDN reactie zelf. De HG route voor DBT HDS wordt meer geremd door carbazool dan de DDS route. Daarom wordt HDN meer dan HDS geremd door carbazool aangezien de HDN reactie pas na ringhydrogenering kan optreden.

De invloed van de transformatie van niet-basische pyrrolische typen stikstofverbindingen tijdens HDS werd onderzocht met behulp van tetrahydrocarbazool, het gehydrogeneerde (sterk basische) tussenprodukt in HDN van carbazool. Tetrahydrocarbazool werd toegevoegd om het verschil in remmende invloeden te zien tijdens HDN van carbazool vóór en na de hydrogeneringsstap. Het gehydrogeneerde tussenprodukt vertraagt de HDS van DBT beduidend meer dan de originele stikstofverbinding, waarschijnlijk wegens zijn sterkere basiciteit.

Ontwikkeling van zeer actieve katalysatoren

Om hoogst actieve katalysatoren voor diesel ultra diepe HDS te ontwikkelen, zijn er verscheidene denkbare manieren om de activiteit van katalysatoren te verbeteren in ontzwaveling van de meest hardnekkige zwavelmoleculen in diesel brandstof, zoals β -gesubstitueerde dibenzothiofeen.

In de eerste plaats kan het aantal actieve plaatsen worden verhoogd door de actieve metaalbelading zo veel mogelijk te verhogen, op voorwaarde dat de dispersie van actieve metalen hoger wordt gehouden dan bij conventionele katalysatoren met vergelijkbare metaalbelading. In hoofdstuk 3 en 4, rapporteerden wij dat type II katalysator belovend is omdat de actieve fase een hogere dispersie kan hebben als die van type I, bij beladingen boven monolaag oppervlakedekking. Bovendien kan de hydrogenering efficiënter zijn. Één effect kan zijn dat de sterische belemmering van β -gesubstitueerde groepen zwakker is na de hydrogenering van de oorspronkelijke DBTs. Het andere effect is dat de elektronendichtheid van zwavelatoom na de hydrogenering hoger is dan daarvoor, resulterend in hogere reactiviteit. In Hoofdstuk 4 leken NiMo type II katalysatoren veelbelovend te zijn voor diesel in het diepe HDS bereik.

Men heeft gerapporteerd dat de NiW katalysator een hoogst actieve katalysator voor β -gesubstitueerde DBT HDS kan zijn. Over het algemeen staan NiW katalysatoren bekend als hoogst actief voor de hydrogenering van aromaten en zij worden vaak toegepast in de productie

(hydrofinishing) van smeerolie. Om van de toepassing van hoge hydrogeneringsfunctie van W te profiteren, werd de uitwisseling van W voor Mo onderzocht op type II NiMo katalysatoren bij hoge Mo lading, boven monolaag oppervlaktedekking.

Als modificatie van de drager is titania genoemd als één van de efficiënte componenten om HDS te verbeteren, vooral via de HG reactieroute voor 4,6-DMDBT. Onlangs heeft men gerapporteerd dat W gemakkelijker inzwavelt op TiO_2 dan op Al_2O_3 , vanwege de zwakkere interactie met TiO_2 . NiW katalysatoren tonen een hogere activiteit in het geval van een titania drager dan in het geval van een alumina drager. Daarom werd ook de toevoeging van TiO_2 aan Al_2O_3 uitgevoerd om een mogelijk synergetisch effect te onderzoeken van de toevoeging van W op een NiMo katalysator.

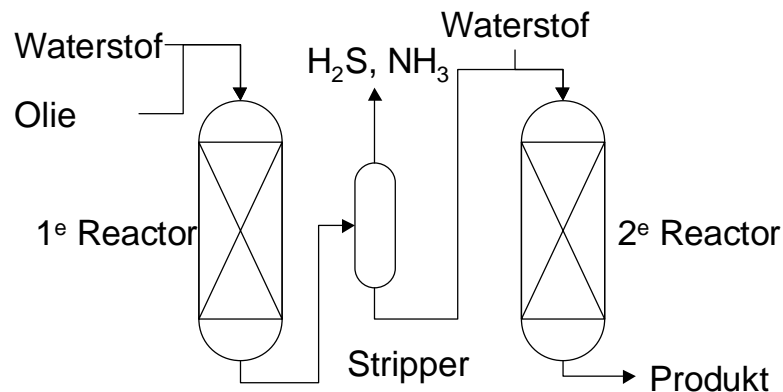
In dit werk is de uitwisseling van W en Mo op een NiMo katalysator getest. De activiteit voor 4,6-DMDBT werd verhoogd in een vroeg stadium van het verhogen van de W verhouding, maar voor DBT was het tegengestelde het geval. Van karakteriseringsstudies zoals TPR en TPS metingen, concludeerden we dat de coëxistentie met Mo de inzwaveling van W verbetert. Het effect van toevoeging TiO_2 op Al_2O_3 in NiMo is ook onderzocht, bij variërende hoeveelheid TiO_2 . Bij stijgende hoeveelheid TiO_2 op Al_2O_3 stegen de activiteiten van de NiMo katalysatoren voor DBT HDS. De activiteiten voor 4,6-DMDBT HDS werden ook, maar beduidend meer, verhoogd. Voorts rapporteerden wij dat de NiMoW/ Al_2O_3 katalysatoren met de toevoeging van TiO_2 een hogere HDS activiteit voor DBT, en een extreem hogere HDS activiteit voor 4,6-DMDBT vertoonden dan de katalysatoren zonder toevoeging van TiO_2 . Het synergetische effect van de uitwisseling van W voor Mo en toevoeging van TiO_2 op Al_2O_3 is waargenomen in NiMo katalysatoren. Het synergetische effect is bevestigd voor een realistische voeding, te weten diesel.

Een denkbaar proces voor ultra diepe ontzwaveling van diesel

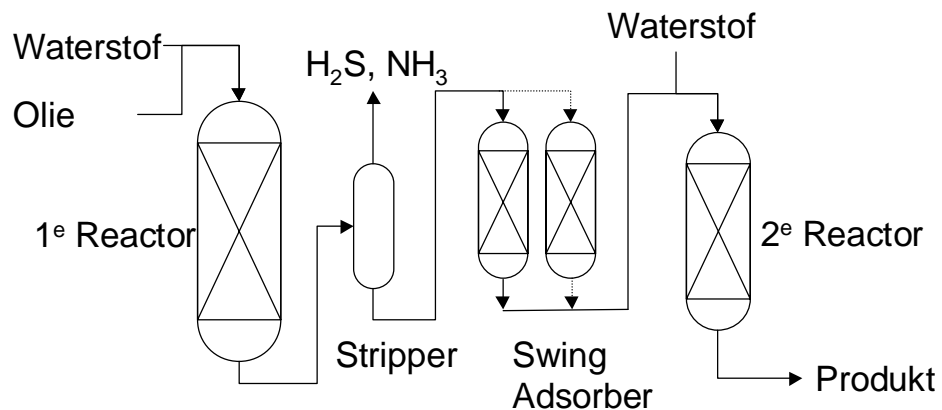
In Hoofdstuk 3 en Hoofdstuk 4 was de NiMo type II hoog beladen katalysator veelbelovend voor ultra diepe ontzwaveling van diesel, aangezien deze een hoge hydrogeneringsactiviteit vertoont, resulterend in een hoge activiteit voor 4,6-DMDBT. Bovendien concludeerden we dat type II NiMo katalysator vooral zeer actief is voor 4,6-DMDBT in de afwezigheid van H_2S . Vanuit deze resultaten wordt een voorstel voor het proces getoond in Fig. 3a die een H_2S stripper bevat tussen twee HDS reactoren om de H_2S partiaalspanning in de tweede reactor te verlagen. Voor de tweede reactor wordt een type II hoog beladen NiMo katalysator voorgesteld, aangezien na de eerste reactor de hardnekkige zwavelcomponenten, zoals 4,6-DMDBT, nog moeten worden ontzwaveld. In Hoofdstuk 7 werd NiMoW/ TiO_2 - Al_2O_3 ontwikkeld als een nieuwe, hoogst actieve HDS katalysator voor 4,6-DMDBT, met vooral verbeterde hydrogeneringsactiviteit. Daarom is deze katalysator een veelbelovende kandidaat voor de katalysator in de tweede reactor. Voor de toekomst zouden de gevoeligheid voor H_2S van NiMoW/ TiO_2 - Al_2O_3 , en de stabiliteit op lange termijn, moeten worden onderzocht.

Voor de eerste reactor zou de CoMo katalysator met hogere DDS selectiviteit aan te bevelen zijn aangezien zijn kleinere waterstofconsumptie ten opzichte van NiMo voordelig is. In Hoofdstuk 5 en Hoofdstuk 6 lieten we zien dat het remmende effect van stikstof op de HDS en vooral op de hydrogeneringsroute significant is. Wat betreft de katalysator typen werden hoog

beladen type II NiMo katalysatoren het meest geremd. Daarom zou het geen goed idee zijn om hoog beladen type II NiMo katalysatoren voor de eerste reactor toe te passen.



a) Tweetrapsproces met tussenliggende stripper



b) Tweetrapsproces met tussenliggende stripper en swing adsorbers

Figuur 3. Denkbaar proces en combinatie van katalysatoren voor ultra diepe ontzwaveling van diesel.

Betreffende de reductie van de remming van de stikstofsamenstelling, is het aan te bevelen om de hoog beladen type II NiMo katalysatoren in de tweede reactor te situeren. Hoewel, we hebben geconcludeerd dat de sterkst remmende stikstofverbinding tijdens HDN van carbazoles het tussenproduct is, na gedeeltelijke hydrogenering. Dit tussenproduct wordt verondersteld een hogere basiciteit te hebben. Een denkbaar proces dat rekening houdt met deze remming wordt getoond in Fig. 3 b; de tussenliggende stripper en sequentiële swing adsorbers zullen de basische stikstofverbindingen, omgezet in de eerste reactor, verminderen. Silica gel [3] en actieve kool [4] zouden bijvoorbeeld kunnen worden toegepast voor de selectieve adsorptie van deze basische stikstofverbindingen. De selectiviteit van de stikstofadsorptie zonder adsorptie van andere koolwaterstoffen, de capaciteit van adsorptie, en de regeneratie van adsorbens zijn essentieel voor het volgende stadium, en moeten worden onderzocht.

Voor de tweede reactor is onze ontwikkelde nieuwe hoogst actieve katalysator NiMoW/TiO₂-Al₂O₃ één van de beste keuzen, aangezien deze geen (dure) edelmetalen bevat . Deze zal niet alleen voor de HDS activiteit veelbelovend zijn, maar ook voor verbetering van het cetaangetal die nodig is volgens de hoge dieselkwaliteit specificatie, aangezien deze katalysator een uiterst hoge hydrogeneringsactiviteit heeft.

Referenties

- [1] H.Schweiger, P.Raybaud, and H.Toulhoat, *Journal of Catalysis*, **212** (2002) 33.
- [2] M.Sun, A.E.Nelson, and J.Adjaye, *Journal of Catalysis*, **226** (2004) 32.
- [3] D.D.Whitehurst, K.G.Knudsen, I.V.Nielsen, P.Wiwel, P.Zeuthen, *Abstracts of Papers of the American Chemical Society, Div. of Petroleum Chemistry*, **219** (2000) 367.
- [4] Y.Sano, K.H.Choi, Y.Korai, and I.Mochida, *Applied Catalysis B: Environmental*, **53** (2004) 169.

List of Publications

Patents

N. Kagami and J. A. Moulijn, Hydrotreating catalyst for hydrocarbons, its manufacturing method, and ultra deep desulfurization process for diesel using the catalyst, JP2005-262173, A(09/29/2005).

N. Kagami, R. Iwamoto, and T. Hirano, Hydrogenation catalyst for hydrocarbon oil and method of hydrogenating hydrocarbon oil, JP2002-85975, A(03/26/2002).

N. Kagami, and R. Iwamoto, Refractory inorganic oxide carrier treated to carry metal compound and hydrogenation catalyst using the carrier, JP2002-001115, A(01/08/2002).

N. Kagami, and R. Iwamoto, Hydrogenation catalyst for hydrocarbon oil and method for hydrogenating hydrocarbon oil, JP2001-300316, A(10/30/2001).

Publications

Proceedings

N. Kagami, R. Iwamoto, M. Amano, and T. Tani, Application of Datamining Method (ID3) to Correlation of Feed Properties and Reactivity for HDS of Diesel Fuel, Preprint Paper of Am. Chem. Soc., Div. Fuel Chem., 2003, **48**(2).

N. Kagami, B. M. Vogelaar, A. D. van Langeveld, and J. A. Moulijn, Relationship between Catalyst Structure and HDS Reaction Mechanism, Preprint Paper of Am. Chem. Soc., Div. Fuel Chem., 2003, **48**(2).

B. M. Vogelaar, N. Kagami, A. D. van Langeveld, and J. A. Moulijn, Active sites and activity in HDS catalysis: The effect of H₂ and H₂S partial pressure, Preprint Paper of Am. Chem. Soc., Div. Fuel Chem., 2003, **48**(2).

Regular articles

N. Kagami, R. Iwamoto, and T. Tani, Application of Datamining Method (ID3) to Data Analysis for Ultra Deep Hydrodesulfurisation of Straight-run Light Gas Oil -Determination of Effective Factor of the Feed Properties to Reaction Rate -, Fuel. **84** (2005) 279.

N. Kagami, B. M. Vogelaar, A. D. van Langeveld, and J. A. Moulijn, Reaction pathways on NiMo/Al₂O₃ catalysts for hydrodesulfurization of diesel fuel catalysts, Applied Catalysis A. **293** (2005) 11.

R. Iwamoto, N. Kagami, and A. Iino, Effect of Polyethylene Glycol Addition on Hydrodesulfurization Activity over CoO-MoO₃/Al₂O₃ Catalysts, Journal of the Japan Petroleum Institute, **48** (2005) 237.

R. Iwamoto, N. Kagami, Y. Sakoda, and A. Iino, Effect of Polyethylene Glycol Addition on NiO-MoO₃/Al₂O₃ and NiO-MoO₃-P₂O₅/Al₂O₃ Hydrodesulfurization Catalyst, Journal of the Japan Petroleum Institute, **48** (2005) 351.

In preparation

Effect of nitrogen compounds to DBT HDS reactions on NiMo Alumina catalysts, Applied catalysis A / in preparation (Chapter 6).

Presentations

Oral presentations

ACS National meeting in New York (September 2003)

Application of Datamining Method (ID3) to Correlation of Feed Properties and Reactivity for HDS of Diesel Fuel, N. Kagami, R. Iwamoto, M. Amano, and T. Tani,

ACS 226th National Meeting, New York, USA, from 7/9/2003 until 11/9/2003 2003.

ACS National meeting in New York (September 2003)

Relationship between Catalyst Structure and HDS Reaction Mechanism, N. Kagami, B. M. Vogelaar, A. D. van Langeveld, and J. A. Moulijn,

ACS 226th National Meeting, New York, USA, from 7/9/2003 until 11/9/2003 2003.

Application of Datamining Method (ID3) to Correlation of Feed Properties and Reactivity for HDS of Diesel Fuel, N. Kagami, R. Iwamoto, M. Amano, and T. Tani,

invited lecture at Total refinery, Antwerpen, The Netherlands, July 2003.

Relationship between Structure and HDS Reaction Mechanism of NiMo Catalysts, N. Kagami, B. M. Vogelaar, A. D. van Langeveld, and J. A. Moulijn,

invited lecture at Universite des Sciences et Technologies de Lille, Lille, France, December 2003.

Relationship between Structure and HDS Reaction Mechanism of NiMo Catalysts, N. Kagami, B. M. Vogelaar, A. D. van Langeveld, and J. A. Moulijn,

invited lecture at Total ERTC, Le havre, France, June 2003.

Application of Datamining Method (ID3) to correlation of feed properties and reactivity for HDS of diesel fuel, N. Kagami, R. Iwamoto, M. Amano, and T. Tani,

invited lecture at Total ERTC, Le havre, France, June 2003.

Poster presentations

Understanding the Active phase and Hydrodesulfurization Catalysts, N. Kagami, B. M. Vogelaar, A. D. van Langeveld, and J. A. Moulijn, Gratama Workshop 2003, Utrecht, The Netherlands, 12-15 May 2003.

Reaction mechanism of hydrodesulfurization of thiophene and (substituted) dibenzothiophene over NiMo alumina catalysts, B. M. Vogelaar, A. D. van Langeveld, and J. A. Moulijn, NCCC V (March 2004).

Understanding the relation between the structure of NiMo catalysts and HDS activity for thiophene and (substituted) dibenzothiophene, N. Kagami, B. M. Vogelaar, A. D. van Langeveld, and J. A. Moulijn, 13th ICC in Paris (July 2004).

Acknowledgement

I would like to thank many people for their support in helping me accomplish my Ph.D. study. I was very lucky to get the opportunity to study in one of the best-known laboratories in the field. I acknowledge Dr. Iwamoto (Idemitsu Kosan Co., Ltd.) for encouraging me to study abroad and helping me apply for financial support from JCCP (Japanese Cooperation Center, Petroleum).

First of all, I would like to thank Prof. dr. Jacob A. Moulijn for accepting me as a Ph.D. student. Jacob, without your direction and encouragement, it would have been impossible to finalize my writing thesis. Your enthusiasm for science impressed me and has motivated me to do my best in R&D progress. Besides the scientific side, I would like to personally thank you and your wife Floor, for your kindness to my wife, Kiyomi and I.

I am much obliged to the following people for their contributions on scientific discussion and technical assistance. I thank Dick and Sonja for your knowledge, experience and stimulating discussions about my HDS study. Rob, you helped me a lot for consulting numerical fitting. Bas, you were my daily adviser, and I enjoyed working with you very much, discussing the HDS study. I really thank you for solving the technical problems of high-pressure autoclave, high-pressure micro flow reactor, TPS, Raman spectroscopy, SCD, and also translating my summary into Dutch. I will always remember our friendship. Thank you Thomas, for introducing a micro flow reactor at atmospheric pressure, Edwin for introducing TPR measurement, Ingrid for the trick maintaining GC, and Harry for the maintenance of equipment. It is my pleasure to thank Johan for the experiments of SO₂, and Delia for the measurement of catalyst composition.

Thanks to my roommates for a nice atmosphere in room 0.484 (Agus, Edwin, Jasper, and Nakul). I enjoyed a lot of our conversations and discussions about cultural, social, and scientific things. It was very special for me coming from Japan to such a cosmopolitan country. Edwin, Jasper, thanks for all the translating of Dutch into English, and teaching me special Dutch expressions, although I could not use them. Sometimes I was able to play mini-soccer, thanks to Hiro, Gerben, Guido, Xander, Peng, Augustin, Bram, et al. in the R&CE team. Jasper, Ignacio, Tilman and Kalyani, it was a nice experience to take the NIOK course for catalysis in Schiermonnikoog together, and Freek, thanks for your good lectures. Thanks for the short conversations at the smoking place just outside our office, Jorrit, Ingrid, and Weidong. I would like to thank Michiel for his administration of finance and safety issues, and Els, Daniella, and Elly (the secretaries) for all their wonderful assistance.

Thanks to all our Japanese neighbours in Delft for making our stay in the Netherlands so enjoyable. Hiro, thanks a lot for helping in the laboratory and also for leisure activities. Good luck with your thesis! Thanks to Mr. & Mrs. Ono, and Mr. and Mrs. Kodama for your friendship, it was very nice staying in Delft together under similar circumstances. Mr. and Mrs. Ishihara, thanks for a lot of useful information about life in the Netherlands from a Japanese perspective. We thank Mr. and Mrs. Stegeman (the owners of our apartment) for making our life comfortable. We are also grateful to the Dutch hosts of the international neighbour group supported by TU Delft for holding lots of enjoyable events where we could experience Dutch culture.

Of course, I cannot finish without offering special thanks to my wife. It is not so common for Japanese to show their thankfulness directly to their partners, but I learned in the Netherlands that it is sometimes good to show feelings and emotions. Kiyomi, thanks for your unlimited

understanding, endless support, and for your love. These make me happy and encourage me a lot. Finally many thanks to my parents for all their support and love.

Curriculum Vitae

Narinobu Kagami was born on May 28th, 1969 in Osaka Japan. He received his bachelor degree in Applied Chemistry in March 1992 from the Faculty of Science and Engineering at Waseda University. He completed his master's degree in Applied Chemistry specializing in catalysis in March 1994 from the Faculty of Science and Engineering at postgraduate school of Waseda University under the supervision of Prof. dr. E. Kikuchi. He has been working in catalysis for fuel processing technology at Idemitsu Kosan Co., Ltd. since April 1994. His PhD. study at Delft University of Technology started in September 2002, in the Reactor and Catalysis Engineering section under the supervision of Prof. J.A. Moulijn.